GEOPHYSICAL INTERPRETATION OF THE NORTHEAST THELON BASIN

GEOPHYSICAL AND GEOLOGICAL INTEGRATION AND INTERPRETATION OF THE NORTHEAST THELON BASIN, NUNAVUT

By VICTORIA LYNN TSCHIRHART, B.Sc.

A Thesis Submitted to the School of Graduate Studies in Partial Fulfillment of the Requirements for

the Degree of Doctorate of Philosophy

McMaster University DOCTORATE OF PHILOSPHY (2013) Hamilton, Ontario

TITLE: Geophysical and geological integration and interpretation of the northeast Thelon Basin, Nunavut
AUTHOR: Victoria Lynn Tschirhart, B.Sc. (McMaster University)
SUPERVISOR: Dr. William A. Morris
NUMBER OF PAGES: xii, 196

Abstract

The northeast Thelon Basin, Nunavut, is a rapidly developing albeit poorly studied, frontier exploration domain for unconformity-associated uranium deposits. Critical criteria for unconformity –associated uranium deposit models are knowledge of the basement geology, fault history and depth to unconformity surface. This thesis sets forth to derive working geological and geophysical models for the northeast Thelon Basin through the implementation of integrated geophysical techniques.

A physical rock property database is compiled defining average density and susceptibility values for key map units for integration into subsequent modelling iterations. Forward and inverse potential field modelling using these petrophysical with geological controls define the structure and geometry of the Shultz Lake intrusive complex and northeast Amer Belt, both of which are present below the Thelon sedimentary cover. Implementation of a new source edge detection technique estimates fault development and location within the basin. This provides a quantitative analysis of fault timing, identifying potentially reactivated faults which have an increased likelihood to serve as conduits to transport uranium-rich fluids and focus deposition. Corroborating the geophysical signatures on the aeromagnetic map with petrophysical properties and outcrop observations, a predictive geological map is developed for area beneath the sedimentary cover sequences. Inversion and interpretation of several discrete aeromagnetic anomalies provides local source depth estimates. Knowledge of fault locations is employed to delineate fault block boundaries. Interpreted geological model profiles include abrupt changes in sediment thickness with faults while abiding with the integrated source depth estimates. Integrating the results from a number of profiles provides a pseudo-3D rendition of the unconformity surface and its relationship to known faults. The geological-geophysical models which are presented herein incorporate all currently available data while providing a framework for the inclusion of future information as the knowledge gap for this remote region diminishes.

Acknowledgements

I am very fortunate to have had an excellent trio of supervisors: Bill, Charlie ('Crazy C') and Pierre. Their guidance and support is much appreciated. They were always willing to lend a helping hand and direct my sometimes divergent focus. Bill provided unconditional support in all the endeavours I undertook while at McMaster. I would also like to thank Charlie for always being up for a good bet. The multiple bottles of scotch I won helped with the headaches associated with writing a thesis.

I would like to thank my now former lab mates for their constant companionship throughout the duration of my time at McMaster. Petey Pabs, Billy, MadDog, Lindsay and Sara were part of many laughs, pranks, made-up religions/cults/blogs and general quests for world domination in our avoidance of doing work.

My parents and siblings exhibited amazing levels of patience dealing with the ever present mood fluctuations associated with a doing a PhD. Simon provided endless support, comfort and non-judgemental feline companionship.

I would like to thank my friends in Guelph, Hamilton and my former teammates for always being up for a good time on the weekend (and to a lesser, but nevertheless present extent, the weekdays). Despite most of them having virtually no idea about what a rock doctor does, they were always willing to lend a sympathetic ear to my vociferous complaints about "the system."

My fieldwork from 2008 to 2012 included several awesome and consecutive summer seasons on the Tundra that spurred my interest in integrating geology and geophysics. Petey Pabs, Crazy C, Scooter, and Stieber ably assisted in trudging "the box" over swamp and hill. Collaborators including Brian McEwan, Dr. Tony Peterson, Dr. Joe White, Dr. Kathy Bethune and Dr. Sally Pehrsson provided valuable and insightful discussions on the Thelon geology. Fieldwork was supported by the Geomapping for Energy and Mineral – Uranium Project, and funding was provided by a NSERC doctoral scholarship. Ookpik Aviation and AREVA Resources Canada provided logistical support and accommodations in the field. Special thanks to Carey Gagnon and Diane Jobin for providing the gravimeters, training and offering trouble-shooting advice.

In memory of Papa 2013.10.22.

Table of Contents

List of Figures

Chapter Two

Chapter Three

Chapter Four

Chapter Five

Chapter Six

List of Tables

Chapter Two

Chapter Three

Chapter Four

Chapter Five

1. Introduction

Basin modeling of potential field data has long been employed by the oil and gas industry to generate comprehensive framework geometries of prospective basins. By analyzing the gravity and magnetic data, the company can assess the viability of the basin by mapping fault (trap) locations and depth to basement, while minimizing risk and exploration costs. Such knowledge, ranging from reconnaissance to very detailed, can guide industry toward favorable areas for drilling. This methodology can be applied to mineral exploration in similar sedimentary basins. Unconformity-associated uranium deposits typically form in Paleoproterozoic basins at the intersections of high angle reactivated faults near the basement-sandstone unconformity interface (Jefferson et al., 2007). Thus, a crucial step in understanding the exploration problem is having a sound understanding of the basement geology, depth to basement, and the geometries and histories of faults in the area of interest. This thesis presents a geological-geophysical framework for basement rock assemblages within and surrounding the northeast Thelon Basin, the creation of 3D models, and revised geological maps for this prospective uranium region.

1.1 The Aberdeen Sub-basin (northeast Thelon Basin) region

The Thelon Basin is an intracontinental basin covering ~85 000 km^2 located in the western Churchill Province. The basin post-dates the uplift of the Hudsonian Orogeny by 100 Ma, yet its location appears to be controlled by reactivated faults that developed during the indenture of the Rae Province by the Slave Craton. That collision was part of the late-stage, global scale amalgamation of Laurentia. Filled dominantly by flat-lying siliciclastic sedimentary sequences of the Thelon Formation, sedimentation within the Thelon Basin is constrained to after 1.75 Ga and before the 1.54 Ga mafic eruptions (Davis et al., 2011). The deposition of the Thelon Formation represents the remnants of a large flat-lying cratonic sand sheet that unconformably overlies highly deformed Neoarchean (Woodburn Lake group) and Paleoproterozoic (Amer and Ketyet) supracrustal belts, Archean gneiss and a wide range of plutonic rocks (Palmer et al., 2004). These packages are cross-cut by strike-slip and dip-slip faults that were reactivated periodically during the 200 Ma depositional history.

The northeast Thelon Basin, here termed the Aberdeen Sub-basin, is prospective for unconformity-associated uranium deposits. As of 2009 Canada was producing 22% of

the global uranium supply, entirely from unconformity-associated deposits in the Athabasca Basin (Jefferson et al., 2007). Active exploration is currently underway in a number of basins known to host deposits but the challenge is to locate and develop economic deposits that can provide nuclear energy fuel in a timely and dependable manner. Key to understanding the uranium potential of the Thelon Basin is the geology and structure of the underlying supracrustal belts and intrusive suites.

Sustainable exploration and development of the Thelon Basin is the primary driver for this thesis. Preliminary exploration and research in the 1970's and 1980's located uranium prospects in the Thelon Basin region that are similar to those in the Athabasca Basin, but the magnitudes and spatial extents of these resources were incompletely documented (Fuchs and Hilger, 1989; Gandhi, 1989; Hasegawa, et al., 1990; Miller and LeCheminant, 1985). The second millennium's nuclear energy revival brought with it renewed exploration vigour. Companies operating in the Thelon Basin region have since acquired new ground and airborne geophysical data within their property limits. This thesis study was logistically integrated with the Geomapping for Energy and Minerals (GEM) Program-supported Northeast Thelon compilation project led by C.W. Jefferson of the Geological Survey of Canada (GSC). This comprehensive GEM project acquired and is now integrating and interpreting aeromagnetic, radiometric, satellite and geological data including published and unpublished industry sources for the northeast Thelon Basin region. This thesis aims to provide new information on the tectonic framework and subsurface geology using potential field interpretation routines that integrate geological and petrophysical data. Five journal articles have been written regarding these studies:

1) Geophysically constrained inverse modeling of the structure and geometry of the northeast Amer Belt.
2) Modeling the framework geology of the Shultz Lake intrusive complex using joint gravity and magnetic forward modeling under geological and petrophysical control.
3) Development of a new fault identification technique to estimate fault timing and intersections within the interior of the Aberdeen Sub-basin.
4) Construction of a new remote predictive geological map for magnetic-lithologic basement terranes below the Thelon Formation cover.

5) Regional 3D modeling of the framework of the Thelon Formation and underlying Amer Belt using integrated source depth routines.

Chapter 2 of this thesis models the structure of the northeast Amer Belt synform. This structure is the most northeasterly extension of a broad fold and thrust belt stretching over 100 km in strike length that extends southwesterly beneath the central part of the Aberdeen Sub-basin. Uranium occurrences are stratabound within the Showing Lake formation (Davidson and Gandhi, 1989) and have potential to host unconformity type deposits below the Thelon Formation cover. Sparse outcrop has resulted in limited structural data and speculative geological interpretations with multiple geometries possible, however distinctive quartzite ridges provide good regional geometric constraints including the overall synform and multiple structures within it (Patterson, 1986). Distinct linear aeromagnetic anomalies accentuate the northeastern end of the Amer synform as a flattened bulls' eye. 2D geometries of synthetic inverse models mimic an isolated oval anomaly within the bulls' eye in the interior part of the synform that has virtually no outcrop. The 2D models are incorporated into the reference model within the UBC-GIF interface in the near-absence of geological controls to generate a geophysically constrained inversion. A major innovation of this study is the integration of geophysically derived constraints that maintain structure at depth and the concept of a partially constrained inversion. This solved the problem of inadequate outcrop, lithologic and structural constraints, and thereby substitutes for insufficient in-place petrophysical data. The inversion results are corroborated with coincident gravity transects and a balanced geological cross-section generated in collaboration with the University of New Brunswick that is consistent with structural style in available outcrops.

Chapter 3 aims to constrain the geometry and context of the Shultz Lake intrusive complex (SLIC) with respect to adjacent uranium-hosting metasedimentary rocks. The SLIC comprises Hudson granite and Martell syenite which is a product of mingling between lamprophyre and Hudson granite magmas. The SLIC is expressed aeromagnetically as a broad overall high with an internal reticulate appearance and abrupt northeast-trending margins. The reticulate appearance results from cross-cuts by intersecting demagnetized fault zones one of which hosts the Tatiggaq uranium deposit of Cameco (R. Hunter, oral presentation, Nunavut Mining Symposium, 5 April, 2011). Extensions of these intersecting faults into the magnetically low metasedimentary rocks also host numerous uranium deposits of the Kiggavik camp. The SLIC is modelled using joint forward modelling of gravity and magnetic data coupled with new petrophysical and geological mapping constraints. Through a collaborative feedback process with project

geologists, the form of the complex is tested via three hypotheses. The petrophysical characteristics of the main rock units are derived. These are input as constraints into the final forward models and corroborated between intersecting profiles.

The location and timing of faults that controlled the development of the Aberdeen Sub-basin is discussed in Chapter 4. For every magnetic peak the Blakely algorithm (Blakely and Simpson, 1986) calculates a strike and dip direction based on the trend of adjacent maxima and source geometries, respectively, with the dip direction being a function of the down-slope gradient of the magnetic source. As a result, the calculated dip direction is always perpendicular to strike and points away from the magnetic source body. Gridding the dip direction helps to identify blocks of similar magnetic-lithologic character from which magnetic lineaments marking fault offsets can be identified. Used in corroboration with a digital elevation model (DEM), these lineaments can be matched with surficial features to deduce fault timing and reactivation. This methodological combination has never before been reported.

Chapter 5 details the construction of a geological map along the basal unconformity surface of the Aberdeen Sub-basin. Known unconformity associated uranium occurrences are located outside the sub-basin at the intersection of hydrothermally altered, reactivated faults within the Woodburn Lake group (Fuchs and Hilger, 1989; Gandhi, 1989; Hasegawa, et al., 1990; Miller and LeCheminant, 1985). Recent studies have emphasized the importance of identifying favourable basement lithological associations that host unconformity-associated uranium deposits (P. Wollenberg, oral presentation, Nunavut Mining Symposium, 5 April, 2011; R. Hunter, oral presentation, Nunavut Mining Symposium, 5 April, 2011). For exploration to progress successfully beneath the Aberdeen Sub-basin to sites analogous to the most recent findings in the Athabasca Basin there must be a thorough understanding of the subsurface geology from which to identify such prospective lithological associations. Through an analysis of source edge detection products, detailed outcrop mapping and pre-existing geological maps, a magnetic-lithologic remote predicted map is derived. A series of gravity profiles within and adjacent to the sub-basin perpendicularly transect the main lithostructural belts, constraining major contacts, fault geometries and offsets.

Chapter 6 addresses the architecture of the Aberdeen Sub-basin as a whole. Covered by non-magnetic strata of the Amarook and Thelon formations, the anomalies

visible on the aeromagnetic map are attributed to the underlying basement terrane (Nabighian et al., 2005). Sparse seismic refraction shot points and limited drill-hole data provide the only documented unconformity depths (Overton, 1979; Davis et al., 2011). This paper utilizes a combination of automatic and inverse source depth routines to compute depth estimates on idealized source bodies corresponding to known basement packages. Multiple methodologies improve the reliability of the depth estimates. By constructing numerous intersecting profiles that incorporate all calculated depth estimates a pseudo-3D model of the sub-basin generates new information on the architecture in an area of little direct control.

1.2 Potential field theory

Potential field techniques have long been implemented in the mining and minerals exploration industry, of which gravity and magnetics are the oldest and most common methods in use. They are used extensively for bedrock mapping due to their ability to map regional geology, structure, and alteration associated with ore deposits based on the apparent physical property contrasts between laterally adjacent geologic units. The measurements are taken on the ground or in the air using a magnetometer or gravimeter, respectively. The magnetometer records the sum contribution of all magnetic sources below the sensor in the presence of the Earth's magnetic field. The gravimeter records the apparent gravity field based on the subsurface mass distribution. The point measurements are then transformed to a 2D surface using a gridding algorithm. The resulting grid can be enhanced using any number of mathematical formulas to generate additional information on the structure and texture that is not apparent on the initial map. It may also be expanded into the third dimension to generate knowledge on the subsurface contributions (magnetic susceptibility and density distributions) of the signal and their location in x, y, z space (Blakely, 1996).

1.2.1 Geophysical modelling

Geophysical modelling provides the most fundamental way to generate 3D information from a 2D image. Coupled with a sound knowledge of the geology, geophysical modelling allows one to achieve a better understanding of the subsurface geological framework via the distribution of physical properties assigned to designated lithologic units. This methodology allows the interpreter to generate a wealth of information from an otherwise non-unique signal. In magnetics this assumes a magnetic

susceptibility distribution, and for gravity, a density distribution. Fundamentally, geophysical modelling is undertaken by two main approaches: inverse and forward modelling.

Inverse modeling is an automated numerical procedure that constructs a model of subsurface geology from measured magnetic or gravity data and any other *a priori* information with the additional condition that input data be reproduced within the error tolerance. Generally differences between the observed and calculated models are assumed to be negligible. Inverse models are non-unique on the basis that there are an infinite number of inaccurate measurements. More than one model can be obtained with the same accuracy and many subsurface distributions can produce the exact same surface response. There is no inherent depth information associated with a potential field signal so the observed response can be replicated by a thin near surface highly magnetic slab. As a result, whereas the inversion results are geophysically accurate, the resultant model does not necessarily satisfy the true geology. Uniqueness is introduced to the solution by including constraints where available in the original reference model as physical property bounds to pre-defined lithologic units, borehole data and/or previous inversions.

Forward modeling of potential field data calculates a response at some set of observed locations for a specific distribution of model parameters (magnetic susceptibility and/or density). A solution is obtained by manually adjusting a series of polyhedra with predefined parameters to obtain a match between the observed and computed data. The polyhedra are constructed using geologic principles and adhere to known surficial observations. Deviations between the observed and calculated responses are attributed to discrepancies in the mapped geology and assigned physical property distributions. Forward modelling assumes a set physical property for each unit in consideration and does not account for variability in mineralogy resulting in a heterogeneous density or magnetic susceptibility distribution. For a given set of parameters there is a unique solution.

Depending on the nature of the problem to be addressed and the available information one method may be more applicable than the next. Forward modelling presents the best results for abundant *a priori* information. It is best used in corroboration with geologists to ensure that the geological data is geophysically reasonable. It is implemented to test hypothesis involving multiple geometries that produce

distinguishable responses. Isolated anomalies can be modelled to generate information regarding the dip, depth and geometry of source bodies. Abundant petrophysical information allows for better control of the modelled units. A larger population of samples will be more representative of the true geology. By incorporating borehole data, absolute pierce points provide constraints on the interpretation. Inverse modelling is more appropriate where there are few known variables. The only requirement is a set of observed values; no other *a priori* information is needed. Accuracy of the solution is improved with the addition of constraints, but they are by no means essential to the inversion process.

Ultimately the goal of potential field modelling is to produce information as to where economic commodities of interest are located. This powerful tool provides information on the subsurface through an environmentally benign and non-invasive means. This level of regional scale modelling is essential to companies operating in remote and frontier regions where the cost of gathering detailed geological information greatly exceeds risk-benefit analysis. Prospective rock packages can however be identified geophysically for aerially constrained detailed follow-up thereby minimizing financial risks. The quality of the geophysical model is however a function of the pre-existing geological knowledge, the quality and density of the geophysical data, and how well the geophysical data can be related to the geological knowledge. Geophysics provides a means to supplement geological knowledge and thereby add value and precision to the geological interpretation.

1.3 Contributions by the author to this thesis

This thesis includes five chapters in addition to the introduction and conclusion. Each chapter includes a published, accepted or in preparation for submission manuscript by the student Victoria Tschirhart[1]. As each chapter represents an individual entity, material is repeated throughout chapters, particularly the geological setting, survey specifications and data reduction techniques. Each manuscript has three to six co-authors, with Bill Morris[1] and Charlie Jefferson[2] co-author on all publications. Chapters 2 and 3 were published in Geophysical Prospecting (Tschirhart et al., 2013b) and Canadian Journal of Earth Sciences (Tschirhart et al., 2013c), respectively. Chapter 4 has been accepted for publication in Uranium in Canada: Geological Environments and

[1] McMaster Applied Geophysical and Geological Imaging Center, Hamilton, Ontario, Canada
[2] Geological Survey of Canada, Ottawa, Ontario, Canada

Exploration Developments a Special Issue of Exploration and Mining Geology (Tschirhart et al., 2013a). Chapter 5 has been submitted to Precambrian Research and Chapter 6 has been submitted to Interpretation. The student wrote all the first-draft manuscripts, undertook the primary acquisition of local gravity data, and completed the data reduction, processing, petrophysical measurements, interpretation and geophysical images used in the manuscripts. Charlie Jefferson provided the geological maps and direct input on the geology used in all manuscripts in a feed-back process, whereby the geological maps were constrained by the geophysical data and by the third-dimensional knowledge provided by the geophysical interpretations. Bill Morris helped to direct research undertakings, provided technical feedback and direction through consultative discussions.

1.4 Presentations

Tschirhart, V., Morris, W.A. and Jefferson, C.W. 2010. Improved mapping of basement faults in the northeast Thelon Basin, Nunavut by source edge processing of aeromagnetic data. Presented at: *British Columbia Geological Survey Symposium on Uranium Exploration*, Vancouver, Canada, November 4, 2010.

Tschirhart, V., Morris, W.A. and Jefferson, C.W. 2010. Improved mapping of basement faults in the northeast Thelon Basin, Nunavut by source edge processing of aeromagnetic data. Presented at: *Yellowknife Geoscience Forum*, Yellowknife, Canada, November 17, 2010.

Tschirhart, V. Morris, W.A., Ugalde, H. and Jefferson C.W. 2010. Northeastern Thelon Basin, Nunavut: preliminary 3D geophysical modeling of the Aberdeen Sub-basin. *Presented at: GeoCanada 2010,* Calgary, Canada, May 16, 2010.

Tschirhart, V., Morris, W.A. and Jefferson, C.W. 2011. Preliminary geophysical analysis of the northeastern Thelon Basin region, Nunavut. Presented at: *Northeast Thelon Consortium Workshop*, Hamilton, Canada, March 10, 2011.

Tschirhart, V., Morris, W.A. and Jefferson, C.W. 2011. 3D geophysical inversions of the northeast Amer Belt and their relationship to geologic structure. Presented at: *Geological Association of Canada 2011,* Ottawa, Canada, May 27, 2011.

Tschirhart, V., Morris, W.A. and Jefferson, C.W. 2012. Framework modeling of the Shultz Lake igneous suite, basement to the northeast Thelon Basin, Nunavut. Presented at: *Geological Association of Canada 2012*, St. John's, Canada, May 26, 2012.

Tschirhart, V., Pehrsson, S., Peterson, T.P., Grunsky, E., Jefferson, C.W. and Morris, W.A. 2012. Geophysical characterization and spatial analysis of bimodal 1750 Ma Pitz calderas associated with gold and silver across the Kivalliq region of Nunavut. Presented at: *Nunavut Mining Symposium*, Iqaluit, Canada, April 17, 2012.

Tschirhart, V., Morris, W.A. and Jefferson, C.W. 2013. Geophysical framework modelling of key basement packages within and surrounding the northeast Thelon Basin, Nunavut. Presented at: *Prospectors and Developers Association of Canada - Student Minerals Colloquium*, Toronto, Canada, March 5, 2013.

1.5 References

Blakely, R. 1996. Potential theory in gravity and magnetic applications. Cambridge University Press, New York.

Blakely, R., and Simpson, R. 1986. Approximating edges of source bodies from magnetic or gravity anomalies. *Geophysics*, 51, 1494‑1498, doi:10.1190/1.1442197.

Davis, W.J., Gall, Q., Jefferson, C.W., and Rainbird, R.H. 2011. Fluorapatite in the Paleoproterozoic Thelon Basin: structural-stratigraphic context, in-situ ion microprobe U-Pb ages, and fluid flow history. *Geological Society of America Bulletin*, 123, 1056-1073.

Davidson, G.I., and Gandhi, S.S. 1989. Unconformity-related U-Au mineralization in the Middle Proterozoic Thelon sandstone, Boomerang Lake prospect, Northwest Territories, Canada. *Economic Geology*, 84, 143-157.

Fuchs, H.D. and Hilger, W. 1989. Kiggavik (lone gull): An unconformity related uranium deposit in the Thelon Basin, Northwest Territories, Canada. Uranium Resources and Geology of North America: International Atomic Energy Agency, Tech. Doc. 500, 429–454.

Gandhi, S.S. 1989. Geology and uranium potential of the Thelon Basin and adjacent basement in comparison with the Athabasca Basin region. Uranium Resources and Geology of North America: International Atomic Energy Agency, Tech. Doc. 500, 411-428.

Hasegawa, K., Davidson, G.I., Wollenberg, P. and Lida, Y. 1990. Geophysical exploration for unconformity-related uranium deposits in the northeastern part of the Thelon Basin, Northwest Territories, Canada. *Mining Geology*, 40, 83-95.

Jefferson, C.W., Thomas, D.J., Gandhi, S.S., Ramaekers, P., Delaney, G., Brisbin, D., Cutts, C., Portella, P., and Olson, R.A. 2007a. Unconformity-associated uranium deposits of the Athabasca Basin, Saskatchewan and Alberta: *in* Jefferson, C.W. and Delaney, G., (eds.), EXTECH IV: Geology and Uranium EXploration TECHnology of the Proterozoic Athabasca Basin, Saskatchewan and Alberta; Geological Survey of Canada, Bulletin 588, 23-68.

Miller, A. R., and LeCheminant, A.N. 1985. Geology and uranium metallogeny of Proterozoic supracrustal successions, central District of Keewatin, N.W.T. with comparisons to northern Saskatchewan*: in* Sibbald, T.I. and Petruk, W., (eds.), Geology of Uranium Deposits: Canadian Institute of Mining and Metallurgy Special Volume 32, 167-185.

Nabighian, M., Grauch, V., Hansen, R., LaFehr, T., Li, Y., Peirce, J., Phillips, J., and Ruder, M. 2005. The historical development of the magnetic method in exploration. *Geophysics*, 70, 33ND–61ND.

Overton, A. 1979. Seismic reconnaissance survey of the Dubawnt Group, districts of Keewatin and Mackenzie. Geological Survey of Canada, Current Research, Part B, Paper 79-1B, 397-400.

Palmer, S.E., Kyser, T.K., and Hiatt, E.E. 2004. Provenance of the Proterozoic Thelon Basin, Nunavut, Canada, from detrital zircon geochronology and detrital quartz oxygen isotopes. *Precambrian Research*, 129, 115-140.

Tschirhart, V., Morris, W.A. and Jefferson, C.W. 2013a. Faults affecting the northeast Thelon Basin: improved basement constraints from source edge processing of aeromagnetic data: *in* Potter, E., Quirt, D. and Jefferson, C.W., (eds.), Uranium in Canada: Geological Environments and Exploration Developments; Volume 21, Special Issue of Exploration and Mining Geology (CIM).

Tschirhart, V., Morris, W.A., Jefferson, C.W. 2013b. Framework geophysical modelling of granitoid vs supracrustal basement to the northeast Thelon Basin around the Kiggavik uranium camp, Nunavut. *Canadian Journal of Earth Science*s, 50, 667-677.

Tschirhart, V., Morris, W.A., Jefferson, C.W., Keating, P., White, J.C. and Calhoun, L. 2013c. 3D geophysical inversions of the north-east Amer Belt and their relationship to geologic structure. *Geophysical Prospecting*, 61, 547-560.

2. 3D geophysical inversions of the north-east Amer Belt and their relationship to structure

Tschirhart, V.[1], Morris, W.A[1]., Jefferson, C.W[2]., Keating, P[2]., White, J.C[3]. and Calhoun, L[3].

1. *MAGGIC, School of Geography & Earth Sciences, McMaster University, Hamilton, Ontario, Canada L8S 4K1*

2. *Geological Survey of Canada, 601 Booth St., Ottawa, Ontario, Canada K1A 0E8*

3. *Department of Earth Sciences, University of New Brunswick, P.O. Box 4400, Fredericton, New Brunswick, Canada E3B 5A3*

Reproduced with permission from Tschirhart, V., Morris, W.A., Jefferson, C.W., Keating, P., White, J.C. and Calhoun, L. 2013. 3D geophysical inversions of the north-east Amer Belt and their relationship to structure. *Geophysical Prospecting*, 61, 547-560.

2.1 Abstract

The Amer Lake area is located within the Churchill Structural Province in the Kivalliq Region of Nunavut, approximately 160 km north-west of Baker Lake. Two distinct geophysical-geological entities are structurally intercalated: an Archean mixed granitoid gneiss – metasedimentary-metavolcanic basement and the unconformably overlying Paleoproterozoic Amer Group metasediments. From east of Amer Lake stretching toward the south-west, these two entities form the Amer fold and thrust belt. At the north-east end of this belt, high-resolution aeromagnetic data define a distinctive oval shape that has been interpreted as a south-west trending doubly plunging synform. The outcrop within the interior of this structure is sparse resulting in limited structural data and speculative geological interpretations with multiple geometries possible. The high-resolution aeromagnetic data compiled through an industry-government consortium and newly acquired detailed gravity profiles were modelled to provide constraints on the geometry of this synform.

We document a geophysical-geological feedback process whereby the available geological and geophysical data were used to derive constraints on inversion models for the synform. Starting with available limited litho-structural data the presence of a double plunging synform was directly inferred from the aeromagnetic data. Segments of the aeromagnetic data have 2D morphology and so can be modelled using a simple parametric 2D dipping slab inversion approach. Models of profiles extracted from the aeromagnetic data were used to provide preliminary dip and magnetic susceptibility constraints for the Three Lakes mudstone with iron formation and the Five Mile Lake basalt. Landsat imagery outlined the spatial limits of the stratigraphically underlying, non-magnetic Ayagaq quartzite. Incorporating these outputs as bounds in the input / reference model for a UBC-GIF 3D magnetic inversion helped to accentuate the geological structure in the output mesh: an enhanced inversion that incorporates both geological and geophysical constraints. The validity of the resulting inversion model was tested by computing 2D forward models of the gravity profile data. The inversion model generated by this study emphasizes the importance of integrating information from as many knowledge sources as one can find. More trust can be placed on forward and inversion models where there is agreement among all data sets and a coherency of structural style.

2.2 Introduction

The Thelon Basin, transecting the border of Nunavut and Northwest Territories, Canada, (Figure 2.1) has been subject to periodic vigorous exploration efforts. One driver has been its historically documented similarities with the Athabasca Basin (Figure 2.1; Miller and LeCheminant 1985; Gandhi 1989), one of the world's largest uranium producers (Jefferson et al. 2007). Due in part to the Thelon Basin's remote location, exploration has been comparatively limited and many questions remain regarding the structure, geometry and tectonic framework of the basin and its underlying lithologic units. Of critical importance to the location of uranium deposits is a thorough understanding of the basement geology and structure, including reactivated faults and geochemically favourable trap rocks and how such attributes constrain transport of uranium from sources to focused deposits (Jefferson et al. 2007).

Geophysical inversions are applied in order to gain an understanding of the subsurface physical property distribution of a defined volume. For aeromagnetic data, this invokes a magnetic susceptibility distribution; and for gravity, a density distribution. An unconstrained inversion is a mathematical procedure that minimizes an objective function to provide a best match between the effect of the calculated physical property distribution and the observed data within a defined margin of error. Although the calculated inversions may be mathematically accurate, they can be geologically unrealistic. Constraints are incorporated based on the known rock types and their physical properties to ensure the inversion is as geologically realistic as possible. The graphical user interface of the University of British Columbia's inverse algorithm software (UBC-GIF Mag3D) when integrated with ModelVision permitted the incorporation of geological and geophysical constraints to calculate the structure at depth that is consistent in style with known surface structures of the Amer fold and thrust belt that trends south-westwardly beneath the Thelon Basin. We document how parts of a larger aeromagnetic anomaly map can be modelled using a series of individual 2D parametric inversion models and how these solutions can then be integrated into the full 3D inversion to improve the chance of obtaining the most geologically feasible solutions. By first solving elements of the aeromagnetic data on an individual basis rather than an initial bulk-susceptibility model, a best-fit solution is achieved for the model objective function that incorporates known, integrated geophysical and geological constraints.

2.3 Geologic setting

The Thelon Basin is late Paleoproterozoic, intracratonic and relatively undeformed. It covers approximately 85 000 km^2 of the western Churchill Structural Province (Figure 2.1). It is a primary repository of dominantly siliciclastic strata whose pre-erosional extent was once much greater. This complex sedimentary basin is filled by mainly fluviatile sequences with minor ultrapotassic mafic lavas and dolomite of the Barrensland Group that records a 200 million year depositional and diagenetic-hydrothermal history including reactivated faults (Chamberlain et al. 2010; Davis et al. 2011). The Barrensland Group unconformably overlies the Wharton and Baker Lake groups. These three major siliciclastic and volcanic sequences constitute the 1.83–1.5 Ga Dubawnt Supergroup (Rainbird et al. 2003; Peterson et al. 2010). The Dubawnt Supergroup unconformably overlies >2.2–1.9 Ga epicontinental strata of the Amer Lake (Figure. 2.2a) and Ketyet River groups (Rainbird et al. 2010), 2.7–2.6 Ga Archean supracrustal rocks with basalt and iron formation magnetic markers and older Archean gneiss, all of which were multiply deformed and structurally intercalated with each other before about 1.83 Ga (Pehrsson et al. 2010). The entire area was extensively glaciated during the last Ice Age, leaving a variably thick cover of till, sand and gravel constituting a variety of complex landforms (McMartin and Dredge 2005; McMartin, Dredge and Aylesworth 2008).

The Amer fold and thrust belt underlies the central axis of the Thelon Basin, is exposed along a 100 km strike length from the north-east end of the Thelon River toward the study area, has an average width of 50 km and terminates about 30 km north-east of Amer Lake. The multiply deformed and metamorphosed Amer Group (Figure 2.2b) comprises four early Paleoproterozoic sequences (Figure 2.2a) with multiple informal formations (Young 1979; Patterson 1986; Rainbird et al. 2010): Ps1: Ayagaq formation quartzite and conglomerate; Ps2: Resort Lake formation graphitic mudstone, siltstone and nonmagnetic sulphide iron formation, Aluminum River formation dolostone and Five Mile Lake basalt; Ps3: mixed grey-green mudstone and siltstone (Three Lakes formation) with an upper magnetite iron formation (Calhoun et al. 2011) and calcareous sandstone with local uranium concentrations (Showing Lake formation); and Ps4: grey to red sandstone with desiccation cracked red mudstone (Itza Lake formation). Sandstone hosted uranium prospects within the Showing Lake formation have themselves been targeted by exploration companies and are potential metal sources for unconformity associated

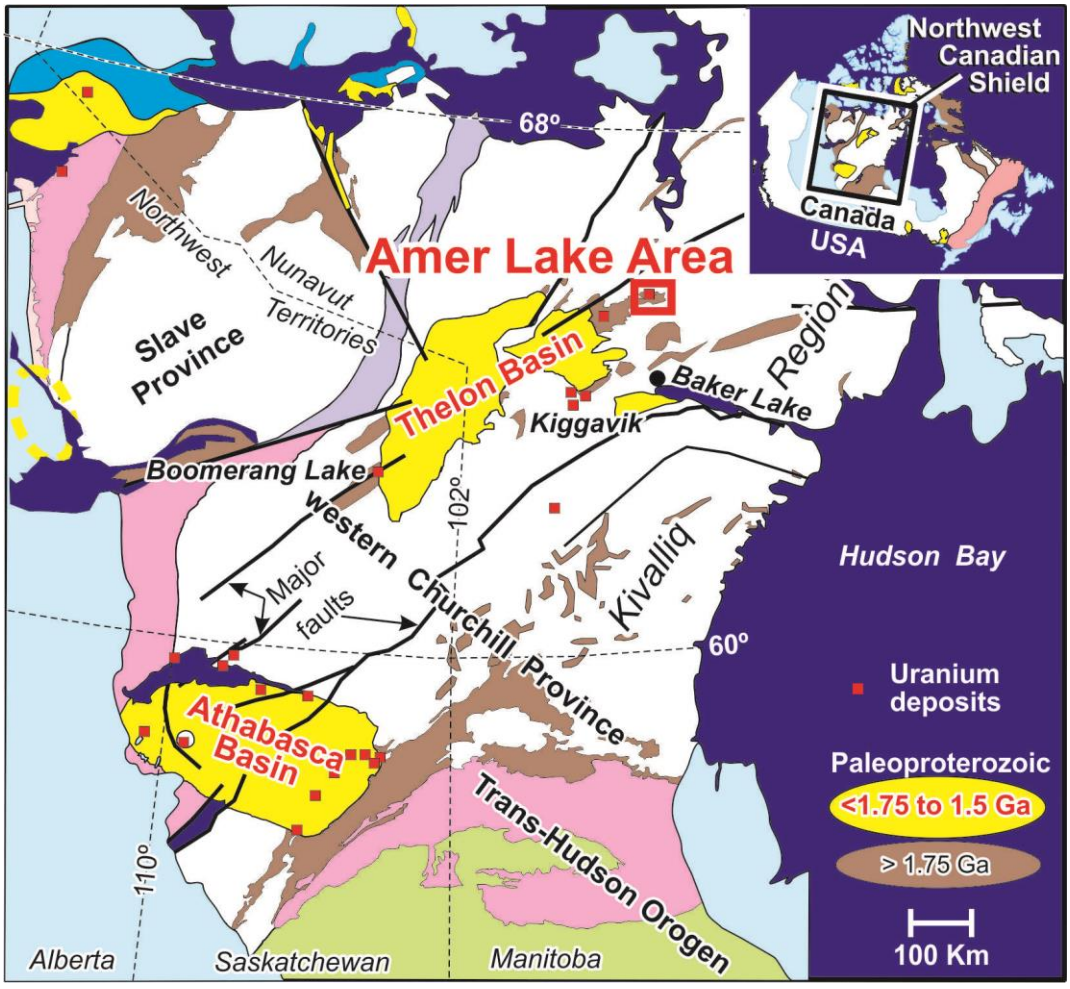

Figure 2.1 Geological setting of Thelon Basin in the northeastern Canadian Shield, after Pehrsson et al. (2010). Thick red rectangle outlines the northeast Amer Belt study area (Figures 2.2b and 2.3).

uranium deposits near and beneath the Thelon Formation conglomerate and sandstone. The Amer Belt has been intersected by drilling beneath the north-east Thelon Basin (Davis et al. 2011), is exposed south of Aberdeen Lake and is inferred to be contiguous in the subsurface with metasedimentary units at the southern tip of the Thelon Basin that host the Boomerang Lake uranium prospect (Figure 2.1), which has structural and lithologic similarities to Athabasca-style deposits (Davidson and Gandhi 1989).

The north-east Amer synform east of Amer Lake (Figure 2.2b) is outlined by the resistant Ayagaq quartzite and bounded to the east and south by thrust repeats of the basement with the quartzite. Previous mapping (Knox 1980; Smith 1984; Patterson 1986; Tella 1994) and more recent geological studies of this structurally complex belt suggest that this structure is a broad south-west trending canoe-shaped D2 synform that refolds D1 nappes and structural discontinuities (Calhoun et al. 2011). The outcrop of the relatively recessive Ps2 through Ps4 fine grained strata within the interior of this synform is sparse, although a good outcrop of the Ps1 Ayagaq quartzite constrains the overall structure (Figure 2.2; Patterson 1986). The Showing Lake formation contains strata bound sandstone hosted uranium prospects along the length of the Amer Belt north-east of the Thelon Basin (Gandhi et al. 2010). Such occurrences are known in the northern and southern parts of the study area (Figure 2.2b) but have not yet been reported in the Showing Lake formation as mapped in the core of the synform being modelled here. This synform can serve as a training area for future modelling of the Amer Belt farther to the south-west close to and underlying the Thelon Formation.

A compilation of high-resolution aeromagnetic data from the industry and new surveys (Harvey et al. 2011; Tschirhart, Morris and Oneschuk 2011) outlines an east-west elongated bulls-eye pattern of linear aeromagnetic highs in the synform of interest. Based on detailed mapping of a key outcrop by Calhoun et al. (2011), the strongest linear aeromagnetic anomaly is known to be associated with a mudstone containing disseminated euhedral magnetite in the Three Lakes formation of Ps3. This magnetic marker is structurally and stratigraphically separated by D1 discontinuities and sequence Ps2 from the outer, locally broken ring of Ps1 Ayagaq quartzite. Moderate linear magnetic highs and lows are also associated with disseminated magnetite in the mudstone of the Showing Lake formation whose complex structure cannot be connected geologically due to the sparse outcrops. Interpretations of the interior structure must

a)

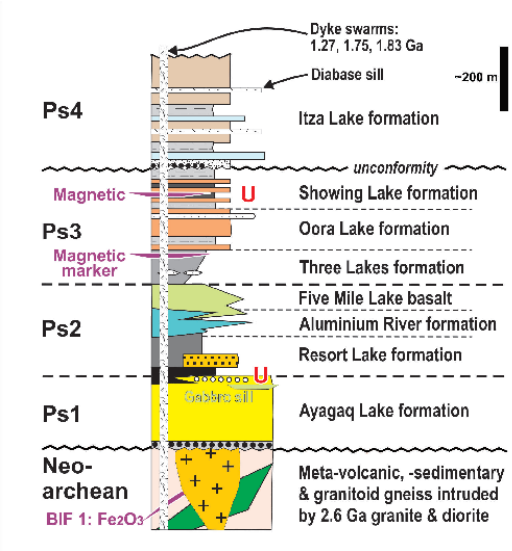

b)

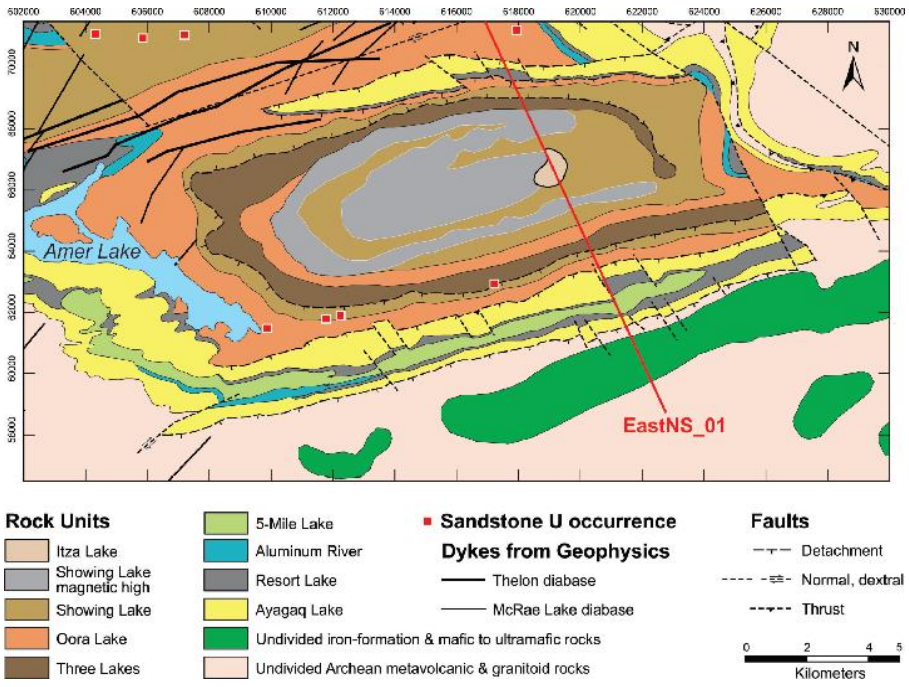

Figure 2.2 a) Simplified lithostratigraphic succession of the Amer Belt (after Pehrsson et al., 2010). **b)** Simplified geological map of the northeast Amer Lake synform based on detailed ground traverses and subjective consideration of aeromagnetic compilation. Map units are keyed to Figure 2.2 a); Transect EastNS_01 is keyed to Figures 2.3 and 2.6.

Informal Formation [code]	Description	Average Susceptibility (SI x 10^-3)	Range	Average Density (g/cm^3)	Range	n
Itza Lake [Ps4 Afs]	Arkosic sandstone	0.154	0.014- 0.298	2.72	2.60 – 2.80	7
Showing Lake [Ps3 Afms]	Sandstone and mudstone	0.109	0.015 - 0.174	2.81	2.7 – 2.95	8
Oora Lake [Ps3Afs]	Feldspathic sandstone	0.071	0.016 – 0.110	2.76	2.73 – 2.81	4
Three Lakes [Ps3 Afm]	Mudstone and iron-formation	20.63	20.63	NA	NA	1
Five Mile L. P_{Av} [Ps2Amv]	Basaltic tuff and flows	37.095	35.95 – 38.24	2.86	2.85 – 2.86	2
Aluminium River [Ps2Ad]	Dolostone	Not present in modeled transects				
Resort L. [Ps2Agm]	Graphitic mudstone	0.100	0.012 – 0.157	2.78	2.70-2.83	6
Ayagaq Lake [Ps1Aq]	Quartzite and conglomerate	0.008	0.007 – 0.011	2.64	2.63 – 2.64	4
Archean granitoids	Granitoid and volcanic rocks	NA	NA	2.67*	NA	NA
Archean magnetic unit	Iron-formation and mafic rocks	NA	NA	2.83*	NA	NA

Table 2.1 Average measured physical properties. *denotes estimate of physical property when no samples are available.

therefore build on the excellent geophysical data keyed to the few known outcrops. In addition to the high-resolution aeromagnetic compilation and targeted geological mapping in 2010 over the synform, multiple intersecting detailed gravity transects were completed during the summer of 2010. A suite of representative samples was petrophysically analysed to characterize the key lithologic units constituting the synform (Table 2.1).

2.4 Geophysical modelling: inverse and forward

Inverse modeling is the estimation of model parameters (density, magnetic susceptibility, and where appropriate magnetic remanence) from the observed data. It is a numerical procedure that constructs a model of the physical property distribution of the subsurface from measured magnetic or gravity data and any other prior information with the condition that input data be reproduced within a specified error tolerance (Li and Oldenburg, 1996). A model objective function (ϕ_m (m)) is used to solve multiple linear equations which describe physical property variations in the proposed model which has a predefined "smoothness" in 3 directions. The UBC Mag3D algorithm iteratively modifies the physical property variations until a predetermined "misfit" between the observed and computed model data is achieved. The equation reflects the "smallness" and "smoothness" of the desired output model (ϕ_m (m)):

$$\begin{aligned}\phi_m(m) = {} & \alpha_s \int_v w_s \{w(z)[m(\mathbf{r}) - m_0]\}^2 dv \\ & + \alpha_x \int_v w_x \left\{\frac{\partial w(z)[m(\mathbf{r}) - m_0]}{\partial x}\right\}^2 dv \\ & + \alpha_y \int_v w_y \left\{\frac{\partial w(z)[m(\mathbf{r}) - m_0]}{\partial y}\right\}^2 dv \quad \text{(Li and Oldenburg, 1996)} \\ & + \alpha_z \int_v w_z \left\{\frac{\partial w(z)[m(\mathbf{r}) - m_0]}{\partial z}\right\}^2 dv \qquad (1)\end{aligned}$$

The first term of equation (1) is a measure of the smallness (difference) between the reference model, m_0, and the recovered model, m (**r**). The remaining three terms control the smoothness in 3 orthogonal dimensions. They distribute the difference between m (**r**) and m_0 equally through the whole model. The Alpha weight function

controls these terms, α_s, for smallness and α_x, α_y, α_z, for smoothness, with w_s, w_x, w_y, and w_z spatially dependent weighting functions for these parameters. These parameters drive the inversion and can be adjusted to achieve the desired spatial and physical limits (Williams, 2008; Spicer et al., 2011). The amount of "smoothing" can be varied to increase the discernible structure: a higher ratio of smallness to smoothness will reproduce the reference model more closely at the expense of smoothness, but may introduce excess structure. A lower ratio of smallness to smoothness will create a smoother model with less structure. By changing the parameters in x, y and z to reflect a "smoother" anomaly, the fall-off distance of the signal in x, y and z will increase resulting in smoothed magnetic units. A trade-off must be determined so that excess structure is not introduced, but that the ratio of small to smooth is high enough that structure is discernible. The level of "smoothness" must also be a function of the reliability placed in the reference model in the event there is a rapid transition zone between adjacent cells.

A depth weighting function (w (z)) is applied to allow for equal chance susceptibility for cells at different depths. With no depth weighting, the anomaly source would be focussed near surface with the model being a thin highly magnetic slab atop a large low susceptibility body. The depth weighting function is:

$$w(z) = (z_0 + z_j)^{-\beta/2} \qquad (2)$$

In equation (2) (Li and Oldenburg, 1996), z_j is the depth to the jth cell and z_0 is adjusted to obtain a best match between the kernel's weighting function with depth. The UBC-GIF Mag3D and Grav3D code, which is constructed from a volume of prisms, employs a fixed rate of signal decay with distance from the source; for gravity $\beta = 2$ while for magnetics $\beta = 3$. More recently Cella and Fedi (2012) have shown that when a source body is approximated by a series of prisms the cumulative effect results in signal decay rates that are not uniform but rather are variable and linked to overall geometry of source body. This could produce minor depth inconsistencies in the output model.

The inversion of a potential field is non-unique and, therefore, an infinite number of models can give the same observed field (Li and Oldenburg, 1996). The non-uniqueness associated with the inverse problem stresses the importance of incorporating physical constraints into the starting reference model to force some geologic form on the resulting output model. Procedures for incorporating geological constraints have been described by Spicer et al., (2011). Williams (2008) shows that it is possible to increase

confidence in the output model by progressively increasing the amount of geological constraints in the initial input model. Williams (2008) had limited constraints; primarily some physical rock property data; some near surface lithological contact information that was mainly derived from airborne geophysics and a limited number of borehole studies.

For this study we use: a) satellite imagery which provides direct control on the distribution of the Ayagaq quartzites; b) a limited number of physical property data; and c) near surface geology inferred from patterns in an airborne magnetic survey. There was no borehole data available. We introduce a method for incorporating additional geophysically derived constraints into the UBC-GIF reference model. Many of the magnetic anomalies in the study area are narrow, elongate and closely associated to a specific geological horizon. As such, in a 2D sense, perpendicular to strike, these anomalies can be approximated by simple dipping slabs. Parametric inversion modeling of 2D profiles using a simple dipping tabular body has fewer variables than the myriad of voxels used in a full 3D inversion. The position, strike and width of the top of the body are directly controlled by the resolution of the geophysical data set. Knowing the susceptibility of the unit, the only remaining variables are the depth to top, depth extent and dip of the tabular body. In the absence of any direct evidence for magnetic remanence, all of our models are based on magnetic susceptibility fluctuations. We recognize that, if present, magnetic remanence could affect the dips of our output models (Tschirhart and Morris, 2011). Depth to top can only have a small limited variation as overburden thicknesses in the region are overall less than 10 m (Thomas, 1981). Depth to base of the slab can be treated as infinite since this will have minimal impact on the solution. Susceptibility is then directly controlled by the amplitude of the observed magnetic signal. The only other parameter the dip of the slab is controlled by asymmetry in the geometry of the magnetic anomaly profile. Consistency of computed dip between adjacent profiles and compatibility of the computed dip with limited direct observations provides confidence in the model outcome. Furthermore, a 2D inversion forces the geological “contacts” to be on parallel surfaces. Often a full 3D inversion will produce a dispersion of the anomaly source with increasing depth. This is a consequence of the anomaly equivalence of a volumetrically limited source of higher susceptibility and dispersed model with lower susceptibility. The parallel contacts of a 2D inversion output are obviously more in keeping with our perception of a geological unit. Interpretation of a series of these 2D model profiles provides the basis for the construction of a dipping

geological unit with a known physical property which can then be introduced as a constraint in the full 3D inversion. Knowledge of the dip of this magnetic unit provides a guide for locating the immediately overlying quartzite unit whose presence was established by analysis of Landsat imagery. Patterson (1986) and Calhoun et al. (2011) provided detailed maps for the synform which were considered in constructing the geophysical model, and summarized in Figure 2b. The best exposed unit, the Ayagaq quartzite, is non-magnetic and constitutes the rim of the synform. On air photographs (the primary mapping base for Patterson, 1986) and LANDSAT imagery, the quartzite is evident as broad, linear, white ridges. The quartzite is also evident on the DEM as linear topographic highs.

The output of the magnetic anomaly inversions were tested using independent forward modeling of gravity data. In contrast to inverse theory, forward modeling calculates an observed response at data locations for a user defined geometric model and physical property parameters (density or magnetic susceptibility). An optimum solution, as defined by a minimum Root Mean Square (RMS) error, is obtained by the operator manually adjusting the position and geometry of geological contacts and the physical properties of the units to optimize the match between the observed and computed data. Forward models can be constructed to mimic the structure depicted in the inversion.

In summary, we present a presents a geological model of the northeast Amer which was derived through progressive 2D modelling followed by full 3D inversion of the aeromagnetic data. The geometries of this output model were then tested by forward modelling of gravity data collected on a profile across the structure. More reliability can be attributed to structural hypothesis which satisfies both the inverted aeromagnetic data and the forward modelled gravity data.

2.5 Methodology

2.5.1 Magnetic data reduction

The aeromagnetic data used for the study was acquired by Uranium North and the Geological Survey of Canada (GSC) at 200 m and 400 m spacing, gridded to 50 m and 100 m using minimum curvature, respectively (Harvey et al., 2011; Tschirhart et al., 2011). The Uranium North data were re-gridded to 100 m and upward continued from 70 m to 120 m to be consistent with the GSC data. The two surveys were stitched together

with a final grid node spacing of 100 m. Both surveys had been tie-line levelled. The Uranium North survey was micro-levelled to remove flight line effects and along line corrugations. The merged grid was upward continued 2000 m and subtracted from the original stitched grid to produce a residual grid in which the short wavelength, near surface features of interest are enhanced (Figure 2.3). Data preparation prior to interpretation using UBC-GIF Mag3D followed the methodology described by Spicer et al., (2011) using Pitney Bowes' ModelVision software to incorporate geological and geophysical constraints into input / reference model mesh. A voxel size of 150 m was defined for the mesh with a depth extent of 3000 m. Prior to the inversion process, it is necessary to define a noise (uncertainty) level that is acceptable with the data. This uncertainty envelope addresses the level of anomaly deviation that is to be modeled in the computed fit between the observed and calculated model response (Williams, 2008). Following the removal of the regional field, the aeromagnetic data has a dynamic range of 3603 nT. Williams (2008) and Spicer et al., (2011) have suggested that the uncertainty level should be set at between 3 – 5% of the total dynamic range. An uncertainty value of 3%, or 108nT, was employed in the inversion procedure. Setting the bound at this level serves to focus the computed solution on the more strongly magnetic horizons. Williams (2008) further recommended upward continuing the aeromagnetic data by at least the distance of the individual voxel size to ensure that high frequency signal produced by smaller cell sizes is not included in the resulting inversion model. In this instance the data was upward continued by 150m, which with the flight terrain clearance and overburden thickness means that the total distance between source and sensor point is greater than 270 m. Upward continuation serves to minimize the presence of high amplitude, high frequency signals which because the optimum match is sought through a RMSE calculation could significantly distort the "misfit" being sought by the model algorithm (Williams, 2008; Spicer et al., 2011).

2.5.2 Geologic and geophysical constraints

Reference models, which form the input into the inversion algorithms, are improved by the incorporation of all geologic and petrophysical constraints for the area. The primary spatial constraint for near surface voxels in the reference mesh is provided by the existing geologic map coupled with physical property measurements for the respective units. As noted above the bounds of the Ayagaq quartzite is well-defined by both topographic and satellite imagery. The contacts of other lithological units

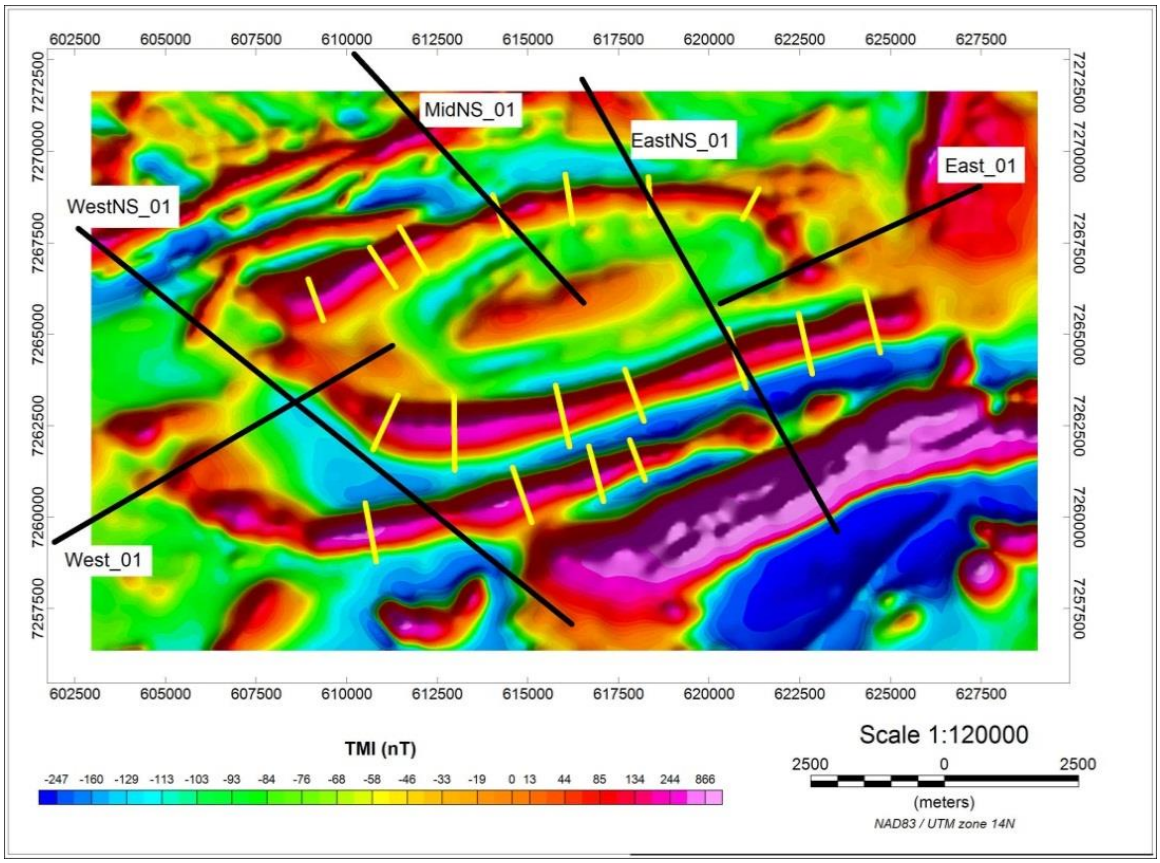

Figure 2.3 Residual magnetic intensity grid encompassing northeast Amer Belt. Locations of PotentQ profiles are shown in yellow; Locations of gravity transects shown in black.

especially those within the interior of the synform are less well constrained. Outcrop is limited and no previously geological maps have been published. Figure 2.2b is the first such attempt resulting from interdisciplinary discussions within the northeast Thelon compilation team.

An attempt was made to extend these near surface spatial constraints to three dimensions by continuing the quartzite prism models 300 m below surface based on the average mapped dip and strike of each lithological unit. Susceptibility ranges were assigned to the units based on measurements of samples from 2008 through 2010 field seasons, especially those collected along the ground gravity transects (Table 2.1). Petrophysical measurements performed on the quartzite were included as boundaries in the reference model. While the inversion process seeks to explain the observed magnetic anomaly pattern by a subsurface distribution of magnetized voxels, by incorporating a region (the quartzites) which is permitted to have only minimal magnetic susceptibility, the solution is forced to place more signal strength (susceptibility) into more geologically appropriate regions of the mesh model (i.e. Three Lakes formation and volcanics).

Incorporating more subsurface constraints into the reference model is a challenge. Due to its remoteness, the northeast Amer Belt has been subject to minimal investigation and no previous geophysical analysis. To overcome the lack of comprehensive continuous geological information for the study area, we develop geophysical reference models from a combination of the known detailed geology and aeromagnetic data to help drive the inverse algorithm. A series of profiles were extracted from the aeromagnetic database over the most magnetic units - Three Lakes formation BIF and Five Mile Lake volcanics. Using Oasis Montaj's PotentQ software 2D inversions of the magnetic profile data was computed for a dipping slab model with only susceptibility, width and dip being allowed to vary. Strike length, height and depth were held constant for each profile, with values estimated from the apparent strike of the unit on the aeromagnetic map and the unconstrained inversion results (Figure 2.3 and Figure 2.4). These were set to 600 m, 1000 m and -220 m, respectively, for the Three Lakes Formation and 600 m, 800 m and -220 m for the Five Mile Lake volcanics. This procedure was applied to fourteen profiles across the Three Lakes Formation and four profiles across the Five Mile Lake volcanics (Figure 2.3) generating eighteen 3D geophysical reference models. The maximum allowed RMS error for the observed versus computed responses was 14.5, with all other RMS errors for the profiles below 10.

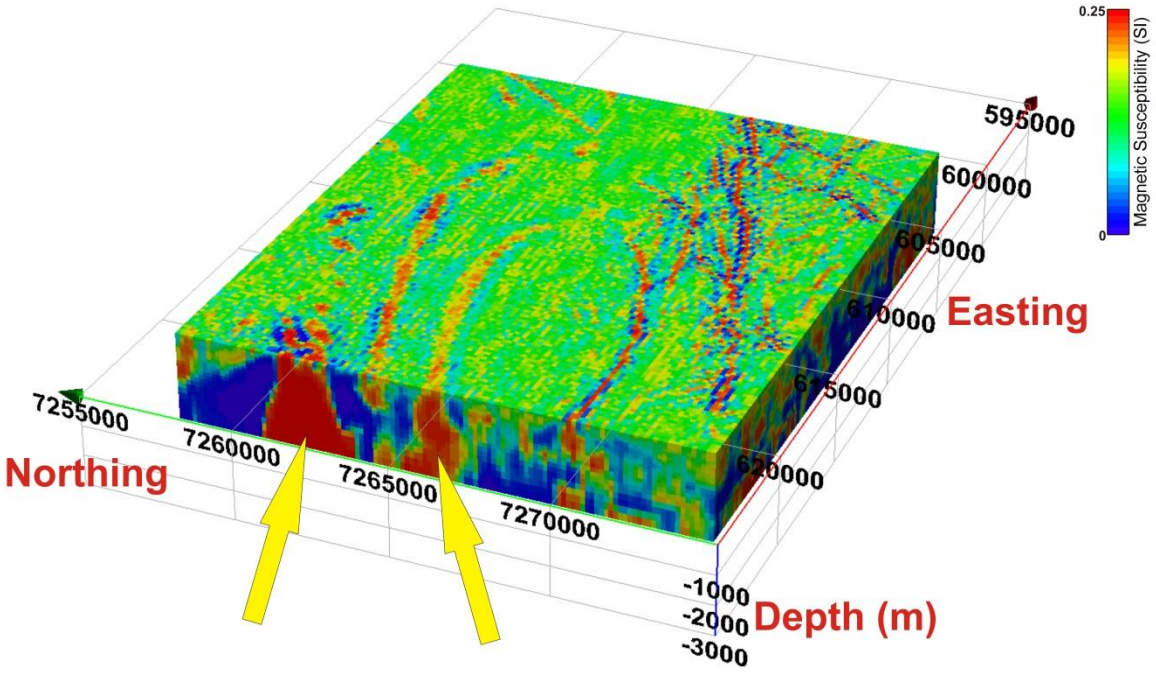

Figure 2.4 Unconstrained inversion of residual magnetic intensity (RMI) data. "Smooth blob" denoted by yellow arrows.

Integrating the individual 2D profile results from the same geological unit into a single model provides a method for estimating the subsurface form of these geophysically defined lithological units. The 2D inversions also provide an estimate of the susceptibility bounds that should be applied to these units. Ideally, as in this study, these computed physical property bounds are compatible with any directly measured values. The lithological contacts provided by the satellite imagery and the 2D geophysical inversions together with the observed and computed physical property limitations helped impose a geological rigour to the input (reference) model (Figure 2.5). The final outcome of the inversion model is then controlled by the mathematical constraints of smoothness and smallness associated with the inversion algorithm and the prior geological knowledge.

2.5.3 Gravity data reduction

Ground gravity transects were acquired in July and August 2010. The station spacing ranged from 50 to 500 m depending on the lateral distance of the previously mapped lithologic contacts. LaCoste and Romberg model G meters G0074, G0173 and G0790, with a reading resolution of 0.01 mGal, were tied to the Canadian Gravity Standardization Net through the Baker Lake gravity base station. The vertical and horizontal locations were determined through differential GPS using a ProMark GPS and computed using GNSS Solutions. An elevation precision of better than 7 cm was determined for all measurements. The first corrections to the field data include latitude, instrument drift, elevation and Earth's tide. Terrain corrections were made for the most eastern northwest-southeast transect where the greatest local topography was encountered. No terrain corrections were made for the other stations, but care was taken at each station to ensure that the field observation was at least 40 m away from steep inclines.

The Free Air anomaly correction (correcting for the variation of gravity effect with increases of height) was the final step before using the data in all subsequent forward models. GM-SYS Solutions was used to compute the forward models, with the bounds of each lithology polyhedron being successively modified to reflect the known surface geology and petrophysical properties to obtain a best-fit between the observed and calculated anomalies (Figure 2.6).

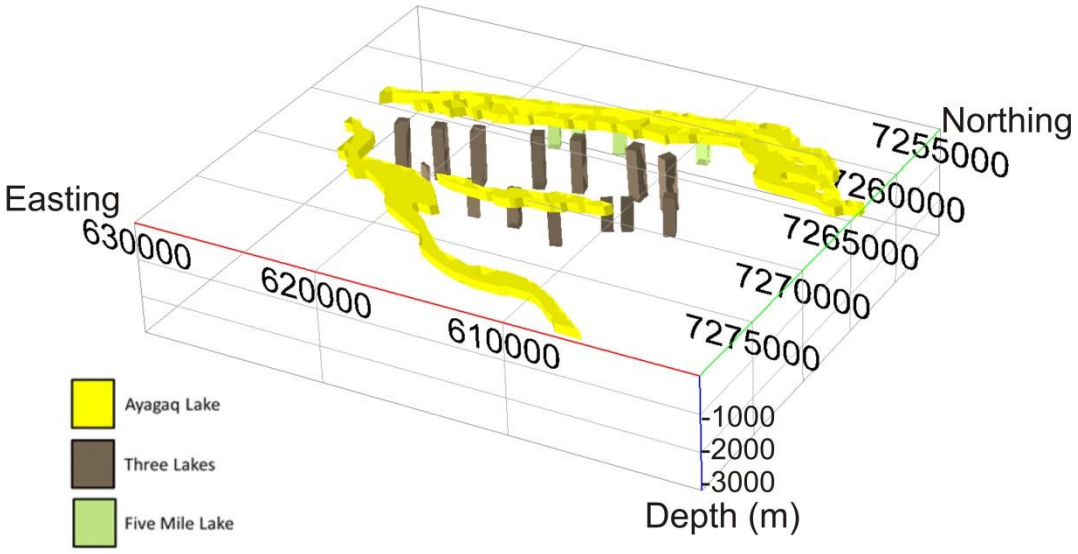

Figure 2.5 Reference model of susceptibility values visible in three dimensions with constraints imposed at depth. The Five Mile Lake volcanics and the Three Lakes formation are continued 800 m and 1000 m, respectively, into the subsurface with the plunge dictated by the PotentQ models. The Ayagaq quartzite is continued 300 m below the subsurface.

The density constraints imposed on the units were derived from the samples acquired during the gravity transects. Whereas the limited number of samples (due to sparse outcrop) prevented determination of absolute values, the range was used to provide boundaries for the density constraint. Three NW-SE and two E-W profiles were generated. As suggested by Reid (2010) the profiles modeled the Free Air gravity anomaly since this allows the interpretation to incorporate the interaction between geological contacts and the topographic surface. To provide further corroboration, the last three authors independently produced geologic cross-sections for the western and easternmost NW-SE cross-sections which corroborated with the NW-SE forward models. Finally, the outlines of the optimum forward models were draped over the inversion results, and then interrogated to ascertain corroboration of results. There is a general agreement in the geometry of the synform with the geophysically constrained inversion results.

2.6 Results and discussion

2.6.1 Inversions

Because inversions are non-unique, the observed responses associated with a magnetic anomaly pattern can be replicated by an infinite number of magnetic susceptibility distributions. Only after assigning values to the petrophysical parameters, focusing on units with sufficient contrast and providing geological control through outcrop mapping can one place confidence in the output. Using the northeast Amer aeromagnetic data, one unconstrained and a series of constrained inversions were computed with varying levels of smoothness, smallness and initial constraints. Ideally, given the lack of reliability placed on the geologic and geophysical constraints due to the sparse sampling and coarse mapping for the region, there should be a lower smallness to smoothness ratio to allow for greater deviation from the reference model. Unfortunately in doing so, structure is lost due to smoothing. The best results obtained from the data resulted from a low "smoothness" to accommodate the abrupt structural contrasts within the highly magnetic units that characterize the area and a low "smallness" to emphasize more detailed structure in the calculated model. The result of this geophysically constrained inversion is shown in Figure 2.7a, b.

a)

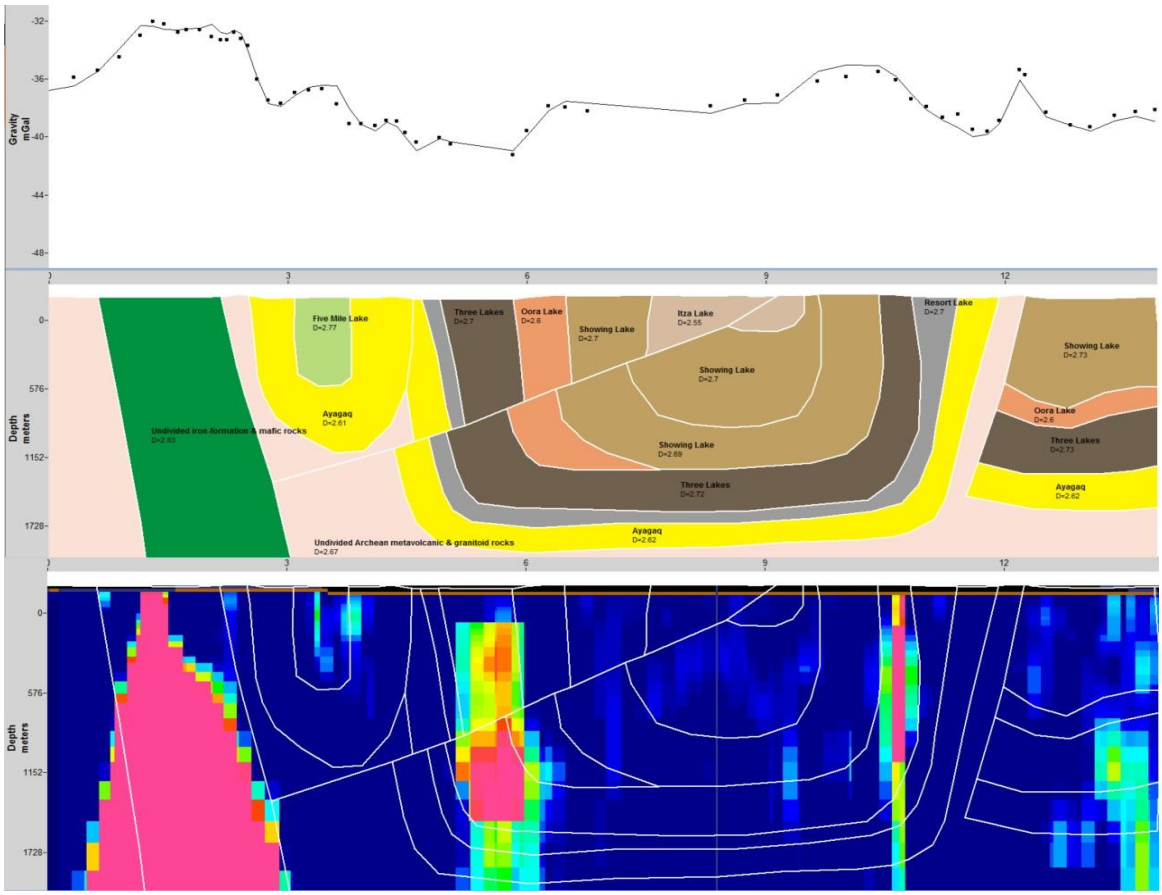

Figure 2.6a Results of gravity profile for EastNS_01**. a)** Top panel: forward modelled gravity profile, units and densities as labelled. Bottom panel: inversion splice draped behind forward model. There is general agreement for the magnetic highs between gravity and magnetic datasets.

b)

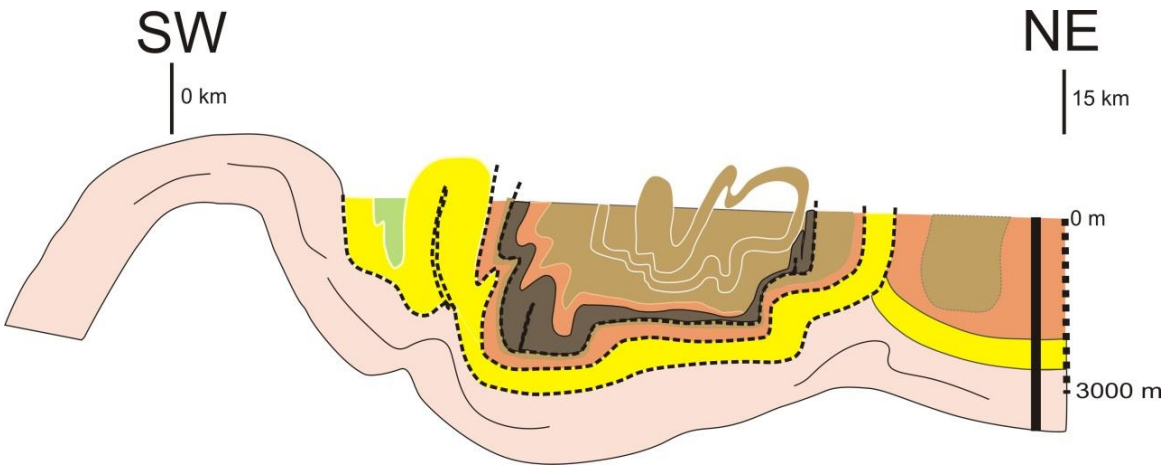

Figure 2.6b Geological cross section for EastNS_01 developed by feedback between geophysical data and structural style of surrounding geological observations. Major detachment surfaces are outlined by black dotted line. The basement rocks are combined as a single unit coloured medium pink, a magnetic component of the Showing Lake formation is distinguished by light brown, and the remaining units are coloured as in part (a) above.

a)

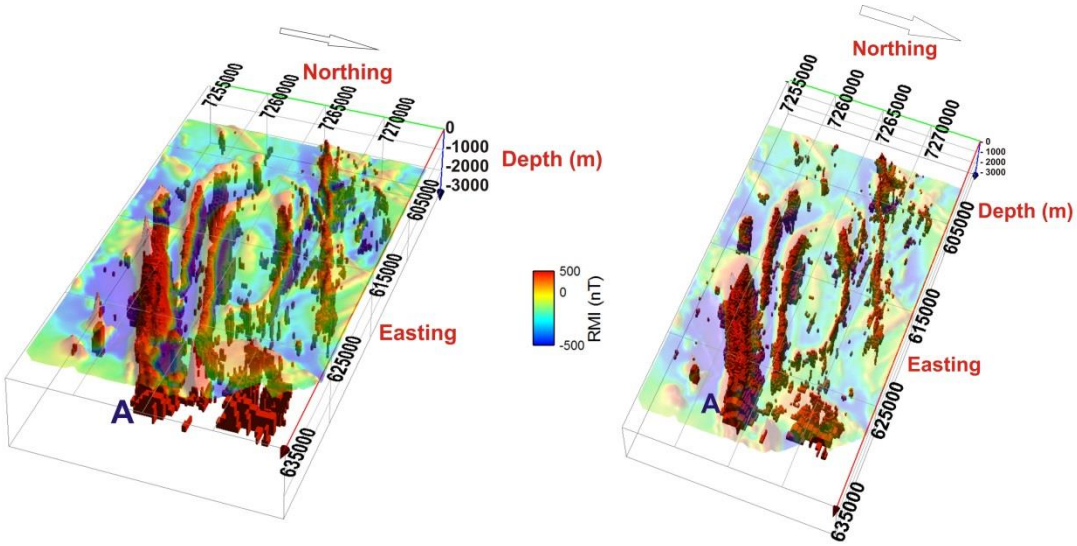

b)

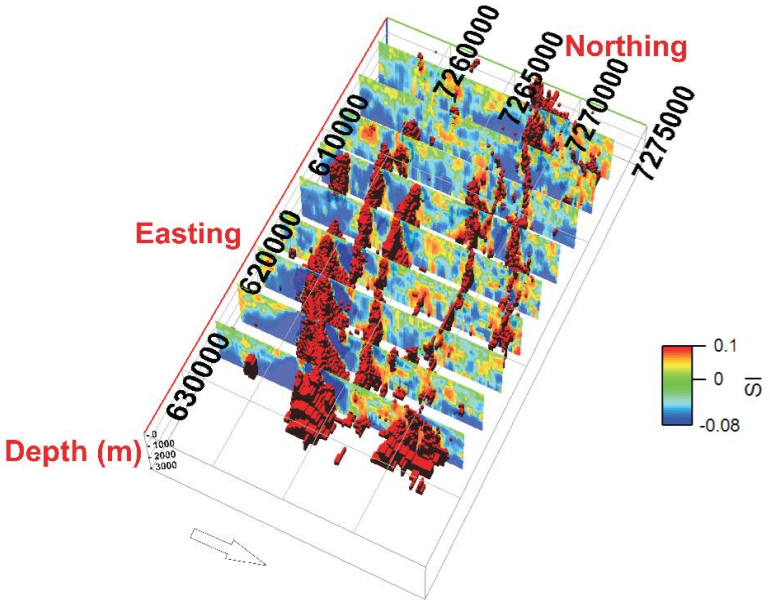

Figure 2.7a Magnetic inversion isolated with a susceptibility range 0.019 to 0.220077 SI displayed below the transparent residual magnetic intensity (RMI) map. Point A marking signal interference within Archean volcanics. **b)** Isolated susceptibility range 0.019 to 0.220077 SI with constrained inversion vertical slices.

From the geophysically constrained inversion, it is evident that incorporating the 2D geophysical reference models into the inversion as constraints helped to force continuity of the strike and dip of magnetic units at depth by minimizing the "smoothed blob" problem. The smooth blob results from the inverse algorithm focussing longer wavelength features at depth with the high susceptibility values spreading out from the main anomaly with increasing depth. Although this replicates the observed signal, the output model shows a body with very minor variations in susceptibility, which obscures any discernible structure (Spicer et al., 2011) and is inconsistent with field knowledge of strong variations in susceptibility in geological samples. With the Three Lakes formation constituting a relatively continuous inner magnetic edge of the synform at surface, the constrained inversion model retains its lateral extent at depth to create the canoe-shaped structure. The unconstrained inversion model drives toward a thicker magnetic unit at depth which is geologically unrealistic (Figure 2.4). After introducing the geophysical constraints where the structure of Three Lakes is constrained to 1000 m depth, the inversion results are truer to geologic knowledge. The susceptibility distribution of the geophysically constrained inversion shows the Three Lake formation dipping almost vertically but slightly toward the centre of the synform with a relatively uniform thickness (Figure 2.7b). The Archean mafic volcanic and diorite units that are associated with the strong aeromagnetic high south of the Ayagaq quartzite did not have any constraints imposed because of signal interference (point A, Figure 2.7a). Both the Three Lakes formation and Five Mile Lakes volcanics could easily be modelled as isolated dipping slabs, but the more complex signal associated with the Archean volcanics and diorite made it impossible to model them using a simple 2D shape approximation. For these reasons, the solution to the Archean volcanic and diorite units approximates a smooth blob. No structure is imposed at depth, driving the shape of the susceptibility distribution toward a wider feature and thus longer wavelength, making it harder to derive deep structural interpretations from the inverse model.

2.6.2 Forward models

As part of the geophysical and geological feed-back process, a series of gravity transects were forward modelled and draped with coincident inverse splices. The shape of the gravity profiles and the inverse results are in general agreement (Figure 2.6). Both show the units of the synform dip near vertically at the edges and flatten out toward the bottom, in agreement with geological interpretations of the structure. Complications arise

when flat-lying strata are encountered. Geophysical anomalies result from lateral discontinuities in the physical properties within rock units. When strata are flat lying, there is no means of positioning the absolute depth to source using only the geophysical data. The parameter controlling the computed depth estimate is the amplitude of the observed gravity anomaly and the density assigned to the source body. But there is a direct trade-off between varying density and depth: increase depth so increase density and vice versa. So the only real external constraint is provided by having physical property (density) measurements on the lithological unit. It is possible to determine maximum and minimum possible depth values by iterating density and depths for the appropriate layers and setting some threshold on the variation of the RMS fit; a signal sensitivity analysis. However, our intent is to derive broad geometrical form for the Amer syncline we are not developing exact geological models.

In the case of the magnetics inversion, the model objective function of the UBC-GIF algorithm includes a parameter which controls the distribution of source bodies with depth. This serves to concentrate all high frequency anomalies near the surface, and as such, would be unable to image a thin horizontal magnetic unit at depth. This complicates the interpretation as there is no control of these units at depth. Interpretations must therefore rely on existing geologic knowledge and the forward modelling results. Alternatively, the units may extend to considerable depth and, as such may not be visible on the inversion which only extends 3000 m below surface. The flat-bottomed canoe-shaped F2 synform is favoured by the gravity modeling and by outcrop observations of flat-bottomed minor F2 folds together with the rectilinear shapes of the east and west ends of the synform.

2.7 Conclusions

High resolution aeromagnetic data for a poorly exposed portion of the northeast Amer Belt were inverted to generate a flat-bottomed canoe shaped synform in agreement with forward models of high resolution strategic gravity transects. These are in agreement with recent regional and local detailed geological knowledge of the structure. The "smooth blob" effect was avoided by generating geophysical reference models that guided body shape and dip with increasing depth. This is evident when compared to the unconstrained inversion of the aeromagnetic data. The inversion results developed here demonstrate that the preferred solution is a compromise between the global and individual solutions, with full use of constraints to drive a more accurate solution. For remote areas

of poor outcrop requiring solutions, knowledge of structural style and boundary conditions in the surrounding area can be applied to high quality geophysical data for developing geophysical models of important lithostructural markers. These marker models constrain 2D inversions which in turn guide the full 3D inversion to produce an integrated model consistent with known structural style in the region as well as providing guidance for further geological interpretations in other poorly exposed areas. We stress the need for data integration from as many knowledge sources as possible, even when there is access to ample high resolution geophysical data but geological information in the immediate problem area is scant. More merit can be placed on forward and inversion geophysical models where there is agreement among all data sets and coherency of structural style.

2.8 Acknowledgements

Field work and aeromagnetic data collection reported in this study were financially supported by the Northern Uranium for Canada Project under NRCan's Geomapping for Energy and Minerals Program led by CWJ. Student support for V. Tschirhart was provided by a NSERC Doctoral fellowship. Laboratory and computer costs were supported by a NSERC Discovery Grant to WAM. P. Tschirhart provided meaningful discussions about the modeling, Dr. J. Patterson (Concordia University) co-supervised geological mapping, and D. MacIsaac (University of New Brunswick) contributed to geological knowledge of the synform area.

2.9 References

Calhoun, L.J., White, J.C., MacIsaac, D., Jefferson, C.W., and Patterson, J.G. 2011. Basement-cover relationships in the Paleoproterozoic Amer Group, Nunavut (Abstract). Geological Association of Canada – Mineralogical Association of Canada – Society of Economic Geologists Joint Annual Meeting, Ottawa, May 2011, Abstract volume.

Cella, F. and Fedi, M. 2012. Inversion of potential field data using structural index as weighting function rate decay. *Geophysical Prospecting*, 60, 313-336.

Chamberlain, K.R., Schmitt, A.K., Swapp, S.M., Harrison, T.M., Swoboda-Colberg, N., Bleeker, W., Peterson, T.D., Jefferson, C.W., Khudoley, A.K. 2010. In-situ U-Pb (IN_SIMS) micro-baddeleyite dating of mafic rocks: Method with examples. *Precambrian Research*, 183, 379-387.

Davidson, G.I., and Gandhi, S.S. 1989. Unconformity-related U-Au mineralization in the Middle Proterozoic Thelon sandstone, Boomerang Lake prospect, Northwest Territories, Canada. *Economic Geology*, 84, 143-157.

Davis, W.J., Gall, Q., Jefferson, C.W., and Rainbird, R.H. 2011. Fluorapatite in the Paleoproterozoic Thelon Basin: structural-stratigraphic context, in-situ ion microprobe U-Pb ages, and fluid flow history. *Geological Society of America Bulletin*, 123, 1056-1073.

Gandhi, S.S. 1989. Geology and uranium potential of the Thelon Basin and adjacent basement in comparison with the Athabasca Basin region. Uranium Resources and Geology of North America: International Atomic Energy Agency, Tech. Doc. 500, 411-428.

Gandhi,S.S., Prasad, N., Chorlton, L.B., Richer, C.,and Lentz, D. 2010. Canadian Uranium-Thorium Deposits and Occurrences. Geological Survey of Canada, digital update of Open File Report 551, web access at http://apps1.gdr.nrcan.gc.ca/gsc_minerals/index.phtml.

Harvey, B.J.A., Coyle, M., Buckle, J.L., Carson, J.M., and Hefford, S.W. 2011. Geophysical Series, airborne geophysical survey of the northeast Thelon Basin, Nunavut, NTS 66 A, parts of 66 B, 66 C, 66 G and 66 H. Geological Survey of Canada, Open File 6510, 2011; 10 sheets, scale 1:250,000; doi:10.4095/288204.

Jefferson, C.W., Thomas, D., Quirt, D., Mwenifumbo, C. J., and Brisbin, D. 2007. Empirical models for Canadian unconformity associated uranium deposits: *in* Milkereit, B., (ed.), Proceedings of Exploration 07: Fifth Decennial International Conference on Mineral Exploration, 741-769.

Knox, A.M. 1980. The geology and uranium mineralization of the Aphebian Amer group, south-west of Amer Lake, District of Keewatin, N.W.T. Unpublished M.Sc. thesis, University of Calgary.

Li,,Y., and Oldenburg, D.W. 1996. 3-D inversion of magnetic data. *Geophysics*, 61, 394-408.

McMartin, I., and Dredge, L.A. 2005. History of ice flow in the Schultz Lake and Wager Bay areas, Kivalliq region, Nunavut. *Geological Survey of Canada, Current Research*, B2: 1-12. Available from http://www.gsc.nrcan.gc.ca/bookstore.

McMartin, I., Dredge, L.A., and Aylesworth, J.M. 2008. Surficial Geology, Schultz Lake South. Geological Survey of Canada, Map 2120A, Scale 1:100,000.

Miller, A. R., and LeCheminant, A.N. 1985. Geology and uranium metallogeny of Proterozoic supracrustal successions, central District of Keewatin, N.W.T. with comparisons to northern Saskatchewan*: in* Sibbald, T.I. and Petruk, W., (eds.), Geology of Uranium Deposits: Canadian Institute of Mining and Metallurgy Special Volume 32, 167-185.

Patterson, J.G. 1986. The Amer Belt: remnant of an Aphebian foreland fold and thrust belt. *Canadian Journal of Earth Sciences*, 23, 2012-2023.

Pehrsson, S., Jefferson, C.W., Peterson, T., Scott, J., Chorlton, L.B., Hillary, B. 2010. Basement to the Thelon Basin, Nunavut – Revisited; Special Session on Geological Environments hosting Uranium Deposits, GeoCanada 2010 - Working with the Earth, Calgary, May 10-14th, 4 p abstract.

Peterson T.D., and Pehrsson, S.J. 2010. Proterozoic (1.85-1.7 Ga) igneous suites of the Western Churchill Province: constraints on tectonic assembly and crust-mantle dynamics. GeoCanada 2010 Abstracts (on-line publication).

Rainbird, R.H., Hadlari, T., Aspler, L.B., Donaldson, J.A., LeCheminant, A.N., and Peterson, T.D. 2003. Sequence stratigraphy and evolution of the Paleoproterozoic intracontinental Baker lake and Thelon Basins, western Churchill Province, Nunavut, Canada. *Precambrian Research*, 125, 21-53.

Rainbird, R.H., Davis, W.J., Pehrsson, S.J., Wodicka, N., Rayner, N., and Skulski, T. 2010. Early Paleoproterozoic supracrustal assemblages of the Rae domain, Nunavut, Canada: Intracratonic basin development during supercontinent break-up and assembly. *Precambrian Research*, 181, 167-186.

Reid, A. 2010. Forgotten truths, myths and sacred cows of potential field geophysics. *SEG Technical Program Expanded Abstracts*, 1198-1201.

Smith, S. 1984. Sedimentology of Amer Group rocks, district of Keewatin, N.W.T. Unpublished B.Sc. thesis, Carleton University.

Spicer, B., Morris, B. and Ugalde, H. 2011. Structure of the Rambler rhyolite, Baie Verte Peninsula, Newfoundland: inversions using UBC-GIF Grav3D and Mag3D. *Journal of Applied Geophysics*, 75, 9-18.

Tella S. 1994. Geology, Amer Lake, 66 H, Deep Rose Lake (66 G), and parts of Pelly Lake (66 F). Geological Survey of Canada Open File, 2969, scale 1: 250 000.

Thomas, R D. 1981. Surficial Geology, Amer Lake, District of Keewatin Geological Survey of Canada, Preliminary Map 9-1981, 1981; 1 sheet, doi:10.4095/109304.

Tschirhart, P. and Morris, W.A. 2011. Grenville age deformation of the Sudbury impact structure; evidence from magnetic modelling of the Sudbury diabase dyke swarm. *Terra Nova* (in press). Doi:10.1111/j.1365-3121.2011.01 056.x.

Tschirhart, V., Morris, W.A. and Oneschuk, D. 2011. Geophysical series, geophysical compilation project, Thelon Basin, Nunavut, NTS 66A, B, and parts of 65N, O, P, 66C, F, G and H. Geological Survey of Canada, Open File 6944, 1 sheet, doi:10.4095/288806.

Williams, N. 2008. Geologically-constrained UBC-GIF gravity and magnetic inversions with examples from the Agnew-Wiluna Greenstone Belt, Western Australia. Ph.D Thesis, University of British Columbia.

Young, G.M. 1979. Geology of the Western Part of the Amer Belt (NTS Sheets 66G1, G2, H5, H6 and parts of G8 and H4), Keewatin; Western Mines Ltd (operator). Mineral Assessment Report 081047, Department of Indian Northern Affairs, Yellowknife, 37 p., 7 maps, 50000 scale.

3. Framework geophysical modelling of granitoid versus supracrustal basement to the northeast Thelon Basin around the Kiggavik uranium camp, Nunavut

Tschirhart, V[1]., Morris, W.A[1]. and Jefferson, C.W[2].

1. *MAGGIC, School of Geography & Earth Sciences, McMaster University, Hamilton, Ontario, Canada L8S 4K1*

2. *Geological Survey of Canada, 601 Booth St., Ottawa, Ontario, Canada K1A 0E8*

Reproduced with permission from Tschirhart, V., Morris, W.A. and Jefferson C.W. 2013. Framework geophysical modelling of granitoid versus supracrustal basement to the northeast Thelon Basin around the Kiggavik uranium camp, Nunavut. Canadian Journal of Earth Science, 50, 667-677.

3.1 Abstract

The northeast Thelon Basin in the Kivalliq region of Nunavut is prospective for uranium deposits. Recently discovered basement-hosted, unconformity-associated prospects west of Kiggavik are restricted to deformed and metamorphosed Neoarchean psammitic enclaves of the Woodburn Lake group within 1.83 Ga Hudson granite and Martell syenite that together comprise the Shultz Lake intrusive complex (SLIC). The depth and geometry of the intrusive complex are relatively unknown as the geological constraints are poor; the drilling is sparse and of shallow depth extent as it was not targeting the basement but shallower multiply faulted and highly altered demagnetized zones. This study aims to constrain the geometry and context of the Shultz Lake intrusive complex with respect to the ore-hosting Neoarchean metasedimentary rocks and intersecting reactivated fault arrays through geophysical modelling of detailed aeromagnetic and gravity data integrated with new geological knowledge. By integrating detailed gravity, aeromagnetic, and structural geology observations measured along a series of transects with a petrophysical rock properties database, it is possible to derive constraints on the depth and thickness (200–300 m) of the SLIC. Quantitative comparison and integration of multiple hypothetical geometries favours a model wherein the SLIC, together with metasedimentary and older basement gneiss, has been structurally emplaced over the Neoarchean metasediments.

3.2 Introduction

The Thelon Basin, straddling the border of Nunavut and the Northwest Territories (Figure 3.1), has long been a frontier exploration region for unconformity-associated uranium deposits based on its similarity to the Athabasca Basin (Miller and LeCheminant 1985). Recent exploration has focused on the northeast Thelon Basin, particularly in and near the Kiggavik camp, an area of unconformity-associated, basement-hosted deposits being developed by AREVA Resources Canada. The deposits are located at hydrothermally altered intersections of reactivated faults cutting structurally intercalated Neoarchean and early Paleoproterozoic supracrustal rocks of the Woodburn Lake and Ketyet River groups, respectively (P. Wollenberg, oral presentation, Nunavut Mining Symposium, 5 April 2011). The supracrustal rocks were intruded by a variety of igneous rocks throughout the study region (Figure 3.1). The most extensive make up the 1.83 Ga Hudson granite and Martell syenite of the composite Shultz Lake intrusive complex (SLIC) that flanks the Kiggavik camp on the west and is represented by a broad

aeromagnetic high with relatively abrupt margins on the east and west (Figure 3.2). Recent discoveries within and west of the SLIC reported by Cameco Corporation are actually hosted by metasedimentary enclaves at otherwise similar hydrothermally altered fault intersections that transect the SLIC along with its supracrustal enclaves (R. Hunter, oral presentation, Nunavut Mining Symposium, 5 April 2011).

The spatial importance of hydrothermally altered intersecting reactivated faults, the 1.75 Ga Nueltin suite of intrusions, and Neoarchean supracrustal assemblages for uranium exploration in the northeast Thelon Basin region was outlined by Jefferson et al. (2011a, 2011b). The recent focus of exploration has been on locating and testing small, intense gravity lows, which are associated with zones of greatest alteration that produced lower-density clays (Miller and LeCheminant 1985). The altered faults and their associated gravity lows are coincident with more extensive hydrothermally hematitized and demagnetized zones that are most evident in rocks with high magnetic susceptibility. In this context, knowledge of the overall shape and depth extent of the highly magnetic SLIC provides an important exploration parameter because a network of intersecting faults is expressed by demagnetized lineaments in the aeromagnetic data (Tschirhart et al., in preparation). Exploratory drilling in the SLIC area to date has been focused along and near the Gerhard fault (Figure 3.1), although numerous additional faults may also be prospective. In this study we present a geophysical investigation of the geometry of the SLIC and provide a modern 2.5-dimensional context for more advanced exploration.

Geophysical modelling has increasingly taken a “black-box” approach within the mining industry through the vigorous application of geophysical inversion software. Although inversions are useful, where unconstrained they may create a void between the interpreter and the geologist as a result of unrealistic and (or) improbable results created by the non-unique nature of the inversion process. In the case of strong near-surface magnetic anomalies and few a priori constraints, as is the case for the SLIC, inversion algorithms will drive solutions toward a thin magnetic slab sitting atop a non-magnetic body (Li and Oldenburg 1996). Inversions are always better at defining the top surface of a source: the lower boundary is only weakly constrained, especially in the absence of physical property constraints. Such solutions do not necessarily represent reality, and as such an alternative modelling method must be considered if we are to realistically test alternative interpretations of the subsurface geology of such areas. By using a forward-

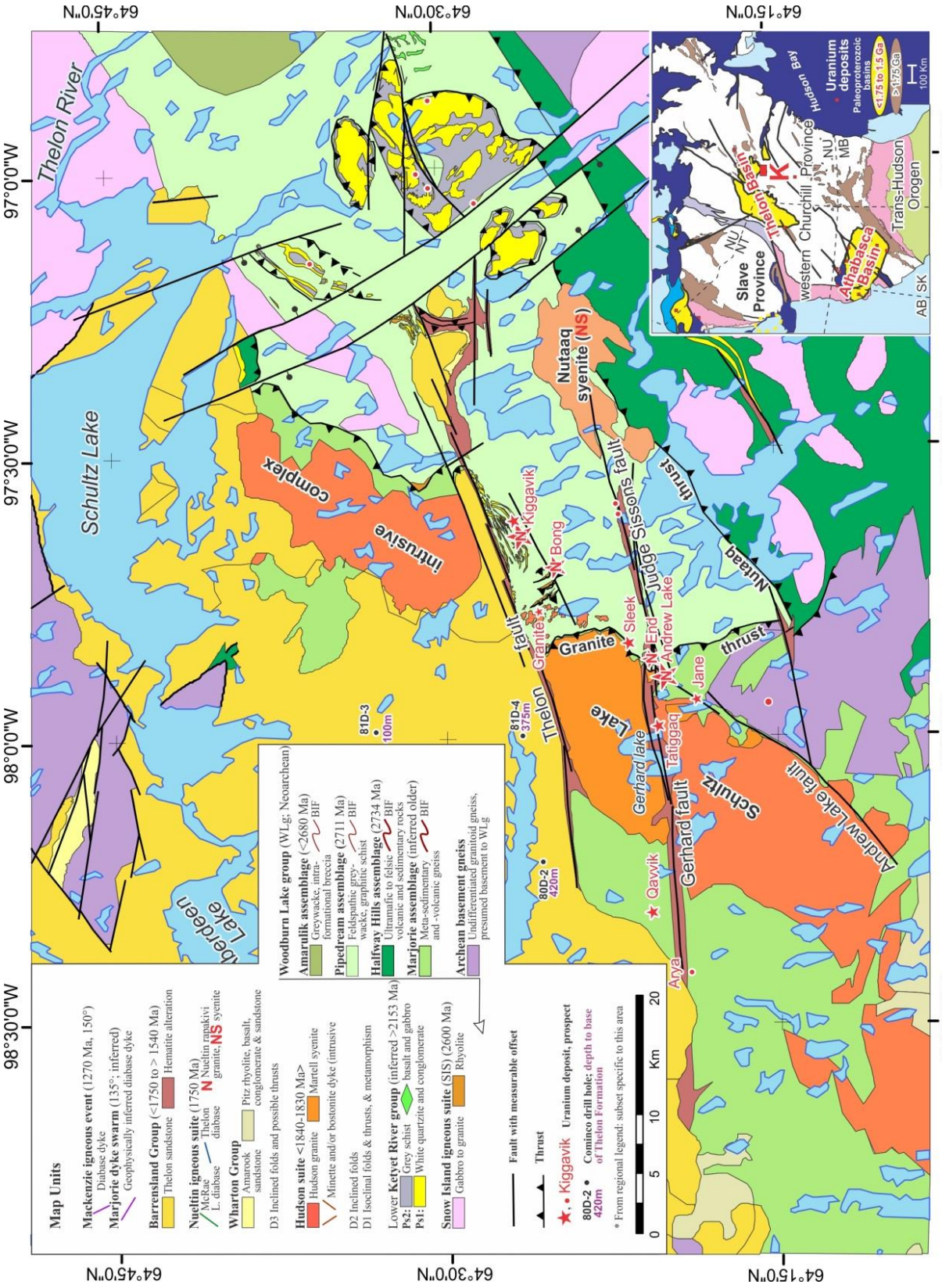
Thelon River
Schultz Lake
Aberdeen Lake
intrusive complex
Nutaaq syenite (NS)
Granite
Kiggavik
Bong
Sleek
End
Andrew Lake
Judge Sissons fault
Nutaaq thrust
thrust
fault
Thelon
Lake
Gerhard lake
Gerhard fault
Schultz
Andrew Lake fault
Tatiggaq
Jane
Qayvik
Arya
81D-3 100m
81D-4 375m
80D-2 420m
Map Units
Mackenzie igneous event (1270 Ma, 150°)
Diabase dyke
Marjorie dyke swarm (135°; inferred)
Geophysically inferred diabase dyke
Barrensland Group (<1750 to > 1540 Ma)
Thelon sandstone
Hematite alteration
Nueltin igneous suite (1750 Ma)
McRae L. diabase
Thelon diabase
Nueltin granite, NS syenite
Wharton Group
Amarook sandstone
Pitz rhyolite, basalt, conglomerate & sandstone
D3 Inclined folds and possible thrusts
Hudson suite <1840-1830 Ma>
Hudson granite
Martell syenite
Minette and/or bostonite dyke (intrusive
D2 Inclined folds
D1 Isoclinal folds & thrusts, & metamorphism
Lower Ketyet River group (inferred >2153 Ma)
Ps2: Grey schist
Ps1: basalt and gabbro
White quartzite and conglomerate
Snow Island igneous suite (SIS) (2600 Ma)
Gabbro to granite
Rhyolite
Woodburn Lake group (WLg; Neoarchean)
Amarulik assemblage (<2680 Ma)
Greywacke, intra-formational breccia
BIF
Pipedream assemblage (2711 Ma)
Feldspathic grey-wacke, graphitic schist
BIF
Halfway Hills assemblage (2734 Ma)
Ultramafic to felsic volcanic and sedimentary rocks
BIF
Marjorie assemblage (inferred older)
Meta-sedimentary and -volcanic gneiss
BIF
Archean basement gneiss
Undifferentiated granitoid gneiss, presumed basement to WLg
Fault with measurable offset
Thrust
Kiggavik Uranium deposit, prospect
80D-2 Cominco drill hole; depth to base of Thelon Formation 420m
* From regional legend: subset specific to this area
0 5 10 20 Km
64°45'0"N
64°30'0"N
64°15'0"N
97°0'0"W
97°30'0"W
98°0'0"W
98°30'0"W
Slave Province
western Churchill Province
Trans-Hudson Orogen
Hudson Bay
Uranium deposits
Paleoproterozoic basins
<1.75 to 1.5 Ga
>1.75 Ga
100 Km
Thelon Basin
Athabasca Basin
NU
NT
MB
AB
SK

Figure 3.1 Geology of the Kiggavik uranium camp (from Jefferson et al., 2012). “K” in the inset map of the northwestern Canadian Shield indicates the location of this camp.

modelling approach, it is possible for the interpreter to modify the geometry of a series of polyhedra with predefined physical properties that describe preconceived geological models until a suitable match can be found between the computed and observed signals. Constraints are introduced to keep the solution geophysically accurate; physical rock property data are integrated with the near-surface geology, and lithostructural field data provide geometrical constraints on the lithologic units. In this type of model approach, the interpreters are then responsible for ultimately deciding the most geologically realistic and geophysically feasible solutions to the observed signals.

During the summer of 2010 a series of coincident gravity and geological transects were measured over the SLIC and adjacent magnetically contrasting supracrustal rocks (Figure 3.2) to test whether the SLIC is a plug (kilometres thick) or a sheet (hundreds of metres thick), and whether its relationship to the laterally adjacent supracrustal rocks is intrusive (laterally tapered) or structural (faulted in one or more ways). Preliminary analysis of synthetic models mimicking the aeromagnetic signature demonstrated that the degree of observed demagnetization along the transecting arrays of steeply dipping reactivated faults could only occur if the SLIC forms a sheet (Tschirhart et al., in preparation). The magnetic anomaly grid over the nearby Snow Island suite (SIS) granitoid batholiths south and east of Judge Sissons Lake (Figure 3.2) does not exhibit the same pattern of intense linear magnetic lows despite being just as riddled with demagnetized faults as the SLIC. It is thought that the much greater depth extent (SIS pluton rather than SLIC sheet) serves to obscure the narrow effects of demagnetization along fault zones.

Forward modelling of joint gravity and aeromagnetic profiles in this paper therefore uses the assumption that the SLIC is a sheet and now tests whether its lateral boundaries are intrusive or structural. The physical rock property database was populated through measuring density and magnetic susceptibility of samples collected in and around the study area from 2006 through 2011. Statistical analysis of data for the lithologic units used in the models helped to discriminate distinct geophysical characteristics of each rock unit (Appendix 3-1). Alternative structural models of the contact between the east side of the SLIC and supracrustal rocks were tested using joint gravity and aeromagnetic forward models. Using the most realistic model, a series of cross sections were generated to exemplify one possible integrated geological–geophysical solution at depth.

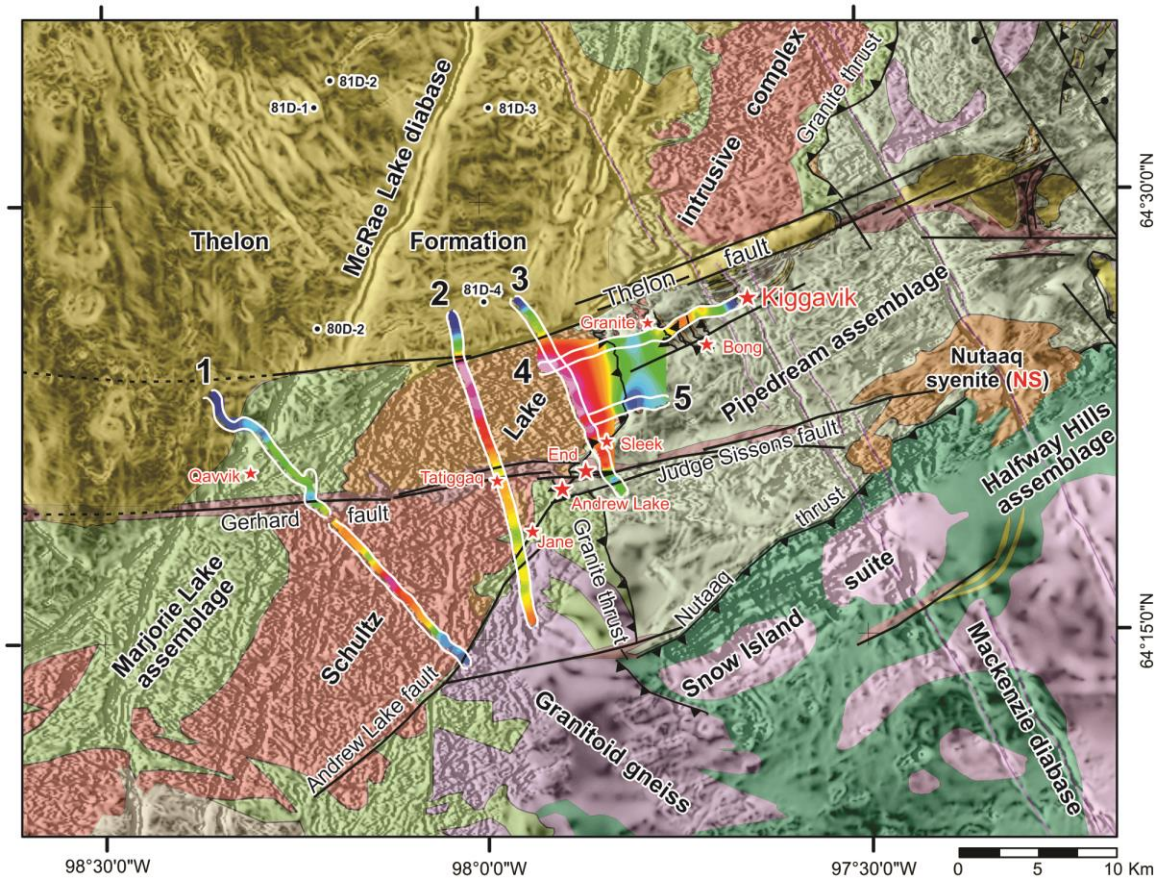

Figure 3.2 Locations of primary gravity lines modelled in this paper (1-5) with respect to transparent geology from the central part of Figure 3.1, draped on a horizontal gradient of total magnetic intensity. The contrasting degrees of resolution of the magnetic data reflect the different flight line spacings of regional verses detailed airborne surveys that were compiled and levelled to make up the base (Tschirhart et al., 2011). The map units, uranium deposits (stars), and faults are as in Figure 3.1.

3.3 Geologic setting

Located in the western Churchill Structural Province (Figure 3.1), the Thelon Basin is a remnant of a somewhat thicker and broader repository that is thought to have covered much more of the Kiggavik map area but is now preserved only to the north and west. The following summary is after geological reports by Davis et al. (2011); Hadlari et al. (2004); Jefferson et al. (2011a, 2011b); Peterson et al. (2010); Rainbird et al. (2003, 2010); Renac et al. (2002), and Zaleski et al. (2000). The Barrensland Group filled the Thelon Basin and represents the upper 1–3 km of the Dubawnt Supergroup, which was deposited after 1.83 Ga as the result of strike-slip extensional faulting during the late stages of, and following, the Trans-Hudson Orogeny. The Dubawnt Supergroup is overall flat lying and unmetamorphosed but in places pervasively altered. It unconformably overlies earlier Paleoproterozoic and Archean basement and consists of three major groups: Baker Lake, Wharton, and Barrensland. The 1.83 Ga Hudson suite granite and Martell syenite components of the SLIC variably intrude the earlier Paleoproterozoic and Archean basement.

As noted in the Introduction, the focus of this study is on the relationship between the SLIC and Woodburn Lake group supracrustal rocks, both of which unconformably underlie the Barrensland andWharton groups. Basement supracrustal rocks host all known significant uranium prospects in this area. The Neoarchean supracrustal rocks are informally referred to as the Woodburn Lake group, which in the map area includes the Marjorie, Halfway Hills, Pipedream, and Amarulik assemblages. These are intruded by 2.6 Ga granitoid rocks of the Snow Island suite and capped by rhyolite inferred to be its extrusive component. The Woodburn Lake group is overlain by and structurally intercalated with early Paleoproterozoic siliciclastic, minor carbonate, and mafic volcanic rocks of the Ketyet River group. The two supracrustal assemblages most closely associated with the SLIC are the Marjorie and Pipedream. The undated Marjorie assemblage is metamorphosed to amphibolite grade and highly deformed, including mafic dykes that are transposed subparallel to compositional layering. It is recrystallized and poorly exposed so that the protolith is uncertain, but graded bedding observed in a few places and the presence of both banded magnetite–chert and garnet–amphibole silicate facies iron formation attest to its metasedimentary origin. The SLIC intruded at mid-crustal levels and enclosed rafts of the Archean Marjorie assemblage and older granitoid gneiss. The assemblage that hosts the Kiggavik deposits is also undated but most closely

resembles thinly bedded feldspathic metagreywacke of the Pipedream assemblage that was dated by Zaleski et al. (2000) as 2711 Ma by U–Pb on zircon from rhyolite. The Pipedream assemblage also includes subordinate banded chert–magnetite and silicate iron formation, as well as felsic metavolcanic rocks, but it is much thinner bedded than the Marjorie assemblage and is of greenschist metamorphic grade with moderately well-preserved primary sedimentary textures and structures, despite multiple deformations.

Generally undeformed, widely distributed mid-crustal intrusions of the 1.83 Ga Hudson granitic suite and Martell syenite are important sheet-like crustal components in the Schultz Lake map area and comprise the SLIC (Peterson et al. 2010). The Hudson granite is interpreted as a product of mid-crustal melting, whereas the contemporaneous ultrapotassic low-silica volcanic rocks of the Christopher Island Suite (CIF) in the Baker Lake Basin reflect mantle melting. Mingling of lamprophyre (minette) magma from the CIF with the Hudson granite sheets is interpreted to have formed the Martell syenite that also is expressed as multiple arrays of bostonite dykes. The bostonite and minette dykes form a compositional spectrum and multiple irregular arrays trending 000°, 045°, and 090°. The SLIC is a continuous belt of mixed Hudson granite and Martell syenite south of the Thelon fault, with predominately Hudson granite south of the Gerhard fault, Martell syenite north of the Gerhard fault, and Hudson granite north of the Thelon fault. The SLIC is contained within and has inclusions of the Archean Marjorie assemblage and older granitoid gneiss. The Pipedream assemblage is also intruded by all components of the Hudson suite as relatively thin (a few to hundreds of metres) sheets, dykes, and, in the Granite Grid deposit area (Figure 3.1), small plugs of granite with pyritic aplite and pegmatite border phases.

High-resolution aeromagnetic data from industry integrated with data newly acquired in 2010 (Tschirhart et al. 2011) highlight the SLIC as a distinct, highly magnetic band crosscut by several arrays of demagnetized faults (Figure 3.2). The most prominent faults are steeply north dipping, are dextral oblique-slip, and trend 080°. These intersect with steeply dipping 015° and 165° cross-faults. Diabase dykes trending 010°–025° and 070°–090° represent the mafic trigger for porphyritic granite of the ca. 1.75 Ga Nueltin suite (Scott et al. 2010; Peterson et al. 2010). These intrusions were contemporaneous with rhyolite and rare basalt of the Pitz Formation (T. Peterson, personal communication, May 2012), plus aeolian to alluvial siliciclastic deposits, all part of the Wharton Group. The Thelon Basin was initiated at an unknown time after 1.75 Ga, bounded by arrays of

faults trending parallel to the dyke sets mentioned earlier as well as several other trends. Major bounding faults include reactivated curvilinear shear zones such as the 060° Turqavik fault and 080° Thelon fault array (Jefferson et al. 2011a, 2011b; Tschirhart et al. 2013). The latter faults, some of which are occupied by the Thelon diabase dyke swarm, have right lateral offsets of up to 20 km, or more, and dip-slip offsets of tens to hundreds of metres, north-side down. The dykes are evident as linear magnetic highs that exceed the amplitude of the SLIC granitoid units. The entire area was extensively glaciated during the last ice age, leaving a variably thick layer of till with drumlins that locally also have an aeromagnetic expression as high-frequency magnetic "pimples".

3.4 Methodology

3.4.1 Data reduction

A series of ground gravity transects were conducted over the SLIC and adjacent packages in July and August 2010 (Figure 3.2). The station spacing along line ranged from 100 to 400 m depending on the lateral distance between previously mapped geologic contacts; a minimum of two stations were occupied over each unit. LaCoste and Romberg model G meters G0074, G0173, and G0790, were tied to the Canadian Gravity Standardization Net through the Baker Lake, Nunavut, gravity base station, with a reading resolution of 0.01 mGal (1 Gal = 1 cm/s^2). The vertical and horizontal locations were calculated by differential global positioning system (GPS) using a ProMark GPS and computed using GNSS Solutions. An elevation accuracy of better than 7 cm was determined for all measurements. The ground gravity data were corrected for latitude, instrument drift, elevation, and the Earth's tides. No terrain corrections were made, as the topography of the area is relatively flat and care was taken to ensure that the station locations were at least 40 m away from steep inclines. The Free Air Correction was the final data rectification. A regional gravity grid consisting of 12–15 km spaced stations was acquired from the Canadian Geoscience Data Repository. Values interpolated from this grid were subtracted from each profile line, to calculate the residual signal, free of the long-wavelength basement components. These data were used in all subsequent modelling.

The aeromagnetic data used in this study area were extracted from a stitched and re-levelled compilation by Tschirhart et al. (2011). Flight lines within the study area are spaced 200 m and gridded to 50 m using minimum curvature (Figure 3.2). For this study

the merged grid was upward continued 5000 m and subtracted from the original grid to produce a residual image accentuating short wavelength near-surface features and removing the long-wavelength background signal that is not under consideration in the modelling. The aeromagnetic profiles used in the forward modelling were sampled from this grid along the ground gravity lines.

3.4.2 Petrophysical analysis

Physical properties were measured on samples from the 2006 through 2011 field seasons (Appendix 3-1). Magnetic susceptibility was measured using a KT-10 meter, and density was calculated using the standard Archimedes' principle submersion approach. The heterogeneous compositions of the major rock units within the study area created a highly variable sample set. As such, the calculated average property values of many of the units are not necessarily representative. The rock properties data were analyzed statistically (Figure 3.3). Histograms illustrate the variations in density and magnetic susceptibility of both igneous (Hudson versus Martell), and metasedimentary (Marjorie versus Pipedream) assemblages.

3.4.3 Geophysical modelling

GM-SYS Solutions software was used to compute the forward models beginning with a set of polyhedra, with the station topography input as the top surface, that were iteratively modified to obtain the best fit between the observed and computed gravity and magnetic signals. The geometry of the polyhedra are based on the known geology, structural measurements, and the petrophysical measurements (magnetic susceptibility, density). As it was possible to adequately model the magnetic data with induced field magnetization controlled by known susceptibility values, remanence was assumed not to be present in the magnetic units. The root mean square (RMS) error was kept <10 nT and <0.5 mGal for magnetics and gravity cases. The area is extensively till covered, but the wide station spacing along the profiles did not permit discrimination of thin (<10 m) till deposits, and, therefore, till was not modelled in the profiles.

3.5 Results and discussion

3.5.1 Petrophysics

Rock properties clearly differ between the SLIC granitoid phases and Woodburn Lake group supracrustal units, so they can be modelled with some certainty; however,

differences within the granitic and supracrustal arrays are subtle. The granitic components of both the Hudson and Nueltin suites are relatively homogenous in density (both with an average density of 2.63 g/cc) and variable in magnetic susceptibility (Appendix 3-1). These can be differentiated from some Martell syenite samples (average density 2.77 g/cc); however, the syenite grades into the granite as a continuum—the syenite and granite are mixed on the outcrop scale and vary in proportion from one part of the SLIC to the next. As a product of mixing between Hudson granite and denser, more mafic lamprophyre dykes, the Martell syenite ranges from feldspathic with a small mafic component (low density, 2.61 g/cc) to mafic with a substantial magnetite content (high density, 2.90 g/cc) (D. Quirt and T. Peterson, personal communications, May 2012). Nevertheless, as a starting point, a density ranging from 2.66 to 2.85 g/cc was used for syenite in the first stage of modelling.

As modelling of the gravity data progressed, the density of the Hudson blocks was held within 0.02 g/cc of the average density, whereas different densities were applied to different blocks of Martell syenite within the 0.29 g/cc range of the seven measured non-altered rock samples to provide best fits to the measured gravity profiles. If the density of the Martell had been held constant (which is geologically incorrect based on the varying mafic to feldspathic components), the depth extent would have had to fluctuate to compensate for the lateral variation in signal amplitude. Such a variable depth extent is also incompatible with the thin (50–400 m) sheet configuration required by the aeromagnetic models (Tschirhart et al., in preparation).

It was more difficult to geophysically differentiate the Pipedream assemblage from the Marjorie assemblage as their average density and magnetic susceptibility values are quite similar. Two opposing hypotheses are under investigation: Marjorie assemblage is a more highly metamorphosed variant of the Pipedream assemblage, or they are two different primary units (Jefferson et al. 2013). The Pipedream assemblage hosts the historic Kiggavik, Bong, Andrew Lake, and End Grid deposits (Figure 3.1), around which historical exploration and geologic mapping were focused. The Marjorie assemblage hosts the newly discovered Tattigaq and Qavvik deposits and the Arya prospect (Figure 3.1). Although fewer Marjorie samples were measured compared with Pipedream (Figures. 3.3c, 3.3d), they are geophysically indistinguishable. For the purposes of modelling, they were tagged as two different units, albeit with similar physical properties.

Altered samples of all rock types were not used for the bulk properties assigned to major blocks in the models but only to characterize the altered fault zones.

With respect to magnetic susceptibility, an initial compilation of each intrusive "unit" as a group over the entire region showed similar broad ranges and average values, making it difficult to differentiate because they were so heterogeneous. Regional intrusive susceptibility values are particularly variable, with multiple peaks based on limited samples, especially in the case of the Martell syenite. This variability suggested to the writers that the geological classification was too generalized, and the data were re-examined spatially. This re-examination demonstrated that, for example, the Nutaaq syenite is geophysically discrete from the SLIC syenite, reinforcing petrologic differences that are also emerging through parallel research (T. Peterson, personal communication, September 2012). It was therefore decided to use only data within the area of Figure 3.1 for each specific map unit in these models. It is these data that were used to generate Figures 3.3a, 3.3b.

Nevertheless, another documented variant is intrinsic to the SLIC: the outcrops and rock properties are heterogeneous because of the intermingled nature of the primary Hudson granite and Martell syenite magmas (D. Quirt, personal communication, May 2012). In particular, that part of the SLIC between the Gerhard and Thelon faults contains a much higher proportion of syenite than the portions to the north and south, and this is evident by its higher susceptibility. To incorporate this intrinsic heterogeneity in the model, the susceptibility of the intrusive bodies was changed laterally from one model block to the next, within the measured range of values, following the same procedures as for density.

The varied rock property data may also be influenced by the measurement method. When using a small-diameter sensor coil (Bartington MS2E) on coarse-grained igneous rocks, it is quite possible to experience localized nugget effects. For each sample we took three measurements on three different faces of the sample. For example, a local coarse magnetite crystal in a mass of feldspar and quartz can result in an inappropriate and artificially high magnetic susceptibility reading (Lee and Morris 2012). Nevertheless, clear and consistent differences in the physical properties are documented between the intrusive versus metasedimentary packages, with the latter having a higher average bulk

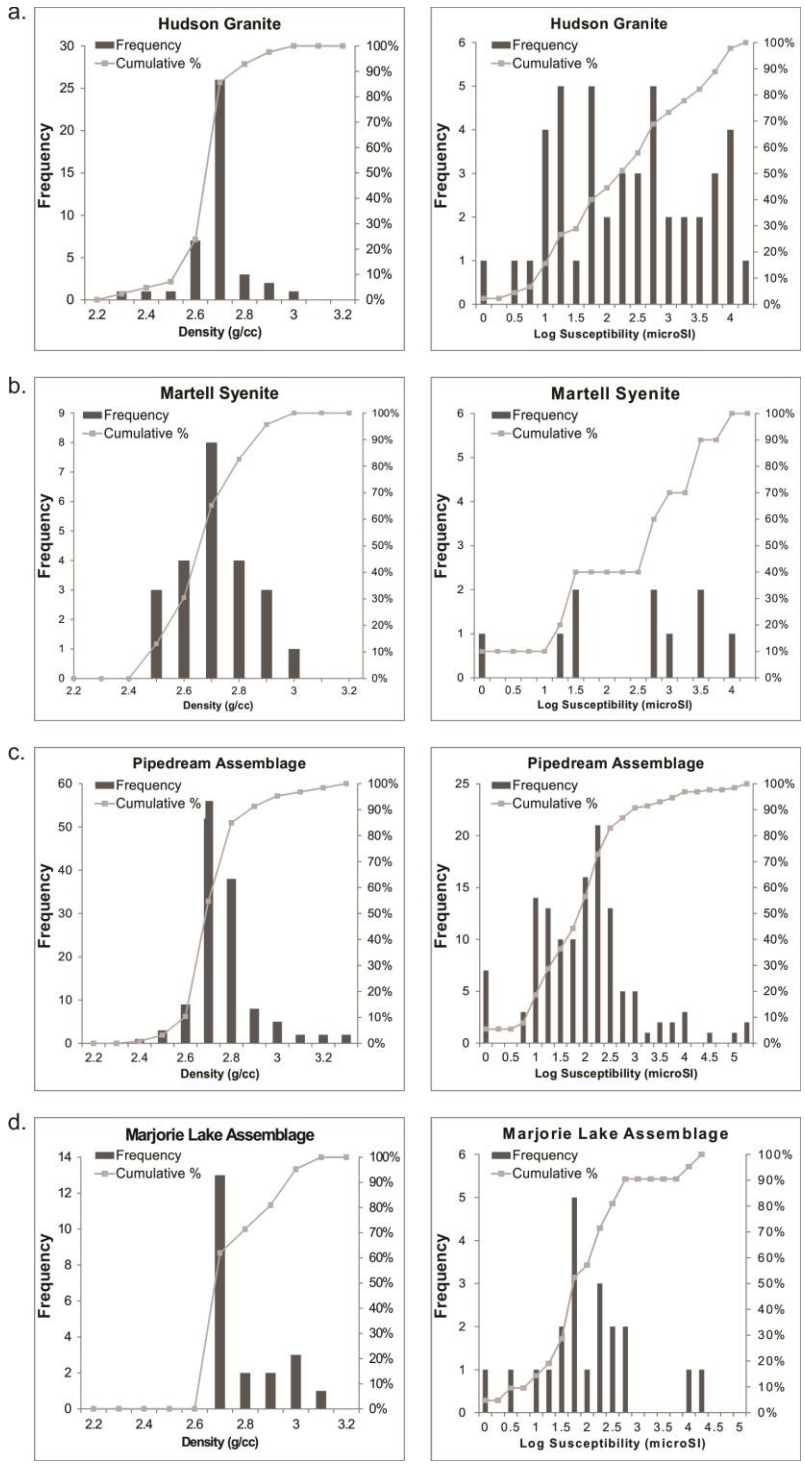

Figure 3.3 Physical property distributions: density and magnetic susceptibility distribution, respectively of **a)** Hudson granite; **b)** Martell syenite; **c)** Pipedream assemblage; **d)** Marjorie assemblage.

density, lesser average magnetic susceptibility, and higher standard deviation (Appendix 3-1).

3.5.2 Structural hypothesis

The SLIC–Pipedream contact is not exposed in outcrop, although it is constrained in some closely spaced outcrops and was intersected in drill core from Andrew Lake, End, and Sleek deposits that were made available to the third author in 2012. Nevertheless the drill intersections are confusing (in some places the contact is sub-horizontal, in others near vertical), so the true structural relationship remains elusive and geophysical modelling provides the only camp-scale 3D method to constrain the bulk geometry. The first step in forward modelling involved testing three possible geometries for the contact, each of which is compatible with the limited geological information: thrust fault, reverse fault, and horst (Figures 3.4a–3.4c). Profile 4 was chosen as the test profile, as it is perpendicular to the contact and extends several kilometres on either side. Although many geometries are possible within the specified error tolerance, particularly in the calculated gravity (there is less variation in the density values and a smoother observed curve), subtleties in the shape of the calculated magnetic response favour a thrust fault, where Archean Marjorie and older granitoid gneiss structurally overlie the 2.711 Ga Pipedream assemblage that hosts thinner (in the order of a few to several tens of metres) and more localized Hudson–Martell sheets and small plugs on the order of 0.5–2 km in diameter (Figure 3.4a). In the reverse fault model (Figure 3.4b), older Marjorie and Archean granitoid bodies are east of Pipedream, with younger Hudson and (or) Martell laccoliths cut off by the fault. Owing to the dip required by a reverse fault, the magnetic response associated with the Martell decays sharply toward the west, in disagreement with the observed aeromagnetic profile that decays gradually to the east. With the laccoliths cut off by the fault plane, the low-density Hudson granites do not contribute to the calculated signal where they are required to lower the response to get a better curve match. The horst – normal fault model (Figure 3.4c) offers the second most favourable match in terms of the RMS error between the observed versus computed aeromagnetic profiles. However, in this model the contact creates an abrupt magnetic contrast, with the SLIC not being thrust over the Marjorie but, rather, emplaced as a sheet that was later cut off by the fault. The horst model cannot replicate the long wavelength of the SLIC curve that is observed within the thrust model. It also implies that the Archean basement extends to depth. Because the Archean basement has lower density than Marjorie and

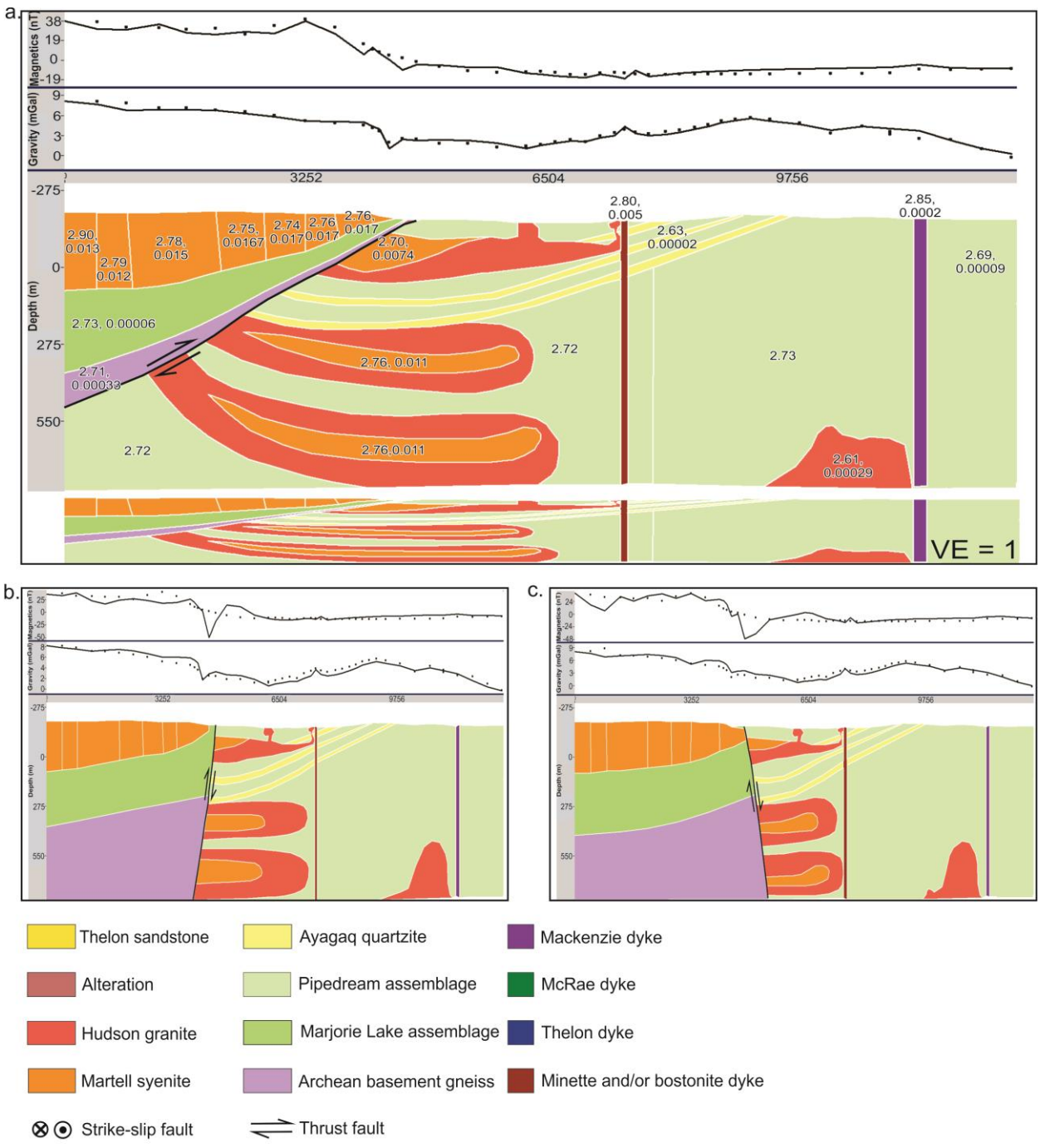
a.
Magnetics (nT)
Gravity (mGal)
3252
6504
9756
Depth (m)
2.90, 0.013
2.79 0.012
2.78, 0.015
2.75, 0.0167
2.74 0.017
2.76 0.017
2.76, 0.017
2.70, 0.0074
2.80, 0.005
2.63, 0.00002
2.85, 0.0002
2.69, 0.00009
2.73, 0.00006
2.71, 0.00033
2.76, 0.011
2.72
2.73
2.72
2.76,0.011
2.61, 0.00029
VE = 1
b.
c.
Thelon sandstone
Alteration
Hudson granite
Martell syenite
Strike-slip fault
Ayagaq quartzite
Pipedream assemblage
Marjorie Lake assemblage
Archean basement gneiss
Thrust fault
Mackenzie dyke
McRae dyke
Thelon dyke
Minette and/or bostonite dyke

Figure 3.4 Alternative hypothetical models to explain the gravity and aeromagnetic data for profile 4. Top panels: dotted line, observed magnetic field; solid line, calculated magnetic field. Middle panel: dotted line, observed gravity anomaly; solid line, calculated gravity anomaly. Second-from-bottom panel: forward model with numbers in polygons denoting density and magnetic susceptibility, respectively; unit colours are consistent with Figure 3.1; **a)** Thrust fault model. The profile is shown at true scale in an extra bottom panel. Values for profile a. apply to b and c; **b)** Reverse fault model; **c)** Normal fault model. VE, vertical exaggeration. 1 Gal = 1 cm/s^2.

Pipedream, the calculated gravity curve is shifted below the observed. The very low-density, high-magnetic-susceptibility Hudson laccoliths are still needed to lower the calculated gravity and smooth the calculated magnetic curve immediately to the west of the fault plane. The thrust model, though not perfect, most accurately replicates the observed response. It is in agreement with the limited geological mapping of sparse outcrop and drill core analysis by the third author indicating thrust or reverse faults in the vicinity of the Andrew Lake, End Grid, and Sleek deposits (Figure 3.1) but outside of the transect area, and with the subtle but abrupt topographic drop at the eastern edge of the complex (Jefferson et al. 2013).

3.5.3 Forward models

Given that the thrust fault model best explains the geophysical data for profile 4 and that the SLIC forms a thin (200–300 m) sheet within the Marjorie assemblage structurally overlying the Pipedream assemblage, five geophysical cross sections were created using the thrust model to explain coincident gravity and aeromagnetic profiles (Figure 3.5). In all profiles across the SLIC the depth of Martell and (or) Hudson is held relatively constant at 40–70 m below sea level, in agreement with the thin sheet hypothesis. Profiles 4 and 5 depict the thrust fault hypothesis with mixed Hudson–Martell laccoliths at depth within the structurally underlying Pipedream assemblage. Mapped "lava lamp" Hudson granite plugs are here interpreted as derived from these laccoliths. Geophysically these plugs satisfy the observed gravity lows immediately adjacent to the contact between SLIC–Marjorie and Pipedream. Pipedream metagreywacke is much denser than Hudson granite and by itself would not create a low of this magnitude. The SLIC is modelled as a 200–300 m thick sheet overlying denser Marjorie assemblage. Industry drilling and mapping is consistent with this order of thickness and has documented metasedimentary enclaves, but, owing to limited vertical and lateral extents, they were not incorporated in the models except for profile 2, which transects the drilled Tattigaq deposit hosted by one such enclave (R. Hunter, oral presentation, Nunavut Mining Symposium, 5 April 2011). The resolution of the gravity profiles is insufficient to discriminate such enclaves without other evidence such as detailed mapping and (or) drilling. Profile 3 intersects profiles 4 and 5. For geological correctness, at each intersection point the profiles were iteratively adjusted to ensure agreement in the depth extent of the geologic units and their physical properties.

The en echelon Gerhard and Judge Sissons faults are marked by a major east–west zone of mapped alteration. Where crossed by profiles 1 and 2 the Gerhard fault is marked by strong demagnetization and a moderate but abrupt gravity low. The Judge Sissons fault is at the south end of profile 3 and corresponds to a sharper and more substantive gravity low. These and other fault zones were subject to both greater paleoweathering and hydrothermal alteration relative to unfractured rock on either side. These processes dramatically reduced the bulk density within the alteration zones because of removal of quartz and changes in mineralogy to hematite and clay (Appendix 3-1). Profile 3 also extends northwesterly across the Thelon fault into the northeast Thelon Basin, where the data record a significant and sustained drop in gravity and the magnetic field. The drop in gravity is equivalent to a thick mass of low-density Thelon sedimentary rock overlying denser supracrustal basement rocks inferred to be Marjorie assemblage. Discussions with industry representatives at a workshop in St. John's, Newfoundland, (May 2012) support the interpretation of the aeromagnetic low primarily as a result of demagnetization of the basement supracrustal rocks accompanying faulting, perhaps further decreased by the blanket effect of the overlying thick Thelon sandstone (thickness from Davis et al. 2011).

The Hudson–Martell laccolith in the southern portions of profiles 1 and 2 is modelled at depth to fit the gravity low adjacent to the Andrew Lake fault that juxtaposes SLIC with granitoid gneiss and Marjorie assemblage (Figure 3.2). The distinct reticulate magnetic texture associated with the SLIC can be seen to continue (somewhat attenuated) to the east of the Andrew Lake fault, below the Marjorie and granitoid gneiss. This feature is represented in profiles 1 and 2, which model the sheet as thickening to the east before abrupt termination, and the same concept is used for profiles 3 through 5 (Figures 3.4, 3.5). The major faults were identified on the both aeromagnetic and gravity profiles as abrupt lows, which correspond to the alteration discussed above. The dip of the hypothesized granite thrust was modelled as being very shallow based on the shape of the observed aeromagnetic anomaly. Geological mapping indicates that foliated and compositional layering in the region are generally shallow, and structural discontinuities logged by the third author in drill core at Andrew Lake, End, and Sleek deposits are generally also shallow. On the other hand, the demagnetized faults are all steeply dipping.

Sparse drill-hole data in the Thelon Basin flanking the Thelon fault provided constraints on the depth to the unconformity at the base of the Thelon Formation (Table 3.1; Figure 3.2). The unconformity was intersected at 205 m (local depth) at the north end

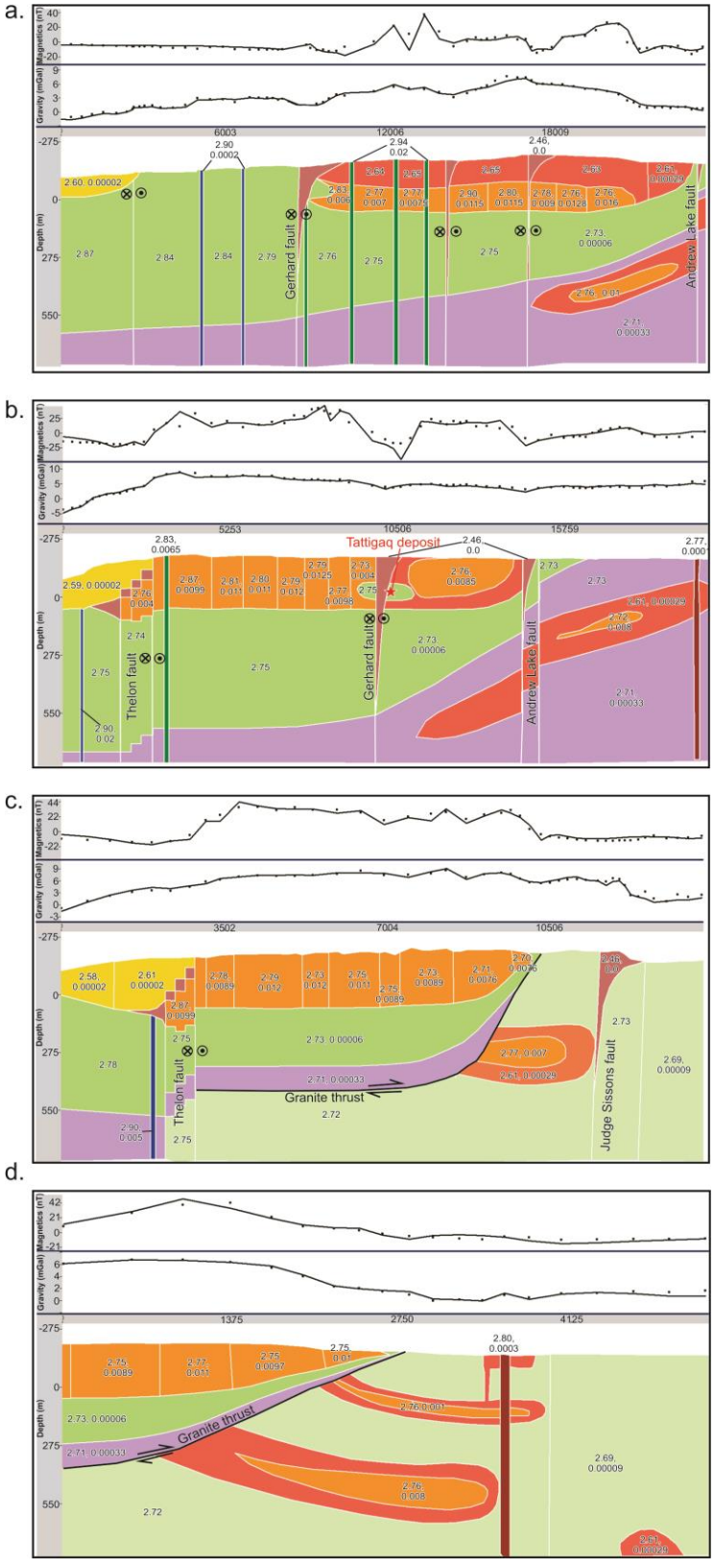
a.
Magnetics (nT)
Gravity (mGal)
Depth (m)
Gerhard fault
Andrew Lake fault
b.
Tattigaq deposit
Thelon fault
Gerhard fault
Andrew Lake fault
c.
Thelon fault
Granite thrust
Judge Sissons fault
d.
Granite thrust

Figure 3.5 Models for profiles 1 **(a)**, 2 **b),** 3 **(c)** and 5 **(d)**, applying the thrust hypothesis as tested in Figure 3.4. Number in polygons denote density and magnetic susceptibility, respectively; unit colours are consistent with Figure 3.1. Values for profile 1 apply to other profiles, except where otherwise specified.

of profile 3 (Cominco drill hole 81 D-4, Davis et al. 2011) and at 420 m within 2 km of the Thelon fault, halfway between profiles 1 and 2 (Cominco drill hole 80 D-2, Davis et al. 2011). The depth to the unconformity shallows northwesterly to about 100 m some 12 km north of profile 3 (Cominco drill hole 81 D-3, Davis et al. 2011) and to about 200 m some 16 km north of profiles 1 and 2 (Cominco drill hole 81 D-2, Davis et al. 2011). These depths work well for the modelling of profiles 2 and 3 (thick Thelon Formation close to the Thelon fault, thinning away toward the northwest). In the case of profile 1, the gravity low is not as pronounced as on the profiles to the north, requiring only a few to 20 m of Thelon Formation over denser Marjorie assemblage. This result is also consistent with geological and aeromagnetic data that indicate the Thelon fault is north of the end of profile 1. The geophysical data suggest there is very little to no alteration at this contact.

3.6 Conclusions

A series of synthetic models support the hypothesis that the SLIC intrudes and encloses enclaves of old Archean Marjorie assemblage supracrustal gneiss and granitoid gneiss. This package was thrust over the Neoarchean Pipedream supracrustal assemblage that is intruded at depth by an eastern extension of the SLIC. Petrophysically, the intrusive SLIC is distinct from the metasedimentary packages in being considerably less dense and more magnetic, placing a high degree of reliability on the modelling. The modelling that requires a relatively thin sheet of granitoid intrusion, as opposed to a deep pluton, is consistent with available drill core and outcrop data. The physical property distribution of the intermixed Martell syenite and Hudson granite required for the models is consistent with strong lateral variability in their densities and magnetic susceptibilities as measured in representative samples and as observed in limited outcrop and drill core. Given a previous analysis of demagnetization along faults, and the gravity constraints, the SLIC was modelled as a series of slabs on the order of 200–300 m thick. Corroborations between gravity and magnetic profiles using the measured physical properties are well within the RMS error tolerance for all of the profiles, re-affirming the validity of the cross sections. The model provides a semi-quantitative conceptual 3D geometric framework for the SLIC and adjacent rock masses, to a depth and spatial extent exceeding that of drilling to date. Aspects of this proposed model could be tested by further drilling; by incorporating high-resolution airborne gravity and electromagnetic data, as well as very

DDH	Company	Latitude	Long.	Precision*	Collar Elev.**	Un-conf.	Units	Notes
80D-2	Cominco	-98.21061	64.42809	50	200	420	metres	
81D-1	Cominco	-98.22462	64.56065	50	110	~157	metres	fault inferred between this and 81D-2
81D-2	Cominco	-98.20348	64.57709	50	120	205	metres	
81D-3	Cominco	-97.9841	64.56363	50	200	100	metres	
81D-4	Cominco	-97.98182	64.44849	50	100	375	metres	

* Locations obtained in Arc GIS from geo-registered unpublished Cominco map

** Collar elevations estimated visually from topographic map

Table 3.1 Drill-hole data for the Thelon Formation on the north side of the Thelon fault.

high-resolution ground geophysical data; and by expanding the gravity transects to the north side of the Thelon fault.

3.7 Acknowledgements

This project is part of the northeast Thelon compilation activity of the GEM Uranium project (Geomapping for Energy and Minerals Program) delivered by the Geological Survey of Canada (GSC). The high-resolution geophysical data were acquired through a Letter of Agreement involving nine companies, the GSC, and McMaster University, whereby GSC acquired new geophysics to fill priority gaps in the data. In the study area of this paper the key industry partners were AREVA Resources Canada, Cameco Corporation, Bayswater Uranium, Forum Uranium, and Nunavut Tunngavik Inc. Financial support to V. Tschirhart was provided by a Natural Sciences and Engineering Research Council (NSERC) Doctoral fellowship. Laboratory and computer costs at McMaster University were supported by a NSERC Discovery Grant to W.A.M. P. Tschirhart and C. Stieber ably assisted in field data collection. Geological ideas and data were shared by P. Wollenberg, J. Scott, T. Riegler, S. Pehrsson, T. Peterson, B. McEwan, T. LeCheminant, R. Hunter, and K. Bethune. Logistical support by Ookpik Aviation was contracted through Polar Continental Shelf Project. P. Keating provided much-appreciated guidance and critical comment.

3.8 References

Davis, W.J., Gall, Q, Jefferson, C.W., and Rainbird, R.H. 2011. Diagenetic fluorapatite in the Paleoproterozoic Thelon Basin: structural-stratigraphic context, in situ ion microprobe U-Pb ages and fluid flow history. *Bulletin of the Geological Society of America*, 123, 1056-1073.

Hadlari, T., Rainbird, R.H., and Pehrsson, S.J. 2004. Geology, Schultz Lake Nunavut. Geological Survey of Canada Open File 1939, scale 1:250 000. doi: 10.4095/215673.

Jefferson, C.W., Chorlton, L.B., Pehrsson, S.J., Peterson, T., Wollenberg, P., Scott, J., Tschirhart, V., McEwan, B., Bethune, K., Calhoun, L., White, J.C., Leblon, B., LaRocque, A., Shelat, Y., Lentz, D., Patterson, J., Riegler, T., Skulski, T., Robinson, S., Paulen, R., McClenaghan, B., Layton-Matthews, D., MacIsaac, D., Riemer, W., Stieber, C. and Tschirhart, P. 2011a. Northeast Thelon Region: Geomapping for Uranium in Nunavut. Geological Survey of Canada, Open File 6962. doi:10.4095/289037.

Jefferson, C.W., Pehrsson, S., Peterson, T., Chorlton, L., Davis, W., Keating, P., Gandhi, S., Fortin, R., Buckle, J., Miles, W., Rainbird, R., LeCheminant, A., Tschirhart, V., Tschirhart, P., Morris, W., Scott, J., Cousens, B., McEwan, B., Bethune, K., Riemer, W., Calhoun, L., White, J., MacIsaac, D., Leblon, B., Lentz, D., LaRocque, A., Shelat, Y., Patterson, J., Enright, A., Stieber, C., Riegler, T. 2011b. Northeast Thelon region geoscience framework - new maps and data for uranium in Nunavut. Geological Survey of Canada, Open File 6949. doi:10.4095/288791.

Jefferson, C.W., Pehrsson, S., Peterson, T., Wollenberg, P., Tschirhart, V., Riegler, T., McEwan, B., Tschirhart, P., Scott, J., Chorlton, L., Davis, W., Bethune, K., Riemer, W., Patterson, J., Morris, W.A., Anand, A., and Stieber, C. 2012. Bedrock geology of the western Marjorie-Tehek supracrustal belt and Northeast Thelon Basin margin in parts of NTS 66A and 66B, Nunavut; Geological Survey of Canada, Open File 7241 (in press).

Lee, M. D., and Morris, W.A. 2012. Comparison of magnetic susceptibility meters using rock samples from the Wopmay orogen, Northwest Territories, Canada. Current Research. Geological Survey of Canada, Open File (in press).

Li, Y. and Oldenburg, D. 1996. 3-D inversion of magnetic data. *Geophysics*, 61, 394-408.

Miller, A.R. and LeCheminant, A.N. 1985. Geology and uranium metallogeny of Proterozoic supracrustal successions, central District of Keewatin, N.W.T. with comparisons to northern Saskatchewan: *in* Sibbald, T.I.I. and Petruk, W., (eds.), Geology of uranium deposits, Canadian Institute of Mining and Metallurgy, Special Vol., 167-185.

Peterson, T., Pehrsson, S., Jefferson, C., Scott, J., and Rainbird, R. 2010. The Dubawnt Supergroup, Canada: a LIP with a LISP. December 2010 LIP of the month [online]. Available from http://www.largeigneousprovinces.org/LOM.html, [accessed 18 September 2012].

Rainbird, R.H., Hadlari, T., Aspler, L.B., Donaldson, J.A., LeCheminant, A.N. and Peterson, T.D. 2003. Sequence stratigraphy and evolution of the Paleoproterozoic intracontinental Baker Lake and Thelon basins, western Churchill Province, Nunavut, Canada. *Precambrian Research*, 125, 21–53.

Rainbird, R.H., Davis, W.J., Pehrsson, S.J., Wodicka, N., Rayner, N., and Skulski, T. 2010. Early Paleoproterozoic supracrustal assemblages of the Rae domain, Nunavut, Canada: Intracratonic basin development during supercontinent break-up and assembly. *Precambrian Research*, 181, 167-186.

Renac, C., Kyser, T.K., Durocher, K., Dreaver, G., O'Connor, T. 2002. Comparison of diagenetic fluids in the Proterozoic Thelon and Athabasca Basins, Canada: implications for protracted fluid histories in stable intracratonic basins. *Canadian Journal of Earth Science*, 39, 113-132.

Scott, J., Peterson, T.D., Jefferson, C.W., Cousens, B. 2010. Proterozoic (1.85-1.7 Ga) granitoid rocks and uranium in the Baker Lake – Thelon Basin region, Nunavut. *In* GeoCanada 2010 Extended Abstracts, Calgary, AB, 4 pp.

Tschirhart, V., Morris, W.A. and Oneschuk, D. 2011. Geophysical series, geophysical compilation project, Thelon Basin, Nunavut, NTS 66A, B, and parts of 65N, O, P, 66C, F, G and H. Geological Survey of Canada, Open File 6944. doi:10.4095/288806.

Tschirhart, V., Morris, W.A., Jefferson, C.W. 2012a. Faults affecting northeast Thelon Basin: improved basement constraints from source edge processing of aeromagnetic data: *in* Potter, E., Quirt, D., and Jefferson, C.W., (eds.), Uranium in Canada: Geological Environments and Exploration Developments, Special Issue of Exploration and Mining Geology (CIM), (in press).

Tschirhart, V., Morris, W.A., Jefferson, C.W. and Keating, P. 2012b. Geophysical modeling of faults transecting the Schultz Lake intrusive complex, basement to the northeast Thelon Basin. Current Research. Geological Survey of Canada, Open File (in press).

Zaleski, E., Pehrsson, S., Duke, N., Davis, W.J., L'Heureux, R., Greiner, E., Kerswill, J.A. 2000. Quartzite sequences and their relationships, Woodburn Lake group, western Churchill Province, Nunavut, Current Research, Geological Survey of Canada, Paper 2000-C7.

3.9 Appendix 3-1

Major map unit	Unit map code	Map unit geological description	Avg Susc	Avg Susc (log10)	Min	Max	St. Dev	Avg. Density	Range	St. Dev	n
Mackenzie Event	Mck-dy	Diabase dyke, 1270 Ma, 150° swarm	0.030280	0.030280	n/a	n/a	n/a	3.04	n/a	n/a	1
	Mck-dy-clay		0.000034	0.000300	n/a	n/a	n/a	2.52	n/a	n/a	1
Thelon Formation	Th2-cg	Quartz pebbly feldspathic quartzarenite	0.000018	0.000004	0.000000	0.00004	0.00002	2.59	2.42-2.68	0.11765	4
	Th1-slt	Red hematitic siltstone	0.000007	0.000002	0.000000	0.00001	0.00001	2.58	2.49-2.69	0.08477	4
	Th1-ss	Pink feldspathic quartzarenite	0.000008	0.000000	0.000000	0.00001	0.00002	2.48	2.21-2.62	0.14666	12
	Th1-cg-sil	Polymict conglomerate interlayered with sandstone and siltstone	0.000003	0.000001	0.000000	0.00001	0.00000	2.62	2.59-2.64	0.02327	5
	Th1-cg	Polymict conglomerate with quartzose, commonly silicified feldspathic quartzarenite matrix	0.000034	0.000021	0.000004	0.00014	0.00004	2.64	2.56-2.85	0.06953	18
Nueltin suite	Nlt-gr	Sanidine porphyritic (rapakivi) granite	0.002047	0.000234	0.000000	0.01234	0.00324	2.63	2.58-2.71	0.03500	27
	Thl-dy	Thelon diabase dyke (050° to 080° swarm cuts McR-dy)	0.027399	0.025958	0.025897	0.02602	0.00009	2.92	2.75-2.98	0.16486	2
	McR-dy	McRae Lake diabase dyke (010° to 025° swarm)	n/s	n/s	n/s	n/s	n/s	n/s	n/s	n/s	n/s
Wharton Group	Ptz-rhy	Pitz Formation rhyolite, mixed rhyolite-basalt and local basalt (extrusive part of Nueltin suite, in Wharton Group)	Not included in gravity modelling								
	Wh-Ak	Amarook Formation (basal Wharton Group) polymict conglomerate and aeolian quartzarenite	Not included in gravity modelling								
Hudson suite	Bstn-dy	Bostonite (syenite) dyke	0.000880	0.000254	0.000013	0.00256	0.00099	2.65	2.58-2.71	0.04183	11
	Mntt-dy	Minette (lamprophyre) dyke	0.000172	0.000099	0.000010	0.00051	0.00020	2.71	2.62-2.77	0.04913	6
	Mrt-sy (SLIC)	Martell syenite (Hudson granite mingled with minette)	0.002003	0.000762	0.000000	0.01436	0.00243	2.77	2.71-2.92	0.10669	7
	Mrt-sy-clay	Clay altered Martell syenite	0.000022	0.000022	0.000020	0.00002	0.00000	2.50	2.47-2.53	0.04708	2
	Hds-gr	Hudson granite: equigranular, includes minor pegmatite and aplite	0.001785	0.000290	0.000007	0.01264	0.00301	2.63	2.55-2.80	0.07668	38
	Hds-gr-clay	Clay altered Hudson granite	0.000004	0.000003	0.000001	0.00001	0.00000	2.42	2.28-2.62	0.14014	4
	Hds-peg	Pegmatite dykes cutting Pipedream Assemblage and part of Hudson plutons	0.000103	0.000052	0.000014	0.00019	0.00013	2.60	2.57-2.63	0.04677	2
Ketyet R. group	Ayg-qz	Quartzarenite with local conglomerate at base and top	0.000066	0.000013	0.000000	0.00051	0.000126	2.68	2.53-2.91	0.0763	19
Snow Island Suite	Snw-rhy	Quartz-feldspar porphyritic rhyolite	Not included in gravity modelling								
	Snw-gr	Intrusion, undivided gabbro to mainly quartz monzonite, locally porphyritic	Not included in gravity modelling								
Pipedream assemblage of Woodburn Lake group	Ppd-BIF	Iron formation: banded chert magnetite and garnet-amphibole-magnetite	0.030897	0.002414	0.000046	0.16461	0.05529	3.04	2.74-3.39	0.22143	12
	Ppd-clay	Intensely clay altered supracrustal rock of uncertain parentage	0.000004	0.000004	n/a	n/a	n/a	2.31	n/a	n/a	1
	Ppd-fv	Felsic metavolcanic rocks: tuff, lapilli tuff, tuffaceous argillite: samples measured are from outside study area	0.000055	0.000034	0.000006	0.00018	0.00006	2.70	2.57-2.80	0.06046	11
	Ppd-gw	Thin bedded feldspathic metagreywacke with graded bedding and schistose partings	0.000532	0.000094	0.000000	0.00855	0.00156	2.70	2.54-2.91	0.06757	79
	Ppd-gw-clay	Partially clay altered Ppd-gw preserves primary and metamorphic textures	0.000018	0.000013	0.000006	0.00004	0.00002	2.49	2.44-2.57	0.05101	5
	Ppd-gw-hem	Intensely hematite altered Ppd-gw preserves primary & metamorphic textures	0.000015	0.000011	0.000005	0.00003	0.00001	2.65	2.64-2.67	0.02624	2
	Ppd-mv	Amphibolite with hornfels appearance adjacent to Mackenzie dyke	0.000245	0.000244	0.000036	0.00027	0.00012	2.95	2.94-2.96	0.06187	2
	Ppd-md	Metapelite, thin bedded to laminated, in places graphitic and strong conductor; interbedded with Ppd-gw in places.	0.000055	0.000029	0.000008	0.00014	0.00007	2.75	2.68-2.86	0.09460	3
	Ppd-qz	Neoarchean brownish white quartzite (not present in Kiggavik study area)	0.000009	0.000004	0.000000	0.00006	0.00002	2.65	2.59-2.70	0.03475	13

Marjorie	Ml-BIF	Iron formation: banded magnetite-chert with high magnetic susceptibility enclosed in garnet-amphibolite schist (silicate facies iron formation)	0.000046	0.000045	0.000036	0.00006	0.00001	2.95	2.84-3.05	0.14781	2
	Ml-gw	Metagreywacke: thick graded beds highly recrystallized and transposed parallel to lenticular foliation; commonly described as metasedimentary gneiss (includes minor undivided ML-fv and ML-mv)	0.000131	0.000062	0.000001	0.00039	0.00012	2.69	2.62-2.92	0.08338	10
	Ml-gw-hem	Intensely hematite altered ML-gw preserves primary and metamorphic textures	0.000012	0.000007	0.000037	0.00022	0.00001	2.65	2.63-2.68	0.03158	3
	Ml-fv	Felsic metavolcanic rocks: aphanitic to saccharoidal rhyolite (minor component)	0.004344	0.002919	0.000362	0.01008	0.00493	2.79	2.66-3.00	0.14855	4
	Ml-mv	Amphibolite interpreted as mafic metavolcanic or highly transposed metagabbro dyke (minor component)	0.000033	0.000033	0.000030	0.000036	n/a	2.90	2.84-2.97	n/a	2
Gneissic	A-gtoid	?meso-Archean granitoid gneiss (generally tonalitic) with biotitic metasedimentary and amphibolitic enclaves	0.001117	0.000327	0.000015	0.00646	0.00205	2.71	2.62-2.80	0.04944	12
basement	A-gtoid-clay	Clay altered A-gtoid preserves metamorphic textures	0.000005	0.000005	n/a	n/a	n/a	2.52	n/a	n/a	1

4. Faults affecting the northeast Thelon Basin: improved constraints from source edge processing of aeromagnetic data

Tschirhart, V[1]., Morris, W.A[1]. and Jefferson, C.W[2].

1. *MAGGIC, School of Geography & Earth Sciences, McMaster University, Hamilton, Ontario, Canada L8S 4K1*

2. *Geological Survey of Canada, 601 Booth St., Ottawa, Ontario, Canada K1A 0E8*

Reproduced with permission from Tschirhart, V., Morris, W.A. and Jefferson, C.W. 2013. Faults affecting the northeast Thelon Basin: improved constraints from source edge processing of aeromagnetic data: *in* Potter, E., Quirt, D. and Jefferson, C.W. (eds.), Uranium in Canada: Geological Environments and Exploration Developments; Volume 21, *Special Issue of Exploration and Mining Geology (CIM).*

4.1 Abstract

A new method for mapping faults within basement rocks underlying the Thelon Formation and glacial overburden was developed and tested in the Aberdeen Sub-basin. This method utilizes newly acquired aeromagnetic data, the Blakely algorithm for defining magnetic source edges, a calculated dip-direction map, a digital elevation model (DEM) derived from the Canadian Digital Elevation Database, and the positions of identified, inferred and newly mapped faults that are within and adjacent to this sub-basin. Combining these data revealed three age groups of faults. One group is seen only on the DEM; these faults are young brittle structures that have no effect on the sub-Thelon basement unconformity, and are not visible on the dip direction map. A second group is evident on the dip direction map but not the DEM; these faults are old basement structures that did not propagate upward through the Thelon Formation. The third group is expressed on both the DEM and dip direction map; these faults are also old structures that propagated upward during and/or after deposition of the Thelon Formation. The latter group of faults may be of greatest interest for uranium exploration, with reactivation increasing their potential to serve as conduits to transport uranium-rich fluids and focus deposition at or near the unconformity surface. This methodology has promise for comprehensive mapping of basin faults and tracking the tectonic development of the whole Thelon Basin through time.

4.2 Introduction

Exploration for unconformity-associated uranium deposits is focused by identifying intersecting high-angle reactivated faults at the basement-sandstone contact (Jefferson et al., 2007). The importance of defining fault loci and determining fault displacement history as critical aspects of exploration for uranium is highlighted by Babu (2007). Analysis of geophysical data from frontier basins can help elucidate: a) the depth to the basement-sandstone contact, b) the loci of pre-existing basement structures, and c) which faults have been reactivated.

The Paleoproterozoic Thelon Basin is a frontier basin with known unconformity-associated uranium deposits (Miller and LeCheminant, 1985; Davidson and Gandhi, 1989) but relatively little exploration. The Thelon Basin is very remote, straddling the border between Nunavut and Northwest Territories in the interior of the Churchill Province (Rainbird et al., 2003). This study is focused on the Aberdeen Sub-basin (Figure 4.1) as part of a larger multidisciplinary project under the Geomapping for Energy and

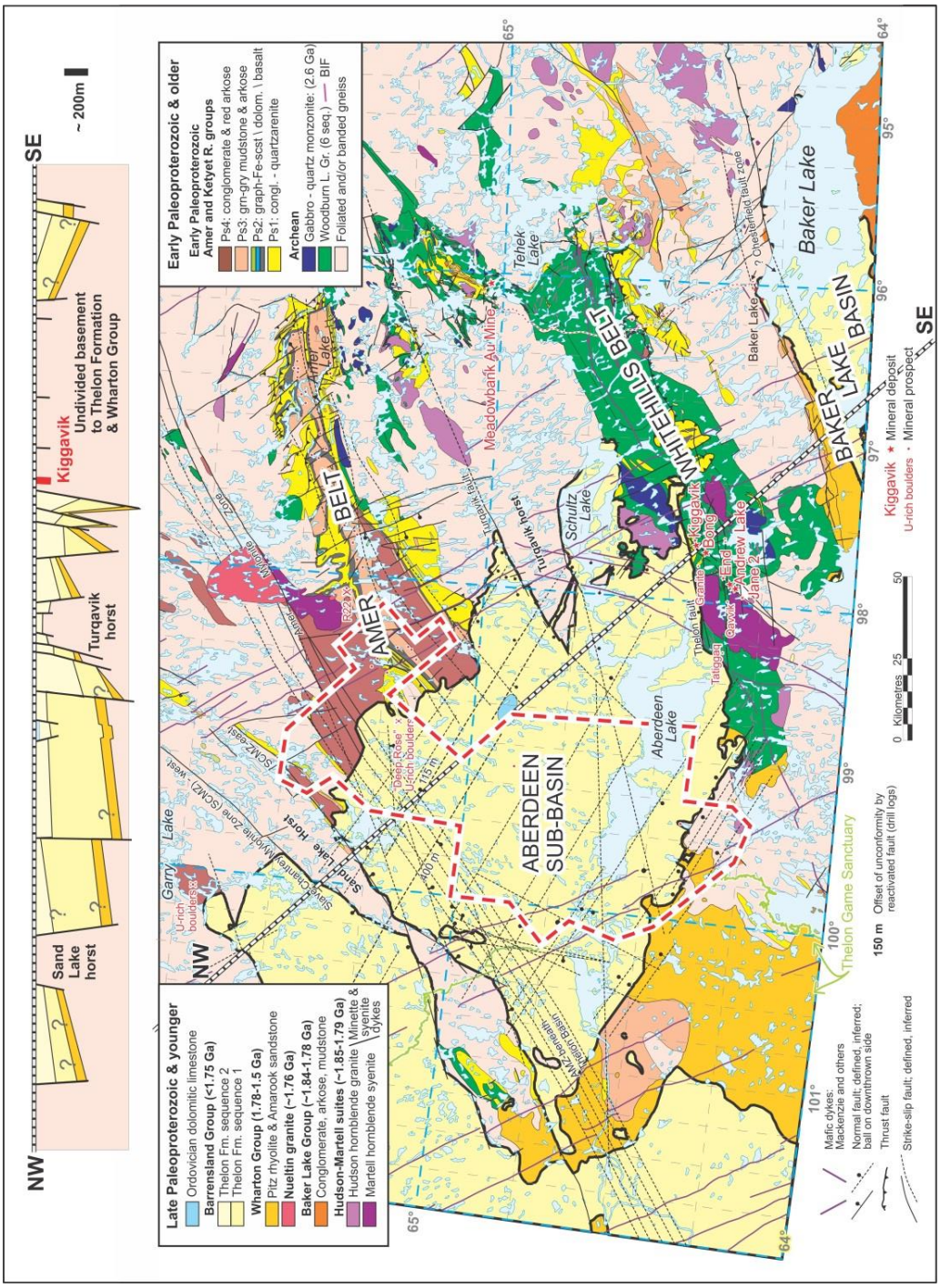
NW
SE
~ 200m
Sand Lake horst
Turqavik horst
Kiggavik
Undivided basement to Thelon Formation & Wharton Group
Late Paleoproterozoic & younger
Ordovician dolomitic limestone
Barrensland Group (<1.75 Ga)
Thelon Fm. sequence 2
Thelon Fm. sequence 1
Wharton Group (1.78-1.5 Ga)
Pitz rhyolite & Amarook sandstone
Nueltin granite (~1.76 Ga)
Baker Lake Group (~1.84-1.78 Ga)
Conglomerate, arkose, mudstone
Hudson-Martell suites (~1.85-1.79 Ga)
Hudson hornblende granite \ Mineite & syenite \ Martell hornblende syenite
Early Paleoproterozoic & older
Early Paleoproterozoic
Amer and Ketyet R. groups
Ps4: conglomerate & red arkose
Ps3: grn-gry mudstone & arkose
Ps2: graph-Fe-scst \ dolom. \ basalt
Ps1: congl. - quartzarenite
Archean
Gabbro - quartz monzonite; (2.6 Ga)
Woodburn L. Gr. (6 seq.)
BIF
Foliated and/or banded gneiss
AMER BELT
WHITEHILLS BELT
ABERDEEN SUB-BASIN
BAKER LAKE BASIN
Baker Lake
Aberdeen Lake
Schultz Lake
Tehek Lake
Meadowbank Au Mine
Kiggavik
Andrew Lake
Thelon Game Sanctuary
Mafic dykes: Mackenzie and others
Normal fault; defined, inferred; ball on downthrown side
Thrust fault
Strike-slip fault; defined, inferred
150 m Offset of unconformity by reactivated fault (drill logs)
0 Kilometres 25 50
Kiggavik ★ Mineral deposit
U-rich boulders • Mineral prospect

Figure 4.1 Geological map, simplified from the Arc GIS geodatabase of the Uranium - Northern Canada Project [http://www.nrcan.gc.ca/earth-sciences/about/current-program/geomapping/energy/6693], showing the location of the study area (dashed red line) in the Aberdeen Sub-basin, with respect to the Amer and Whitehills belts, a number of uranium deposits, and the approximate position of a vertically exaggerated, NW-SE cross-section (top). The heavy black line marks the contact of the Barrensland Group.

Minerals Program, which is aimed at delineating the geology and structure in order to help understand the potential for unconformity-associated uranium deposits around and beneath the northeastern Thelon Basin (Jefferson et al., 2011). In the Aberdeen Sub-basin the unconformity is located at depths as great as 1000 m, based on integration of existing seismic reflection data, regional geological knowledge, and 2-D forward modelling of regional-scale gravity and aeromagnetic data (Tschirhart et al., 2011a).

Faults have been identified within the Aberdeen Sub-basin through visual analysis of linear features on a DEM (Digital Elevation Model of topographic data), satellite imagery, air photographs, and total magnetic intensity (TMI) maps, in concert with traditional geological field work. This visual approach to mapping basement faults is limited in many ways: 1) there is bias toward near-surface structures; 2) thick sandstone cover attenuates the response of magnetic units at depth; and 3) lineaments in glaciated terrain may be unrelated to faults. Ground truthing of lineaments to confirm that they are really faults is limited to a few summer months and is costly in this remote area. Another method is clearly needed to identify and discriminate basement faults that may have offset the unconformity but are not necessarily reflected in the surface topography, or do not have an obvious magnetic expression.

In this paper, we test a new fault-identification utility that is based on a grid of approximated source edge dip directions calculated from the total field horizontal gradient (TF-hgm) and the tilt horizontal gradient (TDX) aeromagnetic data, using the Blakely algorithm (Blakely and Simpson, 1986). These data are a subset of newly acquired aeromagnetic data over the central part of the Aberdeen Sub-basin in the northeast Thelon region (Harvey et al., 2011; Tschirhart et al., 2011a). We use the resulting dip direction map to identify possible new faults and to test known faults that were interpreted from air photographs, DEMs, and field mapping by Jefferson et al. (2011). An analysis of the DEM and dip-direction grids yields relative ages of the faults, providing useful information for uranium exploration by identifying reactivated faults within the basin.

4.3 Geologic setting

The Thelon Basin is filled by the late Paleoproterozoic Barrensland Group, which developed in an intracratonic setting, is relatively undeformed (Rainbird et al., 2003). It covers approximately 85,000 km2 of the Rae Craton in the western Churchill Province,

stretching across Northwest Territories and Nunavut. Dominantly fluviatile siliciclastic strata (sequences 1 and 2, Figure 4.1) of the Thelon Formation record an initial basin configuration close to, but locally larger than, its present shape. This fault-bound sedimentary basin, which is topped by minor Ordovician ultrapotassic mafic lava and dolomite, records a 200 million year depositional and diagenetic-hydrothermal history and is cut by reactivated basement faults (Chamberlain et al., 2010; Davis et al., 2011). The Barrensland Group unconformably overlies the Wharton and Baker Lake groups. Collectively, these three groups constitute the 1.83–1.5 Ga Dubawnt Supergroup (Rainbird et al., 2003; Peterson et al., 2010). The Dubawnt Supergroup unconformably overlies >2.2– 1.9 Ga epicontinental strata of the Amer and Ketyet groups (Rainbird et al., 2010), 2.7–2.6 Ga Archean supracrustal rocks that contain magnetic marker units, and older Archean gneisses to the east and south of the study area (Figure 4.1), all of which were multiply deformed and structurally intercalated before ca. 1.83 Ga (Pehrsson et al., submitted). The late- to post-tectonic Hudson granite (1.83 Ga) intruded mid-crustal Archean gneiss and supracrustal rocks, while adjacent fault-controlled troughs were filled with conglomeratic red beds and volcanic rocks of the Baker Lake Group (Rainbird et al., 2003; Peterson et al., 2010). The early Paleoproterozoic Amer and Ketyet groups are structurally intercalated with Archean supracrustal rocks of the Woodburn Lake Group (Figure 4.1) in two extremely complex fold-and-thrust belts, the Amer Belt and the Whitehills Belt, respectively, that are exposed beside and plunge beneath, the Aberdeen Sub-basin. The Amer Belt stretches across a 100 km strike length from east of Amer Lake southwest toward the northern part of the study area. The Whitehills Belt extends from the vicinity of the Meadowbank Au Mine, through the Kiggavik cluster of uranium deposits, toward Aberdeen Lake in the southern part of the study area. The correlative Amer and Ketyet groups include strongly magnetic marker units that can be traced below cover rocks of the Thelon Formation as linear highs (Figure 4.2). Northwest-trending en echelon linear magnetic highs are visible on the map (Figure 4.2), which represent the MacKenzie diabase dike swarm that transected the area at ca. 1127 Ma (LeCheminant and Heaman, 1989), The entire area was extensively glaciated during the last ice age, leaving a variably thick cover of till, sand and gravel forming a variety of complex landforms, mainly with north-northwest and east-west orientations (McMartin and Dredge, 2005).

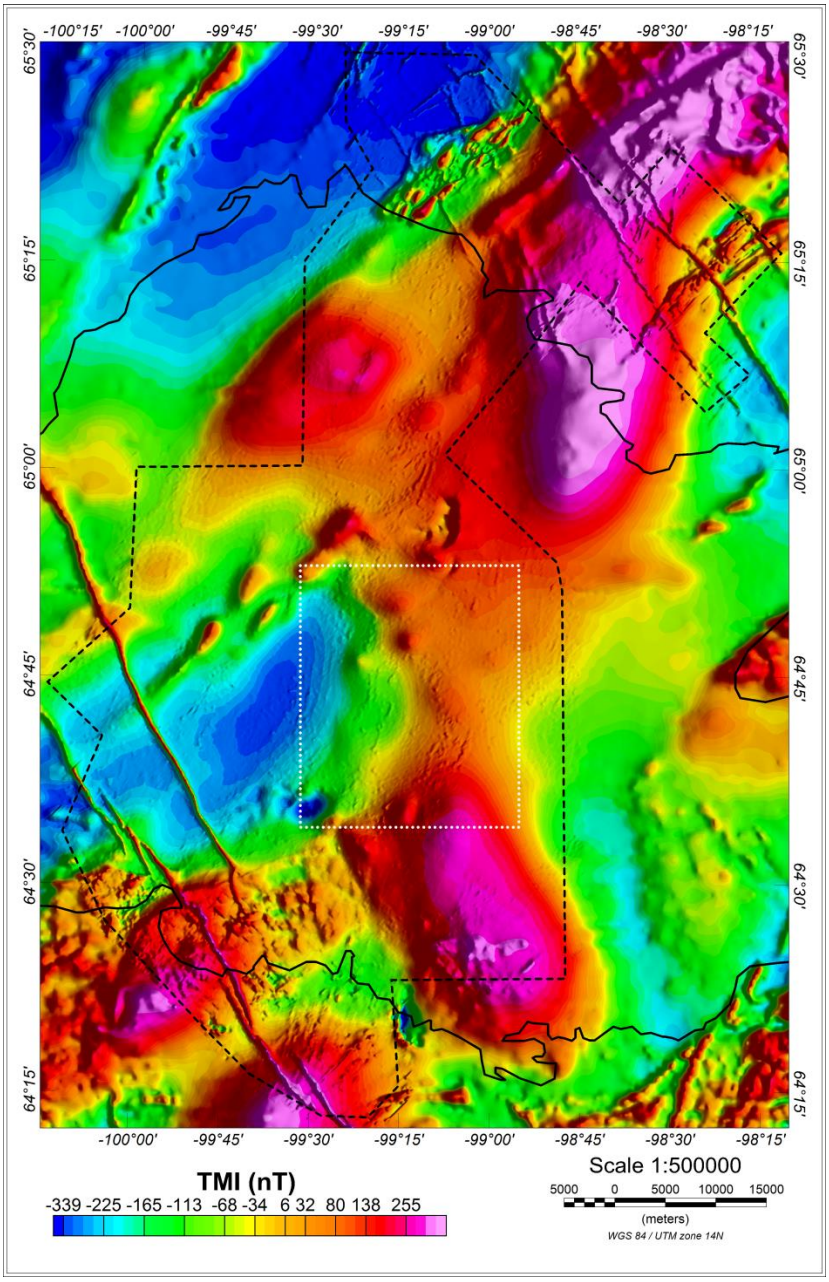

Figure 4.2 Total magnetic intensity (TMI) map of the study area (dashed black line). The outline of the Aberdeen Sub-basin (solid black line) is also shown along with a rectangular area (white dotted line), where glacial overburden produces a stippled pattern in the TMI map.

Rock Type	Number of Samples	Mean Susceptibility (cgs x 10^-6)
Woodburn Group Metasediments	29	49.2
Woodburn Group Gneiss	6	156.5
Amer Group	51	1.7
Nueltin Granite	13	26.4
Hudson Granite	2	3.4
Thelon Formation Sedimentary Cover	26	3.5

Table 4.1

Physical-property measurements were done on archived samples collected within and around the Aberdeen Sub-basin, which represent most of the aforementioned units (Table 4.1). These measurements are consistent with the magnetic expressions of units in the TMI image (Figure 4.2). The majority of the anomalies in the TMI map reflect signatures associated with basement units, such as the Woodburn Lake Group, Neoarchean gabbro (2.6 Ga; Hadlari et al., 2004), and Hudson-Martell granitoid plutons (ca. 1.85–1.79 Ga) that are evident as near-circular magnetic highs (here termed "layer three"). The Thelon Formation itself is relatively non-magnetic.

4.4 Aeromagnetic theory and fault detection

In an aeromagnetic survey, the signal at each observation point represents the sum of the contributions from all magnetic sources within a given distance of the sensor. The scalar magnitude of this observation is then a result of the variable distance to, and the magnetic properties of, the various source body contributions. In the study area, there are essentially three layers (surfaces) that contribute to the total magnetic signal. The uppermost layer (layer 1) comprises glacial overburden, along with topographic elements such as lakes and swamps, which serve to mask the underlying bedrock contacts and structure. Magnetically, surficial materials (overburden) generally cause short wavelength, low-amplitude dampening of signals from bedrock. In some instances, narrow and elongate, positive magnetic anomalies are associated with glacial overburden; but they generally can be linked to erosional or constructional ice-flow features (Gay, 2004). The second layer (layer 2) is the flat-lying, sedimentary rocks of the Thelon Formation, which unconformably overlie plutonic and metamorphic basement rocks (layer 3). The sedimentary cover sequence generally has weak magnetic properties and contributes little to the overall magnetic response. Iron-rich strata may be locally present but, being flat-lying, they generally do not produce discrete magnetic anomalies; therefore, layer 2 is essentially magnetically transparent (Thomas and McHardy, 2007). Layer 3 is magnetically heterogeneous because it comprises a variety of deformed and metamorphosed rocks, including iron formation and plutons. Mapping faults using aeromagnetic data is based on the identification of sharp contrasts in magnetic anomaly patterns, and the displacement of continuous marker horizons.

Determining the timing of faulting is of critical significance for uranium exploration in the northeast Thelon Basin. Previously mapped faults (Figure 4.1) were identified through lineament analysis of topographic data, geologic mapping, and abrupt

offset of anomalies in the TMI map (Jefferson et al., 2011). Faults within the basement (layer 3) may terminate at the unconformity with the Thelon Formation (layer 2), or if reactivated, they may extend upward into layer 2, causing displacement of the unconformity, or may even continue upward to surface. The majority of these faults are shown to have cross cut both layers. Facies changes and diagenesis indicate that some of these faults were active and/or reactivated before, during, and after deposition of the Thelon Formation (Davis et al., 2011). In some cases, reactivated steep faults may terminate upward by refraction into sub-horizontal bedding planes (e.g., Tourigny et al., 2007). Where a fault is terminated within the sedimentary cover, it has little or no surficial expression. Thick glacial overburden can also obscure the surficial expression of through-going, reactivated faults, especially where the till has a dominant ice-transport direction. If there is no magnetic contrast between adjacent rock units, it is impossible to detect faults on a TMI map. Even where moderate magnetic contrasts exist between units, the resulting magnetic expression may be suppressed by cover rocks and the fault may not be detected at surface because of loss of the high-frequency signal. However, the expression of basement magnetic units at surface can be enhanced using edge detection techniques.

4.5 Source edge detection theory

Edge detection techniques have been used extensively by geophysicists for providing useful information regarding geological structures and geometry of magnetic source bodies. A magnetic source edge defines the contact between two laterally adjacent bodies that have magnetic susceptibility contrasts. An edge represents a physical property boundary that can be of stratigraphic, intrusive, or tectonic origin. Source edge techniques use mathematical equations to calculate inflection points in the potential field data, which enhance physical property contrasts that are not otherwise obvious. Depending on the nature of the edge being detected, some data enhancement procedures are more applicable than others (Pilkington and Keating, 2004). Pilkington and Keating (2009) compared the results of twelve potential field enhancements for detecting edges in magnetic data. Tilt (TI), tilt horizontal gradient (TDX), theta map (TH), and vertical gradient (VG) were found to overlap, with TDX or TH representing all four techniques. Analytic signal (AS) and local wave-number (LW) were found to be useful, but are susceptible to noise as they make use of second derivatives.

Theoretically, source-edge-detection grids generate ‘peaks’ associated with the magnetic contacts. Blakely and Simpson (1986) proposed a spatial filter to isolate ridge crests by comparing the value of a central cell with its eight nearest neighbours and by fitting a second-order polynomial to the eight surrounding points. This converts an edge detection grid to a dot map that outlines the spatial distribution of source edges, i.e., peaks (Blakely and Simpson, 1986; Cordell and Grauch, 1987). As implemented in Oasis Montaj ™, the Blakely and Simpson (1986) edge detection filter has been modified to output a strike and dip direction symbol. The computed dip direction provides a more complete view of the peak form as derived by the edge detection routine, displaying the dip direction with a range of 360º versus strike direction that only has a range of 180º. Using the grid peak solutions as input to a second gridding of the dip direction data results in an image that isolates blocks of crust within which the dips of the edge detection peaks are similar, i.e., within a single block there may be many parallel contacts.

It is not always possible to determine what type of contact (fault or lithological) a specific source edge represents; however, a number of features present on a magnetic map can assist in the direct identification of faults. These features include (a) clear linear displacement of a magnetic lithological boundary, and (b) equal displacement of a series of cross-cutting magnetically-defined patterns, i.e., the lateral continuity of a lineament. Further corroboration of a possible fault may be the orientation of a linear feature transecting known geological trends. Where source edges are parallel to lithological strike, it is difficult to discriminate between a tectonic boundary and a lithologic contact. However, this is no different than distinguishing stratigraphic repetition from structural repetition in geological mapping. Source edge detection offers a data-driven, three-dimensional perspective to structural analysis.

4.6 Methods

A regional aeromagnetic survey was conducted by the GSC as part of a project entitled, Geo-mapping for Energy and Minerals (GEM) Northeast Thelon, in the summer of 2009. Flight lines were oriented 135º, spaced 400 m apart and the survey was flown at 130 m mean terrain clearance. The original data collection involved three cesium vapor magnetometers arranged in an orthogonal horizontal gradient array; two wing-tip magnetometers and a tail sensor. This study is based on the results from one of the three

magnetometers. Prior to public release, the total-magnetic intensity (TMI) data were corrected by Harvey et al. (2011) to account for diurnal errors and then tie-line leveled.

The data were gridded for this study using minimum curvature with 100 m node spacing. Anomalous high-frequency features in the TMI grid (Figure 4.2) are attributed to glacial landforms and cannot be ignored. To diminish the high-frequency noise associated with the glacial landforms, the aeromagnetic grid was upward continued by a distance of 100 m. In order to place the source edge contacts over their geological sources, the data were further reduced-to-pole; although given the already steep inclination of the local magnetic vector in the study area, this procedure had only limited effect. Finally, source edge detection grids were computed using TF-hgm (Figure 4.3) and TDX (Figure 4.4) methods.

The Blakely algorithm has four levels of peak detection representing the significance level of the data (Blakely and Simpson, 1986). The eight neighboring cells in four directions (x-direction, y-direction, and both diagonals) are compared to find the maximum through which a second-order polynomial is fitted. The significance level is a function of those surrounding values, i.e., a significance level of 4 means that all the neighboring grid points have a lower value, and a significance level of 1 means that only one set of neighboring grid points has a lower value. The Blakely and Simpson (1986) method was applied to the TF-hgm and TDX grids using a peak level of 3. The contact maxima (peaks) are shown on the grids as black dots (Figure 4.3, 4.4).

For every peak detected, Blakely calculates a strike direction, based on the trend of adjacent peak maxima, and approximate dip direction, based on the geometry of the peak. By examining the symmetry of each individual peak in signal form, it is possible to estimate the dip direction of that source body based on the signal's down-sloping gradient. As a result, dip direction is always perpendicular to strike and points away from the magnetic source body. The dip direction of each located peak is sampled from a database of the TF-hgm and TDX grids, and gridded using a minimum curvature algorithm with a 400 m node separation (Figure 4.5). TDX better delineates edges as is evident by the coherency of dots on Figure 4. Tilt, from which TDX is calculated, is the ratio of the vertical to horizontal derivatives, essentially acting as an automatic gain control filter. This retains the spatial integrity of the signal and emphasizes low-amplitude features that are lost in TF-hgm results.

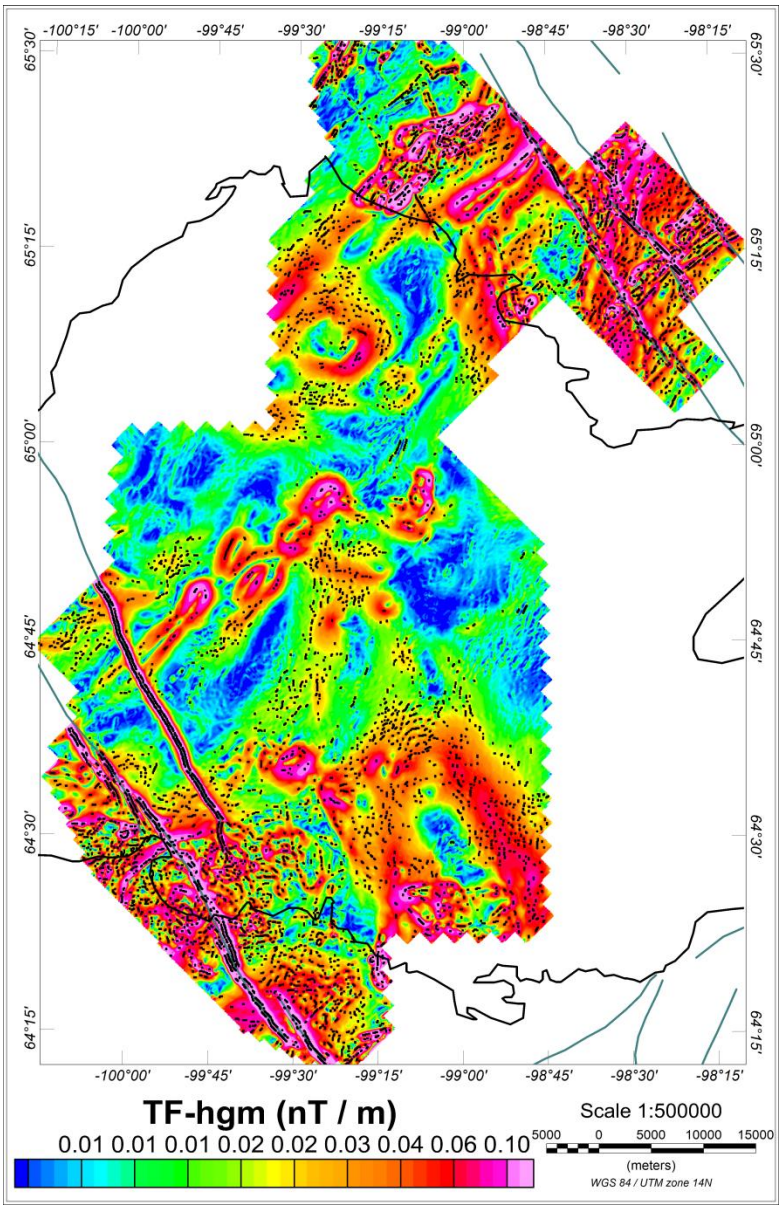

Figure 4.3 Total magnetic field, horizontal gradient magnitude (TF-hgm) map of the study area (derived from TMI data) showing contact maxima (black dots), the outline of the Aberdeen Sub-basin (black line), and diabase dikes (purple lines).

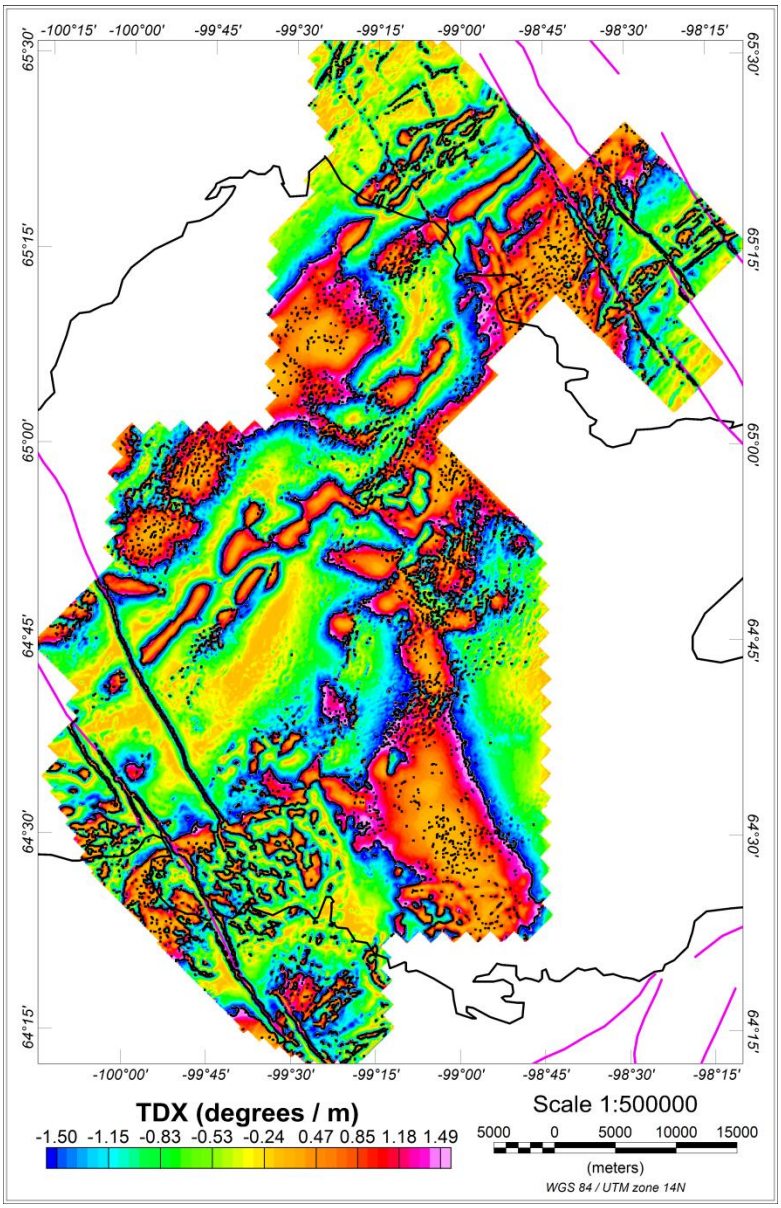

Figure 4.4 Tilt derivative (TDX) map of the study area (derived from TMI data) showing contact maxima (black dots), the outline of the Aberdeen Sub-basin (black line), and diabase dikes (purple lines).

Figure 4.5 shows blocks with similar dip direction based on the fall-off vector of the calculated source edge as defined by the Blakely algorithm. We have chosen to portray dip direction in color, as opposed to traditional strike and dip symbols, in order to improve the visualization of similar magnetic-lithological blocks. A digital elevation model (DEM) was produced for the area from the Canadian Digital Elevation Database (CDED) and re-gridded to a 100 m grid cell size (Figure 4.6). Figure 4.7 shows the dip direction map draped over this DEM.

4.7 Discussion

Figure 4.5 shows the dip direction image (map) that was computed using the Blakely algorithm on the TDX and TF-hgm grids with respect to previously mapped, inferred, and newly mapped faults. The previously identified and inferred faults were extracted from the geodatabase of Jefferson et al. (2011), and updated from a much more regional compilation map by Skulski (in prep). Previously mapped or 'identified' faults were delineated using field geology, the old regional TMI (800 m line spacing) image, LANDSAT, air photographs, and the DEM; whereas 'inferred' faults were interpreted from the DEM and regional TMI map. 'Newly defined' faults represent trends within the dip direction map. The identified, inferred, and newly defined faults are shown as solid, dashed, and dotted lines, respectively (Figure 4.5). This map mainly reflects magnetic geological units in the basement (layer 3) because the Thelon Formation (layer 2) is relatively non-magnetic; thus, this map provides information about the structure at the unconformity surface.

Some identified faults (solid lines) in basement rocks can easily be seen as lineaments and discontinuities in the dip direction map, which are reflected by abrupt changes in color. For example, three previously mapped faults in the Amer Belt are obvious in the dip direction map (Figure 4.5: locations 1, 2, 3). South of Aberdeen Lake, however, a series of mapped northwesterly trending faults is not well manifested in the dip direction map (Figure 4.5: location 6). Notably, outcrop is sparse in this area and the mapped faults were based on their surficial expression; however, it appears that this expression does not reflect basement structure. Another example can be seen in the north, near 99º15' and 99º00', where two SE- and SSE-trending faults can be seen cross-cutting distinct positive anomalies with no noticeable offset (Figure 4.5: location 7). These identified faults are either wrongly located or the dip direction map is reflecting deeply

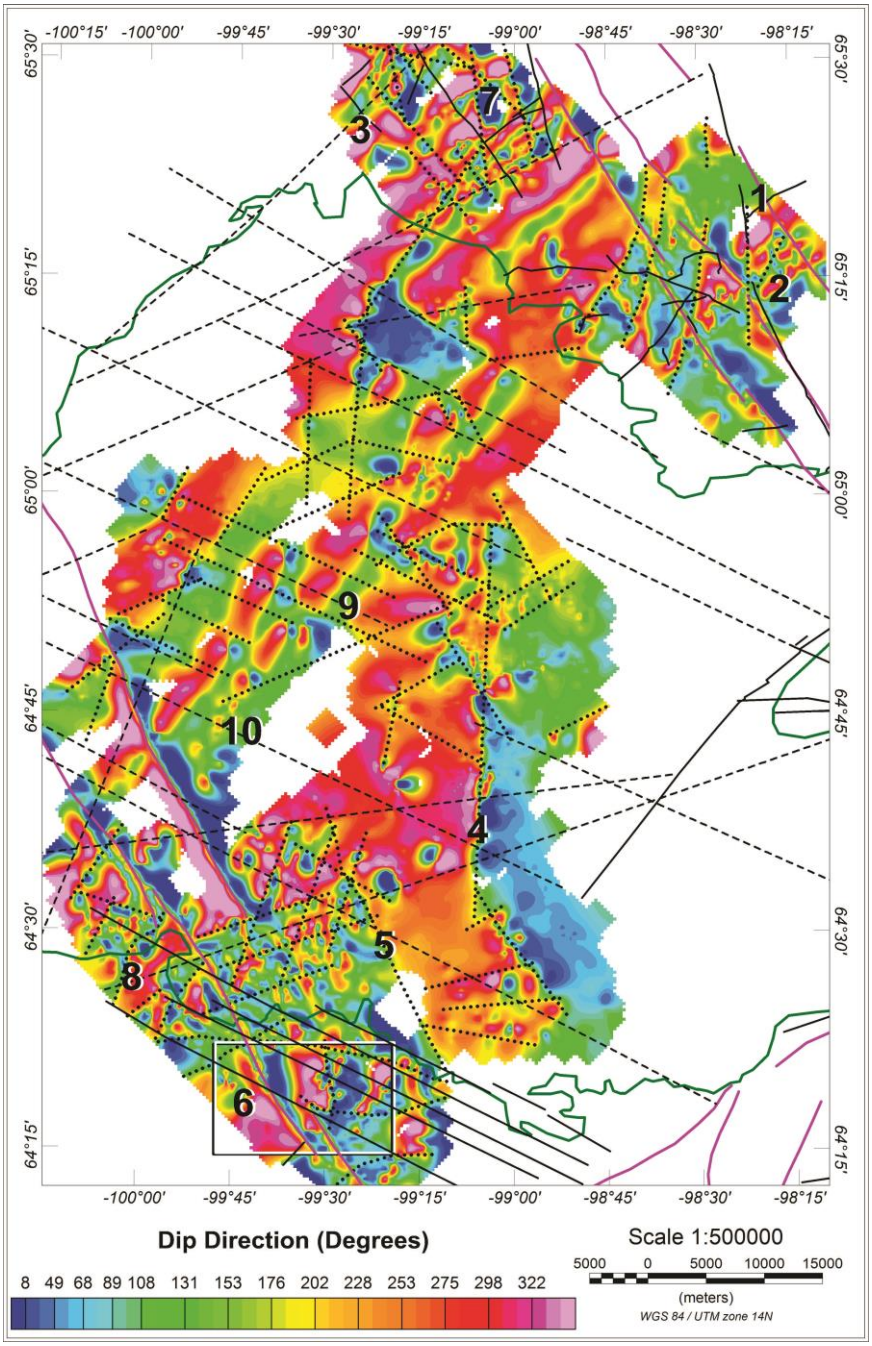

Figure 4.5 Gridded dip-direction map of the study area, calculated from the TF-hgm and TDX grids using the Blakely algorithm. Previously mapped or `identified´ (solid), `inferred´ (dashed), and `newly mapped´ (dotted) faults are shown as black lines. Black numbers refer to locations discussed in the text; the outline of the Aberdeen Sub-basin (green line) and diabase dikes (purple lines) are also shown.

buried, basement units that have been overlain by faulted non-magnetic basement units on which the mapping was based.

Several inferred faults (dashed lines) within the Aberdeen Sub-basin are manifested on the dip direction map, (Figure 4.5: locations 8, 9). As these faults have both basement (magnetic) and surface topographic (DEM) expressions, they are interpreted as reactivated faults that cut the Thelon Formation. In some cases, inferred faults from surface lineaments do not exactly line up with lineaments on the dip direction map, possibly indicating a dipping structure if it is one and the same lineament. Higher resolution DEM and aeromagnetic data sets would more accurately locate and minimize any discrepancies that might have arisen due to the initial geo-referencing of inferred faults. Other inferred faults have no expression in the dip direction map; in fact, they cross cut positive anomalies (Figure 4.5: location 10) and either are not real or they are brittle faults within the Thelon Formation that have no basement expression.

Many newly mapped faults were added to Figure 4.5 (dotted lines) based on features in the dip direction map. New faults are indicated by (a) a noticeable change in linear-trending dip direction, (b) clear displacement of boundaries of magnetic lithological units, or (c) equal displacement of points along the same magnetic lithological feature. Some of these faults are discussed below. At location 4 (Figure 4.5), a very strong N-S-oriented change in dip direction is interpreted as a basement fault. The linearity of the anomaly may represent a fault-bounded magnetic basement unit (i.e., magnetic granitoid). At location 5, an unmapped, NW-trending fault is also demarcated by an abrupt change in dip direction. Locations 4 and 5 are in parts of the Aberdeen Sub-basin that are poorly exposed, either suggesting that these faults are not reflected in the Thelon Formation or they are obscured by glacial overburden. As these faults trend northerly, they are coincident with the predominant glacial direction and may have been interpreted as glacial topographic features.

To investigate the possibility that the dip direction map is detecting faults terminating at the unconformity surface, the map and faults were draped over a DEM (Figure 4.6) to produce the image in Figure 4.7. First, it is clear from the DEM that many identified and inferred faults follow prominent topographic ridges and/or valleys, or they follow lateral offsets in topographic lineaments (Figure 4.6: locations 1, 2). At location 2, an identified fault is parallel to a ridge, whereas at location 1, an identified fault

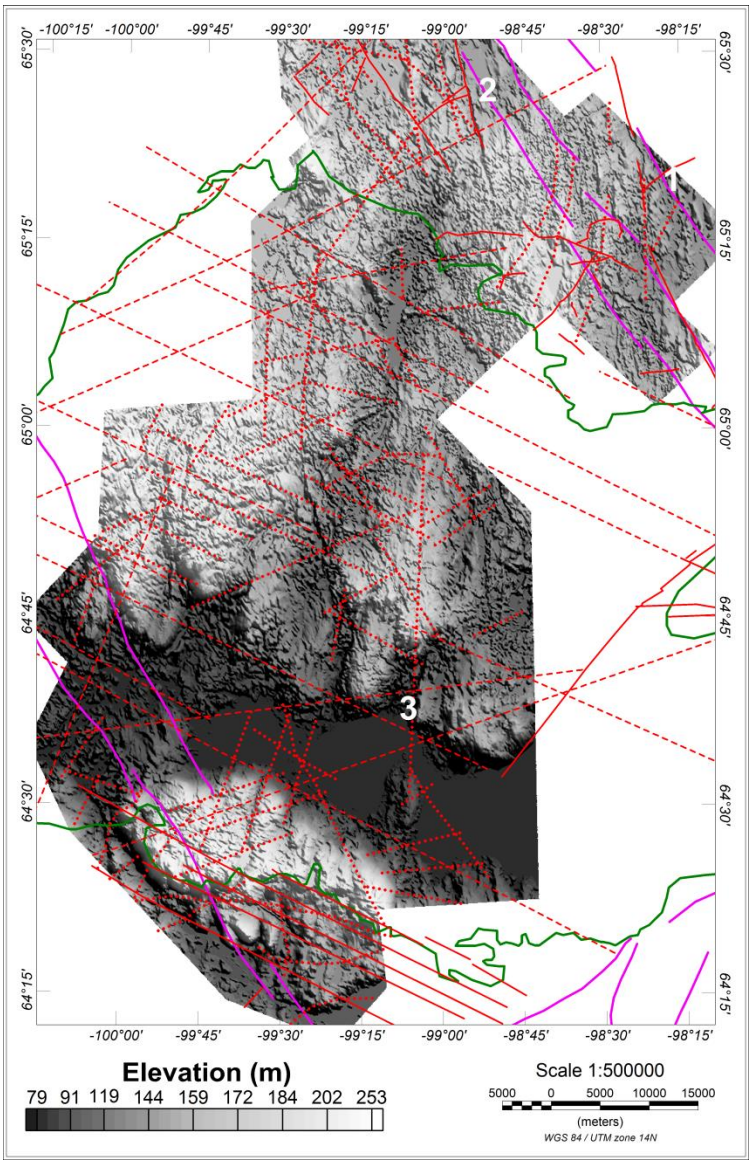

Figure 4.6 A digital elevation model (DEM) derived from the Canadian Digital Elevation Database with `identified´ (solid), `inferred´ (dashed), and `newly mapped (dotted) faults (red lines) superimposed; faults are evident as lineaments or discontinuities on the DEM. White numbers refer to locations discussed in the text; the outline of the Aberdeen Sub-basin (green line) and diabase dikes (purple lines) are also shown.

cuts across several topographic ridges. In many cases, newly mapped faults have no topographic expression, suggesting they are old basement structures that did not propagate through the sedimentary cover sequence or they have been obscured by glaciation. However, one newly mapped fault that trends approximately 005º (Figure 4.6: location 3) has a topographic expression, which was ignored by Jefferson et al. (2011) because it is oriented parallel to the dominant glacial direction. This structure is more pronounced in Figure 4.7 (location 3), which shows that many newly mapped faults can be extended farther along topographic lineaments (e.g., Figure 4.7, location 4), although this was not done in this study.

By comparing Figures 4.6 and 4.7, it is possible to assign various faults within the Aberdeen Sub-basin to three different groups (Figure 4.7). Different sun angles were applied to the DEM (Figure 4.6) in order to visualize lineaments of various orientations, which were compared with the dip direction map (Figure 4.5). The first group (blue in Figure 4.7) is seen only on the DEM; these faults are young brittle structures that have no effect on the basement unconformity, and as such are not visible on the dip direction map. The second group (red in Figure 4.7) is evident on the dip direction map but not the DEM; these faults are old basement structures that did not propagate upward through the Thelon Formation. The third group (yellow in Figure 4.7) has an expression on both the DEM and the dip direction map; these faults are also old structures but they propagated upward during and/or after deposition of the Thelon Formation. Some of these show appreciable basement topography and are thought to be relatively important as conduits for transport of uranium-bearing fluids; those that cut favorable basement rocks are prime targets for unconformity-associated uranium exploration.

Because the study area has been extensively glaciated, caution must be taken in assigning faults to the groups above. Glaciation has camouflaged northerly trending lineaments in the area but enhanced east-west ones in the DEM. Thus, a number of lineaments that are visible in the basement (dip direction map) and that propagated through the Thelon Formation are no longer evident at surface. Ultimately, ground truthing may be needed to validate some of the relative ages assigned here. Adjacent to the Aberdeen Sub-basin, it is difficult to assign faults to groups because the Thelon Formation is absent and hence, no cover exists to establish relative timing of faults. Nevertheless, faults form arrays, and knowledge of an array gained from within the

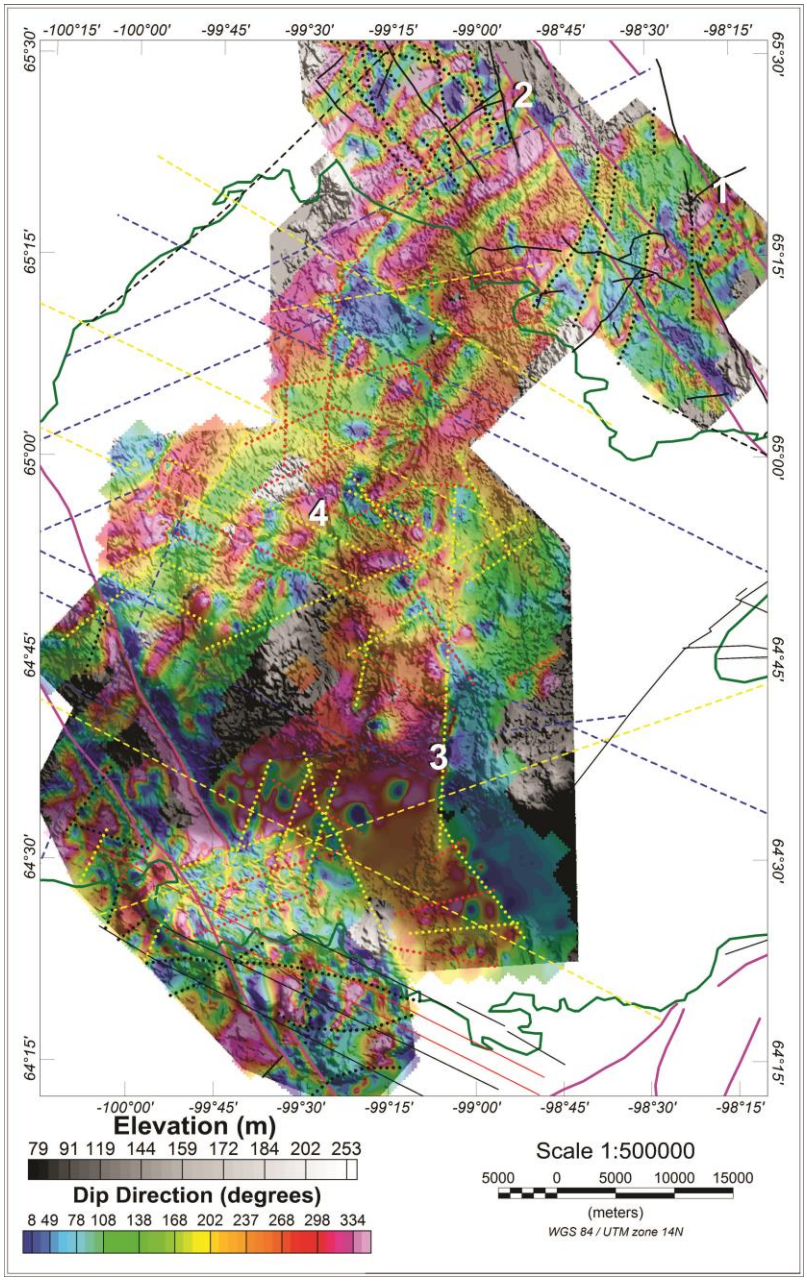

Figure 4.7 The dip direction map (Figure 4.5) draped over the DEM (Figure 4.6), with `identified´ (solid), `inferred´ (dashed), and `newly mapped´ (dotted) faults superimposed and color coded as to age as follows; blue = post-Thelon (intraformational); red = pre-Thelon (basement); and yellow = re-activated faults. White numbers refer to locations discussed in the text; the outline of the Aberdeen Sub-basin (green line) and diabase dikes (purple lines) are also shown.

Aberdeen Sub-basin can be extrapolated to members of that array that now lie outside the basin. Despite this shortcoming, the dip direction map draped over the DEM provides a valuable utility for establishing the history of faulting within and adjacent to the Thelon Basin as a whole.

4.8 Conclusions

A new method for mapping faults within basement rocks underlying the Thelon Basin was developed and tested in the Aberdeen Sub-basin. First, a dip direction grid was derived from newly acquired, tilt horizontal gradient (TDX) and total field horizontal gradient magnitude (TF-hgm) aeromagnetic data, using the Blakely algorithm for defining magnetic source edges. For every inflection point on a source edge, the algorithm was used to calculate a dip direction for the magnetic body, based on the symmetry of that point. Subsequent gridding of these data yielded a color image or lineament map with offsets and abrupt changes in dip direction, which helped to accentuate the presence of faults. A digital elevation model (DEM) was produced using data from the Canadian Digital Elevation Database (CDED); identified, inferred, and newly mapped faults were superimposed on both the DEM and the dip direction map, and comparison of the two maps revealed three age groups of faults. The first group is seen only on the DEM; these faults are young brittle structures that have no effect on the basement unconformity and are not visible on the dip direction map. The second group is evident on the dip direction map but not the DEM; these faults are old basement structures that did not propagate upward through the Thelon Formation. The third group has an expression on both the DEM and the dip direction map; these faults are also old structures but they propagated upward during and/or after deposition of the Thelon Formation The third group of faults may be of greatest interest for uranium exploration, with reactivation increasing their potential to serve as conduits to transport uranium-rich fluids and focus uranium deposition at or near the unconformity surface.

Future work will focus on the geometry of the potentially reactivated structures and expand the fault analysis to the aeromagnetic data set in and around the Aberdeen Sub-basin of the northeast Thelon region (Tschirhart et al., 2011a). For faults that have been corroborated by topographic lineaments but appear to be slightly offset from those interpreted from the dip direction image, there is the potential to calculate the dip of the fault plane if the depth to the unconformity surface is known. Using standard trigonometry, the distance between surficial and basal fault expression is known, allowing

calculation of geological dips. Knowing the distribution, location, and geometry of basal faults, exploration efforts can focus on unconformity-associated uranium deposits located at high-angle fault intersections. Further analysis of source edge detection and dip direction maps will help generate a predictive basement geology map. By demarcating the signature and contrasts of the units peripheral to and extending beneath the Thelon cover, the geology of the unconformity surface can be mapped. Identifying the favorable geology and structure can help companies to focus on intersections with the greatest potential for unconformity-associated uranium deposits.

4.9 References

Babu, V.R., Ram, S. and Sundararajan, N. 2007. Modeling and inversion of magnetic and VLF-EM data with an application to basement fractures: A case study from Raigarh, India. *Geophysics*, 72, B133-B140.

Grauch, V.J.S. and Cordell, L. 1987. Limitations of determining density or magnetic boundaries from the horizontal gradient of gravity or pseudogravity data. *Geophysics*, 52, 118-121.

Davidson, G.I. and Gandhi, S.S. 1989. Unconformity-related U-Au mineralization in the Middle Proterozoic Thelon sandstone, Boomerang Lake prospect, Northwest Territories, Canada. *Economic Geology*, 84, 143-157.

Davis, W.J., Rainbird, R.R., Gall, Q. and Jefferson, C.W. 2008. In situ U-Pb dating of diagenetic apatite and xenotime; paleofluid flow history within the Thelon, Athabasca and Hornby Bay Basins. *Geochemica Cosmochimica Acta*, 72 (12S), A203.

Davis, W.J., Gall, Q., Jefferson, C.W., and Rainbird, R.H. 2011. Fluorapatite in the Paleoproterozoic Thelon Basin: structural-stratigraphic, in-situ ion microprobe U-Pb ages, and fluid flow history. *Geological Society of American Bulletin*, 123, 1056-1073.

Blakely, R.J. and Simpson, R.W. 1986. Approximating edges of source bodies from magnetic or gravity anomalies. *Geophysics*, 5, 1494-1498.

Gay, S.G. 2004. Glacial till: a troublesome source of near-surface magnetic anomalies. *The Leading Edge*, 23, 542-547.

Hadlari, T., Rainbird, R. H., and Pehrsson, S. J. 2004. Geology, Schultz Lake, Nunavut. Geological Survey of Canada, Open File 1839, 1 sheet, scale 1:250 000.

Harvey, B.J.A., Coyle, M., Buckle, J.L., Carson, J.M., and Hefford, S.W. 2011. Geophysical Series, airborne geophysical survey of the northeast Thelon Basin, Nunavut, NTS 66 A, parts of 66 B, 66 C, 66 G and 66 H. Geological Survey of Canada, Open File 6510, 2011, 10 sheets, doi:10.4095/288204.

Holden, E., Dentith, M. and Kovesi, P. 2008. Towards the automated analysis of regional aeromagnetic data to identify regions prospective for gold deposits. *Computers and Geoscience*, 34, 1505-1513.

Jefferson, C.W., Thomas, D., Quirt, D., Mwenifumbo, C.J. and Brisbin, D. 2007. Empirical models for Canadian unconformity-associated uranium deposits: *in* Milkereit, B., (ed.), Proceedings of Exploration 07: Fifth Decennial International Conference on Mineral Exploration, 741-769.

Jefferson, C.W., Chorlton, L.B., Pehrsson, S.J., Peterson, T., Wollenberg, P., Scott, J., Tschirhart, V., McEwan, B., Bethune, K., Calhoun, L., White, J.C., Leblon, B., LaRocque, A., Shelat, Y., Lentz, D., Patterson, J., Riegler, T., Skulski, T., Robinson, S.,

Paulen, R., McClenaghan, B., Layton-Matthews, D., MacIsaac, D., Riemer, W., Stieber, C. and Tschirhart, P. 2011. Northeast Thelon Region: Geomapping for Uranium in Nunavut: Geological Survey of Canada, Open File 6862, Power Point Presentation, 38 slides.

Lee, M., Morris, W.A., and Ugalde, H. 2010. Calibrating apparent magnetic susceptibility and the identification of fractures: A case study from the Eye-Dashwa lakes pluton, Atikokan, Ontario. *Geophysics*, 75 (3), B147.

LeCheminant, A.N. and Heaman, L.M. 1989. Mackenzie igneous events, Canada: Middle Proterozoic hotspot magmatism associated with ocean opening. *Earth and Planetary Science Letters*, 96, 38-48.

Miller, A.R., and LeCheminant, A.N. 1985. Geology and uranium metallogeny of Proterozoic supracrustal successions, central District of Keewatin, N.W.T. with comparisons to northern Saskatchewan: *in* Sibbald T.I.I., and Petruk, W., (eds.), Geology of Uranium Deposits: Canadian Institute of Mining and Metallurgy, Special Volume 32, 167-185.

Pilkington, M. and Keating, P.B. 2004. Contact mapping from gridded magnetic data – a comparison of techniques. *Exploration Geophysics*, 35, 306-311.

Pilkington, M. and Keating, P.B. 2009. The utility of potential field enhancements for remote predictive mapping. *Canadian Journal of Remote Sensing*, 35, S1-S11.

Rainbird, R.H., Hadlari, T., Aspler, L.B., Donaldson, J.A., LeCheminant, A.N. and Peterson, T.D. 2003. Sequence stratigraphy and evolution of the Paleoproterozoic intracontinental Baker Lake and Thelon basins, western Churchill Province, Nunavut, Canada. *Precambrian Research*, 125, 21–53.

Rainbird, R.H., Davis, W.J., Pehrsson, S.J., Wodicka, N., Rayner, N. and Skulski, T. 2010. Paleoproterozoic supracrustal assemblages of the Rae domain, Nunavut, Canada: intracratonic basin development during supercontinent break-up and assembly. *Precambrian Research*, 181, 167-186.

Thomas, M.D., and McHardy, S. 2007. Magnetic insights into basement geology in the area of McArthur River uranium deposit, Athabasca Basin, Saskatchewan: *in* Jefferson, C.W., and Delaney, G., (eds.), EXTECH IV: Geology and Uranium EXploration TECHnology of the Proterozoic Athabasca Basin, Saskatchewan and Alberta: Geological Survey of Canada, Bulletin 588, 425-440.

Tourigny, G., Quirt, D.H., Wilson, N., Wilson, S., Breton, G., and Portella, P. 2007. Geological and structural features of the Sue C uranium deposit, McClean Lake area, Saskatchewan: *in* Jefferson, C.W., and Delaney, G., (eds.), EXTECH IV: Geology and Uranium EXploration TECHnology of the Proterozoic Athabasca Basin, Saskatchewan and Alberta: Geological Survey of Canada, Bulletin 588, 229-248.

Tschirhart, V., Morris, W.A. and Oneschuk, D. 2011a. Geophysical series, geophysical compilation project, Thelon Basin, Nunavut, NTS 66A, B, and parts of 65N, O, P, 66C, F, G and H. Geological Survey of Canada, Open File 6944, 1 sheet, doi:10.4095/288806.

Tschirhart, V., Morris, W.A., Ugalde, H., and Jefferson, C.W. 2011b. Preliminary 3D geophysical modelling of the Aberdeen sub-basin, northeast Thelon Basin region, Nunavut. Geological Survey of Canada, Current Research 2011-4, 12 pp., doi: 10.4095/287165.

5. Basement geology beneath the northeast Thelon Basin, Nunavut: Insights from integrating new gravity, magnetic and geological data

Tschirhart, V[1]., Jefferson, C.W[2]. and Morris, W.A[1].

1. *MAGGIC, School of Geography & Earth Sciences, McMaster University, Hamilton, Ontario, Canada L8S 4K1*

2. *Geological Survey of Canada, 601 Booth St., Ottawa, Ontario, Canada K1A 0E8*

A version of this manuscript has been submitted to *Precambrian Research* (October 2013) as: Tschirhart, V., Jefferson, C.W. and Morris, W.A. Basement geology beneath the northeast Thelon Basin, Nunavut: insights from integrating new gravity, magnetic and geological data.

5.1 Abstract

The <1.75 to >1.27 Ga Thelon Basin in the Kivalliq region of Nunavut has undergone several exploration campaigns because of its' prospectively for unconformity-associated uranium deposits. However, no basement geology map currently exists and much of the surface geology has been only crudely mapped because it is such a remote, frontier area. As part of a regional geoscience compilation, new areal and 3-D insights are here provided by extending detailed outcrop and geophysical knowledge from adjacent exposed basement rocks to the unconformity surface beneath the northeastern part of the Thelon Basin, the Aberdeen sub-basin. We use primary and derived aeromagnetic imagery including source edge detection, ground gravity transects, petrophysical properties, magnetic textural correlations, and structural trends and discontinuities derived from geophysical markers as elements in the mapping. These geophysical data were calibrated with compiled and new outcrop geological data adjacent to the sub-basin. The gravity profiles are forward modeled in four cross sections that transect the main lithostructural belts in outcrop and beneath the basin, constraining major contacts, fault geometries and offsets. The new geological map of the basement below the Aberdeen sub-basin and the cross sections delineate six main lithotectonic entities: Archean mixed granitoid and amphibolitic gneiss; Neoarchean metasedimentary and metavolcanic rocks tentatively assigned to the ca 2.7 Ga Woodburn Lake group; the latest Neoarchean Marjorie Hills metasedimentary gneiss; the Amer Mylonite Zone with inferred associated 2.6 Ga mafic intrusions; other igneous intrusions of 2.6, 1.83 and 1.75 Ga vintage, and the <2.3 to >1.84 Ga Amer Group. Four main brittle regional fault arrays (040-060°, 075-90°, 120° and 150°) controlled development and preservation of the Aberdeen sub-basin. The reactivated intersections of such faults are key foci for uranium deposits.

5.2 Introduction

Overlapping the border between Northwest Territories and Nunavut, the Thelon Basin (Figure 5.1) is similar in many ways (Miller and LeCheminant, 1985) to the Athabasca Basin, known for its very high grade unconformity-associated uranium deposits (Jefferson et al., 2007a). Although several exploration and mapping campaigns have targeted the Thelon Basin, its remoteness, exploration moratoria and lack of infrastructure have limited the growth of knowledge about its geology, geometry and structure. Even the northeastern part of the Thelon Basin - here termed the Aberdeen sub-basin (Figure 5.1), which is closest to tide water at Baker Lake, remains poorly defined.

Current uranium prospects are basement hosted and located outside of the sub-basin at the intersections of hydrothermally altered, reactivated faults within the Neoarchean Woodburn Lake group and early Paleoproterozoic Ketyet River group (Fuchs et al., 1986; Miller and LeCheminant, 1985). With continued exploration and development of the region, it is expected that the search for new deposits will progress to greater depths to find buried deposits beneath the Thelon sandstone, analogous to most of the recent discoveries in the Athabasca Basin that are covered by hundreds of metres of undeformed sandstone (see reviews by Jefferson et al., 2007a, b). Recent studies of locales peripheral to the Aberdeen sub-basin have served to emphasise the importance of identifying lithological associations that provide favourable sites within basement rocks for unconformity-associated uranium deposition (P. Wollenberg, oral presentation, Nunavut Mining Symposium, 5 April, 2011; R. Hunter, oral presentation, Nunavut Mining Symposium, 5 April, 2011; Jefferson et al., 2013a, b; V. Tschirhart et al., 2013b).

The purposes of this paper are twofold. First we estimate the depth to basement along a series of strategic transects that model the shape of the unconformity between the underlying supracrustal and crystalline basement rocks and the overlying conglomerate and sandstone that filled the Aberdeen sub-basin. Second we remotely map the main geological units that lie beneath the basal unconformity, both as depth slices along the strategic transects and aerially as a geological map of the unconformity surface. As part of the second aim, we also improve both the accuracy and detail of mapping around the periphery of the sub-basin, particularly in the large areas of basement supracrustal rocks where there is less than 1% outcrop.

Within the Aberdeen sub-basin (Figure 5.1), little knowledge is available regarding the basement geology at and below the unconformity at the base of the Thelon Formation. Only 10 documented boreholes actually intersect the unconformity; the remainder provide only minimum depth constraints (Davis et al., 2011). The boreholes that did intersect the basal unconformity penetrated only a few to several 10's of metres into the basement rocks, offering little guidance regarding the spatial extent or structure of the underlying basement rock units. Sparse seismic shot points collected by Overton (1979) were used by Davis et al. (2011) to infer the depth to basement but these interpretations are uncertain in places, and the seismic data do not identify the basement lithology. Faults have been mapped in the surrounding basement rocks (Calhoun et al, 2014; Jefferson et al., 2014 a, b; Tschirhart et al, 2013a, b, c) and as indicated by a few

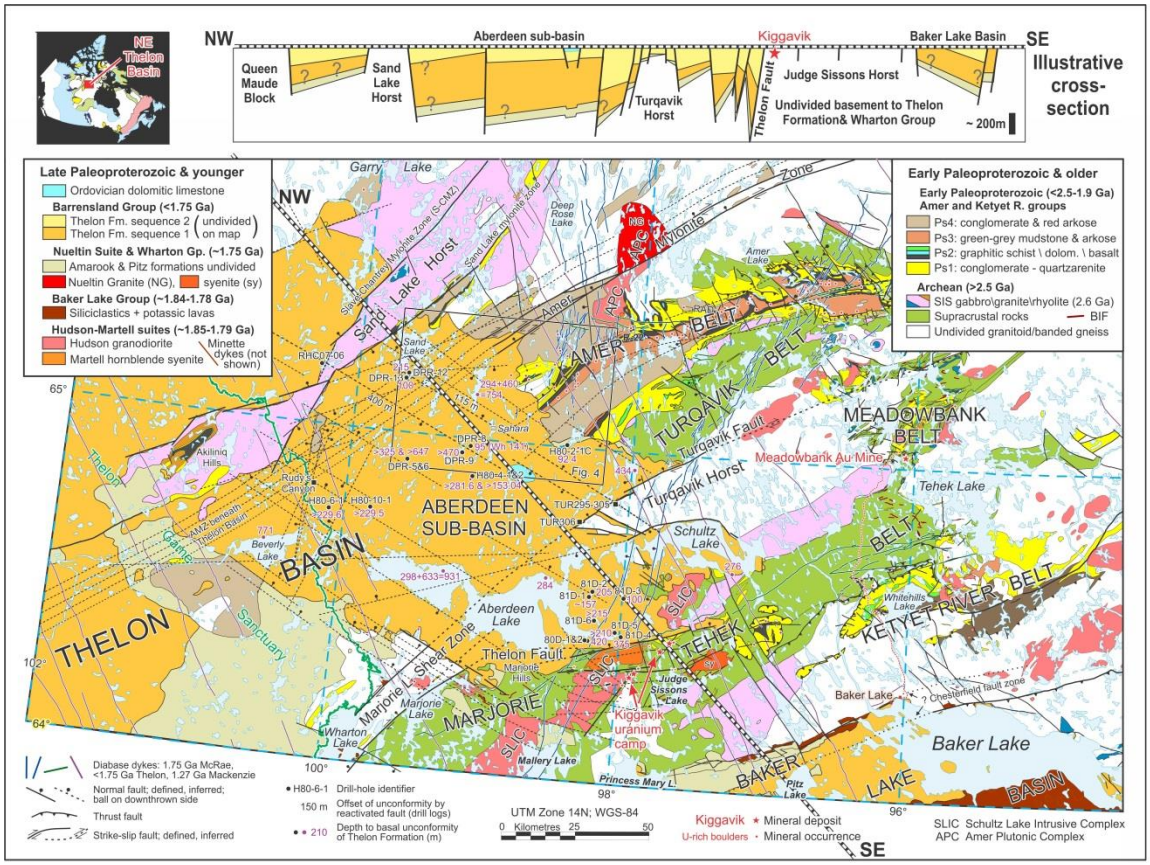

Figure 5.1 Preliminary generalized geology of the Aberdeen sub-basin in the northeastern part of the Thelon Basin (after Tschirhart et al., 2011b; Jefferson et al., 2011b, 2013a, b). Abbreviations not explained on the figure are explained in Table 5.1. Defined faults are geologically mapped; inferred faults are based on one or more of: map patterns, geophysical data, and satellite and air photo imagery. Some inferred faults have defined offsets at certain points but their extrapolated trend is uncertain. New interpretations of these preliminary faults are developed in this paper. Location of Figure 5.4 is outlined. Depths to basal unconformity shown beside purple dots are from Overton (1979); those beside black drill holes dots are from Davis et al., 2011.

Group / Suite	Map Unit	Map Code	Lithology	Magnetic susceptibility traits at map scale	*	Average Susc. (SI)	Susc. (log10)	Minimum	Maximum	Standard Deviation	Density Avg. g/cc	n
Mackenzie	Mackenzie diabase	Mck-dy	diabase	high, 150° straight	1	0.030280	0.030280	n/a	n/a	n/a	3.04	1
Event	(1.17 Ga)	Mck-dy-clay	altered diabase	na	n	0.000034	0.000300	n/a	n/a	n/a	2.52	1
Barrensland	Thelon	Th2-cg	conglomerate	transparent	2	0.000018	0.000004	0.000000	0.000043	0.000019	2.59	4
Group	Formation	Th1-slt	siltstone	transparent	2	0.000007	0.000002	0.000000	0.000014	0.000006	2.58	4
(<1.75 Ga)	(apatite cement	Th1-ss	sandstone	transparent	2	0.000008	0.000000	0.000000	0.000009	0.000024	2.48	12
	1.68 Ga)	Th1-cg-sil	interbedded	transparent	2	0.000003	0.000001	0.000000	0.000009	0.000004	2.62	5
		Th1-cg	conglomerate	transparent	2	0.000034	0.000021	0.000004	0.000137	0.000036	2.64	18
Nueltin Suite	Nueltin granite	Nlt-gr	granite	high to low areal	3	0.002047	0.000234	0.000000	0.012343	0.003243	2.63	27
intrusive	Thelon River diabase	Thl-dy	diabase	mod.-hi, 075° straight	1	0.027399	0.025958	0.025897	0.026020	0.000087	2.92	2
components	McRae Lake diabase	McR-dy	diabase	mod-hi, 350-020° straight	1	0.030229	0.023206	0.010857	0.049600	0.027395	2.80	2
Wharton	Pitz Formation	Pitz-rhy	rhyolite	mod., dappled area	4	0.002347	0.000091	0.000017	0.026250	0.007534	2.63	12
Group	Amarook Fm.	Wh-Ak-cg	conglomerate	low (transparent)	2	0.000043	0.000016	0.000002	0.000206	0.000069	2.54	9
(1.75 Ga)		Wh-Ak-qz	quartzarenite	low (transparent)	2	0.000014	0.000011	0.000004	0.000034	0.000012	2.56	5
Hudson	Bostonite dyke	Bstn-dy	fine syenite	mod., 000+125° straight	1	0.000880	0.000254	0.000013	0.002559	0.000991	2.65	11
Suite	Lamprophyre dyke	Mntt-dy	lamprophyre	mod., 000+125° straight	1	0.000172	0.000099	0.000010	0.000513	0.000200	2.71	6
(intrusive)	Martell Syenite	Mrt-sy (SLIC)	coarse syenite	high, reticulate area	5	0.002003	0.000762	0.000000	0.014360	0.002434	2.77	7
(1.83 Ga)		Mrt-sy-clay	altered syenite	demagnetized faults	6	0.000022	0.000022	0.000020	0.000024	0.000003	2.50	2
	Hudson Granite	Hds-gr (SLIC)	granodiorite	moderate-high, reticulate	5	0.001785	0.000290	0.000007	0.012640	0.003014	2.63	38
		Hds-gr-clay	altered granodiorite	demagnetized faults	6	0.000004	0.000003	0.000001	0.000008	0.000003	2.42	4
		Hds-peg	pegmatite	na	n	0.000103	0.000052	0.000014	0.000193	0.000126	2.60	2
Amer Group	Ps4: Itza Lake fm.	Itz-fss	arkosic sandstone	transparent	2	0.000053	0.000023	0.000001	0.000298	0.000070	2.64	26
(all	< 1.91 Ga	Itz-fmd	red mudstone	transparent	2	0.000109	0.000080	0.000012	0.000272	0.000047	2.70	8
formation	Ps3: Showing L. fm.	Shw-fsmd	mudstone & siltstone	high, folded linear	7	0.001444	0.000167	0.000015	0.014733	0.004251	2.76	22
names	Ps3: Oora L. fm.	Orl-fss	feldspathic sandstone	low	8	0.000345	0.000196	0.000042	0.000966	0.000359	2.62	11
(fm.) are	Ps3: Three Lakes fm.	3lk-md	grey mudstone & siltstone	very high, folded linear	7	0.004215	0.000480	0.000058	0.020627	0.007826	2.78	7
informal)	Ps2: Five Mile L. bslt.	5ml-v	porphyritic basalt	very high, curvilinear	7	0.007219	0.000890	0.000003	0.054617	0.013888	2.86	31
	Ps2: Aluminium R. fm.	Alm-dol	siliceous dolostone	low	8	0.000035	0.000021	0.000004	0.093010	0.024849	2.81	14
	Ps2: Resort L. fm.	Rsl-fqz	feldspathic sandstone	low	8	0.000067	0.000040	0.000004	0.000215	0.000056	2.71	17
	(<1.95 Ga)	Rsl-mdslt	graphitic meta-mudstone	low but with conductors	9	0.000285	0.000090	0.000000	0.002265	0.000445	2.75	40
	Ps1: Ayagaq L. fm.	Ayg-qzp	pyritic quartzite	low	8	0.000030	0.000012	0.000003	0.000084	0.000037	2.67	5
	(<<2.6 Ga)	Ayg-cgu	conglomerate	low	8	0.000060	0.000007	0.000000	0.000155	0.000064	2.70	12
		Ayg-qzar	quartzarenite	low	8	0.000060	0.000018	0.000001	0.000513	0.000126	2.68	19
		Ayg-srqz	sericitic quartzite	low	8	0.000240	0.000056	0.000010	0.001048	0.000386	2.78	7
Marjorie Hills assemblage		Ml-BIF	clay altered metagreywacke	very high, folded linear	11	0.000046	0.000045	0.000036	0.000055	0.000014	2.95	2
(MHA; informal)		Ml-gw	metagreywacke, thick beds	low to moderate, areal	n	0.000458	0.000089	0.000001	0.004217	0.001052	2.68	17
(<2.63 Ga detrital zircons, V.McNicoll,		Ml-gw-hem	metagreywacke, hematitized	demagnetized	6	0.000012	0.000007	0.000037	0.000218	0.000013	2.65	3
personal communication, March 2013)		Ml-fv	felsic metavolcanic rock	na	n	0.004344	0.001294	0.000362	0.010081	0.004926	2.79	4
		Ml-mv	mafic metavolcanic rock	moderate-high, broad	12	0.028647	0.006921	0.000030	0.093107	0.033950	2.93	6
Snow Island	mafic intrusions	Snw-di, -gb	diorite to gabbro	high, strong peaks	10	0.000260	0.000030	0.000000	0.000446	0.000234	2.79	3
Suite (SIS)	granitoid rocks	Snw-mzdi	grano- to monzodiorite	moderate-high, domal	10	0.003260	0.000230	0.000005	0.015647	0.006923	2.69	5
(2.6 Ga)	volcanic rocks	Snw-rhy	qtz-fsp porphyritic tuff	low	n	0.000213	0.000044	0.000007	0.003643	0.000700	2.66	34
Woodburn	Pipedream	Ppd-BIF	chert-magnetite BIF	very high, folded linear	11	0.030897	0.002414	0.000046	0.164610	0.055292	3.04	12
Lake	assemblage	Ppd-clay	clay altered greywacke	demagnetized	6	0.000004	0.000004	n/a	n/a	n/a	2.31	1
group	(informal)	Ppd-fv	felsic metavolcanic rock	na	n	0.000094	0.000046	0.000006	0.000179	0.000060	2.70	13
(informal)	(<2.71 Ga)	Ppd-gw	metagreywacke, thin beds	weak	n	0.000509	0.000092	0.000000	0.008549	0.001503	2.70	83
		Ppd-gw-clay	clay altered metagreywacke	demagnetized faults	6	0.000018	0.000013	0.000006	0.000043	0.000016	2.49	5
	These values apply to	Ppd-gw-hem	metagreywacke, hematitized	demagnetized faults	6	0.000215	0.000043	0.000005	0.000613	0.000346	2.69	3
	other assemblages in	Ppd-mv	metagreywacke, hematitized	moderate	12	0.000245	0.000244	0.000036	0.000265	0.000122	2.95	2
	study area, e.g. the	Ppd-md	graphitic meta-mudstone	low (locally conductive)	9	0.000055	0.000029	0.000008	0.000137	0.000071	2.75	3
	Turqavik Belt	Ppd-qz	thin yellowish quartzite	na	n	0.000009	0.000004	0.000000	0.000061	0.000016	2.65	13
Undivided	Granitoid gneiss	A-gtoid	granitic gneiss	moderate, areal	n	0.000778	0.000268	0.000015	0.006456	0.002053	2.72	14
Archean		A-gtoid-clay	clay altered gneiss	demagnetized	6	0.000005	0.000005	n/a	n/a	n/a	2.52	1
basement	Felsic metavolcanic	A-fv	felsic metavolcanic rock	low	n	0.002481	0.000035	0.000035	0.011587	0.004175	2.72	13
	Mafic metavolcanic	A-mv	mafic metavolcanic rock	moderate-high, broad	12	0.000425	0.000320	0.000068	0.001436	0.000364	2.82	14

*notes: 1) dykes are defined by orientation and strength of linear magnetic anomaly; 2) underlying markers are subdued in intensity; 3) The only large body in the study area is on the north side of the Amer Mylonite Zone; 4) subtle pattern noted in places south of Aberdeen Lake; 5) mainly in the Schultz Lake Intrusive Suite (SLIC); 6) demagnetization records hydrothermal alteration to hematite and/or clay in linear zones along reactivated steep faults, most evident in thin magnetic units; 7) regionally continuous distinct stratigraphic-structural marker; 8) provides contrast to 7; 9) low magnetic susceptibility but good conductors provide local stratigraphic-structural markers; 10) deep plutons not affected by demagnetization along faults, however in places form lenses along ancient shear zones; 11) BIF is locally the highest contrast marker in several greywacke units; 12) indistinct, in places forms crude linear trend; n) non-diagnostic.

Abbreviations in this table and in the figures, in alphabetical order: Avg. = average; BIF = banded iron formation; bslt = basalt; fm. = informal stratigraphic formation name; Ga = billion years; hi = high; L. = Lake; mag. = magnetic susceptibility; mod. = moderate; n = number of samples measured; na = too small a unit to model; Susc. = magnetic susceptibility

Table 5.1 Geophysical properties of map units in the study area, including lithologic details. Bottom row explains abbreviations in figures.

closely spaced drill holes some faults are known to continue into the sub-basin (Davis et al., 2011). Most faults, however, are only inferred in plan based on indistinct surficial lineaments and subjective analysis of airborne magnetic data as total magnetic intensity (TMI) maps. Such faults could be en echelon rather than continuous so their exact locations in plan are highly uncertain.

Remote predictive mapping methods must be applied in order to gain a better understanding of the subsurface geology. Only geophysical anomaly patterns and their signal attributes analysed in the context of geophysical rock property data have the power to characterize key map units at depth. These can also define important exploration parameters for unconformity uranium deposits such as reactivated faults and fertile basement supracrustal belts (Jefferson et al., 2007b). The southwestern corner of the Aberdeen sub-basin is within the Thelon Game Sanctuary and as such our knowledge is limited to a single field traverse by the second author and compiled data from early mapping such as reported by LeCheminant et al. (1983). Inferences on the subsurface geology in that area are bolstered here by geophysical correlations traced geophysically beneath the Aberdeen sub-basin from better known areas to the northeast.

5.3 Geological and geophysical setting

The following descriptions refer to Figure 5.1 and Table 5.1 (geophysical properties) that lists rock types in order by increasing age. Located in the western Churchill Province, the intracratonic Thelon Basin was filled during the late Paleoproterozoic after 1.75 Ga (Miller and LeCheminant, 1983) and mostly before eruption of the 1.54 Ga ultrapotassic Kuungmi mafic lavas (Chamberlain et al., 2010). The basin was filled by the Barrensland Group, comprising the dominantly fluvial Thelon Formation sandstone, thin Kuungmi lavas and the Lookout Point Formation dolostone (Rainbird et al., 2003).The latter two units are not preserved in the Aberdeen sub-basin region.

The focus of this study is the Aberdeen sub-basin that is separated on its western side from the rest of the Thelon Basin by the Sand Lake Horst. Normal and strike slip faults, which controlled the shape of the sub-basin, were reactivated multiple times, and are described in detail at the end of this section. Uranium-rich fluorapatite cemented both brittle basement faults and soft sediment faults within the sandstone at 1.667 ± 5 Ma (Davis et al., 2011), however the sparse distribution of this cement and poor exposure

preclude linkage to any particular fault array. The Thelon Formation sandstone is magnetically transparent so that the observed geophysical signatures are those of underlying rocks in the basement, most notably the McRae Lake and Thelon River diabase dyke swarms defined regionally by Buchan and Ernst (2004) and described below in detail for this study area.

Topped only by an isolated outlier of fossiliferous Ordovician dolomite (Bolton and Nowlan, 1986) in the Aberdeen sub-basin, the dominantly fluviatile, clay altered feldspathic sandstone and conglomerate of the Thelon Formation unconformably overlies the 1.75 Ga Wharton Group. In the Baker Lake Basin, the Wharton Group unconformably overlies the 1.83 -1.81 Ga Baker Lake Group, but the Baker Lake Group is absent from the area of the Aberdeen sub-basin. The Baker Lake, Wharton and Barrensland groups make up the 1.83 to <1.54 Ga Dubawnt Supergroup (Rainbird et al., 2003; Peterson et al., 2010).

The Wharton Group in the Baker Lake Basin comprises two distinct units: the Amarook Formation quartzarenite and the overlying Pitz Formation volcanic and epiclastic rocks (Rainbird et al., 2003). In the study area, on the southern flank of the Aberdeen sub-basin, the Wharton Group is represented only by the Pitz Formation – bimodal rhyolite and basalt, which are the extrusive components of the Nueltin porphyritic granite plutons (Peterson et al., in prep). The Pitz Formation also includes cross bedded epiclastic sandstone and conglomerate derived from the lavas. Exposed Nueltin Granite in the study area is restricted to rapakivi granite at the north end of the Amer Plutonic Complex (APC), and small intrusions in the Kiggavik area. On the north and east sides of the Aberdeen sub-basin the Wharton Group is represented only by the older Amarook Formation – feldspathic arenite to quartzarenite with aeolian cross beds. Although silicified and highly lithified compared to the almost friable Thelon sandstone, the Amarook sandstone is unmetamorphosed, generally gently dipping, geophysically indistinguishable from the Thelon sandstone, less than 100 m thick and outcrops as very narrow discontinuous units along fault zones at the margins of the Aberdeen sub-basin, and in two inliers near its northeast margin. Therefore the Amarook and Thelon sandstone units are considered together as the fill of the sub-basin for the purposes of geophysical modeling. Recognition of the presence or absence of the Amarook Formation as a separate layer is useful, however, as it provides geological constraints for geophysical modeling. In particular it helps to define faults on the basis of its presence or absence, and

dips of up to 40° within the formation beneath the sub-horizontal Thelon sandstone unconformity indicate local block tilting.

At the margins of the Aberdeen sub-basin the Thelon Formation and Wharton Group unconformably overlie progressively older rocks, the first of these being gently folded almost unmetamorphosed sandstone, conglomerate and mudstone of Ps4 - the Itza Lake formation (informal name by Young, 1979). This and its equivalent in the Ketyet River Belt along the shores of Whitehills Lake contain clasts of the granitoid 1.83 Ga Hudson Suite and isoclinally folded clasts of Ps1 quartzite (Pehrsson et al, 2010). The highly deformed Ps1 through Ps3 supracrustal rocks are the lower ¾ of the Amer and Ketyet River groups, range in age from <2.3 to > 1.84 Ga (Pehrsson et al., 2013a) and are intruded by the Hudson granodiorite and contemporaneous Martell syenite (Rainbird et al., 2010). The Amer and Ketyet River groups unconformably overlie 2.6 Ga rhyolite, basalt and gabbro to granite of the Snow Island suite (SIS) (LeCheminant and Roddick, 1991; Peterson and Born, 1994; Davis and Zaleski, 1998), 2.8 to 2.68 Ga metavolcanic and metasedimentary rocks of the Woodburn Lake group (Pehrsson et al., 2013a) and the <2.628 Ga (V. McNicoll, personal communication, March 2013) Marjorie Hills assemblage (Jefferson et al., 2014a, b). The Neoarchean rocks are structurally intercalated with the early Paleoproterozoic Ps1 through Ps3 sequences of the Amer and Ketyet River groups. Inferred older Archean (but undated) orthogneiss and amphibolite are exposed in the Turqavik Horst, west of Marjorie Lake, northeast of Sand Lake Horst, and on the southeast side of the Marjorie-Tehek supracrustal belt. Together the 1.83 Ga and older granitoid and highly deformed crystalline and metamorphic complexes and supracrustal belts constitute the basement that flanks and underlies the Aberdeen sub-basin. The less deformed and sub-greenschist-metamorphosed <1.83 Ga Ps4 is also considered "basement" to this sub-basin, but is geophysically also transparent and its rock properties are essentially the same as those of the Amarook and Thelon formations.

The 1.83 Ga Hudson Suite granodiorite and Martell Syenite of the Schultz Lake Intrusive Complex (SLIC) form thin to thick sills (Peterson et al., 2002;Tschirhart, et al., 2013b) within the Neoarchean Marjorie Hills assemblage that includes layers of undated orthogneiss and flanks the southeast corner of the sub-basin. Around Kiggavik, thin mid-crustal sheets of Hudson granodiorite and small plugs of Hudson granite also cut the Pipedream assemblage of the Woodburn Lake group, and all of these rocks are cut by slightly younger bostonite (syenite) and minette (lamprophyre) dykes that are equivalent

to ultrapotassic volcanic flows of the Christopher Island Formation within the Baker Lake Basin.

The early Paleoproterozoic Amer and Ketyet River groups are structurally intercalated with Neoarchean supracrustal rocks of the SIS and Woodburn Lake group in two complex fold and thrust belts - the Amer and Marjorie-Tehek. The Amer fold and thrust belt is exposed along a 125 km strike length northeast of the sub-basin, expands from 25 km to 80 km in width toward the southwest, and is projected to underlie much of the Aberdeen sub-basin. The Amer Belt comprises four early Paleoproterozoic sequences whose stratigraphy was informally defined by Young (1979) and is still viable despite detailed structural studies that have documented extensive refolded thrusts and nappes (Calhoun et al., 2011, 2013). Ps1 is the Ayagaq Lake formation quartzite and conglomerate. Ps2 comprises the Resort Lake formation graphitic mudstone, siltstone and non-magnetic sulphide iron formation, Aluminum River formation dolostone and magnetic Five Mile Lake basalt (a distinctive aeromagnetic marker). Ps3 includes the Three Lakes formation mixed grey-green mudstone and siltstone with an upper unit rich in disseminated magnetite (a second distinctive aeromagnetic marker), Oora Lake formation arkosic sandstone with carbonate marker, and Showing Lake formation composed of alternating mudstone and calcareous sandstone with local uranium concentrations and one or more distinctive magnetic marker units (there may be just one marker here that was repeated by D1 folding). Ps1 through Ps3 were isoclinally deformed and profoundly eroded before being unconformably overlain by Ps4: Itza Lake formation grey to red sandstone with desiccation cracked red mudstone.

Ps4 is very much like the Amarook and the Thelon formations in being transparent aeromagnetically and weakly distinguishable seismically. For example interpretations by Davis et al. (2011) of seismic depth to “basement” from Overton (1979) were subjectively adjusted with high uncertainty where Ps4 is projected beneath the Aberdeen sub-basin because Ps4 is at sub-greenschist metamorphic grade, and the highly metamorphosed crystalline basement below it is probably the main reflector in those locations. Ps4 and the underlying strata were deformed by D2 that produced upright to inclined, open to tight, northeast trending folds that define the regional scale map patterns. D2 is also associated in the Meadowbank River area with peak metamorphism and the growth of monazite (Pehrsson et al., 2013a), although sharp lateral changes in

metamorphic grade to sub-greenschist as in Ps4 and the Baker Lake Basin indicate strong differential uplift.

Detailed mapping of the northeast portion of the Amer Belt has identified the specific stratigraphic sources of the above-described strong magnetic anomalies in the Five Mile Lake basalt and in siltstone of the Three Lakes and Showing Lake formations (Table 5.1; Calhoun et al., 2011, 2014). In all three units the high magnetic susceptibility is caused by disseminated euhedral magnetite concentrated along certain lithological units. These units are herein traced to the southwest on the evidence of their linear aeromagnetic signatures that continue beneath the Thelon Formation. These aeromagnetic marker units also are the basis of interpreting geophysically defined folds and faults that help determine the nature of the intervening lithologic units. Within the Showing Lake formation, sandstone-hosted uranium prospects have been targeted by exploration companies for decades (Miller and LeCheminant, 1985) and are potential source rocks for unconformity related deposits within the basement and sub-basin fill, at the sandstone-basement contact. The Amer Belt has been intersected by drilling that targeted conductive graphitic markers of the Resort Lake formation both external to and beneath the sub-basin (Young, 1979). The Amer Belt has been tentatively extended continuously beneath the axis of the entire Thelon Basin as far as its southernmost tip (Jefferson et al., 2011b) where it hosts the Boomerang Lake uranium prospect (Davidson and Gandhi, 1989).

The poorly known Turqavik Belt (new name) of presumed Neoarchean metasedimentary and metavolcanic rocks obliquely underlies the Amer Belt, with the SIS rhyolite is structurally intercalated with the Amer Group by thrusts and folds, and is tentatively included in the Woodburn Lake group (Jefferson et al., 2014b). Southeast of the Amer Belt, the Turqavik Belt forms the northwest flank of the Turqavik Horst. It has similar lithologic components to the Pipedream and Halfway Hills assemblages, such as metagreywacke, iron formation, komatiites and mafic to felsic volcanics, but there are no geochronological or geochemical data to support time correlation. A fringe of rhyolite between the Turqavik assemblage and the overlying Amer Group has been confirmed as part of the 2.6 Ga SIS (W. Davis, personal communication, May 2013).

The SW-NE trending Marjorie-Tehek Belt flanks the southeast margin of the Aberdeen sub-basin and the Turqavik Horst. It comprises three assemblages of the Woodburn Lake group overlain by volcanic and epiclastic facies of the SIS, and

terminates at its southwest end in the Marjorie Hills assemblage (Jefferson et al., 2014b). The Woodburn Lake group and SIS supracrustal rocks are structurally intercalated with Paleoproterozoic quartzite and grey schist of the Ketyet River group (Pehrsson et al., 2013a). A variant of the Pipedream assemblage of the Woodburn Lake group hosts the Kiggavik deposits and has a similar although distinct detrital zircon assemblage to that of the type Pipedream assemblage in the Meadowbank Belt to the northeast (V. McNicoll, personal communication, March, 2013). The other two assemblages of the Woodburn Lake group in the Marjorie-Tehek Belt include the Halfway Hills (oldest) and Amarulik (youngest). The SIS is represented by rhyolite that is locally preserved only at the interface between the quartzite and the Woodburn Lake group, as well as by epiclastic rocks that appear to form a belt flanking the southeast side of the SLIC. The Pipedream, SIS and Marjorie Hills supracrustal assemblages host all known potentially economic uranium deposits in the region (Jefferson et al., 2014a).

The Neoarchean Marjorie Hills assemblage extends in outcrop southwesterly from the Marjorie Hills, to past the southern edge of the map area. It is delimited on the west by the major ductile Marjorie Lake Fault, is separated from the SIS and Pipedream assemblages on the east by a gently west-dipping fault (Tschirhart et al, 2013b) and is preserved as rafts within the SLIC. South of the area of Figure 1 it has been identified by Peterson et al. (2014) as continuing through the east-central part of map sheet 65O. The Marjorie Hills assemblage is not included in the Woodburn Lake group for multiple reasons, the first being that as a field map unit it has a completely different appearance dominated by a lenticular gneissic fabric, and it is metamorphosed to the extent that it is barely recognizable as supracrustal. It is entirely metamorphosed to amphibolite grade and highly deformed, such that its interpretation as metasedimentary is based mainly on the presence of magnetite and silicate-sulphide iron formation layers (Hunter and Zaluski, 2011). It neither contains nor is intruded by any of the SIS phases and is structurally separated from the Woodburn Lake group on its east side by a major 020° structure. Its detrital zircon ages (V. McNicoll, personal communication, March 2013) have a small population at 2.628 Ga with the balance being ~2.672 Ga. That pattern is distinct from the polymodal populations with youngest zircons 2.680 Ga that characterize all the other metasedimentary assemblages that are included in the Woodburn Lake group. The Marjorie Hills assemblage appears not to be in contact with the Paleoproterozoic Ketyet River group, although vestigial highly metamorphosed and dismembered quartzite lenses

within it might be Ps1. The second author has observed a few instances of very poorly preserved, thick graded bedding disrupted by partial melt layers.

The Pipedream assemblage is of greenschist metamorphic grade in the Kiggavik area, comprises thinly bedded feldspathic wacke with minor magnetite iron formation and in places felsic metavolcanic rocks, and has much thinner, well preserved bedding and primary detrital textures compared to the recrystallized Marjorie Hills assemblage. Neither the Pipedream nor Marjorie Hills assemblages has a distinct geophysical signature, however, the latter is intruded by the SLIC which is manifested on the aeromagnetic map as a high amplitude magnetic anomaly criss-crossed by arrays of demagnetized zones related to faults. It was structurally emplaced on top of the Pipedream assemblage (Tschirhart, et al., 2013b) that includes SIS rhyolite and epiclastic rocks.

Neoarchean strata, with the exception of the Marjorie Hills assemblage, are intruded by granitoid rocks and overlain by volcanic phases of the 2.6 Ga SIS. Extrusive phases of the SIS are the youngest Neoarchean metavolcanic rocks mapped at the stratigraphic interface between the older Neoarchean assemblages and the quartzite at the base of the Paleoproterozoic Amer and Ketyet River groups. The SIS plutons are visible on the aeromagnetic map as high amplitude, broad oval anomalies exceeding 50 km width in places. Although highly faulted, the SIS plutons do not exhibit the same criss-crossed demagnetized pattern as the SLIC. Gravity and magnetic modeling suggest the SIS bodies are deep-rooted cylindrical plutons (P. Tschirhart, et al., 2013). Some of these plutons are exposed, such as at Judge Sissons Lake; others are inferred at depth based on their distinctive magnetic signatures.

Multiple dyke swarms transect the study area, most widespread being the northwest trending ~1.127 Ga Mackenzie diabase dikes that radiate from the Amundsen Gulf area (LeCheminant and Heaman, 1989). Three other dyke swarms are tightly constrained to corridors: the ~170 to 180^{o} and 015 to 025° trending McRae Lake diabase dykes (that represent the mafic trigger for the 1.75 Ga Nueltin suite granite (Peterson et al., 2010 and in prep.; Scott et al., 2010, 2012), and the ~075^{o} to 080° Thelon River diabase dyke array that has the same orientation as faults dextrally offsetting the McRae Lake dykes (Tschirhart, et al., 2013b) and is thought to belong to the same geochemical suite (Peterson et al., in prep.). The primary McRae Lake dyke swarm originates south of

the study area (LeCheminant et al., 1979; Buchan and Ernst, Peterson et al., 2014); its magnetic lineaments are evident through the Thelon Formation cover east of Aberdeen Lake before they cut across the Turqavik Horst, Turqavik and Amer belts, and continue well beyond to the northeast (Jefferson et al., 2013). A subsidiary swarm assumed to be part of the McRae Lake dyke event has a more northerly trend west of the Amer Plutonic Complex. The Thelon River dykes form two sub-parallel swarms axial to the Marjorie-Tehek and Amer supracrustal belts respectively.

Four fault arrays form the boundaries of the Aberdeen sub-basin (Figure 5.1), three of which are brittle reactivations of major ductile shear zones. All of the faults in these arrays have magnetic expressions because rocks within the fault zones have been variably demagnetized and/or are the places across which magnetic intensity abruptly changes (Tschirhart et al., 2013b, c). The faults also have expressions in surface topography visible in DEM, LANDSAT and air photograph images. Extensions of the faults beneath the Thelon Formation can be better constrained using newly available geophysical data (Tschirhart et al., 2013c). The brittle-reactivated curvilinear ductile shear zones of the ~050-060° Turqavik Fault and the eastern strand of the 040-060° Slave-Chantrey Mylonite Zone form the main boundaries with horsts on the east and west sides of the sub-basin, respectively. Pehrsson et al. (2013b) present evidence suggesting the Slave-Chantrey Mylonite Zone may have been reactivated with reverse offset as a far-field effect of the ~1.6 Ga Racklan Orogeny. Although much less demagnetized, the Turqavik Fault is visible on the aeromagnetic map as a sharp edge along the northwestern flank of the horst of Archean granitoid gneiss that trends southwestward beneath the sub-basin. On the aeromagnetic map the horst and its bounding faults continue southwesterly beneath the Thelon Formation. One fault demarking a portion of the southeast side of the Turqavik Horst is curvilinear, arcing 075-90° along the north shore of Schultz Lake before aligning sub-parallel to the Turqavik Fault, albeit much more subtly, on the east side of the Turqavik Horst. The Turqavik Fault has a long history. Early ductile mylonite connects it to a major shear zone crossing Meadowbank River to the northeast, and to the major Marjorie Lake shear zone. Late movement responsible for horst development in part follows the Turqavik Fault but also cuts straight across the sub-basin to the southwest, northwest of and en echelon with the Marjorie Lake shear zone.

The 075° Thelon Fault has a net right lateral offset of at least 18 km as measured by the offset of the SLIC, which comprises about 16 km of movement before intrusion of

the McRae Lake dykes and 2 km of right lateral offset of the McRae Lake dykes. It also has a dip slip offset of at least 400 metres, north-side-down (Davis et al., 2011), between gravity transects 1 and 2 of V. Tschirhart, et al. (2013a). Detailed study of this fault zone suggests an early ductile component followed by a series of later, more restricted brittle movements focused on its sharply defined southern side (Anand et al., 2012).

Two series of relatively straight dip slip faults are clearly identified as surface topographic lineaments trending ~090° and 120° (Figure 5.1). These lineaments are associated with outcrop defined offsets of mapped geological contacts in areas beside the basin, and as demagnetized structures cutting the SLIC (Jefferson et al., 2014a). At a more detailed exploration scale provided by very high resolution ground magnetic data these lineaments exhibit close spatial relationships to uranium zones (Hunter and Zaluski, 2011; Hunter et al., 2012). However the positions of these faults at depth where they should offset the basal unconformity surface cannot be determined without careful modeling of geophysical data. An assessment of one aeromagnetic data set by Tschirhart et al. (2013c) showed that edge detection methods can help locate and position such faults, particularly where they offset other basement linear features at high angles.

The 150° Mackenzie dyke swarm is spatially associated with and is parallel to major faults that significantly offset basement map units (Hadlari et al., 2004; Jefferson et al., 2014a, b). These were important in locally shaping the depth of preservation of the Thelon Formation and basement hosted uranium deposits, however it is assumed here that they were not active during the periods when the Thelon Basin was originally filled and when primary uranium deposits were formed.

One major ductile fault does not seem to have been significantly reactivated during or after deposition of the Thelon Formation. The Amer Mylonite Zone represents a 10 km broad, ~060° trending belt of highly strained to mylonitic rocks with multiple dextral and a later north-side-down dip slip offset as suggested by two features. First, a thick section of the upper Amer Group is preserved on the north side of the mylonite zone across from mid-crustal Hudson granite on the south. Second an upper crustal Nueltin rapakivi granite pluton is preserved on its north side but not on the south. The Nueltin plutons are interpreted as being relatively high crustal level because some have miarolitic cavities and many are pancake shaped such that basement structural magnetic patterns can be seen through them (Jefferson et al., 2013). In the case of the Amer Mylonite Zone it

can be reasonably assumed that the Nueltin granite was intruded straddling the mylonite zone as so some along the Snowbird Tectonic Zone (Jefferson et al., 2013; "Nueltin Irregular Plutons" of Hayward et al., 2013), however the Amer Mylonite Zone does not seem to have played a major role in defining or subdividing the Aberdeen sub-basin. It merely seems to have been a shallow valley area as suggested by a subtle tongue of Thelon sandstone projecting along it toward the northeast.

The entire area was glaciated with multiple ice flow directions during the last ice age, leaving a variable layer of till (McMartin and Dredge, 2005). Notable on the aeromagnetic map are short wavelength, low amplitude magnetic highs within the interior of the basin that are interpreted as drumlins, distinguished here by methods such as reported by Gay (2004). After the end of glaciation, some of the above described faults were reactivated yet again, as indicated by lineaments and low escarpments that in a number of places are visually striking as well as being clearly defined by a digital elevation model (Jefferson et al., 2011a).

5.4 Methodology

5.4.1 Data acquisition

The high resolution aeromagnetic data were acquired through a collaborative Letter of Agreement involving nine companies, McMaster University and the Geological Survey of Canada (GSC) under the Geomapping for Energy and Minerals (GEM) Program of the Earth Sciences Sector of Natural Resources Canada. The companies contributed their airborne geophysical data sets, in-kind support and shared geological and geophysical knowledge. The GSC acquired new geophysics (Harvey et al., 2011) by contracting out to Goldak Airborne Surveys, thereby filling data gaps prioritized by the consortium. The Industry partners were AREVA Resources Canada, Cameco Corporation, Bayswater Uranium, Forum Uranium, Uranium North, Mega Uranium, Titan Uranium, Western Uranium and Nunavut Tunngavik Incorporated. Flight line spacing for the different surveys ranges from 200 m to 400 m, and the Industry lines are oriented in a number of directions depending on the individual survey area. The high-resolution aeromagnetic data were merged to generate a contiguous high resolution aeromagnetic map that encompasses almost all of the Aberdeen sub-basin and surrounding exposed basement rocks. Remaining gaps were filled by stitching to regional

data obtained from the Canadian Geoscience Data Repository, thereby creating a final comprehensive map (Tschirhart et al., 2011a).

As part of the Northern Uranium for Canada Project under the GEM Program, detailed geological mapping projects in the exposed basement terranes (e.g. Calhoun et al., 2014; Jefferson et al., 2014a, b; McEwan, 2012, Peterson et al., 2014 and in prep.; Scott, 2012) documented lithostructural training areas with which to calibrate the geophysics, in particular to define the origins of aeromagnetic marker units, to characterize rock properties such as density and magnetic susceptibility, and to surface calibrate ground gravity transects for integrated structural modeling in exposed parts of the basement belts (e.g. Tschirhart et al., 2013a, b).

During the summers of 2010 and 2011, multiple ground gravity transects were acquired within and peripheral to the Aberdeen sub-basin. The station spacing along these lines ranges from 200 m to 1500 m. LaCoste and Romberg model G meter G0079 was tied to the Canadian Gravity Standardization Net through the gravity base station at Baker Lake, Nunavut; the meter has a reading resolution of 0.01 mGal. The vertical and horizontal locations of each station were calculated by differential GPS using a ProMark GPS and computed using GNSS Solutions. An elevation accuracy of better than 7 cm was determined for all measurements. Four of these transects were selected for the present study (Figure 5.2) and are described under Geophysical modeling below.

Petrophysical properties measured on samples, lithologic boundaries interpreted from edge detection maps (Tschirhart, et al., 2013c), and depth to basement as interpreted from seismic shot points (Overton, 1979) and industry drill-holes by Davis et al. (2011) also provided constraints for the geophysical models.

5.4.2 Data processing

From the aeromagnetic data compilation (Tschirhart et al., 2011a) a single data grid was generated using a 100 m grid cell. The data were reduced to the pole and then the tilt horizontal gradient (TDX) and Theta (TH) grids were computed (Wijins et al., 2005). After applying these source edge detection (SED) algorithms, anomaly maxima (contact source edges) were detected using the Blakely and Simpson (1986) spatial filter. These SED grids are shown in Figure 5.2 and were used in the subsequent contact mapping as detailed in section 5.5.2, and forward modeling as detailed in section 5.5.3 of this paper.

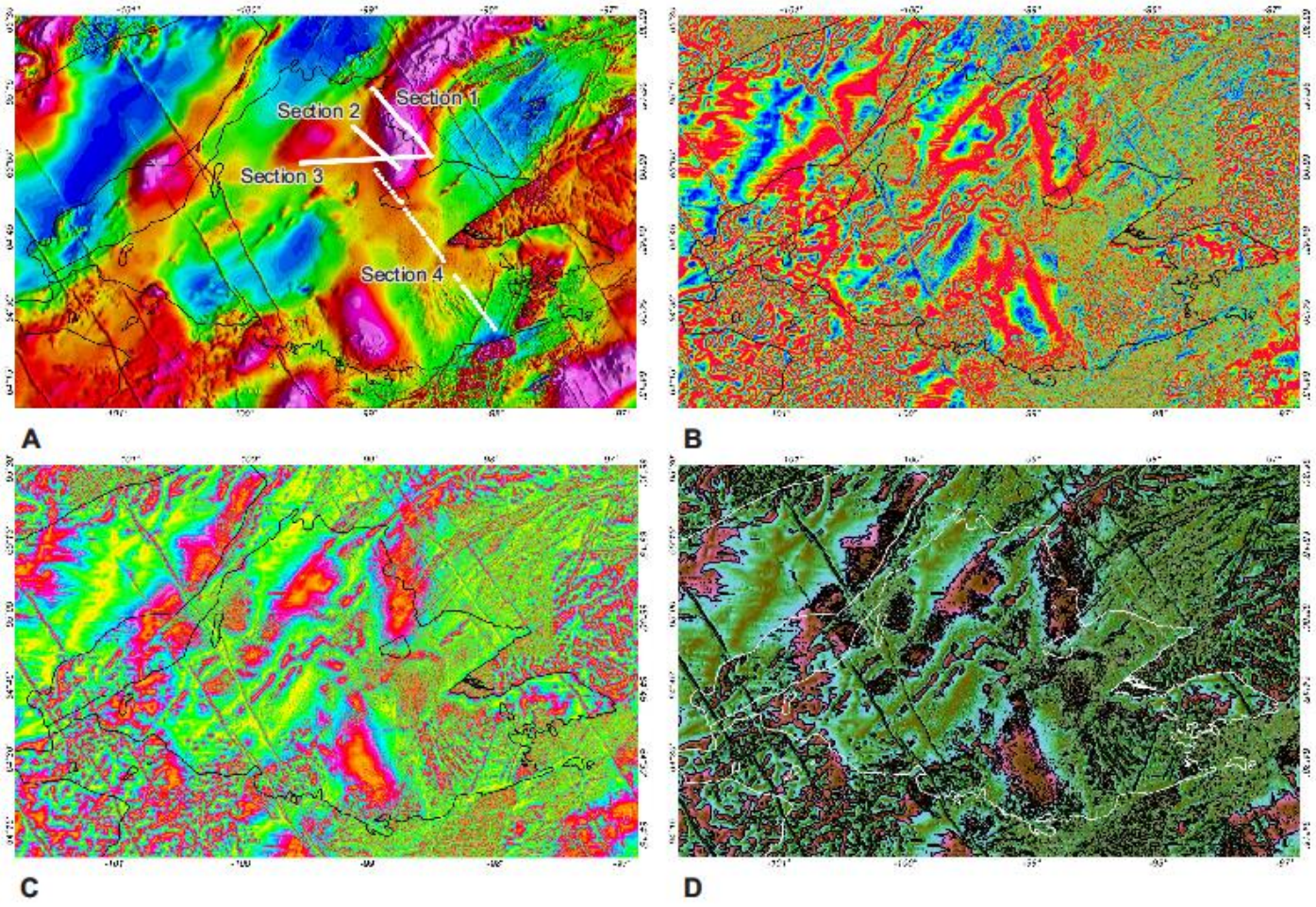
Section 1
Section 2
Section 3
Section 4
A
B
C
D

Figure 5.2 Aeromagnetic data and some low-resolution examples of derivative images of source edge detection grids. High resolution versions of the latter were integrated with other data sets in geospatial software to interpret basement geology. Outline of Aberdeen sub-basin is shown in black, white in 2d); width of view is ~240 km. a) Merged total magnetic intensity image. The locations of integrated magnetic-gravity-geology cross sections are labelled 1 through 4 for reference by subsequent figures, and locations of gravity stations are shown as white dots. b) Colour Theta grid. c) TDX grid (see Figure 5.4b for a detailed greyscale portion). d) Combined TDX pseudocolor image with 60% transparency over greyscale Theta intensity image – an expanded version of this is the background for Figure 5.3. Locations of Blakely and Simpson peaks are shown as black dots.

The ground gravity data were corrected for latitude, instrument drift, elevation and the Earth's tides, followed by application of the Free Air and Bouguer corrections. The data was reduced to a Bouguer slab density of 2.67 g/cc, which is assumed to represent the average density of the earth's crust. No terrain corrections were made as the topography of the area is relatively flat. A regional gravity grid derived from stations spaced 12-15 km apart was acquired from the Canadian Geoscience Data Repository. Values interpolated from this grid were subtracted from the profiles to calculate the residual signal, free of the long wavelength deep basement components. These data were used in all subsequent modeling.

5.4.3 Petrophysical analysis

Physical properties were measured on samples collected by GSC field personnel during the 2006 through 2011 field seasons (Table 5.1). Magnetic susceptibility was measured using a Terraplus KT-10 meter. Density was calculated using the standard Archimedes Principle submersion method. The heterogeneous lithology of many of the map units, together with variable levels of alteration, resulted in wide variations of physical property values. Statistical analysis was used to decide on the appropriate magnetic susceptibilities of these units for modeling (Table 5.1). For the gravity modeling, the density of each polyhedron was held to within 0.03 g/cc of the average value.

Table 5.1 presents mainly two distinct populations of high vs. low magnetic susceptibility. The strongly magnetic population includes: the magnetic marker unit in the upper part of Three Lakes formation (grey slate and schist, Amer Group), Five Mile Lake formation (tholeiitic basalt, Amer Group), mafic dykes (some of the McRae Lake and Thelon River dykes are very thin and thus have only moderate expression at the map scale), Hudson Suite granitoid rocks (especially Martell Syenite in the SLIC), banded iron formation, and mafic to ultramafic metavolcanic rocks (includes amphibolite). The low-magnetic group comprises units that are transparent on the aeromagnetic map: Thelon Formation, Amarook Formation of the Wharton Group, Ayagaq Lake and Itza Lake formation of the Amer Group, and metagreywacke of the Woodburn Lake group and the Marjorie Hills assemblage. Due to lack of exposure, no samples were obtainable for the inferred deep-seated magnetic phases of the SIS plutons or the Amer Mylonite Zone mafic bodies. Proxies were used to provide rock properties for these units as follows: the exposed SLIC granites for the SIS, and Archean amphibolite (metabasalt) for the inferred

deep seated gabbros flanking the Amer Mylonite Zone. Exposed leucocratic portions of the SIS plutons are only weakly magnetic, although these coincide geographically with some of the inferred deeply seated magnetic phases. The abundant bostonite and lamprophyre dykes are weakly to moderately magnetic and have generally low to moderate map-scale expressions that are traceable only with high-resolution data, yet are important to this study because of the large contiguous high-resolution shared data set.

5.4.4 Geophysical modelling

Many lithological units can be distinguished by their magnetic and density characteristics (Table 5.1), especially in their mapped context. Some petrographically different units, like the highly metamorphosed Marjorie Hills assemblage and the greenschist grade Pipedream assemblage, have very similar geophysical properties and therefore cannot be separated on the basis of geophysical signatures alone. Lithostructural marker horizons are particularly useful for tracing contacts on the aeromagnetic map from areas where they are constrained by outcrop (e.g. Calhoun et al., 2014; V. Tschirhart et al., 2013a) to areas where they are deeply buried beneath the Thelon Formation. Magnetically transparent sandstone of the Itza Lake and Thelon formations permit recognition of magnetic anomaly patterns related to the underlying basement rock units. Nevertheless, as a consequence of the increased distance between the basement source and the airborne sensor, the observed basement signal response is dampened and the location of a contact is defined less precisely beneath the Thelon Formation than beneath shallow glacial till with scattered outcrop.

The signal dampening effect makes it difficult to trace the exact extents of lithological units beneath the interior of a basin, especially where the siliciclastic strata are greater than 1000 m thick (Tschirhart et al., 2011b). One approach to addressing this problem is to employ filtering procedures that accentuate the bounding edges of source bodies. SED methods have been used extensively as a predictive tool for lithological contact mapping where there is limited or no exposure (Pilkington and Keating, 2009). Provided there is sufficient contrast between physical properties of the adjacent units, a SED algorithm will generate a peak at the magnetic inflection point, defining the "source edge". This procedure enhances signatures related to subtle contrasts in the aeromagnetic image. The main aeromagnetically traceable units and broad aeromagnetic features in this study are sharply defined by the TDX grid (Figure 5.2, 5.4). The calculated Theta max represents a source edge that is bracketed by two 0 values (Wijins et al., 2005). By

examining the Theta grid interpreters can see subtle contrasts within highly magnetic units that are not emphasized in the TDX grid. By displaying the two images together, the TDX grid highlights source edges while the Theta grid enhances compositional differences within source bodies. Where there is no sharp contrast; the shape, texture, structural style and in many cases the continuity of an anomaly from outside the sub-basin give key insights into what lithologic unit(s) the anomaly might represent (Holden et al., 2008; Pilkington and Keating, 2009). Clearly multiple interpretations are possible and this is an exercise in geophysically constrained remote predictive mapping.

Some of the gravity transects obtained in 2010 and 2011 have already been used to enhance geological and calibrate geophysical knowledge in areas outside the Aberdeen sub-basin: at the north end of the Amer Belt (V. Tschirhart et al., 2013a), and across the Schultz Lake Intrusive Complex (Tschirhart et al., 2013b). Cross Section 1 of this study (Figures 5.2, 5.3, 5.4) transects a relatively well exposed and geologically mapped part of the Amer Belt dominated by Ayagaq formation quartzite that constitutes a strong visual and structural marker unit. Cross Sections 2 and 3 are located along the same structural trend as Cross Section 1 but were obtained over flat lying Thelon Formation sandstone of the Aberdeen sub-basin, designed to extend basement knowledge from nearby Cross Section 1 to the basement beneath the Thelon Formation sandstone. Cross Section 4 is a reconnaissance transect also across flat lying Thelon Formation, extending from the detailed area of Cross Sections 1 to 3, southeast almost to the Thelon Fault where it can be linked directly to modeling of the Schultz Lake Intrusive Complex and the Thelon Fault by Tschirhart et al. (2013b).

The current study employs forward gravity modeling. We generated a series of lithologic polyhedra with predefined physical properties integrated into 2D geological cross-sections along the four selected transects (Figure 5.2). The geometries of the polyhedra on each transect cross section were initially constrained by surface observations of lithology, structural geometry, contacts and their geophysical responses (e.g. Calhoun et al., 2014, V. Tschirhart, et al., 2013a, b).

GM-SYS Solutions^{TM} software was used to compute the forward potential field models. The initial set of polyhedra was individually and iteratively modified to obtain the best fit between the observed and computed gravity signals in keeping with known structural styles from outcrop mapping. Additional constraints on the possible depth

extent and subsurface morphology of a model source body were provided by the density, and by the positions of the unconformity at the base of the Thelon Formation from boreholes (Davis et al., 2011) and/or seismic shot points (Overton, 1979). The root mean square (RMS) error was kept to <0.5 mGal. The area is extensively till covered, but the wide station spacing along the profiles did not permit discrimination of thin (less than ~10 m) till deposits and therefore till was not modeled. This approach was reinforced by the findings of Thomas and Wood (2007, p. 457) in the analogous Athabasca Basin that "sources of short wavelength anomalies may relate to density changes within the stratigraphic sequence rather than variations in overburden thickness".

To delineate the contacts in the remote predictive map of basement geology beneath the Thelon Formation, either fault or lithologic, a number of features present on the map were utilized: a) offsets of linear magnetic boundaries, b) continuity of magnetic lineaments, c) magnetic textural continuity and d) cross-cutting relationships. Further constraints on extrapolating lithologic units were provided by magnetic susceptibility as measured on the units listed in Table 5.1.

5.5 Results

5.5.1 Physical properties

The remote predictive geological map of the basement surface below the Aberdeen sub-basin (Figure 5.3) was begun by interpretation of magnetic anomaly patterns associated with, and detailed ground gravity transects across, basement lithostructural belts. Prior to interpreting the geology it was imperative to gain a thorough understanding of the susceptibility distribution of each unit to establish which formations are capable of producing dependable, regionally traceable anomaly patterns. As the Thelon Formation has weak magnetic susceptibility (Table 5.1), and hence for modelling considerations is essentially non-magnetic, it contributes little to the observed magnetic signal. The thickness of the Thelon Formation does however directly contribute to the distance between the airborne acquisition system and the magnetic sources in the basement. Increased distance between the source (magnetic basement) and sensor effectively dampens the observed signal. It is quite possible that anomalies associated with some stratigraphically thin, or weakly magnetically contrasting units are effectively obscured by the increased source-sensor separation. Locally some iron-rich strata are present within the Thelon Formation, but these strata are flat-lying, generally thin and

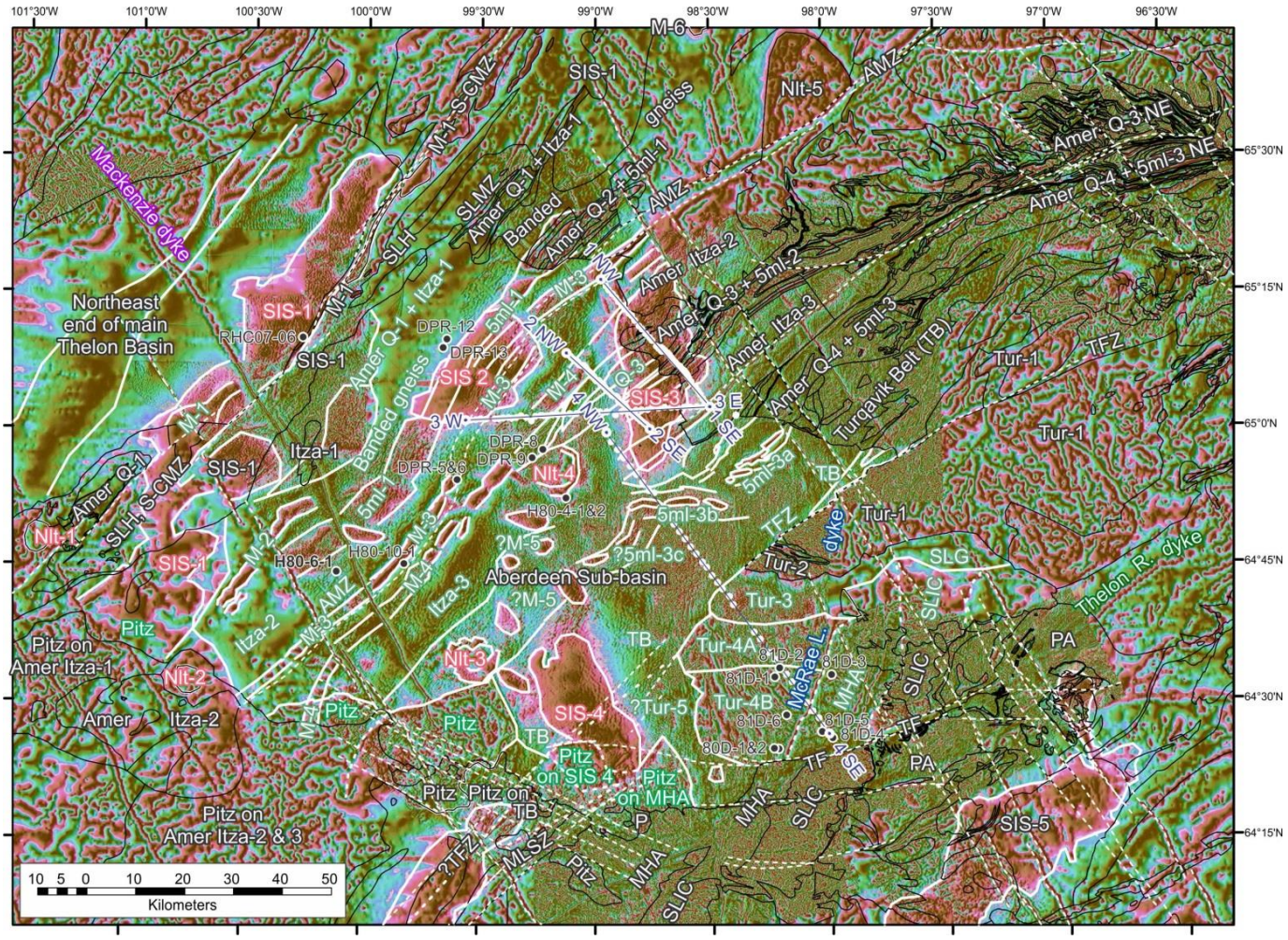
101°30'W
101°0'W
100°30'W
100°0'W
99°30'W
99°0'W
98°30'W
98°0'W
97°30'W
97°0'W
96°30'W
65°30'N
65°15'N
65°0'N
64°45'N
64°30'N
64°15'N
M-6
SIS-1
NIt-5
AMZ
Amer. Q-3 NE
Amer. Q-4 + 5ml-3 NE
Mackenzie dyke
M-1
S-CMZ
SLH
SLMZ
Amer Q-1 + Itza-1
Banded gneiss
Amer Q-2 + 5ml-1
Amer Itza-2
Amer Q-3 + 5ml-2
Amer Itza-3
Amer Q-4 + 5ml-3
Turqavik Belt (TB)
TFZ
Tur-1
Northeast end of main Thelon Basin
RHC07-06
DPR-12
DPR-13
SIS 2
3 W
3 E
DPR-8
DPR-9
DPR-5&6
Itza-1
NIt-4
H80-4-1&2
5ml-3a
5ml-3b
?5ml-3c
TB
TFZ
dyke
Tur-2
SLG
Thelon R. dyke
NIt-1
H80-6-1
H80-10-1
?M-5
Aberdeen Sub-basin
Itza-3
Itza-2
Tur-3
SLIC
PA
Pitz
Pitz on Amer Itza-1
NIt-2
NIt-3
Tur-4A
81D-2
81D-1
81D-3
McRae L.
MHA
Amer
Itza-2
Tur-4B
?Tur-5
81D-6
81D-5
81D-4
TF
SIS-4
80D-1&2
TF 4 SE
Pitz on SIS 4
Pitz on MHA
Pitz on TB
P
Pitz on Amer Itza-2 & 3
?TFZ
MLSZ
SIS-5
10 5 0 10 20 30 40 50
Kilometers

Figure 5.3 Base image is TDX grid 60% transparency over grey scale Theta grid. The outline of the Aberdeen sub-basin and previously mapped geological contacts and labels outside of it are in black (after Jefferson et al, 2014a, b). Newly mapped geophysical units in white are mainly beneath the sub-basin. Some new units or trends extend outside the basin where exposure is poor, where the new unit is projected from beneath a similarly transparent unit such as the Itza Lake formation, or where the geophysical trend differs from the previous reconnaissance geological map. Dashed white lines trace the locations of major block faults as well as shear zones that were reactivated as brittle trans-extensional faults. The Aberdeen sub-basin is separated from the main Thelon Basin by the Sand Lake Horst (SLH) which is flanked by reactivated faults of the Slave-Chantrey Mylonite Zone (S-CMZ). Labelled magnetically defined components are numbered in sequence from west to east, as follows. Nlt 1 to 4 = 1.75 Ga plugs of Nueltin Granite inferred to core volcanic ring structures and Nlt 5 = large exposure of Nueltin rapakivi granite. SIS 1 to SIS 5 = 2.6 Ga plutons projected through overlying Neoarchean to Paleoproterozoic supracrustal belts. M 1 to 4 = mafic phases of SIS (all projected from depth except for M 1). Amer Q1 to 4: 2.2-1.9 Ga belts of Ps1 quartzite through Ps3 mudstone, some including Five Mile Lake (5ml 1 to 3) basalt. The isoclinally D1 folded Amer Q belts were unconformably overlain by and refolded along with Ps4 sandstone and mudstone labelled Amer Itza 1 through 3. The Turqavik Horst (segments = Tur 1 to 5) is flanked on the northwest by the Turqavik Belt (TB) and on the southeast by the Marjorie Hills assemblage (MHA), Schultz Lake intrusive complex (SLIC) and Schultz Lake Graben (SLG). The label “Pitz” refers to flat lying bimodal volcanic rocks dated as 1.75 Ga along the south side of the sub-basin. These units are explained in detail in the text. The area encompassing gravity sections 1, 2, 3 and the northwest end of 4 is detailed in Figure 5.4.

composed of hematite so they do not usually produce magnetic anomalies. All attributes considered, the Thelon Formation is virtually transparent magnetically (cf. Thomas and McHardy, 2007 for the comparable Athabasca Group). The Amarook Formation sandstone and Itza Lake formation sandstone and mudstone are also weakly magnetic (Table 5.1) and gently dipping, and therefore indistinguishable from the Thelon Formation on the aeromagnetic map. Other non-magnetic stratigraphic units within the Amer Group were involved in both D1 and D2 deformation events, and generally have steep dips. These are distinctive on the aeromagnetic map because of their deeply negative aeromagnetic anomalies particularly in contrast to the adjacent high susceptibility units. Some short-wavelength (in the order of 200 m), low-amplitude anomalies associated with variations in thickness of detrital magnetite-bearing glacial till are visible on the map and are particularly evident in the area between the labels for Cross Sections 3 and 4 in Figure 5.2a and Figure 5.2c, but these anomalies just add texture to the underlying units rather than masking them. They do increase the distance between source and sensor, but only by marginal and local amounts because the till depth is generally less than 10 m (McMartin and Dredge, 2005). The longer wavelength, higher amplitude magnetic units visible on the aeromagnetic map are thus attributed to the magnetic basement units under consideration for mapping (Table 5.1).

5.5.2 Geological map of basement to the Aberdeen Sub-basin

Six main magnetically calibrated components characterize the basement geology of the Aberdeen sub-basin, and are outlined by white lines on Figure 5.3. The first component is highly granitoid plutons of the 2.6 Ga SIS - broadly spaced, oval features that have “magnetically domal” signatures – i.e. intensely magnetic in a broad central portion with gradational magnetic “edges” whose shapes are independent of detailed outcrop patterns. The focus in this paper is on the isolated ellipses with dimensions of approximately 30 x 15 km, labelled SIS 1 through SIS 5 from west to east on Figure 5.3. These are explained in detail in the following section, as are the magnetic expressions of 1.75 Ga Nueltin Granite bodies in the same region. The 1.83 Hudson Granite, most prominent in the SLIC, is modelled in a previous study (Tschirhart et al., 2013b) and does not play a key role in this study. The second major magnetically calibrated component is the Amer Group which is exposed mainly northeast of the Aberdeen sub-basin in four northeast trending belts described in detail in section 5.5.2.2. Other distinct magnetic components modelled and traced in the current study include the sharply defined

Turqavik Horst and Turqavik Fault (section 5.5.2.3); the Amer Mylonite Zone and highly magnetic oblong features interpreted as mafic intrusions along the Amer and Slave-Chantry mylonite zones (M-1 through M-5 on Figure 5.3); and the Neoarchean Turqavik and Marjorie Hills assemblages that have overall low aeromagnetic signatures. The local irregular magnetic iron-formations within these assemblages are useful for confirming their supracrustal natures. As noted in the following discussion of the SIS plutons, the south side of the Aberdeen sub-basin is largely blanketed by 1.75 Ga Pitz Formation volcanic rocks that have an overall moderate but dappled magnetic anomaly pattern (Pitz, Figure 5.3) which tends to obscure underlying magnetic units.

5.5.2.1 Granitoid intrusions

The most dominant geophysical anomalies on the aeromagnetic and SED images are attributed to the 2.6 Ga SIS granite intrusions (SIS 1 through SIS 5 on Figure 5.3). Their broad domal magnetic anomalies reach some 550 nT above background, and their sizes range from 25 to 40 km in length and 15 to 25 km in width. SIS 1 has been documented as a major swath along the S-CMZ by LeCheminant et al. (1984) and Tella et al. (1984), and SIS 5 was mapped and compiled in outcrop by the second author and T. Peterson after Hadlari et al. (2004). At the northeast end of SIS 5 a deeper satellite pluton was modeled and inferred to be also SIS by P. Tschirhart et al. (2013). The present study focuses on SIS 2, 3 and 4 which do not outcrop, and compares their gravity signatures and their high amplitude magnetic anomalies with portions of SIS 1 and SIS 5.

The actual area of outcrop (or subcrop beneath Thelon Formation) for these plutons varies depending on the crustal level of erosion but many are unexposed, and the mapped outcrop areas where they are exposed tend to be smaller than the sizes of their aeromagnetic footprint – i.e. the bulk of the strongly magnetic bodies is in the subsurface. A broad area labelled SIS 1 constitutes a nearly continuous swath of granite with local aeromagnetic highs representing more mafic phases distributed along the Slave Chantry Shear Zone, exposed in the Sand Lake Horst and to the north. All of the SIS 1 batholith components as well as vast expanses of non-magnetic SIS phases are exposed in basement uplifts like the Sand Lake Horst, although the northern magnetic part of SIS 1 west of the horst is covered by the Thelon Formation. In the Judge Sissons Lake area (southeast corner of Figure 5.3) about 1/3 of the highly magnetic portion of SIS 5 pluton is exposed, the balance being covered by metavolcanic rocks and gneiss. A satellite SIS pluton northeast of SIS 5 has been modelled as terminating several hundred metres below

surface, below a klippe and with no known surface geological expression (P. Tschirhart, et al., 2013).

The large exposed SIS plutons are known to have smaller (~ 4 km diameter) components that are parts of sub-circular composite 2.6 Ga intrusions south of the northeast Amer Belt, originally mapped by Tella et al. (1984, 1994) and Zaleski (2005) as Archean or Proterozoic. Work by T. Peterson, J. Scott and B. Davis (personal communication, 2012) has documented their 2.6 Ga age as well as a range in compositions from gabbro to granite that have the same differentiation trend as larger exposed SIS plutons such as SIS 5. The highest magnetic intensities are spatially associated with the gabbro phases. The contact zones of these plutons are a very characteristic xenolith-choked agmatite in equigranular dioritic matrix.

SIS 2, SIS 3 and SIS 4 plutons are interpreted herein to be deeply buried beneath other basement rocks and not to be in contact with the unconformity at the base of the Thelon Formation, except possibly SIS 4. The SIS 3 pluton extends north beyond the sub-basin to underlie the Amer belt (Amer Itza-2, Amer Q-3 + 5ml-2 and Amer Itza-3). Lithologic interpretation of the sparse outcrops of granitoid rocks in this area is difficult and geochronological data are unavailable, however the continuity of aeromagnetic lineaments of the Amer Group from northeast to southwest across this pluton (Figures 5.2, 5.3, 5.4) and gravity modeling (Figure 5.5) require that it culminates at least 1.5 km below surface outside the Aberdeen sub-basin. At the south end of SIS 3 distinct linear magnetic anomalies interpreted as Showing Lake formation can be traced beneath the Itza Lake formation and across the pluton (Figure 5.4b), thus at least both of these formations mantle the pluton. Two antiforms above SIS 3 do expose foliated granodiorite that might be SIS, but also exposed are banded gneiss and amphibolite that are clearly not SIS in the middle of Cross Section 1 (Figure 5.4). Furthermore the density of the granitoid gneiss in the antiforms is greater than that of SIS granitoids exposed elsewhere. The outcrops in the antiforms are thus constrained as being geometrically above the aeromagnetically interpreted SIS 3 pluton. This geometry can be interpreted in at least two ways. A simple hypothesis would be that the SIS pluton simply intruded the gneiss and amphibolite but its magnetic portion does not reach the surface. A more complex hypothesis derives from mapping elsewhere in the area of Figure 5.3 that shows the Archean granitoid and supracrustal rocks in the northeast Thelon region to be structurally intercalated with early Paleoproterozoic rocks (e.g. Calhoun et al., 2014; Jefferson et al., 2014a; Pehrsson et al.,

2013a). Structural relationships include SIS granitoid rocks as broad sheets thrust over supracrustal rocks (Thomas, 2012). Thus in the area of Figure 5.4 the gravity data are compatible with the hypothesis that there is a structural detachment between the granitoid gneiss and the underlying SIS pluton, and that all of these rocks including the detachment were uplifted by the broad F2 antiform mapped in the middle of Cross Section 1. Further sampling, geochemistry and geochronology of the surface foliated granitoid rocks would be required to test this hypothesis (only one sample was obtained and that was paleo-weathered beneath the Amer quartzite so its geochemistry is unreliable).

A different set of contextual knowledge in the southern part of the Aberdeen sub-basin is used to infer depth to the top of the SIS 4 pluton. In this region the Pitz Formation is mapped in outcrop along the southern flank of the Aberdeen sub-basin where it has a dapple textured aeromagnetic anomaly pattern. The Pitz Formation in outcrop is flat lying and forms a thin cover on highly deformed basement (Figure 5.3: Pitz on Amer Itza-2&3, Pitz on TB, Pitz on MHA). The dappled magnetic texture continues beneath the Thelon Formation where it is interpreted as a continuation of Pitz Formation being the geological unit located immediately below the Thelon Formation, and as such covering the southern part of the SIS 4 pluton (Pitz on SIS 4, Figure 5.3). The resulting interpretation is that only a small irregularly shaped portion of the SIS 4 pluton is present as subcrop beneath the basal unconformity of the Thelon Formation, analogous to the irregular exposure of SIS 5.

Nlt4 is a distinct semi-circular anomaly located near the centre of the sub-basin (Figures 5.3, 5.4). It consists of an eastern rim and central magnetic low. This is interpreted as a 1.75 Ga Nueltin granite plug surrounded by a volcanic-related gabbro ring structure analogous to one documented at Mallery Lake (T. Peterson in Jefferson et al., 2013; Peterson et al., 2014 and in prep.). The surrounding drill holes provide few insights on this body. DPR-8 intersected Amarook Formation between the base of the Thelon Formation at 94.3 metres and the underlying Itza Lake formation at 139.75 metres (Davis et al., 2011) with no Pitz volcanic rocks as found around the Mallery Lake ring structure, however DPR-8 is located west of a linear aeromagnetic truncation of the Nlt4 ring, interpreted as a fault, and therefore is not a true test of whether or not Pitz Formation is present, let alone gabbro as interpreted from the anomaly. An indication of the uncertainty in this area is given by DPR-9 that was spudded just 2 km to the southwest, and cored 470 m of Thelon Formation sandstone without reaching basement, more direct

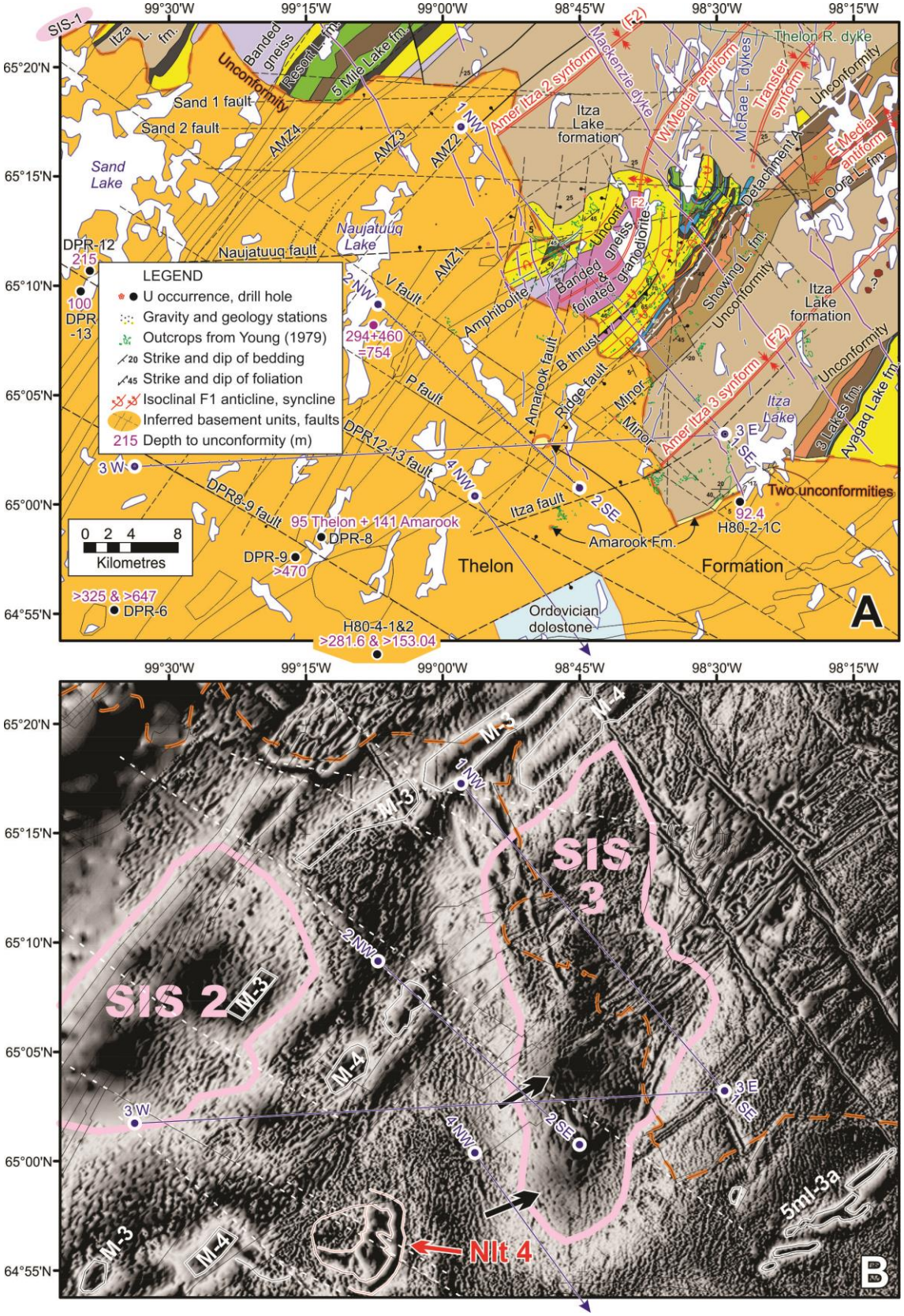
99°30'W
99°15'W
99°00'W
98°45'W
98°30'W
98°15'W
65°20'N
65°15'N
65°10'N
65°05'N
65°00'N
64°55'N
SIS-1
Itza L. fm.
Banded gneiss
Resort L. fm.
5 Mile Lake fm.
Unconformity
Sand 1 fault
Sand 2 fault
AMZ4
AMZ3
AMZ2
AMZ1
1 NW
Ameri Itza 2 synform
Mackenzie dyke
(F2)
Itza Lake formation
W. Medial antiform
McRae L. dykes
Transfer synform
Thelon R. dyke
Unconformity
E. Medial antiform
Detachment A
Oora L. fm.
Sand Lake
Naujatuuq Lake
Naujatuuq fault
DPR-12
215
100
DPR-13
2 NW
V fault
294+460 -754
Amphibolite
Banded gneiss & foliated granodiorite
Unconf.
F2
Showing L. fm.
Unconformity
Itza Lake formation
Unconformity
P fault
Amarook fault
B thrust
Ridge fault
Minor
Minor
Ameri Itza 3 synform
(F2)
Itza Lake
3 E
1 SE
3 Lakes fm.
Avagaq Lake fm.
3 W
DPR12-13 fault
4 NW
DPR8-9 fault
Itza fault
2 SE
Two unconformities
92.4
H80-2-1C
95 Thelon + 141 Amarook
DPR-8
DPR-9
>470
Amarook Fm.
Thelon
Formation
>325 & >647
DPR-6
Ordovician dolostone
H80-4-1&2
>281.6 & >153.04
A
LEGEND
U occurrence, drill hole
Gravity and geology stations
Outcrops from Young (1979)
Strike and dip of bedding
Strike and dip of foliation
Isoclinal F1 anticline, syncline
Inferred basement units, faults
Depth to unconformity (m)
0 2 4 8
Kilometres
M-3
M-4
SIS 3
SIS 2
Nlt 4
5ml-3a
B

Figure 5.4a Maps detailing the context of gravity sections 1, 2 3 and the northwest end of section 4; location outlined in Figure 5.1. a) Surface geology. Map units are labelled once each, except the Aluminium River formation (deep blue). b) Grey scale TDX image base shows enhanced aeromagnetic textures and structures described in text. The edge of the Aberdeen sub-basin is shown by dashed orange line. Black arrows show where linear aeromagnetic units of the Three Lakes and Showing Lake formations can be traced over the deeply buried SIS 3 pluton (outlined in pink straddling the northeast margin of the Aberdeen sub-basin) both in outcrop to the northeast and beneath the Thelon Formation sandstone to the southwest (details in text). Dashed white lines are selected examples of interpreted cross faults. Black lines with white backing outline discrete highly magnetic features interpreted as mafic intrusive (M3, M4) or volcanic rocks (5ml-3a).

evidence of significant fault offsets. The two drill holes south of this anomaly (H80-4-1 & 2) also did not reach basement.

A similar but more attenuated aeromagnetic dimple beneath Aberdeen Lake at is labelled as Nlt3 - another possible Nueltin ring candidate. Finally, previous modeling by the first author (reported by Jefferson et al., 2013) inferred the presence of Nueltin rings at Nlt1 (Akiliniq Hills) and Nlt2 (Beverly Lake). The Nlt1 and Nlt2 rings are spatially associated with bimodal Pitz volcanics but their existence at this point is solely based on geophysics because of poor outcrop and limited field mapping. In each case the geophysical model for the Nueltin rings requires a circular aeromagnetic high ringing a circular relative aeromagnetic low that is at or below background value.

5.5.2.2 Amer Belt

The Amer Group forms four southwest-plunging synformal belts that are traced geophysically beneath the Thelon Formation cover in Figure 5.3. The northwestern two belts are defined by discrete quartzite map units and labelled "Amer Q-1 + Itza-1" and "Amer Q-2 + 5ml-1", respectively. They are poorly known and both are partly covered by Itza Lake formation (Itza 1). The next two belts are large synforms (Itza 2 and Itza 3) cored by Itza Lake formation on opposite sides of a medial antiform with a spine of Ayagaq formation quartzite that includes Five Mile lake basalt infolds (Amer Q-3 + 5ml-2). The F2 medial antiform is a composite en-echelon feature with several components illustrated in Figure 5.4a: West medial antiform, Transfer synform and East medial antiform. These major F2 synform-antiform structures are defined in outcrop in the main Amer Belt on the north side of the sub-basin where Jefferson et al. (2014b) applied the same structural style as established at the northeast end of the Amer Belt by Tschirhart et al. (2013c) and Calhoun et al. (2014). The broad Itza 2 synform is cored by Itza Lake formation and flanked by the Amer Mylonite Zone on the northwest. On the southeast side of the West medial antiform the Itza 3 synform is also cored by Itza Lake formation and is completed by quartzite and basalt (Amer Q-4 + 5ml-3) along its southeastern flank. These two synforms and the medial antiform constitute the main Amer Belt as labelled in Figure 5.1.

The Itza Lake formation forms only small outliers in the northeastern part of the Amer Belt, expands significantly toward the southwest in outcrop as the two synforms deepen, and is interpreted to coalesce into a single swath blanketing the older units

beneath the Aberdeen sub-basin. The Itza Lake formation is the only part of the Amer Group that is exposed on the south side of the sub-basin, in an oval region labelled "Amer Itza-2". The inferred presence of older Amer Group units beneath the Itza Lake formation along the southwest side of the sub-basin cannot be verified due to the extensive cover of the Pitz Formation whose dappled aeromagnetic texture obscures fine underlying magnetic signals. The westernmost part of the Amer Group in the study area is a relatively well exposed and mapped (LeCheminant et al., 1984) outlier (Amer Q-1) resting on SIS rhyolite and granite on the west side of the Sand Lake Horst in the extreme west-centre of Figure 5.3. A poorly exposed inlier of uppermost Amer Group is entirely surrounded by Thelon Formation near the west side of Aberdeen sub-basin (Itza-1). A northwestern belt of Amer Group centred at 100° west was not included in this study, except for being subjectively extrapolated beneath the main Thelon Basin west of the Sand Lake Horst.

In Figure 5.3 the three belts cored by Itza Lake formation are extrapolated southwesterly beneath the Aberdeen sub-basin based on subjective analysis of aeromagnetic data, incorporating constraints from SED (Tschirhart et al., 2013c) and from four integrated gravity-magnetic-geological transects (figures 5.5, 5.6, 5.7, 5.8) whose positions are located on Figures 5.2, 5.3 and 5.4. The "Amer Q-1 + Itza-1" belt trends southwesterly beneath an area of the sub-basin where only low resolution regional aeromagnetic data are available, and the first outcrop along trend is the "Itza-1" inlier interpreted as a horst bounded by faults on all sides. The northwestern flank of the "Amer Q-1 + Itza-1" belt for extrapolation purposes is the weakly foliated SIS-1 granite as exposed along the Sand Lake Horst. The southeastern flank is defined by the next belt: "Amer Q-2 + 5ml-1" that is extrapolated beneath the sub-basin as "5ml-1" starting from distinct linear aeromagnetic highs in its poorly exposed portion north of the Aberdeen sub-basin. These linear aeromagnetic highs are traced toward the southwest under the sub-basin as far as a Mackenzie diabase dyke, just west of drill hole H80-8-1. The "5ml-1" magnetic high is terminated at that Mackenzie dyke which is interpreted as occupying a major block fault with southwest side down. The inferred 5ml-1 basalt is there interpreted to be deeply buried by siliciclastic rocks of the Itza Lake formation which is the only Amer Group unit exposed south of the sub-basin.

As noted above the main exposed part of the Amer Belt is subdivided into two large synforms separated by a medial antiform, grossly separated from northwest to

southeast into four components: Amer Itza 2 (synform), Amer Q-3 + 5ml-2 (antiform), Amer Itza-3 (synform), and Amer Q-4 + 5ml-3 (southeast flank of the main belt). The main Amer Belt is flanked on the northwest by the Amer Mylonite Zone (AMZ on Figure 5.3) and on the southeast by Neoarchean supracrustal rocks: the 2.6 Ga SIS rhyolite and undated metasedimentary-metavolcanic rocks of the Turqavik Belt. The main Amer Belt is extrapolated southwesterly beneath the sub-basin as Itza-2 and Itza-3, with the Q-3 quartzite medial antiform interpreted as plunging and closing off toward the southwest where it is buried by Itza Lake formation beneath the Aberdeen sub-basin. The southeast limb of the Amer Itza-3 synform is also the southeast side of the main Amer Belt, mapped beneath the Thelon Formation by tracing a belt of aeromagnetically distinct basalt infolds (5ml-3) within the Ayagaq formation quartzite. The main Amer Belt is a key focus of the northeast Thelon region compilation (Jefferson et al., 2011b) and of this study.

On the southeast flank of the Amer Q-3 medial antiform, the weak magnetic nature of Itza Lake formation and the overarching signal of the SIS granite make it difficult to trace the very detailed magnetic striping of the Three Lakes and Showing Lake formations (Figure 5.4b) much further than 5 to 10 km beneath the sub-basin margin. Nevertheless it is possible to discern an inflection in these structural trends as they cross the SIS 3 magnetic high in outcrop and continue beneath the Thelon Formation until they fade out toward the southwest with increasing thickness of the sandstone (Figure 5.4b). The deep SIS 3 pluton may have served as a buttress against deformation resulting in a strain gradient from its interior to its exterior that caused the en echelon arrangement of the medial antiform in the area of Figure 5.4, which includes inflection of the Three Lakes and Showing Lake magnetic stripes, although the current interpretations (Figures 5.4, 5.5, 5.6, 5.7) invoke structural detachment between the deep pluton and the upper exposed panel of Amer Group with its immediate basement of inferred older Archean granitoid gneiss. As noted above, this is only one possible interpretation

In the broad "Amer Itza 3" synform the Itza Lake formation is a magnetically translucent axial window through which can be seen the above-noted magnetic striping of underlying units of the Amer Group. These are inferred to be Showing Lake and Three Lakes formations based on detailed work at the northeast end of the Amer Belt (Calhoun et al., 2014; Tschirhart, et al., 2013b) and the middle of the belt (Young, 1979). This magnetic striping becomes less distinct toward the southwest beneath the Thelon Formation where it is slightly deflected transecting SIS 3, but some of the striping is still

visible in the enhanced imagery as far as Cross Section 4 wherein the inferred Amer Group source units are shown at depth (Figures 5.4b, 5.5).

The Five Mile Lake basalt is another useful structural marker unit because it characteristically exhibits an intense linear aeromagnetic high that is paired with the deep linear low of the Ayagaq Lake formation quartzite. At the northeastern termination of the Amer Belt, this basalt is restricted to the core of an upturned F1 syncline along the southeast flank of the belt (Calhoun et al., 2011, 2014; V. Tschirhart et al., 2013a), labelled in Figure 5.3 as "Amer Q4 + 5ml 3 NE". This basalt is not present in the medial antiform of or along the northwest flank of the northeast Amer Belt, even though the quartzite marker is well exposed – this part of the northeast Amer Belt is thus labelled "Amer Q3 NE". From the northeast to the southwest the Amer Belt expands in width and the amount of Itza Lake formation increases as it progressively blankets the older Amer Group units because the two broad synforms plunge southwesterly. Exposures of D1 infolded Five Mile Lake basalt continue along the southeast flank of the Amer Belt where they can be traced aeromagnetically for at least 50 km beneath the Aberdeen sub-basin, labelled as "5ml 3a", "5ml 3b" and "?5ml 3c" in Figure 5.3. The last unit is deeper, less distinct and less certain than the first two. It is possible that one or more of the anomalies labelled "?M5" are also basalt rather than mafic intrusions. Basalt also outcrops and generates aeromagnetic anomalies near the Aberdeen sub-basin margin associated with the medial antiform, labelled "Amer Q3 + 5ml 2" and "Amer Q2 + 5ml 1. No magnetic linear highs are associated with the "Amer Q1 +Itza 1" belt; hence basalt is inferred to be absent there. The twin anomalies associated with "5ml 1" along each limb of a tight upright synform can be traced nearly continuously beneath the Aberdeen sub-basin for more than 80 km southwest where they stop abruptly at a Mackenzie dyke, suggesting that the dyke occupies a significant dip-slip fault. This boundary also represents a magnetic survey boundary between high resolution and low resolution data, which makes it difficult to discern if the basalt is indeed truncated or if it continues southwest of the dyke but is not visible due to the coarser resolution of the data. The anomaly associated with "5ml 2" in outcrop appears to also continue after a jog, southwesterly beneath the sub-basin, however the geophysical style of this anomaly is identical to others interpreted as deep mafic intrusions and would require an illogical sinistral fault offset to be aligned with the "5ml 2" anomaly, therefore it is labelled "M 4". The "Amer Q1 + Itza 1" belt does not have a pronounced geophysical signal, and lies within the low resolution data

once it enters the Aberdeen sub-basin. We infer a southwest trending linear low to represent this belt beneath the sub-basin where it is labelled "Amer Q1". This aeromagnetic low is lost over the powerful highs of SIS 1 and M1 that underlie the Sand Lake Horst which defines the western margin of the sub-basin. However, southward along the horst, a superbly exposed upright F2 synform refolds a nappe involving only sub-greenschist-metamorphosed SIS rhyolite, Amer Q1 and Resort Lake formation, all resting on SIS quartz monzonite. This was mapped by LeCheminant et al. (1984) who noted the 2.6 Ga age of the granite, and the rhyolite was dated also as 2.6 Ga by LeCheminant and Roddick (1991). The refolded nappe may represent the structural style of Q1 at its poorly exposed "outcrop" position north of the Aberdeen sub-basin where it also structurally overlies 2.6 Ga granite dated by Tella et al. (1984). With respect to the sub-basin geological map interpretation, most of the major belts mapped there are thought to be F2 synforms. However in the gravity-magnetic-geological cross sections shown in Figures 5.5 through 5.8, many of the smaller folds are interpreted as F1 isoclinal folds that were reoriented during D2. The type example of this structural style in the northeast Amer Belt was geophysically modeled by Tschirhart et al., (2013b).

5.5.2.3 Turqavik Horst (Tur) and Fault Zone (TFZ)

The Turqavik Horst is the most distinct and prominent structure on the geophysical images, and is transected by a number of half grabens. The north-tilted Tur 2 half graben is mapped in outcrop; those beneath the Thelon Formation are interpreted as similar half grabens dipping to the north because each aeromagnetic break separating them is sharp and the north side of each block has a more subdued aeromagnetic signature, consistent with thicker cover by Thelon Formation sandstone on the down-tilted side. The triangular exposed part of the Turqavik Horst is flanked on the northwest by the Archean Turqavik supracrustal belt and on the south by the Schultz Lake Graben (SLG), an eastern embayment of the Thelon Basin. The exposed portion of the Turqavik Horst (Tur 1 and Tur 2 on Figure 5.3) includes outcrops along its northwest boundary (the Turqavik Fault) and in a cross-cutting half graben (Tur 2) where Amarook and Thelon formations unconformably overlie Archean banded gneiss and amphibolite.

The Turqavik horst is underlain by banded tonalitic and amphibolitic gneiss that is distinct from all supracrustal belts, including the Marjorie Hills assemblage. The gneiss in the horst is at a higher metamorphic grade and has a higher proportion of orthogneiss, amphibolite and Hudson granite than even the Marjorie Hills assemblage; as well it has a

much higher amplitude and distinctive 150° aeromagnetic striping. The horst extends southwesterly beneath the eastern Aberdeen sub-basin through faulted blocks Tur 3, Tur 4A, Tur 4B and ?Tur 5 as the deepest possible block. The horst and bounding faults appear to be on strike with high grade mylonitic and orthogneiss outcrop south of Aberdeen Lake. This southern high grade gneiss and high strain zone flanks the west side of Marjorie Lake and continues through the centre of Wharton Lake (mapped by LeCheminant et al, 1983 as the eastern 8-10 km of their "western domain of deformed potassic intrusive rocks and north-northeasterly trending cataclastic gneisses") and is here termed the Marjorie Lake Shear Zone. The same name is being applied to the continuation of this zone in the map area 65-O due south of Marjorie Lake (Peterson et al., 2014) where it includes a low angle detachment component and a late brittle dip slip component flanked by conglomerate of the Kunwak Formation, the uppermost unit of the Baker Lake Group (Rainbird et al., 2003). Metamorphism reaches upper amphibolite with retrograde chlorite along the Marjorie Lake Shear Zone. The deformation is partitioned into a number of high strain zones separated by moderately foliated granitoid rocks. This zone demarks the western boundary of the Marjorie Hills assemblage south of Aberdeen Lake.

Tur 3 is the first half graben of the Turqavik Horst that was defined by this study beneath the Thelon Formation. It dips north like Tur 2, and both of their bounding faults trend eastward into and are interpreted to also subdivide the Shultz Lake half graben (SLG on Figure 5.3). The northern 075° boundary fault of the SLG flanks the southeast side of the main Turqavik Horst; water and sandstone cover obscure the relationship between this ~035° trending horst and the series of 015° trending belts on its south side: the Marjorie Hills assemblage, the SLIC and the Pipedream assemblage. Tur 4A, the next block defined by this study, is up-thrown with respect to Tur 3 because it has a much more distinct texture and the magnetic signal is less attenuated. Tur 4B is then slightly downthrown with respect to Tur 4A and is thus inferred to have a thicker Thelon cover sequence. The final and deepest graben (?Tur 5) is north-northwest trending, and separates Tur 4A and Tur 4B from Pitz and SIS 4. The trace of the Turqavik Fault is lost across this deepest graben which has the most subdued aeromagnetic response of the entire Aberdeen sub-basin.

Southwest of the ?Tur 5 graben the Pitz domain is inferred to form a thin cover on Archean orthogneiss similar to that of the Turqavik Horst. The area of SIS 4 that

subcrops beneath the Thelon Formation is likely much smaller than outlined in white in Figure 5.3 as discussed in section 5.2.2.1, therefore much of this subcrop is probably also orthogneiss. Similar aeromagnetic textures west of SIS 4 are thought to represent some combination of orthogneiss, supracrustal gneiss like the Turqavik Belt and a thin drape of Pitz Formation. The presence of a magnetically very distinct semicircular aeromagnetic linear anomaly interpreted as iron formation south of the Aberdeen sub-basin in this area is consistent with this being an extension of the Turqavik Belt, although it is covered here by Pitz Formation ("Pitz on TB", Figure 5.3) and could not be verified in outcrop. The Turqavik Fault was also tracked using SED methods by V. Tschirhart et al., (2013a). It is more evident as a brittle reactivation lineament in SED and LANDSAT imagery than in Figure 5.3.

Blocks Tur 4A and Tur 4B underlie the eastern portion of Aberdeen Lake. They are interpreted to represent a direct continuation of the Turqavik horst comprising banded amphibolite and granitoid orthogneiss covered by about 150 to 200 m of Thelon Formation as indicated by drill core (Figure 5.1) and the gravity model (Figure 5.8). A strong macroscopic fabric evident in SED and aeromagnetic images is sub parallel to one of the main ice-flow directions but cannot be correlated with specific Quaternary features, thereby indicating that they may be related to magnetite-rich bands (?amphibolite) in the basement gneiss. The aeromagnetic bands are spaced on the order of 2.5 km, have curvilinear trends about 140°, and are only evident within the area interpreted as the Turqavik Horst beneath the Thelon Formation.

The northwest margin of blocks Tur 3 and Tur 4A is the slightly stepped southwest extension of the Turqavik Fault. The westernmost McCrae Lake Dyke demarks the east-southeast margin of blocks Tur 4A and Tur 4B, and this margin is exposed in outcrop in an outlier of gneiss at the east end of Tur 3. East of these three blocks is the inferred northern extension of the Marjorie Hills assemblage from its observed presence in outcrop on the south side of the Thelon Fault. This inference is consistent with a very distinct change in background magnetic fabric from striped in the Turqavik Horst to mottled in the Marjorie Hills assemblage. The Marjorie Hills assemblage fabric is however disrupted by the 015° linear trends of the McCrae Lake dyke swarm.

5.5.2.4 Amer Mylonite Zone (AMZ)

Examination of the high resolution aeromagnetic data combined with gravity modeling requires a highly magnetic, dense unit at depth under the northwest end of Cross Section 1, near the northwest end of 2 and the west end of 3 (Figures 5.6, 5.7, 5.8). This dense unit coincides spatially with two highly magnetic bands (M3 and M4 on Figure 5.3). M3 is interpreted as a zone of mafic intrusions localized along strands of the Amer Mylonite Zone (AMZ). M4 resembles M3 but is southeast of the AMZ and appears to align with a known occurrence of the Five Mile Lake basalt within Amer Q3 quartzite; however it is here interpreted as a deep intrusion like M3, perhaps along a strand of the AMZ that dies out beneath the Aberdeen sub-basin and is taken over by the AMZ as mapped in outcrop by Tella (1984, 1994). These small aeromagnetic anomalies in the Aberdeen sub-basin are interpreted to be similar to and of the same general age as the gabbroic parts of the SIS plutons described above. In the deepest part of the sub-basin a number of similar sized anomalies are labelled "?M5" and may be of the same type. This interpretation has high uncertainty because other possibilities are reasonable, they are not clearly aligned with a mapped external body, and their shapes are irregular - some are elongate, resembling the highs interpreted as 5ml 3 to the east. Some of the M5 "blips" may indeed be Five Mile Lake basalts but these are at the deepest centre of the Aberdeen sub-basin with no way of distinguishing basalt vs gabbro.

M6, an unknown anomaly at the north edge of Figure 5.3 at 98° 33' W has a similar signature to those at M5 but is well north of the Aberdeen sub-basin. M6 was independently modeled in terms of a body whose upper contact is ~ 1 km below the surface (W. Miles, personal communication, September 2012). The second author had visited the exact site earlier before discussing with Miles, noting that only continuous granitoid gneiss is exposed across abundant outcrop over the anomaly. The field observations are consistent with Miles' independent model that the magnetic body does not reach the surface.

The magnetic band 5ml 1 also resembles M3 and M4 but lines up very directly near the central part of the Amer Mylonite Zone with an outcropping belt of feldspathic sandstone between two quartzite ridges, labelled Amer Q2 + 5ml 1. Here the magnetic zone in the outcrop belt comprises two or more individual linear elements that demonstrate high crustal level and are therefore interpreted as Five Mile Lake basalt hidden beneath magnetically transparent Itza Lake formation sandstone. This belt is

clearly traced continuously under the sub-basin for 80 km as noted earlier, although the detailed breakdown of this belt into bands of basalt between quartzite (Figure 5.9) is speculative. The three magnetic bands labelled 5ml 1, M3 and M4 trend southwesterly, sub-parallel to the Slave-Chantrey Mylonite Zone in the Sand Lake Horst, and they each remain distinct as far southwest as a Mackenzie dyke that is interpreted to occupy a significant block fault. M3 is traced faintly across that dyke but loses distinction beneath a thick cover of Pitz volcanic rocks south of the basin margin. M4 is weakly interpreted to peel off to the south as a series of point highs that again disappear under the Pitz Formation. The M3 and M4 bands are interpreted to be localized along strands of the Amer Mylonite Zone that Jefferson et al. (2011a) have hypothesized to be continuous beneath the main Thelon Basin into the MacDonald Fault Zone and the Great Slave Lake Shear Zone. Multiple northwest trending faults offset these bands as well as the Turqavik Horst, and are represented as demagnetized zones crossing the magnetic units.

The interpreted mafic intrusions M3 and M4 are thought to have been focused along the AMZ in the same way as mafic intrusions that are exposed along the Slave-Chantrey Mylonite Zone (S-CMZ) some 15 km to the northwest along the Sand Lake Horst (Berman et al., 2013) where they are labelled M1. The M2 anomaly is much like M-3 and M-4. It is completely buried under Thelon Formation in the southwest part of the sub-basin and may be aligned with the S-CMZ. Such mafic intrusions along mylonite zones may have Ni-Cu-PGE potential by analogy with ultramafic-hosted intrusions along other shear zones world-wide (P. Lightfoot, oral presentation, Prospectors and Developers Annual Meeting, March 5, 2013). Toward the northeast, the distribution of M3 and M4 between SIS 2 and SIS 3 is problematic, with M3 seemingly disappearing or doubling up. This could represent accommodation at a bend in the Amer Mylonite zone from 063° north of the sub-basin to about 030° beneath the sub-basin in the vicinity of the SIS 2 body where the southwestward continuation of M-3 is unclear. The Slave-Chantry Mylonite Zone shows similar changes along strike, but some mafic bodies are located on straight segments and there is no apparent spatial association between bends and intrusions.

5.5.3 Forward models

5.5.3.1 Cross section 1

The gravity transect of Cross Section 1 is located over exposed bedrock on the northeast flank of the Aberdeen sub-basin (Figure 5.4a), and is modelled in Figure 5.5. It transects the last outcrops of distinctive Ayagaq formation quartzite ridges before the Amer Belt trends beneath the sub-basin. The ridge-forming quartzarenite was isoclinally folded during D1 and subsequently brought up within a large, steep-sided D2 antiform (West medial antiform on Figure 5.4a) flanked by gentle synforms on each side. Isoclinal D1 folds and detachments, although present in the Archean through Ps3 units and some being integral parts of the modeling, cannot be completely resolved geophysically because the folds are relatively small and flattened by D1. The detachments have a large translational component within formations (e.g. "detachment A" within the Three Lakes formation, Figure 5.4a) or at formational boundaries, and thereby preserve the primary stratigraphy (V. Tschirhart et al., 2013a; Calhoun et al., 2013). In the northwest part of Cross Section 1, a thin layer of sub-horizontal Thelon Formation unconformably overlies Itza Lake formation (Ps4), which in turn unconformably overlies and was gently folded with Ps1 Ayagaq Lake and Ps2 Resort Lake formations. The magnetic striping that characterizes the Ps3 Three Lakes and Showing Lake formations is not visible on the SED maps, suggesting that these units were eroded prior to deposition of Ps4. This northwestern part of Cross Section 1 transects a northeast striking aeromagnetic high that is parallel to the Amer Mylonite Zone and is coincident with a strong, long-wavelength gravity high. This combination of data is not explainable by known units in the Amer Group, and is thus interpreted as a deep, dense mafic intrusion, interpreted to be part of the 2.6 Ga Snow Island Suite by analogy with similar intrusions and anomalies that are localized along the Slave-Chantrey Mylonite Zone.

Moving southeast along Cross Section 1, the major eroded west medial F2 antiform exposes a window of Archean granitoid gneiss that is unconformably overlain by the Ayagaq formation, and is thus basement to the Amer Group in this area. The gneiss is interpreted to have been thrust over and/or intruded at depth by a 2.6 Ga SIS pluton (SIS 2) that does not produce a pronounced signature in the gravity profile, but is represented in the magnetic data as a large amplitude (>20 nT), long wavelength anomaly that masks most of the detailed striping associated with the magnetic Amer Group units. The West medial antiform of Archean amphibolite and orthogneiss carrying a northwest-

vergent D1 thrust ("B thrust" on Figure 5.4a) or broken fold is the preferred geological hypothesis that is compatible with both geological and geophysical data, including a break seen on the SED image as a linear magnetic high on strike with the Ayagaq Lake formation. The B thrust and the associated northward-overturned smaller folds on the south limb of the antiform coincide in the profile with a gravity high. This gravity high is explained in the model by thickening of the amphibolite unit (density = 2.80 g/cc) in the basement gneiss complex. In this model the hanging wall of the B thrust carries a complete sequence of the Amer Group: Ayagaq Lake, very thin Resort Lake (not shown at this scale and likely the locus of another D1 detachment), Aluminum River, Three Lakes (locus of the labelled "Detachment A" in Figure 5.4a defined by truncation of aeromagnetic striping visible in Figure 5.4b), Oora Lake and Showing Lake formations resting on amphibolite (2.80 g/cc) and the Turqavik Belt (2.74 g/cc). No petrophysical properties have been collected for the Turqavik Belt, so its density is approximated using the average density of the Marjorie Hills assemblage which is similar in metamorphic grade and aeromagnetic appearance. As modelled, the amphibolite overlies the Turqavik assemblage; alternatively the assemblage may overlie the amphibolite, or the amphibolite may be part of the Turqavik assemblage. The gravity station spacing along the part of the cross section containing the above-discussed thrust and folds, from 18 to 27 km, is much closer than on the ends. The calculated gravity profile was generated by staying true to the average density value for each unit listed in Table 5.1, and the structural style of the geological map.

At the southeast end of Cross Section 1, the broad Amer Itza 3 synform cored by Itza Lake formation is cut longitudinally by the Itza fault near its axis which is marked by a small central antiform that is developed in the lower Amer Group units from Ayagaq Lake through Showing Lake formations, but not in the unconformably overlying Itza Lake formation. This southeast end of Cross Section 1 is the east end of Cross Section 3 that extends westward from this point (Figure 5.4a). In this area outcrop mapping by the first author also suggests dip-slip offsets along several different fault directions within the Itza Lake formation (Figure 5.4a). However as this locality is at the ends of the gravity data for Cross Sections 1 and 3, the small central antiform cannot be fully modeled here. The Itza fault is however visible on the SED images as a linear aeromagnetic high (Figure 5.4b). It is interpreted as northwest-side-down based on geological context, both of the

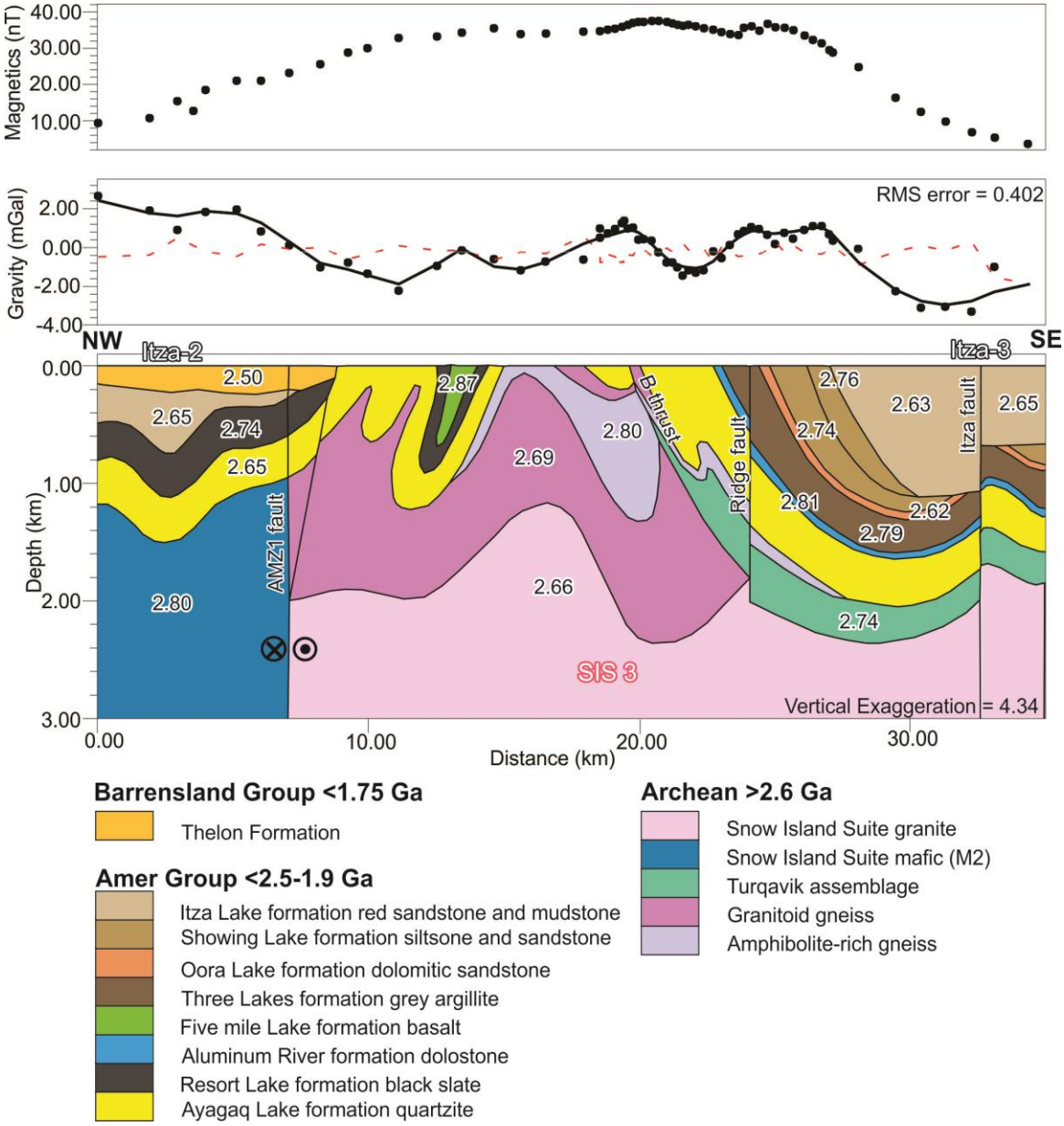

Figure 5.5 Cross Section 1 showing magnetic and gravity data and interpreted forward model. Top panels: dotted line = observed magnetic field. Middle panel: dotted line = observed gravity anomaly, solid line = calculated gravity anomaly, red dashed line = root mean square error between observed and model-calculated gravity anomaly. Bottom panel: forward model of gravity data with numbers in polygons denoting density in g/cc. Legend at bottom.

SED images and the solitary larger gravity anomaly at the last station that suggests a change in near surface density across the fault.

The aeromagnetic TMI and SED images were used qualitatively to guide the gravity forward model as discussed above. Figures 5.4b and 5.5 demonstrate the overwhelming nature of the magnetic high (from 20 to 40 nT) associated with the deep-seated SIS 3 pluton, however the distinct aeromagnetic peaks on the southeast flank of the SIS 3 magnetic high do coincide with the magnetic markers in outcropping Three Lakes and Showing Lake formations. These magnetic stripes can still be seen in a very subtle way crossing the southern part of the SIS 3 (two black arrows in Figure 5.4b), indicating that the Amer Group overlies the pluton even beneath the Thelon Formation. Farther north over the central and northern parts of the pluton, a significant structural and stratigraphic thickness of Amer Group is mapped in outcrop above it, further supporting the deep interpretation.

5.5.3.2 Cross section 2

Sub-parallel to Cross Section 1, Cross Section 2 (Figure 5.6) also transects the West medial antiform of the Amer Belt but the basement geology is completely inferred by geophysics because it is hidden below the Thelon Formation. Starting from the northwest, a minor northwest-side down fault is interpreted as a reactivated strand of the Amer Mylonite Zone (AMZ1). The abrupt gravity low at the northwest end is interpreted to be more an effect of a fold in the Amer Group than because of any thickness change of the Thelon Formation. Two kilometres south of the northwest end of the transect a seismic reflection shot point by Overton (1979) suggests the depth to basement is 754 m, comprising an upper 294 m unit and a lower 460 m unit above crystalline basement (Figures 5.1 and 5.4a). These depths are consistent with the forward model shown in Figure 5.6 if the 294 m unit corresponds to the Thelon Formation, and the 460 m unit is the weakly metamorphosed Amer Group. Southeast of the AMZ1 fault, Itza Lake formation unconformably overlies only the folded Resort Lake and Ayagaq Lake formations; no intervening formations are included in the model here because this belt lacks the magnetic striping of those units, as for Cross Section 1. The crystalline basement here is interpreted as the M2 mafic intrusion which is modelled with a density of 2.81g/cc and is thought to be localized along the Amer Mylonite Zone, again as for Cross Section 1. The third fundamental continuation from Cross section 1 is the West medial antiform - a middle window of Archean basement coring a broad F2antiform of

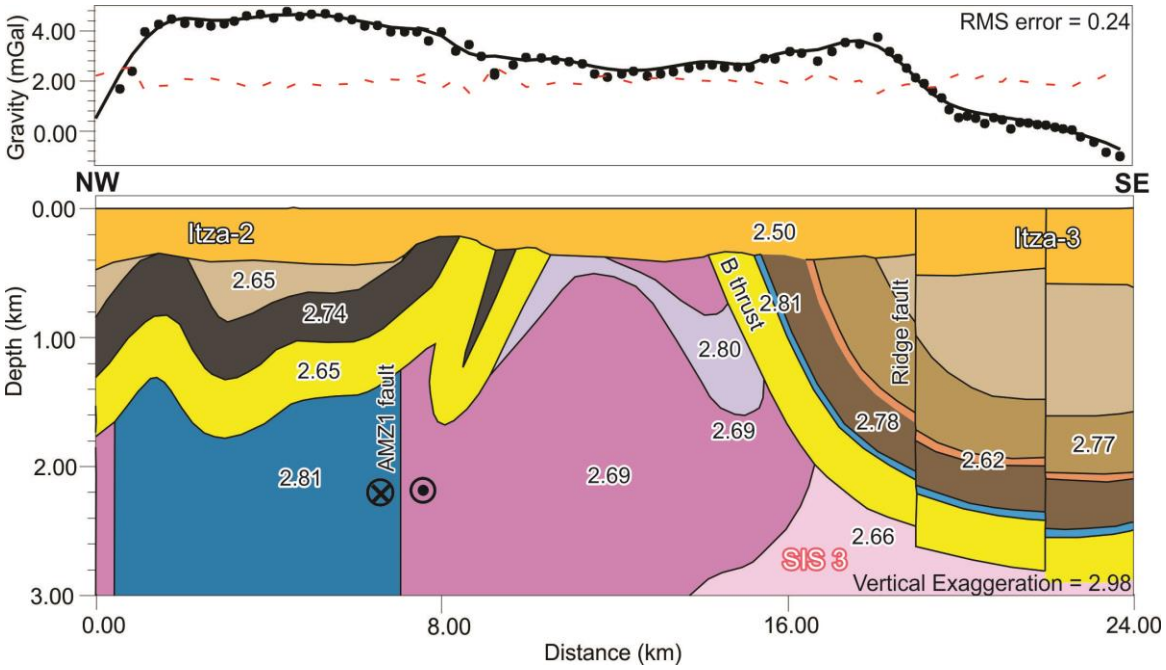

Figure 5.6 Cross Section 2 showing gravity data and interpreted forward model. Numbers in polygons denote density in g/cc; unit colors and line types are as explained in Figure 5.5. Values for each designated unit from Cross Section 1 apply to like units except where otherwise specified.

banded gneiss and foliated granite modeled with density 2.69 g/cc and including amphibolite modeled with a density of 2.80 g/cc. On the northwest flank of the West medial antiform the small D1 syncline is cored by only Resort Lake formation – the Five Mile Lake basalt is no longer present as it was in Cross Section 1. The southeast flank of the West medial antiform includes the same enigmatic northwest-directed B thrust that is shown in Figures 5.4a and 5.5 as a placing foliated granite over Ayagaq quartzite. In Cross Section 2 the B thrust is inferred to continue but is grossly simplified for the purpose of modeling, with the basement gneiss below the hanging-wall Ayagaq quartzite not being shown. The structural site of the B thrust and associated isoclinal folds which has a complex gravity profile in Cross Section 1 has only low amplitude gravity highs coincident with linear on-strike magnetic highs on the SED images. The southeast end of Cross Section 2 is again comparable to Cross Section 1 in having the broad Amer Itza 3 synform continue, here being buried beneath flat lying Thelon Formation Two block faults are shown that step their southeast sides down, with the Ridge fault offset being reflected in the gravity profile as an abrupt low. The geological interpretations at the intersections of Cross Sections 2 and 3 are in agreement.

5.5.3.3 Cross section 3

Cross Section 3 is an east-west transect, mainly beneath the northeastern Aberdeen sub-basin (Figure 5.6), starting at the southeast end of Cross Section 1, crossing the southeastern part of Cross Section 2, running just north of Cross Section 4 and ending at the south end of SIS 2 on the extension of the Amer Mylonite Zone. Starting from the west, the Amer Belt is modeled as a continuation of the Amer Itza 2 synform where the D1 folded Ayagaq Lake and Resort Lake formations are unconformably overlain by Itza Lake formation and in turn unconformably overlain by flat lying Thelon Formation. The 400m southwest-side down DPR8-9 fault is at the west end of the cross section and impacts only the westernmost part with a drop in gravity in the last two stations. The offset on this fault is constrained by logs (Davis et al., 2011) of the two drill holes DPR8 and 9 that straddle the fault (Figure 5.4a). The western drop in gravity is also partly attributed to the SIS 2 pluton that lies west of this cross section. The Amer Itza 2 synform does not have a gravity low but is marked on the gravity profile by a slight decrease in the observed signal toward the east. This gravity drop is interpreted as an east-side-down fault that has not been recognized in surface mapping – it is not included in Figure 5.4a. In the same area the TMI and SED images show a linear magnetic anomaly striking

southwest that is interpreted as a continuation of the M2 mafic body along the Amer Mylonite Zone. Although not contributing to the observed gravity signal significantly, Werner deconvolution suggests the M2 body is buried to a depth greater than 1500 m by the combined thickness of the Thelon Formation and the Amer Group (Tschirhart et al., in prep).

The Amer Itza 2 synform is flanked on the southwest by the West medial antiform, again eroded to have exposed the same window of Archean granitoid gneiss in its core now buried by the Thelon Formation as in Cross Section 2. The medial antiform still is modelled as carrying the B thrust on its southeast flank and to be underlain at depth by the SIS 3 pluton. East of the B thrust, a block of basement has been uplifted exposing a package that has been mapped by the second author as gently dipping Amarook Formation quartzarenite (Figure 5.4a), part of the Wharton Group (Figure 5.1). This appears to be a very narrow block on the cross section because the cross section cuts a small corner across a larger block where the Ridge and Amarook faults intersect at an angle of about 30°. The thin stratigraphic interpretation on this cross section is derived from the forward modeling process. The DPR-8 drill hole 18 km southwest of this outcrop cored 141 m of subhorizontal Amarook Formation sandwiched between Thelon Formation above and Itza Lake formation below; another small outcrop of Amarook Formation is located about 7 km due south of this one; and a strip of Amarook Formation was mapped by the second author southwest of Itza Lake (Figure 5.4a). In terms of densities, the Thelon and Amarook formations are virtually indistinguishable gravitationally, and as such are modelled as one unit – Thelon Formation - on the gravity profiles. Because of the degree of block faulting that either exposes or has allowed erosion to remove the Amarook Formation before deposition of the Thelon Formation, it is important to keep in mind that modeled depth to basement may in places actually be the thickness of Thelon + Amarook formations. East of the Amarook Formation outcrop on this cross section, the gravity decreases significantly into a distinct gravity low, indicating a thickening of Thelon Formation east of the Ridge fault that is modelled as having a ~650 m east-side down throw. Thick Thelon Formation and the Itza Lake formation uncomfortably overlie and are block faulted along with a previously deformed complete sequence of the Amer Group, in turn unconformably overlying the Turqavik assemblage. The Thelon Formation gently on-laps the Itza Lake formation where this cross section intersects the edge of the Aberdeen sub-basin.

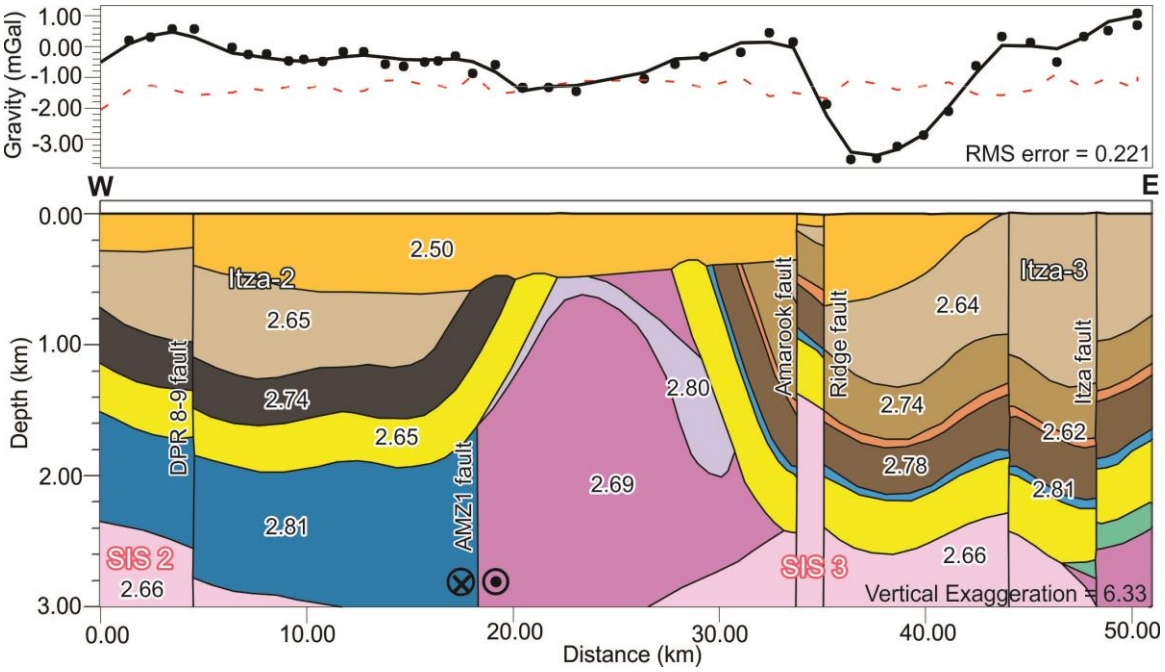

Figure 5.7 Cross Section 3 showing gravity data and interpreted forward model. Numbers in polygons denote density in g/cc; unit colors and line types are as explained in Figure 5.5. Values for each designated unit from Cross Section 1 apply to like units except where otherwise specified.

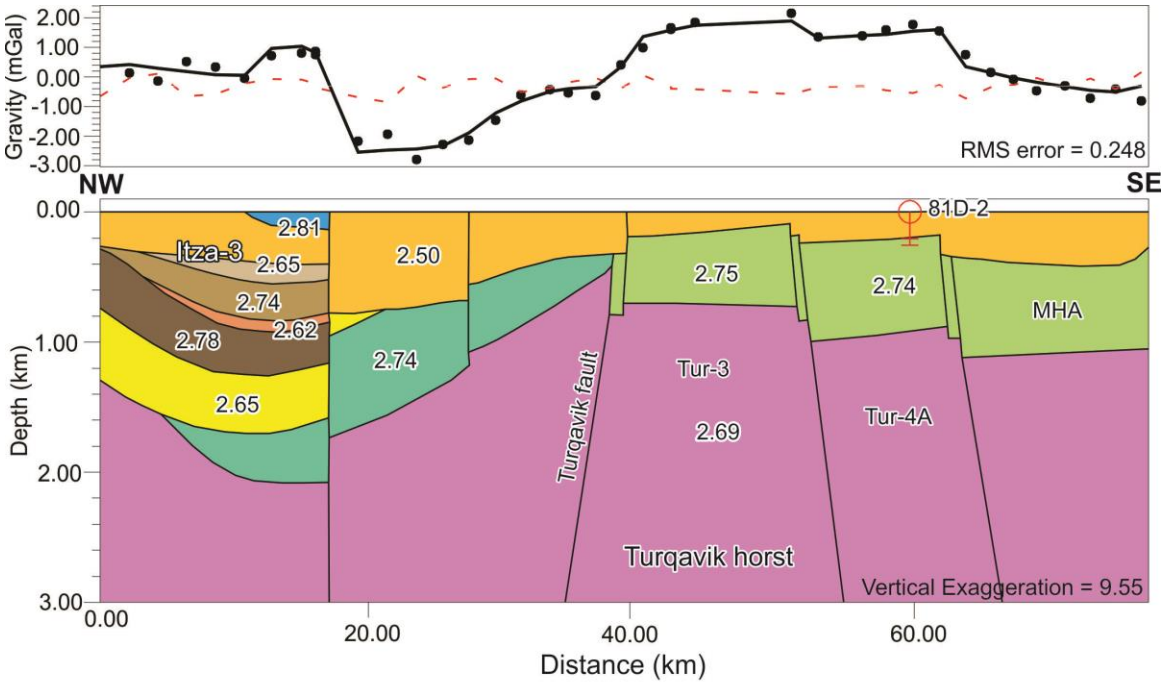

Figure 5.8 Cross Section 4 – the long, regional spaced transect across the eastern Aberdeen sub-basin showing gravity data and interpreted forward model. Numbers in polygons denote density in g/cc; unit colors and line types are as explained in Figure 5.5. Values for each designated unit from Cross Section 1 apply to like units except where otherwise specified.

5.5.3.4 Cross section 4

Cross Section 4 (Figure 5.8) runs southeast from just south of Cross Section 3 in the northwest and stretches ~ 80 km to the southeast joining with profile 2 from Tschirhart et al., (2013b). To the north, the Amer Group is modeled as overlying the Turqavik assemblage in the open Amer Itza 3 synform and unconformably overlain by flat lying Thelon Formation. The SIS 2 granite intrudes at depth beneath northwest corner of the cross section. Whereas it is not expressed in the gravity data, it is visible on the SED maps (Figure 5.4b). This southern tip of the SIS is too deep to be shown on this cross section. The Ordovician strata are reflected in the gravity profile as an abrupt high. This outcrop is inferred to be ~ 200 m thick assuming a density of 2.81 g/cc which is the average density of the Aluminum River dolostone. A fault truncation of the Ordovician dolostone (density 2.81 g/cc) is interpreted for the southeast side of a graben where the basement has been significantly down-dropped to preserve this extremely isolated outlier. A fault is also mapped on the northwest side of the outlier, consistent with the jump in gravity profile between the fifth and sixth stations, but was not included in this cross section model. The gravity low between the Ordovician and the Turqavik fault reflects thickened Thelon Formation (density 2.50 g/cc) overlying a thin, southeast-terminated wedge of Ayagaq Lake formation quartzite (density 2.65 g/cc), overlying the Turqavik assemblage (density 2.74 g/cc) that in turn overlies basement gneiss (density 2.69 g/cc).

The revised basement geological map (Figure 5.9) shows only the Ayagaq Lake and Five Mile Lake formations immediately south of the Ordovician outlier, and these quickly pinch out leaving only the Turqavik assemblage mapped beneath the Thelon formation. The overlying Showing Lake and Three Lakes formations are inferred to be absent here because this is the southwestern margin of the Amer Belt projected beneath the Thelon Formation and these units are eroded from that outcrop area. This is consistent with the gravity profile because these mid-Amer Group units have a much greater density and if present would have created a gravity high. Several dykes cut the profile, but due to the large station spacing, they do not create a marked response in the gravity data.

The step response at 39 000 m to the highest gravity readings of this cross section is located at the Turqavik Fault projected through the Thelon Formation. This part of the cross section begins a transect of the Turqavik Horst that separates the Turqavik Belt from the Marjorie Hills assemblage (TB from MHA in Figure 5.9). The high amplitude gravity signal over the Turqavik Horst is consistent with a thin layer (~157, 205, >215 m

in drill holes 81D-1, 2 and 6 respectively) of Thelon Formation overlying gneissic basement. Drill hole 81D-2 is shown on the cross section because it is right on the line of section. In this model cross section, approximately 500 m of Marjorie Hills assemblage metasedimentary gneiss (densities of 2.75 and 2.74 g/cc) is modeled as mantling granitoid gneiss in blocks Tur-3 and Tur-4A. All of the drill holes that reached basement over this horst intersected metasedimentary gneiss, some orthogneiss and retrogressed amphibolite, all consistent with the Marjorie Hills assemblage (unpublished logs by the second author, partially reported in Davis et al., 2011). A similar result could be obtained however by invoking much thinner Marjorie Hills assemblage over the horst and adding significant amounts of amphibolite (density 2.8 g/cc) to the basement gneiss rock model. It may be that gneissic layering in the Tur-3 and Tur-4A blocks is dipping sufficiently that alternating amphibolite and quartzofeldspathic gneiss could account for the distinct aeromagnetic banding that characterizes these blocks.

Southeast of the Turqavik horst, just past 81D-2 on the cross section, a graben with slightly thicker Thelon Formation modelled to about 400m depth is underlain by a similar modeled ~400 m thickness of Marjorie Hills assemblage (density 2.74 g/cc), then lighter (2.69 g/cc) granitoid gneiss below that. The western boundary fault of the graben is interpreted to follow the westernmost McRae Lake Dyke. The floor of the graben is mapped beneath the Aberdeen sub-basin as the Marjorie Hills assemblage (MHA east of McRae Lake dyke in Figure 5.9). Here an overall subhorizontal attitude of the typically alternating Marjorie Hills paragneiss and orthogneiss and minimal amphibiotic material are invoked to explain the drop in gravity and the loss of magnetic fabric in the MHA map unit.

The Turqavik horst is transected at high angles by a series of half grabens that down-drop the horst in a series of steps toward the southwest, with each segment being covered by a greater thickness of Thelon Formation. The cross-cutting grabens are expressed in the gravity data as a series of steps in the observed responses (Figure 5.8). As the steps deepen toward the southwest the aeromagnetic signal decreases to the point where the Turqavik Fault line and the northwest trending fabric that characterizes the Turqavik blocks lose their magnetic definition. This enigmatic, magnetically indistinct, inferred very deep area is labelled “?Tur 5” in Figures 5.3 and 5.9.

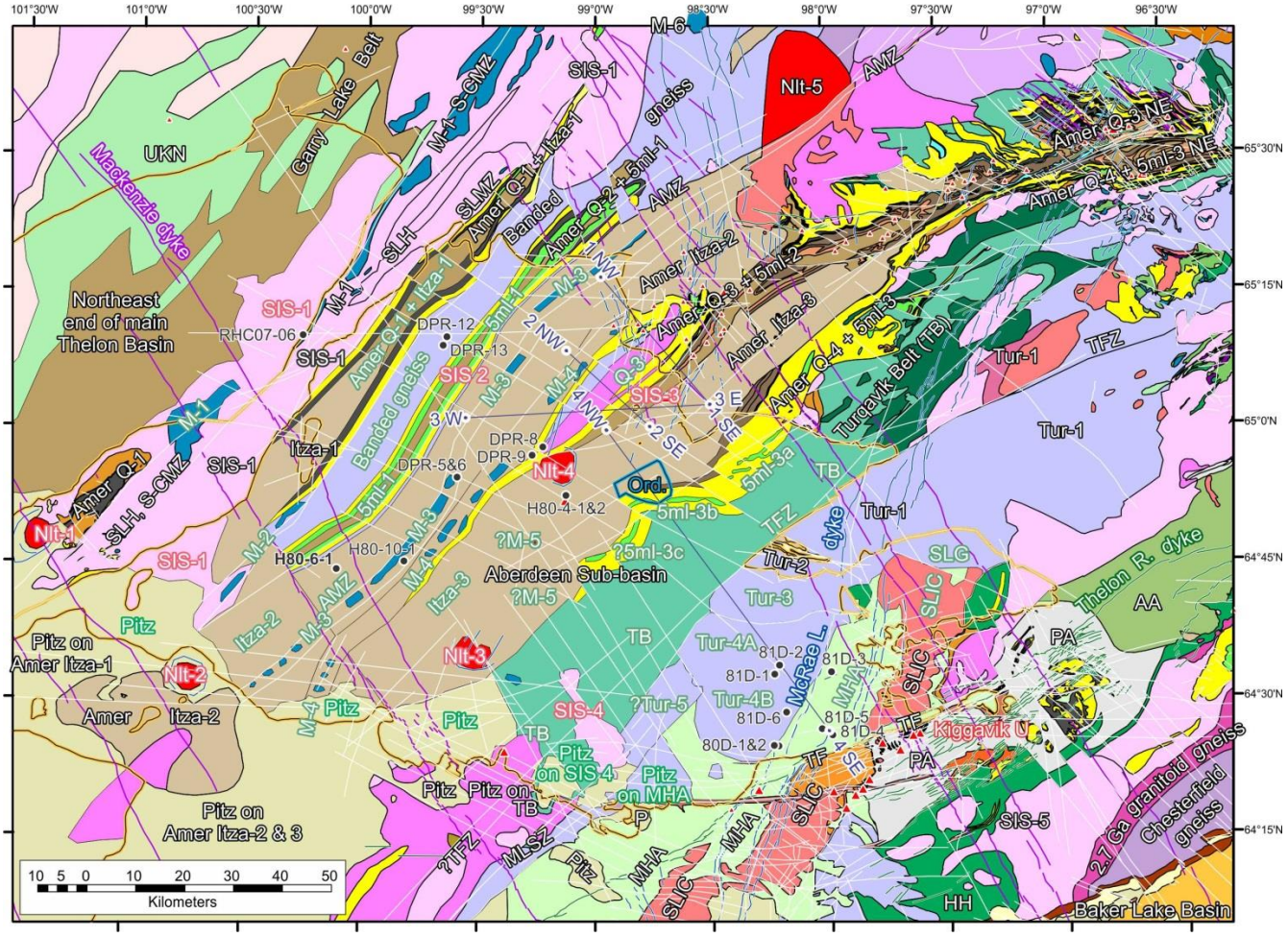

Figure 5.9 Remote predictive map of the geology at the unconformity surface beneath the Thelon Basin, with emphasis on the Aberdeen sub-basin. Outline of Thelon Formation is shown by thin black line on thick orange line. White lines are selected faults. This map covers the same area as Figure 5.3 for cross reference. Legend as in Figures 5.4 and 5.5 except as follows: Ord.= Ordovician dolostone; Snow Island Suite (SIS) pluton outlines are only shown where they outcrop, not the oval shapes outlining their magnetic extent as shown in Figures 5.3 and 5.4. Mafic units M-1 through M-6 are mainly not exposed. Nueltin Granite plutons Nlt-1 through Nlt-4 are not exposed but Nlt-5 is well exposed. Metasedimentary assemblages are: AA, Amarulik; HH, Halfway Hills; MHA, Marjorie Hills; PA, Pipedream; TB, Turqavik; UKN unknown affinity. Unlabelled pink units are non-magnetic SIS. The Garry Lake Belt is undivided Amer Group.

5.6 Conclusions

Integrated analysis of the total aeromagnetic intensity map, derived source edge detection images, gravity profiles and detailed outcrop mapping along supracrustal belts produced a preliminary remote predictive geological map (RPM) of the bedrock at the unconformity surface beneath the Thelon Formation in the Aberdeen sub-basin (Figure 5.9). Correlations between mapped outcrops and their magnetic characteristics with laterally equivalent strata under the Aberdeen sub-basin guided the RPM. The lithologic units are defined by texture, magnetic susceptibility, density and structural continuity as imaged in the magnetic maps. Geological cross sections generated by integrated forward modeling of gravity transects provide further knowledge of the structure and lithology at depth, as well as serving to verify aspects of the proposed RPM geology. The RPM in turn provides constraints for the cross sections.

The new geological RPM of the basement beneath the <1.75 Ga Thelon sedimentary basin comprises six main lithotectonic entities listed here in decreasing order of age: Archean mixed granitoid and amphibolitic gneiss of the Turqavik Horst; Neoarchean metasedimentary and metavolcanic rocks of the Turqavik Belt tentatively assigned to the ca 2.7 Ga Woodburn Lake group; the latest Neoarchean Marjorie Hills assemblage of metasedimentary and orthogneiss; the Amer Mylonite Zone with inferred associated 2.6 Ga mafic intrusions; other igneous intrusions of ca. 2.6, 1.83 and 1.75 Ga ages, and the <2.3 to >1.84 Ga Amer Group. Four main late brittle regional fault arrays (040-060°, 075-90°, 120° and 150°) were involved in development of sedimentary accommodation space for and/or preservation of the Thelon Basin. Reactivated intersections of these faults within supracrustal belts are one of the key foci in the search for unconformity-associated uranium deposits.

Confidence in the remote predictive map of basement geology beneath the Aberdeen sub-basin is high where the magnetic and gravity fabrics of the surroundings can be tracked continuously, such as up to 40 km from the northeast side of the sub-basin, especially features like the Turqavik Horst and the Five Mile Lake volcanics. The linear aeromagnetic highs are speculatively interpreted as mafic intrusions along the Amer Mylonite Zone, but regardless of their true nature they can be traced completely beneath the basin except they are buried both geologically and magnetically by thick Pitz Formation volcanic rocks flanking the southwest side of the sub-basin. Confidence regarding other deep-basin inferences is moderate to low, challenged by increased

attenuation of magnetic signal by the thicker Thelon Formation cover, the southwest-expanded extent and thickness of the older Itza Lake formation sandstone, and the obscuring geological and aeromagnetic blanket of the Pitz Formation along the south side of the sub-basin.

The next iteration of this research will develop a 3D model of the entire Aberdeen sub-basin, accounting for basement geology and further testing depth to basement estimations. The new RPM map product introduced here provides a knowledge framework for developing future exploration programs and a platform for evolving revised geological interpretations as future exploration programs generate new higher resolution information that can provide additional constraints. Advanced drill programs and subsurface geophysical investigation can build on this contribution to further improve the knowledge infrastructure.

5.7 Acknowledgments

This project is part of the northeast Thelon compilation activity of the GEM Uranium project under the Geomapping for Energy and Minerals Program delivered by the Geological Survey of Canada (GSC). Some of the data reported here were obtained under the previous Secure Canadian Energy Supply Program at GSC. As noted in Methodology nine company partners shared not only their data but also their logistics, geological data and knowledge; they also participated in ongoing multiple scientific exchanges, including field trips and several workshops. The data contributed by the GSC under the Letter of Agreement between the Earth Sciences Sector, McMaster University and the nine companies was obtained by a team managed by W. Miles: he procured the contract with Goldak Geophysical Surveys, and oversaw quality controls and field checks of the contract by B. Harvey, M. Coyle, J. Buckle, J. Carson, and S. Hefford. Financial support to V. Tschirhart was provided by a NSERC Doctoral fellowship. Laboratory and computer costs at McMaster University were supported by an NRCan GEM Grant to W.A. Morris. P. Tschirhart and C. Steiber ably assisted in field data collection. Logistical support by Ookpik Aviation was contracted through Polar Continental Shelf Project. P. Keating provided much appreciated guidance, and M. Thomas significantly improved the manuscript and our knowledge base through his comprehensive internal GSC review.

5.8 References

Anand, A., Jefferson, C.W., Pehrsson, S.J., White, J.C., McEwan, B.J., Bethune, K., and Tschirhart, V. 2012. History of reactivated fault systems in the northeast Thelon Basin region: regional to local controls on basin development and hydrothermal fluid flow for uranium (abstract). Geological Association of Canada – Mineralogical Association of Canada Joint Annual Meeting, St. John's, May 2012, Abstract volume, p. 4.

Berman, R. G., Percival, J. A., Harris, J. R., Davis, W. J., McCurdy, M., Normandeau, P., Case, G., Nadeau, L., Hillary, E. M., Girard, E., Jefferson, C. W., Kellett, D., Camacho, A., Bethune, K. M., Pehrsson, S., Hunt, P. 2013. Geo-Mapping Frontiers' Chantrey project: Reconnaissance geology and economic potential of a transect across the Thelon tectonic zone, Queen Maud block, and adjacent Rae craton. Geological Survey of Canada, Open File 7394, 1 sheet, doi:10.4095/292588.

Blakely, R.J. and Simpson, R.W. 1986, Approximating edges of source bodies from magnetic or gravity anomalies. *Geophysics*, 5, 1494-1498.

Bolton, T E and Nowlan, G S. 1979. A Late Ordovician Fossil Assemblage from an Outlier north of Aberdeen Lake, District of Keewatin: *in* Griffin, P.J (ed.), Contributions to Canadian Paleontology, Geological Survey of Canada, Bulletin 321,1-26.

Buchan, K. L. and Ernst, R. E. 2004. Diabase dyke swarms and related units in Canada and adjacent regions. Geological Survey of Canada, "A" Series Map 2022A, 2004; 39 pages (1 sheet), 1 CD-ROM, doi:10.4095/214883.

Calhoun, L.J., White, J.C., MacIsaac, D., Jefferson, C.W., and Patterson, J.G. 2011. Basement-cover relationships in the Paleoproterozoic Amer Group, Nunavut (abstract). Geological Association of Canada – Mineralogical Association of Canada – Society of Economic Geologists Joint Annual Meeting, Ottawa, May 2011, Abstract volume, p. 33.

Calhoun, L., White, J.C., Jefferson, C.W., and Patterson, J. 2014. Integrated geodatabase study of the complexly deformed U-hosting Paleoproterozoic Amer Group, Nunavut. Geological Survey of Canada, Open File 7429, 25 pp.

Chamberlain, K.R., Schmitt, A.K., Swapp, S.M., Harrison, T.M., Swoboda-Colberg, N., Bleeker, W., Peterson, T.D., Jefferson, C.W., Khudoley, A.K. 2010. In-situ U-Pb (IN_SIMS) micro-baddeleyite dating of mafic rocks: Method with examples. *Precambrian Research*, 183, 379-387.

Davidson, G.I., and Gandhi, S.S. 1989. Unconformity-related U-Au mineralization in the Middle Proterozoic Thelon sandstone, Boomerang Lake prospect, Northwest Territories, Canada. *Economic Geology*, 84, 143-157.

Davis, W.J., Gall, Q, Jefferson, C.W., and Rainbird, R.H. 2011. Diagenetic fluorapatite in the Paleoproterozoic Thelon Basin: structural-stratigraphic context, in situ ion microprobe

U-Pb ages and fluid flow history. *Bulletin of the Geological Society of America*, 123, 1056-1073.

Fuchs, H., Hilger, W. and Prosser, E. 1986. Geology and exploration history of the Lone Gull property: *in* Uranium Deposits of Canada, Canadian Institute of Mining and Metallurgy, Special Vol. 33, 286–292.

Gay, S.G. 2004. Glacial till: a troublesome source of near-surface magnetic anomalies. *The Leading Edge*, 23, 542-547.

Hadlari, T., Rainbird, R. H., and Pehrsson, S. J., 2004. Geology, Schultz Lake, Nunavut. Geological Survey of Canada, Open File 1839, 1 sheet, scale 1:250 000.

Harvey, B. J. A.; Coyle, M.; Buckle, J. L.; Carson, J. M.; Hefford, S. W. 2011. Geophysical Series, airborne geophysical survey of the northeast Thelon Basin, Nunavut, NTS 66 A, parts of 66 B, 66 C, 66 G and 66 H. Geological Survey of Canada, Open File 6510, 2011, 10 sheets, doi:10.4095/288204.

Hayward, N., Harris, J.R., Grunsky, E., Beauchemin, M., Jefferson, C., and Peterson, T. 2013. Geo-mapping Frontiers: Predictive Geology Map of the Ennadai Region, Nunavut. Geological Survey of Canada, Open File 7485, 21 p., doi:10.4095/293261.

Holden, E.J., Dentith, M., and Kovesi, P. 2008. Towards the automated analysis of regional aeromagnetic data to identify regions prospective for gold deposits. *Computer & Geosciences*, 34, 1505-1515.

Hunter, R. and Zaluski, G. 2011. Cameco's exploration for basement-hosted unconformity uranium mineralization in the northeast Thelon Basin (abstract). Geological Association of Canada – Mineralogical Association of Canada – Society of Economic Geologists Joint Annual Meeting, Ottawa, May 2011, Abstract volume, p. 98-99.

Hunter, R., Lafrance, B., Lesperance, J. and Zaluski, G. 2012. The Qavvik-Tatiggaq Trend: an evolving unconformity-related uranium corridor of the northeast Thelon Basin, Nunavut (abstract). Geological Association of Canada – Mineralogical Association of Canada Joint Annual Meeting, St. John's, May 2011, Abstract volume, p. 60.

Jefferson, C.W., Thomas, D.J., Gandhi, S.S., Ramaekers, P., Delaney, G., Brisbin, D., Cutts, C., Portella, P., and Olson, R.A. 2007a. Unconformity-associated uranium deposits of the Athabasca Basin, Saskatchewan and Alberta: *in* Jefferson, C.W. and Delaney, G., (eds.), EXTECH IV: Geology and Uranium EXploration TECHnology of the Proterozoic Athabasca Basin, Saskatchewan and Alberta; Geological Survey of Canada, Bulletin 588, 23-68.

Jefferson, C. W., Thomas, D., Quirt, D., Mwenifumbo, C. J. & Brisbin, D. 2007b. Empirical models for Canadian unconformity associated uranium deposits: *in* Milkereit, B., (ed.), Proceedings of Exploration 07: Fifth Decennial International Conference on Mineral Exploration, 741-769.

Jefferson, C.W., Hunter, R., McLaren, M., Peterson, T., Skulski, T., Rainbird, R., Young, G.M., Gandhi, S.S., and Costello, K. 2011a. Northeastern Thelon Basin uranium region: geological compilation for geophysical consortium planning: Geological Survey of Canada, Open File 6950, 1 sheet, doi: 10.4095/288801.

Jefferson, C.W., Pehrsson, S., Peterson, T., Chorlton, L., Davis, W., Keating, P., Gandhi, S., Fortin, R., Buckle, J., Miles, W., Rainbird, R., LeCheminant, A., Tschirhart, V., Tschirhart, P., Morris, W., Scott, J., Cousens, B., McEwan, B., Bethune, K., Riemer, W., Calhoun, L., White, J., MacIsaac, D., Leblon, B., Lentz, D., LaRocque, A., Shelat, Y., Patterson, J., Enright, A., Stieber, C., Riegler, T. 2011b. Northeast Thelon region geoscience framework - new maps and data for uranium in Nunavut. Geological Survey of Canada, Open File 6949, 1 sheet, doi:10.4095/288791.

Jefferson, C.W., Peterson, T., Tschirhart, V., Davis, W., Scott, J.M.J., Reid, K., Ramaekers, P., Gandhi, S.S., Bleeker, W., Pehrsson, S., Morris, W.A., Fayek, M., Potter, E., Bridge, N., Grunsky, E., Keating, P., Ansdell, K., and Banerjee, N. 2013a. LIPs and Proterozoic uranium (U) deposits of the Canadian Shield. Geological Survey of Canada, Open File 7352, 56 pp., doi:10.4095/292377.

Jefferson, Pehrsson, S., Peterson, T., Wollenberg, P., Tschirhart, V., Riegler, T., McEwan, B., Tschirhart, P., Scott, J.M.J., Chorlton, L.B., Davis, W., Bethune, K., Riemer, W., Patterson, J., Morris, W.A., Anand, A., and Stieber, C. 2014a. Bedrock geology of the western Marjorie-Tehek supracrustal belt and Northeast Thelon Basin margin in parts of NTS 66A and 66B, Nunavut. Geological Survey of Canada, Open File 7241, 1 sheet.

Jefferson, C.W., Young, G.M., White, J.C., Patterson, J., Tschirhart, V., Calhoun, L., Peterson, T., Davis, W., and Tella, S. 2014b. Bedrock geology of the Amer Belt, adjacent Neoarchean rocks and flanking northeast Thelon Basin in parts of NTS 66A, B, G and H, Nunavut. Geological Survey of Canada, Open File 7242, 1 sheet.

LeCheminant, A.N., Miller, A.R., Booth, G.W., Murray, M.J. and Jenner, G.A. 1979. Geology of the Tebesjuak Lake map area: a progress report with notes on uranium and base metal mineralization. Geological Survey of Canada, Open File 663, 26 pp.

LeCheminant, A.N., Ashton, K.E., Chiarenzelli, J., Donaldson, J.A., Best, M.A., Tella, S., and Thompson, D.L. 1983. Geology of Aberdeen Lake map area, District of Keewatin: preliminary report. Geological Survey of Canada, Current Research, Part A, Paper 83-1A, 437-448.

LeCheminant, A.N., Jackson, M.J., Galley, A.G., Smith, S.L. and Donaldson, J.A. 1984. Early Proterozoic Amer Group, Beverly Lake map area, District of Keewatin. Geological Survey of Canada , Current Research, Part B, Paper 84-1B, 159-172.

LeCheminant, A.N. and Heaman, L.W. 1989. Mackenzie igneous events, Canada: Middle Proterozoic hotspot magmatism associated with ocean opening. *Earth and Planetary Science Letters*, 96, 38-49.

LeCheminant, A.N. and Roddick, J.C. 1991. U-Pb zircon evidence for widespread 2.6 Ga felsic magmatism in the central District of Keewatin, N.W.T: Radiogenic Age and Isotopic Studies. Report 4, Geological Survey of Canada, Paper 90-2, 91-99.

McEwan, B. 2012. Structural style and regional comparison of the Paleoproterozoic Ketyet River group in the region north-northwest of Baker Lake, Nunavut. Unpublished M.Sc. thesis, University of Regina, 121pp + appendices.

McMartin, I., and Dredge, L.A. 2005. History of ice flow in the Schultz Lake and Wager Bay areas, Kivalliq region, Nunavut. Geological Survey of Canada, Current Research, B2, 1-12.

Miller, A.R. and LeCheminant, A.N. 1985. Geology and uranium metallogeny of Proterozoic supracrustal successions, central District of Keewatin, N.W.T. with comparisons to northern Saskatchewan: *in* Sibbald, T.I.I and Petruk, W., (eds.), Geology of uranium deposits, Canadian Institute of Mining and Metallurgy, Special Vol. 32, 167-185.

Overton, A. 1979. Seismic reconnaissance survey of the Dubawnt Group, districts of Keewatin and Mackenzie. Geological Survey of Canada, Current Research, Part B, Paper 79-1B, 397-400.

Patterson, J.G. 1986. The Amer Belt: remnant of an Aphebian foreland fold and thrust belt. *Canadian Journal of Earth Sciences*, 23, 2012-2023.

Pehrsson, S.J., Berman, R., and Davis, W.J. 2013a. Paleoproterozoic orogenesis during Nuna aggregation: a case study of reworking of the Archean Rae craton, Woodburn Lake, Nunavut. *Precambrian Research*, 232, 167-188.

Pehrsson, S., Ramaekers, P., Fayek, M., Eglington, B.E., Rainbird, R. and St-Onge, M., 2013b. Extent and metallogenic significance of the Racklan-Forward orogen in Canada (abstract) *in* Program with Abstracts, GAC-MAC Joint Annual Meeting, 160.

Peterson, T.D. and Born, P. 1994. Archean and Lower Proterozoic geology of western Dubawnt Lake, Northwest Territories. Geological Survey of Canada, Current Research 1994-C, 157–164.

Peterson, T.D., van Breemen, O., Sandeman, H. and Cousens, B. 2002. Proterozoic (1.85–1.75 Ga) igneous suites of the Western Churchill Province: granitoid and ultrapotassic magmatism in a reworked Archean hinterland. *Precambrian Research*, 119, 73-100.

Peterson, T., Pehrsson, S., Jefferson, C., Scott, J., and Rainbird, R. 2010. The Dubawnt Supergroup, Canada: a LIP with a LISP. December 2010 LIP of the month [online]. Available from http://www.largeigneousprovinces.org/LOM.html, [accessed 18 September 2012].

Peterson, T., Scott, J.M.J., LeCheminant, A., Chorlton, L.B., and D'Aoust, B. 2014. Geology and digital database, Tebesjuak Lake, NTS 65O. Geological Survey of Canada, Canadian Geoscience Map 158, scale: 1:250,000.

Pilkington, M. and Keating, P.B. 2009. The utility of potential field enhancements for remote predictive mapping. *Canadian Journal of Remote Sensing*, 35, S1-S11.

Rainbird, R.H., Hadlari, T., Aspler, L.B., Donaldson, J.A., LeCheminant, A.N. and Peterson, T.D. 2003. Sequence stratigraphy and evolution of the Paleoproterozoic intracontinental Baker Lake and Thelon basins, western Churchill Province, Nunavut, Canada, *Precambrian Research*, 125, 21–53.

Rainbird, R.H., Davis, W.J., Pehrsson, S.J., Wodicka, N., Rayner, N., and Skulski, T. 2010. Early Paleoproterozoic supracrustal assemblages of the Rae domain, Nunavut, Canada: Intracratonic basin development during supercontinent break-up and assembly. *Precambrian Research*, 181, 167-186.

Scott, J., Peterson, T.D., Jefferson, C.W., Cousens, B. 2010. Proterozoic (1.85-1.7 Ga) granitoid rocks and uranium in the Baker Lake – Thelon Basin region, Nunavut. *In* GeoCanada 2010 Extended Abstracts, Calgary, Alberta, 4 pp.

Scott, J.M.J. 2012. Paleoproterozoic (1.75 Ga) Granitoid rocks and uranium mineralization in the Baker Lake – Thelon Basin region, Nunavut. Unpublished M.Sc. Thesis, Carleton University, 127 pp.

Scott, J.M.J., Peterson, T.D., and McCurdy, M.W. 2012. U, Th, REE occurrences within Nueltin granite at Nueltin Lake, Nunavut: recent observations. Geological Survey of Canada, Current Research 2012-1, 11 pp., doi: 10.4095/289393.

Tella, S. 1984. Geology of the Amer Lake (NTS 66H), Deep Rose Lake (NTS 66G), and parts of the Pelly Lake (NTS 66F) map areas, District of Keewatin, NWT. Geological Survey of Canada Open File 1043, 1 sheet, scale 1:250,000.

Tella S. 1994. Geology, Amer Lake, 66 H, Deep Rose Lake (66 G), and parts of Pelly Lake (66 F): Geological Survey of Canada, Open File 2969, 1 sheet, scale 1:250 000.

Thomas, M.D. 2012. Shallow crustal structure in Meadowbank River - Tehek Lake area: insights from gravity and magnetic modellin. Geological Survey of Canada, Open File 7308, 42 pp, doi: 10.4095/292157.

Thomas, M.D., and McHardy, S. 2007. Magnetic insights into basement geology in the area of McArthur River uranium deposit, Athabasca Basin, Saskatchewan: *in* Jefferson,

C.W. and Delaney, G., (eds.), EXTECH IV: Geology and Uranium EXploration TECHnology of the Proterozoic Athabasca Basin, Saskatchewan and Alberta; Geological Survey of Canada, Bulletin 588, 425-440.

Thomas, M.D. and Wood, G. 2007. Geological significance of gravity anomalies in the area of McArthur River uranium deposit, Athabasca Basin, Saskatchewan: *in* Jefferson, C.W. and Delaney, G., (eds.), EXTECH IV: Geology and Uranium EXploration TECHnology of the Proterozoic Athabasca Basin, Saskatchewan and Alberta; Geological Survey of Canada, Bulletin 588, 441-464.

Tschirhart, P., Morris, W.A., and Jefferson, C.W. 2013. Geophysical modeling of the Neoarchean Woodburn Lake and Paleoproterozoic Ketyet River groups, and plutonic rocks in central Schultz Lake map area, Nunavut. Geological Survey of Canada, Current Research 2013-2, 19 pp., doi:10.4095/292116.

Tschirhart, V., Morris, W.A. and Oneschuk, D. 2011a. Geophysical series, geophysical compilation project, Thelon Basin, Nunavut, NTS 66A, B, and parts of 65N, O, P, 66C, F, G and H. Geological Survey of Canada, Open File 6944, doi:10.4095/288806.

Tschirhart, V., Morris, W.A., Ugalde, H. and Jefferson, C.W. 2011b. Preliminary 3D geophysical modelling of the Aberdeen sub-basin, northeast Thelon Bain region, Nunavut. Geological Survey of Canada, Current Research 2011-4, 12 pp., doi: 10.4095/287165.

Tschirhart, V., Morris, W.A., Jefferson, C.W., Keating, P., White, J.C. and Calhoun, L. 2013a. 3D geophysical inversions of the northeast Amer Belt and their relationship to structure. *Geophysical Prospecting*, 61, 547-560.

Tschirhart, V., Morris, W.A. and Jefferson, C.W. 2013b. Framework geophysical modelling of granitoid vs. supracrustal basement to the northeast Thelon Basin around the Kiggavik uranium camp, Nunavut. *Canadian Journal of Earth Sciences*, 50, 667-677.

Tschirhart, V., Morris, W.A. and Jefferson, C.W. 2013c. Faults affecting the northeast Thelon Basin: improved basement constraints from source edge processing of aeromagnetic data: *in* Potter, E., Quirt, D., and Jefferson, C.W. (eds.), Uranium in Canada: Geological Environments and Exploration Developments; Volume 21, Special Issue of Exploration and Mining Geology (CIM).

Wijins, C., Perez, C., and Kowalczyk, P. 2005. Theta map: Edge detection for magnetic data. *Geophysics*, 70, L39-L43.

Young, G.M. 1979. Geology of the Western Part of the Amer Belt (NTS Sheets 66G1, G2, H5, H6 and parts of G8 and H4), Keewatin. Western Mines Ltd (operator), Mineral Assessment Report 081047, Department of Indian Northern Affairs, Yellowknife, 37 pp., 7 maps.(50000 scale).

Zaleski, E. 2005. Geology, Meadowbank River area, Nunavut: Geological Survey of Canada, Map 2068A, scale 1:50,000.

6. Basal unconformity architecture of the northeast Thelon Basin, Nunavut, derived from integration of magnetic source depth estimates

Tschirhart, V[1]., Morris, W.A[1]. and Jefferson, C.W[2].

1. *MAGGIC, School of Geography & Earth Sciences, McMaster University, Hamilton, Ontario, Canada L8S 4K1*

2. *Geological Survey of Canada, 601 Booth St., Ottawa, Ontario, Canada K1A 0E8*

A version of this manuscript has been submitted to *Interpretation* (January 2014) as: Tschirhart, V., Morris, W.A. and Jefferson, C.W. Basal unconformity architecture of the northeast Thelon Basin, Nunavut derived from integration of magnetic source depth estimates.

6.1 Abstract

Exploration for unconformity associated uranium deposits requires detailed 3D knowledge of depth to the unconformity, reactivated intersecting faults and favourable basement lithology as a framework for geochemistry, alteration and drilling. In the absence of high resolution seismic reflection and dense drill data in an established district, high resolution aeromagnetic data can provide surprisingly detailed 3D constraints by combining multiple semi-automated source depth routines. Such routines are applied to the northeastern part of the late Paleoproterozoic Thelon Basin, termed the Aberdeen Sub-basin, in Nunavut. This region is considered prospective for unconformity-associated uranium deposits by comparison with the Athabasca Basin of northern Saskatchewan. Deposits have so far been discovered adjacent to the Aberdeen Sub-basin where they are hosted by structurally complex Neoarchean and early Paleoproterozoic supracrustal rocks. Prior to the current study, little was known about the interior of the sub-basin, such as the locations of intersecting reactivated faults, the distribution of prospective basement host rocks projected beneath the basin, and the depth configuration of the basal unconformity surface. Early products of this study include a remotely predicted map of basement lithology at the unconformity and a preliminary fault map, based on source edge detection, gravity transects and extension of aeromagnetic marker units from detailed outcrop maps. In this paper the morphology of the unconformity surface and the fault geometries are determined by combining multiple analyses of high resolution aeromagnetic data: three semi-automated depth estimation routines (Werner deconvolution, Euler deconvolution and Source Parameter Imaging); and two potential field inversion procedures. Confidence in depth estimates was increased by stacking the output of individual source depth algorithms. Results are consistent with inversion models of several discrete magnetic sources, and previously reported high resolution gravity transects, seismic refraction depth profiles, eight boreholes and outcrop geology around the sub-basin perimeter. An integrated pseudo-3D source depth estimate of the unconformity surface is presented as thirteen north-south profiles. The revised model of the unconformity surface at the base of the Thelon Formation comprises is a complex set of stepped blocks bounded by four major intersecting fault arrays with approximate offsets ranging from tens to hundreds of metres.

6.2 Introduction

The Thelon Basin, straddling the border of Nunavut and NWT, is stratigraphically and tectonically similar to the Athabasca Basin which is known world-wide for its unconformity-associated uranium deposits (Miller and LeCheminant, 1985). Current uranium prospects are located adjacent to the Aberdeen Sub-basin in the northeastern part of the Thelon Basin, positioned at the intersection of hydrothermally altered reactivated faults within Neoarchean metasedimentary rocks of the Woodburn Lake group that were structurally intercalated with early Paleoproterozoic metasediments of the Amer and Ketyet River groups, and cut by the 1.83 Ga Hudson and 1.75 Ga Nueltin intrusions. Critical to the development of prospective uranium deposits is the distribution of favourable basement rock units and intersecting reactivated faults that controlled the flow of uranium bearing hydrothermal fluids to generate focused deposits (Jefferson et al., 2007). With continued exploration and development of the Thelon region it is anticipated that, like the Athabasca Basin, the search for new deposits will progress inward to areas underlying the Thelon Formation. Much of the current uranium exploration in the Athabasca Basin is directed at locating targets near the unconformity surface between the Athabasca Group and the underlying Archean and Proterozoic basement (Jefferson et al., 2007). Prioritizing areas worthy of more advanced exploration can therefore be decided on the basis of three parameters: 1) favorable rock units below the unconformity surface; 2) the basin architecture - identifying areas where the unconformity surface has been modified by post sedimentation brittle faulting; and 3) minimal depth to basement. A previous study (Tschirhart et al., in prep) derived a remotely predicted geological map for the Aberdeen Sub-basin unconformity surface from a combination of source edge detection, forward modeling of gravity data, and new geological mapping around the sub-basin. Justifications for the lithological and structural interpretations in this predictive geological map were based on the lateral continuity of geophysical markers units from outcrop where these markers were defined both geophysically and litho-structurally. In this study we utilize a combination of geophysical methods in order to more accurately determine the architecture of the Thelon Formation and underlying Amer Group as a pseudo-3D volume in much of the Aberdeen Sub-basin, effectively mapping the geometry of the basal unconformity surface which is the prime future exploration target.

Mapping the detailed morphology of an unconformity surface requires knowledge of depth at a sufficient number of points to accurately constrain interpolation. Boreholes,

if available, provide a hard depth constraint. Unfortunately, the number of boreholes is highly dependent on the exploration history of the basin being modeled. Boreholes tend to be clustered together where exploration companies perceive as high potential areas whether for greenfields exploration or to better characterize a known deposit. For example, within the Athabasca Basin, Card et al. (2010) have modelled stratigraphic horizons within the Athabasca Group and the unconformity surface using borehole defined pierce points. The morphology of the computed lithological surfaces ranges from being locally quite complex, to broad and smooth depending on the density of the boreholes. Hathor (2009) have shown how increasing the number of boreholes in a project area can lead to very different geological and mineral deposit models. Within the Aberdeen Sub-Basin of Nunavut only eight boreholes are documented to intersect the unconformity surface, with the remaining twelve providing minimum depth constraints (Davis et al., 2011). Such boreholes are therefore best used to test the viability of results produced by other approaches.

Sandstone and conglomerate of the Thelon Formation (like the Athabasca Group) have petrophysical properties that are quite distinct from the underlying metamorphic basement rocks. The siliciclastic rocks are non-magnetic, much less dense, and are essentially uniform compared to the heterogeneous and locally highly magnetic underlying basement rocks (Mwenifumbo et al., 2004; Thomas and McHardy, 2007; Thomas and Wood, 2007; Tschirhart et al., in prep). The strong physical property contrast across the unconformity surface has previously been employed to derive depth estimates. For example, Overton (1979) presented the results of 35 seismic refraction depth estimates distributed throughout the Thelon Basin. The seismic depths were reinterpreted by Davis et al., (2011) to differentiate between Thelon Formation and underlying unmetamorphosed Paleoproterozoic strata which Overton (1979) had interpreted as a single unit. More recently Tschirhart et al., (2011b) presented a model of the unconformity surface along eight profiles computed from the available Bouguer gravity data. However, as noted by Tschirhart et al., (2011b) the gravity data available for the Aberdeen Sub-basin are regional in scale with an average station spacing of 12 km. The cross-sections are only capable of detecting broad basement features. Short wavelength features attributed to fault zones and alteration that are important for uranium prospecting are undetectable with this type of data (Hasegewa et al., 1990).

In this paper we propose a multi-component integrated geophysical approach to estimate the depth of an unconformity surface by using high resolution aeromagnetic data (Tschirhart et al., 2011a) that are now available for most such basins (Keating, 2004). Within a sedimentary basin, three main sources contribute to the observed total magnetic intensity (TMI): glacial overburden, sedimentary basin fill, and underlying basement rocks. The glacial overburden, generally thin but variable in thickness, in places can produce high frequency anomalies that add texture to the overall observed magnetic signal. Only rarely does the overburden contribute significantly to the overall magnetic anomaly, and this is usually in specific geological settings where highly magnetic basement provides the source for the Quaternary cover (Gay, 2004). Local iron-rich portions of the quartz-dominated sandstone cover sequence are of limited spatial extent. The iron phase is hematite and therefore has limited aeromagnetic response. The Mackenzie diabase dykes outcrop and produce strong magnetic anomalies. These dykes are well known and ignored for the purposes of depth estimation routines. Thus, the main significant magnetic anomalies are attributed to sources within the basement rocks below the basin, ranging from great depth (Tschirhart et al. in prep.) to at or near the basement-cover interface (Nabighian et al., 2005).

Many techniques have been developed to estimate the depth of buried magnetic sources. All are based on the fundamental concept that the observed magnetic signal is a function of the depth, geometry and physical properties of the causative source body. The two approaches to deriving source depth information are semi-automated depth estimate routines and potential field inversion (Goussev and Peirce, 2010). Semi-automated depth estimation routines employ specific attributes of the spatial morphology of the magnetic anomaly pattern. They systematically pass a fixed size search window or profile length through the complete data set and compute a source depth estimate every time the search algorithm satisfies some acceptance criterion. In some instances by adopting a specific search algorithm the operator automatically assumes the source body has a specific geometry. As demonstrated by Li (2003), source depth estimates derived from these various semi-automated depth estimation routines can yield quite different results. The depth estimates obtained from each method depend on variables such as data quality, the size of the search window, interference of neighbouring anomalies and the source geometry. There are no exact values for selecting the input parameters used in these routines, but rather an operator selects a value linked in some logical way to the target

being sought. Ideally, if an operator were able to correctly select the optimum search window and structural index for each depth source routine and each anomaly then one should obtain perfectly coherent depth estimates. A practical innovation used here is to combine the response from a series of search routines, assuming that a greater number of predicted depth solutions provide an increased confidence in the final solution.

Potential field inversion modeling requires the operator to select or window the region of anomalous signal which is considered representative of a buried source body. For a large dataset with multiple source bodies the operator repeats the inversion model for all isolated sources. Inversion model computation describes three groups of parameters that characterize the source body: location (x,y,z), shape (prism, sphere, etc.,), and physical properties (density, susceptibility, remanence). Jessell (2001) recognised three basic approaches to potential field inversion modeling: 1) discrete object; 2) discrete surface; and 3) voxel mesh volumes. In each case the operator seeks an optimum match between the observed and a calculated model signal. Differences between the methods reflect which aspects of the computational model are fixed while seeking the optimum signal match.

In this paper we aim to establish the morphology of the unconformity surface within the Aberdeen Sub-basin by deriving source depth estimates from the analysis of high resolution aeromagnetic data. We assume that the predominant high-frequency magnetic sources are at or near the basement-sandstone interface. To obtain source depth information we employ three semi-automated depth estimation routines: Werner deconvolution, Euler deconvolution and Source Parameter Imaging (SPI); and two potential field modeling procedures: discrete object modeling (Potent) and voxel mesh modeling (University of British Columbia Geophysical Inversion Facility – UBC-GIF). Initial individual depth solutions are integrated in a series of profiles where we derive an optimum depth to the unconformity surface estimate based on the Werner, Euler and SPI solutions. To interpolate the best fit unconformity surface we employed the empirical basement indicators suggested by Goussev and Pierce (2010). This approach resolves source depth by identifying distinct distributions within the solutions that correspond to the basement-sedimentary cover interface. They note six Werner solution empirical basement indicators: 1) lateral alignment; 2) truncations; 3) change of dip; 4) gap; 5) alignment into a cloud; and 6) bounded noise (Figure 6.1). Source edge detection procedures have been used to outline the distribution of magnetic sources which form the

floor to the Aberdeen Sub-basin (Tschirhart et al., in prep.). Many of these sources can be approximated by a two dimensional geometry and therefore can be modeled as discrete object sources. Solving for these bodies provides additional depth constraints. Finally, models of the unconformity surface along a series of profiles are developed to integrate the soft (interpreted) depth constraints provided by the combined semi-automatic magnetic anomaly based depth estimates, the magnetic inverse model depths, and the seismic depth estimates (Overton, 1979) with the limited hard (observed) depth constraints provided by diamond drill-hole (DDH) pierce points (Davis et al., 2011). Boundaries between individual subsections of the unconformity surface are constrained by fault arrays that were derived by Tschirhart et al. (in prep.) from the magnetic data along with a predictive map of the basement geology beneath the Aberdeen Sub-basin (Figure 6.2). The unconformity model profiles presented here are a revised pseudo-3D estimate of the basin framework.

6.3 Geological and geophysical setting

Located in the western Churchill Structural Province, the Thelon Basin is late Paleoproterozoic, and records the deposition of the Barrensland Group in an intracratonic setting. This fault-bound sedimentary basin records a 200 million year depositional and diagenetic-hydrothermal history that was initiated sometime after 1.75 Ga. During the 200 Ma depositional record the basement faults were periodically reactivated (Chamberlain et al., 2010; Davis et al., 2011). The dominantly flat-lying fluviatile siliciclastic undeformed sandstone and conglomerates of the Thelon Formation unconformably overly the 1.75 Ga Wharton and 1.83 - 1.81 Ga Baker Lake groups. These three groups make up the Dubawnt Supergroup (Rainbird et al., 2003). The Wharton Group and Thelon Formation unconformably overly 2.5 - 1.9 Ga epicontinental strata of the Amer and Ketyet groups (Rainbird et al., 2010). The Amer and Ketyet River groups unconformably overlies magnetic 2.6 Ga rhyolite and basalt of the Snow Island Suite, 2.8–2.6 Ga Neoarchean supracrustal rocks of the Woodburn Lake group and Marjorie Hills assemblage, and older Archean orthogneisses and amphibolites to the east and south of the study area (Figure 6.2). The Neoarchean rocks are structurally intercalated with the early Paleoproterozoic rocks that unconformably overly them. 1.75 Ga Nueltin granite and 1.83 Ga Hudson suite granite and Martell syenite of the Shultz Lake Intrusive Complex (SLIC) variably intrude the Paleoproterozoic and Archean

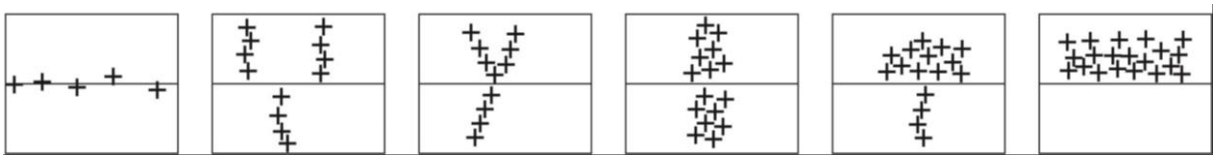

Figure 6.1 Empirical basement indicators modified from Goussev and Pierce (2010). From left to right: lateral alignment, truncations, change of dip, gap, alignment into a cloud and bounded noise.

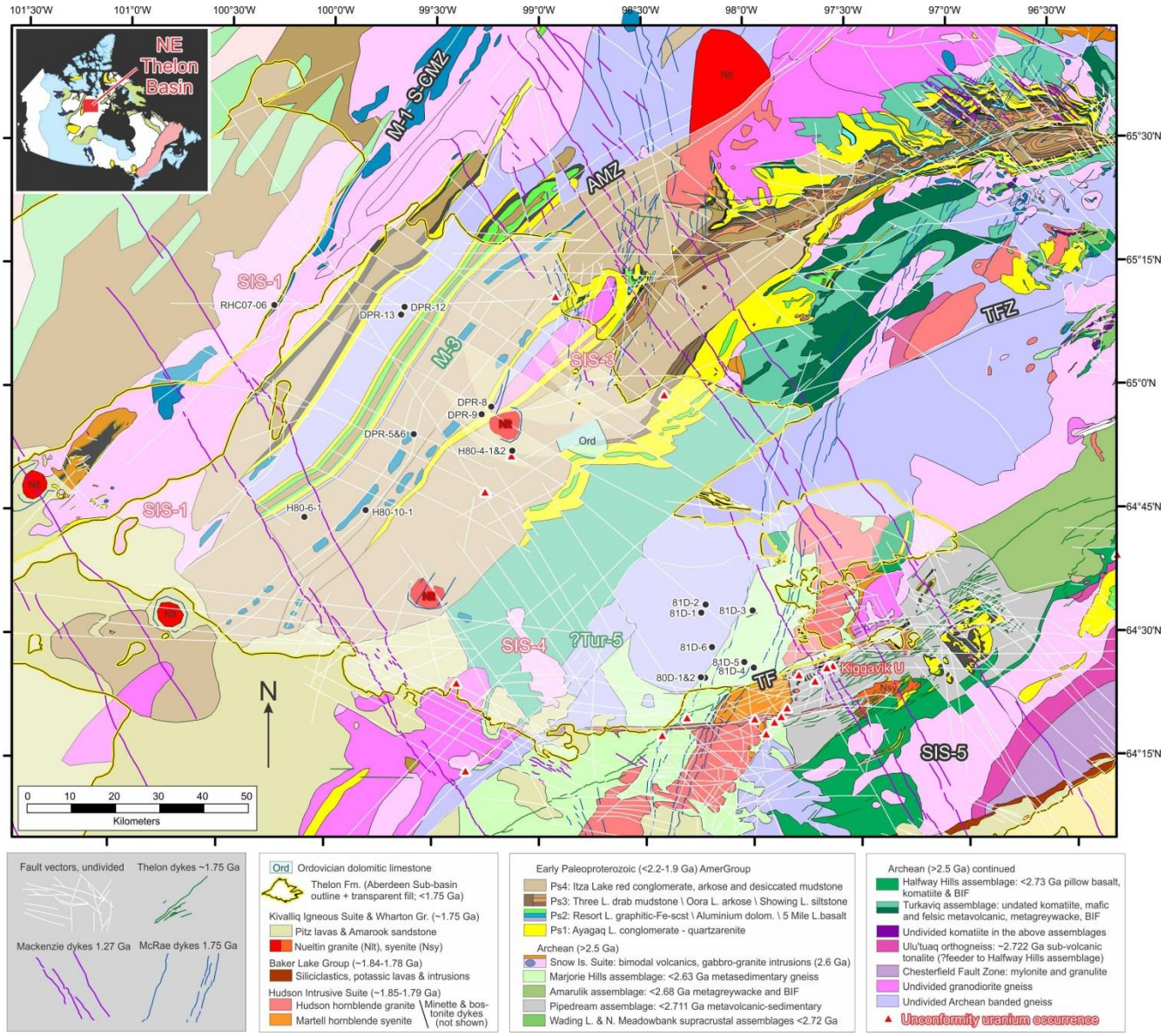

Figure 6.2 Geology of the northeast Thelon region, including remote predicted geology beneath the Aberdeen Sub-basin, modified after Tschirhart et al. (in prep). Codes not explained in legend are: AMZ - Amer Mylonite Zone, TF - Thelon Fault, TFZ - Turqavik Fault Zone, SIS - plutons of the Snow Island Suite, M-3 - mafic intrusion inferred along AMZ, and DDH names shown in black font beside black dots.

basement. Together these belts and complexes constitute the basement to the Thelon Formation.

As the Thelon Formation is magnetically transparent all geophysical signatures visible on the aeromagnetic map are attributed to the magnetic units located at and below the unconformity surface. One exception is the magnetic anomalies associated with the 1127 Ma Mackenzie diabase dyke swarm which are found in surface outcrop and therefore provide no information regarding the unconformity surface. Two notable dyke swarms predate the Thelon Formation and therefore provide distinct calibration of the unconformity surface: the ~350^{o} to 025° McRae Lake diabase (Buchan and Ernst, 2004) and the ~075^{o} to 080° Thelon diabase that has the same orientation as faults dextrally offsetting the McRae Lake dykes (Jefferson et al., 2013). The McRae Lake dyke swarm crops out south of Aberdeen Lake, occupies a 20 km-wide swath beneath the Aberdeen Sub-basin and continues to the northeast across and beyond the Amer Belt (Figure 6.2; Peterson et al., 2010; Jefferson et al., 2013).

As noted above, the basement unconformity surface throughout much of the Aberdeen Sub-basin is underlain by the Amer Group. The Amer Group consists of four supracrustal sequences; Ps1: Ayagaq Lake formation quartzite and conglomerate; Ps2: Resort Lake formation graphitic mudstone, siltstone and non-magnetic sulphide iron formation, Aluminum River formation dolostone and magnetic Five Mile Lake basalt; Ps3: Three Lakes formation mixed grey-green mudstone and siltstone with an upper magnetite iron formation (Calhoun et al., 2011) and Showing Lake formation sandstone with local uranium concentrations; and Ps4: Itza Lake formation sandstone with mudstone that unconformably overlies isoclinally folded Ps1 through Ps3. In the Five Mile Lake, Showing Lake and Three Lakes formations disseminated euhedral magnetite concentrated along certain lithological units is responsible for distinct linear aeromagnetic anomalies that make these marker units so valuable for geophysical analysis (Figure 6.3).

Directly north of the Amer Belt, the Amer Mylonite Zone (AMZ) is a 10 km wide northeast trending belt of highly strained to mylonitic rocks with multiple dextral and a later north-side-down dip slip offset. A mafic extrusive component visible on the aeromagnetic map as a linear magnetic high is interpreted as analogous to 2.6 Ga dioritic rocks discovered along the Slave-Chantry Shear Zone to the northwest (Figure 6.2; Harris et al., 2013). Tracing the magnetic Amer Group and Amer Shear Zone packages

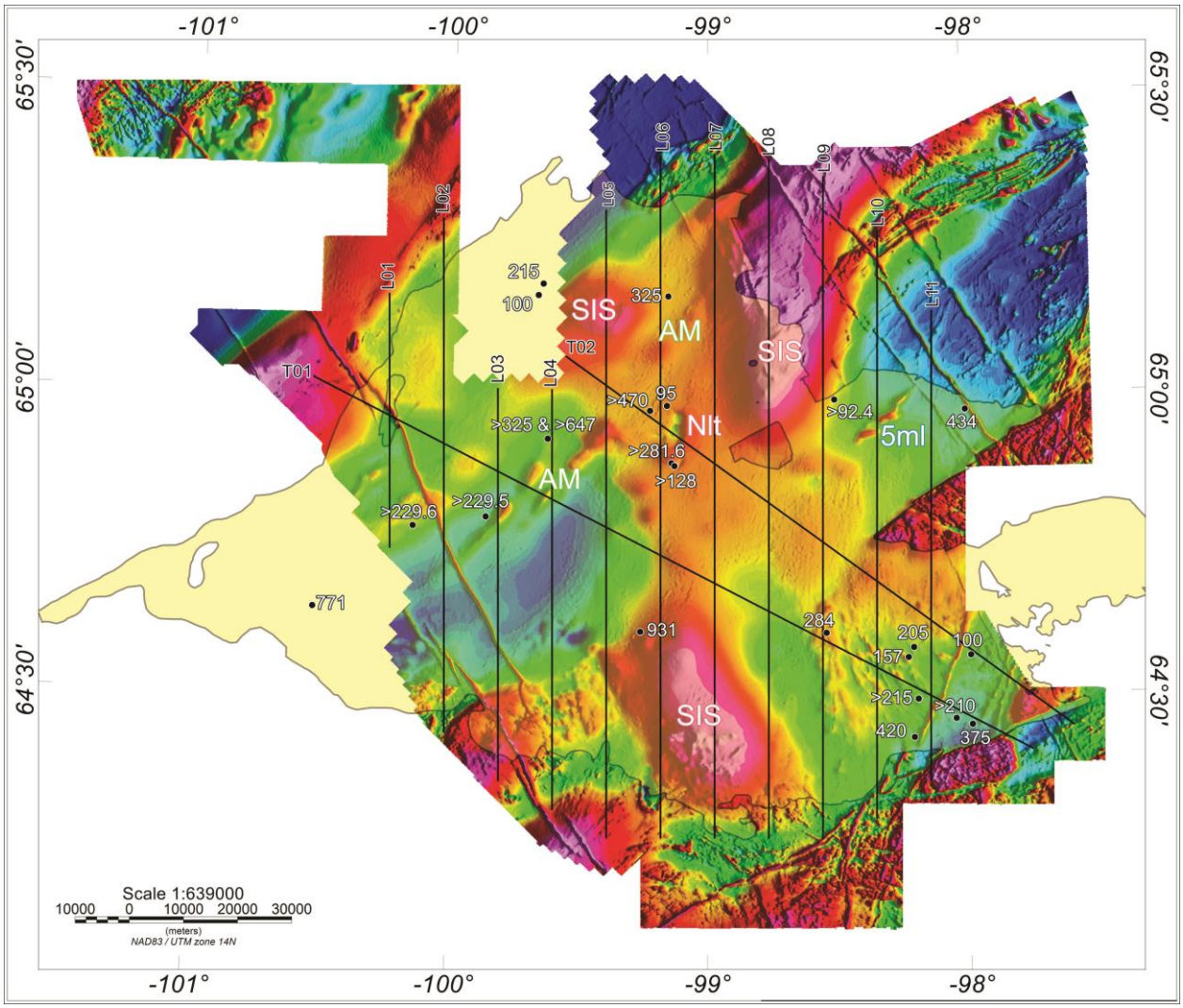

Figure 6.3 Aeromagnetic map of high resolution data encompassing Aberdeen Sub-basin (shown in beige). Source depth profiles are shown as black lines. Publically available DDH and seismic data are black circles; point values correspond to depth to unconformity surface. Magnetic-lithologic units within the sub-basin are as labelled AM (mafic intrusions along the Amer Mylonite Zone); SIS (Snow Island Suite granitoid intrusion); Nlt (Nueltin granite) and 5ml (Five Mile Lake volcanics).

southwest they can be seen to continue beneath the Thelon Formation where their associated magnetic signals are attenuated by the sedimentary cover. With susceptibility and width held equal the attenuation is a direct result of increasing sedimentary cover and thus increasing depth to basement. The eastern third of the sub-basin is underlain by three broad bands that are internally homogeneous but distinct from each other, from west to east: the Neoarchean Turqavik supracrustal belt, Mesoarchean banded gneiss of the Turqavik Horst, and the latest Neoarchean metasedimentary gneiss of the Marjorie Hills assemblage that hosts the distinctive parallel McRae dyke swarm.

6.4 Source depth analysis

Source depth estimation techniques are used extensively to estimate the depth to the magnetic source in the absence of a priori information. Euler and Werner deconvolution are two of the more standard methods and have been in use for decades. Euler deconvolution is based on using Euler's homogeneity equation that solves an over-determined set of linear equations using a least-squares routine. The equation requires that a structural index (SI) be declared for each source, ranging from 0 (contact), 1 (dyke), 2 (horizontal/vertical cylinder) and 3 (sphere) based on the fall-off rate of the field (Thompson, 1982; Reid, 1990). A solution search window designated by the interpreter is generally based on the width of the source.

Werner deconvolution transforms a complex non-linear function magnetic inversion to a simple linear inversion to solve for location, geometry and depth (Hansen and Simmonds, 1993). Like Euler it also uses a moving window (Werner operator) and works for a contact and thin dyke. Both methods use only first derivatives so they are fairly resilient in the presence of noise. However each method can produce erroneous depth estimates where the moving window incorporates interfering signal of broader or adjacent source anomalies.

SPI is a more recent method based on the full analytic signal by computing 3 complex attributes (amplitude, local phase and local frequency) from which source parameters can be computed (Thurston and Smith, 1997). Depth is calculated from the max of the local wavenumber. The method works for SI's from 0 to 2. The maxima obtained from the equations are located over isolated contacts and depth can be estimated without assumptions about the thickness of source bodies. This method works on total field and gradient data, and is not dependent on a user selected window size. The

solutions for dip and susceptibility are valid only at source boundaries, however solutions can be computed at apparent magnetic sources not corresponding to true source boundaries such as magnetic glacial till or noise. Where there is significant curvature, the 2D assumption is violated and poorer solutions arise. SPI uses second derivatives, so it does not hold up in the presence of noisy data.

Simple discrete object modelling is one of the oldest forms of inversion (Jessell, 2001). It is based on the calculation of the magnetic field of a homogeneously magnetized object. We used a dipping prism with horizontal upper and lower surfaces that is aligned parallel to strike (Grant, 1972; Reeves and MacLeod, 1983). The location of the object is selected, and the object is inverted for dip, susceptibility, height, width and depth, with one or more of the properties allowed to be fixed at any given time. An error is calculated based on the deviation between the observed and computed signal.

Although not used directly for its abilities to estimate depth to magnetic source, the UBC-GIF inversion computes a physical property distribution for a 3D volume to account for the 2D observed response (Li and Oldenburg, 1996). It is an automated numerical procedure that constructs subsurface physical property distribution (magnetic susceptibility in this case) which mathematically satisfies the measured magnetic data and any other prior information with the additional condition that the input data be reproduced within a set error tolerance. A model objective function is used to solve the non-linear inverse problem with the model "smooth" in 3 directions and "misfit" the data a predetermined amount. Critical to the inversion is the choice of a depth weighting function which is applied to allow for equal chance susceptibility for cells at different depths. Gaussian noise defines the error tolerance of the data and a positivity constraint is imposed to stabilize the solution by maintaining physical reliability. In a variable geologic environment, no individual source depth routine can be considered ideal and they are best used in conjunction with one another. Issues such as data quality, interference of neighbouring anomalies, source geometry and the inherent non-unique nature of inversion complicate the interpretation. Greater confidence can be placed in the source depths if there is agreement between different routines. Comparison of adjacent lines will further add strength to the solution by looking for consistency of depths. This paper addresses the inherent ambiguity of source depths derived from aeromagnetic data by comparing the results of multiple interpretation algorithms with independent depth

estimates provided by drill-hole data, and seismic points to generate a hypothetical basin architecture of a poorly studied region that has minimal hard geological controls.

6.5 Geological and geophysical assumptions

Source depth routines work on the principle of idealized source geometries. Any deviations from the theoretical bodies introduce error into the depth estimation. Recent studies by Tschirhart et al., (in prep.) compiled a petrophysical property database for rock samples collected in the 2006 to 2012 field seasons from the region around the northeast Thelon Basin. From this data set, six main magnetic geologic (magneto-lithologic) packages have been differentiated (Figure 6.2); Archean mixed granitoid and amphibolitic gneiss; Neoarchean metasedimentary and metavolcanic rocks tentatively assigned to the 2.7 Ga Woodburn Lake group; the Neoarchean Marjorie Hills metasedimentary gneiss; the Amer Mylonite Zone with inferred associated 2.6 Ga mafic intrusions (AM); other igneous intrusions of 2.6, 1.83 and 1.75 Ga vintage, and the <2.2 to <1.9 Ga Amer Group. The 2.6 Ga Snow Island Suite (SIS) plutons are evident on the aeromagnetic map as broad magnetic highs stretching over 50 km wide that punctuate the interior and peripherals of the Aberdeen Sub-Basin (Figure 6.3). They are unconformably overlain by the Ps1 basal quartzite of the Paleoproterozoic Amer and Ketyet Belts. Except where bounded by faults, anomaly patterns associated with the SIS do not display sharp contacts but rather a subtle attenuation. This suggests they are domal bodies that do not correspond to an integer SI (P. Tschirhart et al., 2013). The Neoarchean Marjorie Hills assemblage and the Woodburn Lake group supracrustal rocks show broad mottled anomalies and with the exception of local iron formation are not favorable candidates for computing source depth estimates. Of the magnetic lithostructural marker units noted in Geological and geophysical setting, only the Amer Mylonite Zone mafic intrusions (AM), a central inferred 1.75 Ga Nueltin granite intrusion (Nlt), McRae dykes, and the Amer Group, particularly the Five Mile Lake volcanics (5ml), display idealized source geometry as either a contact, thick dyke or thin dyke. Furthermore, these units are relatively isolated so there is little interference with neighbouring bodies. The northeast-trending 1.75 Ga McRae diabase dykes subcrop at the base of the Thelon Formation unconformity surface within the Marjorie Hills assemblage and are also suitable modelling candidates to determine the depth of the overlying Thelon Formation. The 1.76 Ga Nueltin intrusion inferred beneath the central Aberdeen Sub-basin intrudes the Amer

Group and represents the depth of Thelon Formation. Several DDH close to the intrusion corroborate the depth estimates.

Interspersed in the magnetic geologic packages are several non-magnetic packages, therefore some discretion must be applied when selecting locations to estimate basement depths. The Thelon Formation variably covers the non-magnetic Amarook sandstone of the Wharton Group but this is generally less than 100 m thick. For the purposes of modeling cover thickness it is included with the Thelon Formation. The Amer Group is defined by the 5 m to 600 m thick Ps1 Ayagaq non-magnetic quartzite package and after isoclinal folding, imbricate thrusting was capped with a profound unconformity by the Ps4 Itza Lake formation non-magnetic sandstone, conglomerate and mudstone. The Itza Lake formation is unconformably overlain by the essentially flat lying Wharton Group and Thelon Formation strata. The Ayagaq quartzite, Itza Lake arkose, Wharton Group and Thelon formation are geophysically almost indistinguishable from one another. The Amer Belt as modelled in the profiles does not necessarily incorporate the thickness of the Ayagaq, Itza Lake or Wharton units where these underlie Thelon Formation because they are all magnetically transparent. The depth to the unconformity as profiled here may represent depth of Thelon +Wharton + Itza. In the case of the inferred mafic intrusions along the Amer Mylonite Zone, these underlie the Amer Belt where it transects the centre of the Aberdeen Sub-basin. The modeled depths to mafic source represent the total thickness of Thelon + Wharton + Amer Group, and do not necessarily incorporate the thickness of the Ayagaq formation.

6.6 Methodology

6.6.1 Data reduction

The magnetic data used for this study are from a compilation developed under a Letter of Agreement with nine companies operating in the northeast Thelon Basin, and are publically available from the Canadian Geoscience Data Repository. Flight lines are spaced from 200 m to 400 m, and oriented in a number of directions depending on the individual survey. For depth consistency, each of the industry data sets was upward continued to a common ground clearance of 130 m to match the flight height of the Geologic Survey of Canada data. The high resolution compilation map which was stitched to the regional data provided by the Canadian Geoscience Data Repository was

gridded to 100 m using minimum curvature and reduced-to-pole (RTP) (Tschirhart et al., 2011a).

A series of profiles oriented north-south and spaced 10 000 m apart were extracted from the stitched compilation map, as well as two tie-lines oriented northwest-southeast intersecting several Overton depth points and DDHs (Figure 6.3). The authors chose to work in profile form in order to build a 3D model that can incorporate previous and future 2D geological cross-sections and individual depth points. Werner and Euler deconvolution were run on the extracted profiles in Oasis Montaj. Several passes were run on the profiles using a variety of window sizes to maximize the solutions and determine the ideal moving window width. The ideal moving window size is large enough to enclose one anomaly but small enough to avoid interference of neighbouring anomalies. For Euler deconvolution, a moving window size of 10 000 m, a maximum depth extent of 3000 m and an error tolerance of 10% was chosen. For Werner deconcolution, window length varied from 400 m – 12000 m using an expansion increment of 100 m and a shift increment of 100 m. The depth solutions were corrected for the strike of each anomaly under consideration. The Goussev and Pierce (2010) empirical basement indicators were present in all the extracted profiles (Figure 6.1, 6.4). These guided the interpretation. SPI was run on the RTP aeromagnetic grid using the GX extension in Oasis Montaj. The solutions were extracted to the magnetic profiles and exported into GM-SYS Solutions, along with any drill-hole data or seismic depths that could be projected onto a profile. Using these constraints, the depth slices were generated by modifying a series of polyhedra.

Additional point depth constraints were computed for individual discrete magnetic anomalies using the assumptions described above. Using Oasis Montaj's Potent software 2D inversions of the magnetic profile data across discrete anomalies along the source depth estimates were computed for a dipping dyke model with only susceptibility, depth and dip being allowed to vary. Susceptibility values were held within the range of known physical property characteristics, and the dip was held within 10° of vertical . The width for the McRae dykes was held constant at 100 m and for the Five Mile Lake volcanics at 400 m based on field mapping by the third author and previous forward models, respectively (V. Tschirhart et al., 2013a; 2013b). For anomalies associated with inferred mafic intrusions along the Amer Mylonite Zone, the source width was also allowed to vary as there are no a priori geometrical data for this unit. Strike length and height were

held constant for each profile, with values estimated from the apparent strike of the unit on the aeromagnetic map. As there is no previous sampling or ground-truthing of the Amer Mylonite Zone mafics, the maximum depth extent of the Potent models for this unit was set to 2000 m. This is operating on the assumption that these mafic bodies extend to considerable depth, having intruded along the shear zone. Care was made to ensure the depth model for the estimated source depth were in agreement with the top of the Potent model, taking into account the survey elevation. This procedure was applied to profiles across the Amer Mylonite mafics, the McRae diabase dykes, the Nueltin intrusion and the Five Mile Lake volcanics. The maximum allowed RMS error for the observed versus computed responses was 5 nT. The depth to magnetic source obtained from the models was incorporated into the GM-SYS model to be used in conjunction with the source depth estimates.

The data preparation for UBC-GIF followed the methodology implemented in Spicer, et al., (2011) and Tschirhart et al., (2013a) using ModelVision. A 200 m voxel size was chosen, 3% Gaussian noise was specified as the data error tolerance, a z-increment of 1.11 and the voxel mesh extended to a depth of 3000 m. Individual sub-set areas were selected over isolated anomalies and then submitted for the inversion to save computational time and to focus on areas that are good candidates for an inversion. These areas coincided with fairly confident solutions from the source depth routines over the magnetic Five Mile Lake volcanics in the east.

6.6.2 Unconformity model development - profiles

Estimates of the morphology of the basal Thelon and Amer unconformities were developed for each of the magnetic profiles. Constraints imposed by the geology of the Thelon Formation as mapped in outcrop were enforced in each of the model profiles. For example, at surface where exposed the Thelon Formation is uniformly flat-lying so the integrity of this geologic assumption was maintained throughout all the profiles. The third author has previously mapped a number of faults transecting the sub-basin. For each fault a down-drop direction has been assigned on the basis of remote predictive geology (Tschirhart et al., in prep.). This knowledge was incorporated into each model profile and where appropriate between profiles by forcing abrupt changes in sedimentary thickness to coincide with known fault locations, and utilizing the correct sense of fault down-drop displacement. Coherency was maintained between profiles by ensuring depth to basement of fault blocks were relatively consistent between adjacent profiles.

As explained above due to magnetic transparency, we chose to invert only data over the Thelon Formation and Amer Group. These two packages have undergone extensive studies and contain the most magnetic marker constraints. Less geological knowledge is available in the southwest margin of the sub-basin. Magnetic anomaly patterns in this area are "stippled" making it difficult to generate any reliable depth solutions. Extensive knowledge is available in the southeast, near the Kiggavik exploration camp; however, the units underlying the Thelon Formation here also display non-ideal source geometry, with the exception of the McRae dykes. The depths ascertained in this region are mainly functions of the DDH data, the depth to McRae dykes generated using Potent (i.e. the depth of the Thelon Formation), and the down-drop direction of transecting faults.

Basal unconformity depths on each profile were primarily constrained using the semi-automated depth estimates based on the guidelines provided by Goussev and Peirce (2010). Using information computed for profile L04 (Figure 6.4) highlights five of the indicators, which can be found to varying degrees throughout all the profiles. The sixth indicator is not visible on profile L04, but is identifiable on adjacent profiles as Werner solutions aligned along the basement-sandstone interface (Figure 6.1). Also visible on Figure 6.4 are the Euler and SPI solutions. Euler deconvolution results identified the horizontal position of the contact, and top and horizontal position of a dyke. The SPI algorithm as implemented in Oasis Montaj generates a grid of solutions producing many spurious solutions along the profiles. SPI solutions were only taken into consideration when there was agreement with Euler and/or Werner solutions, and the position along the profile corresponded to an idealized isolated source geometry. For the majority of the depths, the Euler solutions and Werner basement indicators were within general agreement of each other. These depths guided the interpretation along the profile, along with any DDH or seismic information. Several regions on the aeromagnetic map do not contain magnetic anomalies yet generated Werner, Euler or SPI solutions. These areas are extensively glaciated and display small, high frequency anomalies attributed to glacial overburden. These depths were ignored as they are not based on basement units.

Within the Amer Belt there are two magnetic lithostructural units, the Five Mile Lake volcanics and Three Lakes formation. The underlying Three Lakes formation can be identified along some of the profiles within the belt as an apparent empirical basement indicator making it difficult to ascertain the depth to the base of the Amer Belt. DDH

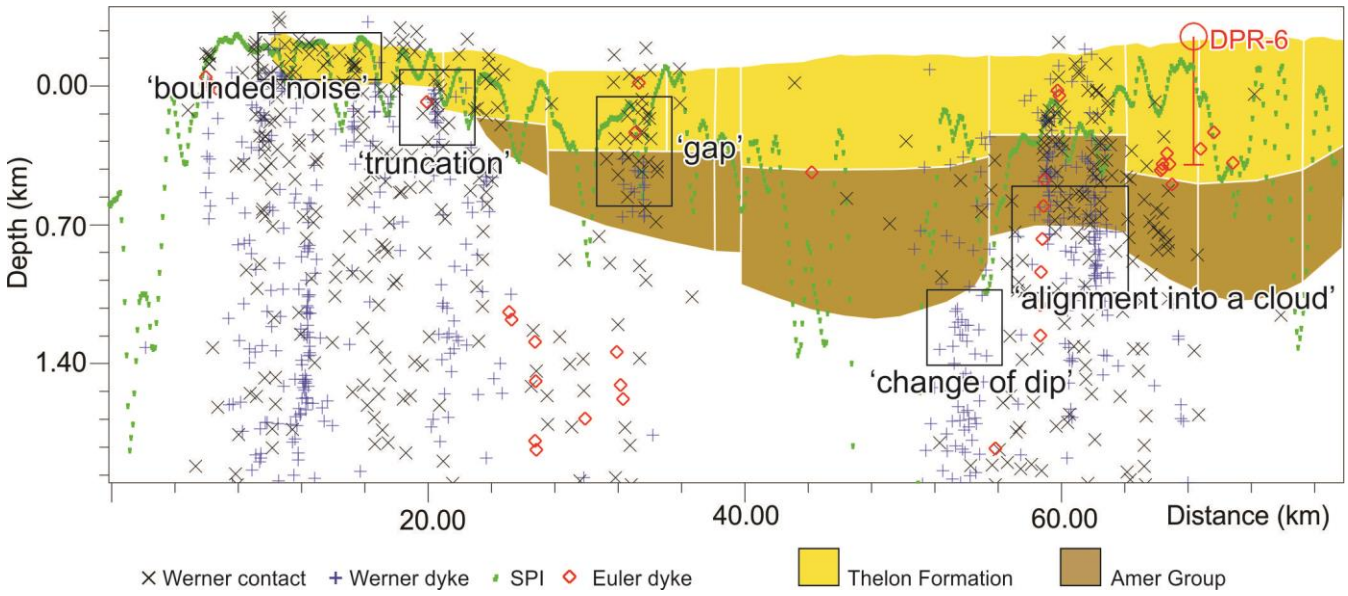

Figure 6.4 L04 cross-section illustrating the source depth solutions and empirical basement indicators shown in Figure 6.1.

information transecting this package to corroborate the depths is very sparse therefore less confidence can be placed in this boundary. Interpretations had to be strengthened through the use of discrete object inversion along these profile lines.

Finally the 3D inversion blocks were draped coincidentally along the profiles and adjacent to the Potent models to look for further corroboration in depth (Figure 6.5). Although not used characteristically for its use in estimating depth to magnetic source, the inversion provided an alternative guideline for identifying depth to source. Commonly the inversions produced depths to the volcanics relatively consistent with the Potent models and source depth interpretations, it poorly defines the basement to the anomalies. The UBC-GIF inversion places increasingly long wavelengths at increasing depths, spreading the anomaly out from its centre at depth. This creates a "smooth blob" anomaly, unrepresentative of the bodies' true form. This can be avoided with the use of geologic and geophysical constraints; however, given the absence of drill-hole data and surficial controls on stratigraphic extents, this is not possible in this area. The inversion looks for consistency between it and the Potent and source depth solutions. The final inversion was draped behind the GM-SYS models to look for consistency of results and compare the solutions. Together with the discrete models, DDH data and 2D profiles, the inversion was integrated into Encom's PA to generate a comprehensive 3D model for the region of the Aberdeen Sub-basin under investigation To demonstrate lateral variations in the depth and morphology of the unconformity surface we have chosen to present the results as series of 2D interpreted profiles located in georeferenced 3D space using Encom PA (Figure 6.6).

6.7 Results and Discussion

Incorporating the aforementioned constraints into each extracted aeromagnetic profile, Figure 6.6 shows the pseudo-3D model of the Thelon Formation and Amer Belt in context with the faults used in the interpretation. The pink body in the centre of the basin corresponds to the circular Nueltin granite intrusion, with a presumed mafic intrusive outer ring. Several DDH located proximal to the body suggest depths > 470 m to the northwest. Several shallow areas punctuate the interior, the most notable being the Nueltin ring structure where depth to basement is modelled at 150-200 m over the mafic exterior and ~ 350 m in the non-magnetic interior. Emplacement of the Nueltin granite at 1.76 Ga predated the unconformity surface. Differences between the depth estimates from the mafic and felsic portions of the intrusion are unlikely to correspond to topography on

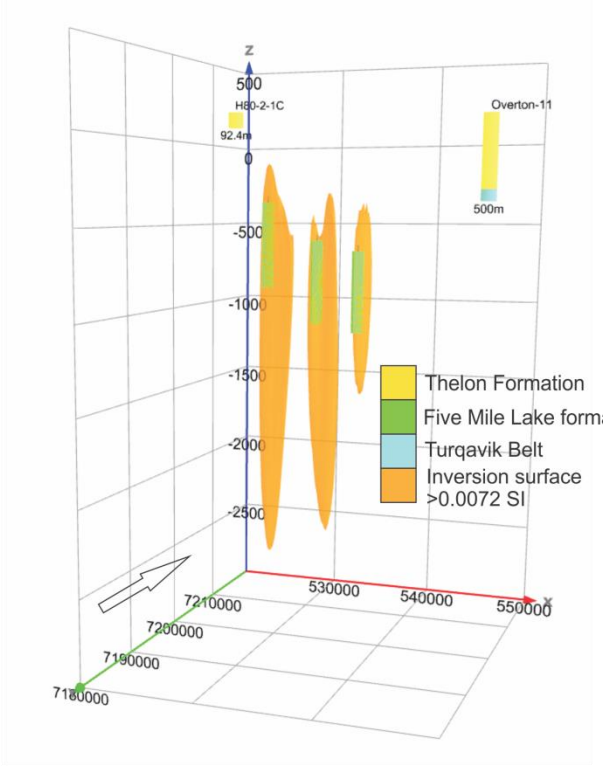

Figure 6.5 Location of Potent models displayed within semi-transparent inversion surface. Nearby DDH and Overton data shown, with maximum depth extent labelled. VE (vertical exaggeration) = 15.

the unconformity surface. It would require faulting between the two mineralogical phases which is not found where similar bodies are found in outcrop. More likely, the difference represents source depth estimate errors possibly associated with the magnetic mineral characteristics of the two phases.

The 3D model shows a highly variable basement topography, with one of the deepest areas of the sub-basin situated within the informally titled ?Tur5 graben (Figure 6.6 point A; Tschirhart et al., in prep.) south and southeast of the Nueltin intrusion. The profile intersecting this area places the depth at ~950 m. However, this depth may be more apparent than real as there are no notable magnetic anomalies in this immediate area. It is possible that the lack of anomalies suggest any sources are deep-seated, or this is a domain of low amplitude magnetic anomalies. The northwest trending fault systems bounding this area have been interpreted as having opposing sense of displacement; both faults exhibit down drop toward the centre of the area creating a graben structure. Work by P. Tschirhart et al. (2013) interpret a significant known horst and graben structure controlled by faults parallel to the Mackenzie dykes termed the Mackenzie fault array. The structure is exposed at surface and provides a direct analogy for the northwest trending horst and graben structures within the Aberdeen Sub-basin that transect the northeast trending Turqavik horst and graben structure. The location and depth extent of ?Tur5 further enhances the Mackenzie fault system as one of the most significant regional structures. The variable nature of the unconformity surface topography may be controlled by these major structures as evidenced by the “lumpy” topography in the central interior of the Aberdeen Sub-basin.

Another fairly deep area is located toward the southwestern part of the sub-basin, within the southwestern extension of the Amer Belt located along L02-L05 (Figure 6.6 point B). This area is also relatively non-magnetic. The southwestern AM are interpreted north of this non-magnetic area, decreasing in observed magnetic amplitude toward the west. The Potent inverse models transecting the AM also decrease in depth toward the southwest if susceptibility, width and height are held constant. This may be a result of increasing thickness of Amer Group and/or Thelon Formation. The Itza Lake formation was mapped in outcrop at the southwest corner of the basin directly south of another presumed Nueltin ring structure (Figure 6.2) suggesting a substantial package of Amer Group likely underlies the Itza Lake formation in this region. Without DDH or seismic data it is impossible to ascertain how much of the decreased magnetic intensity is due to

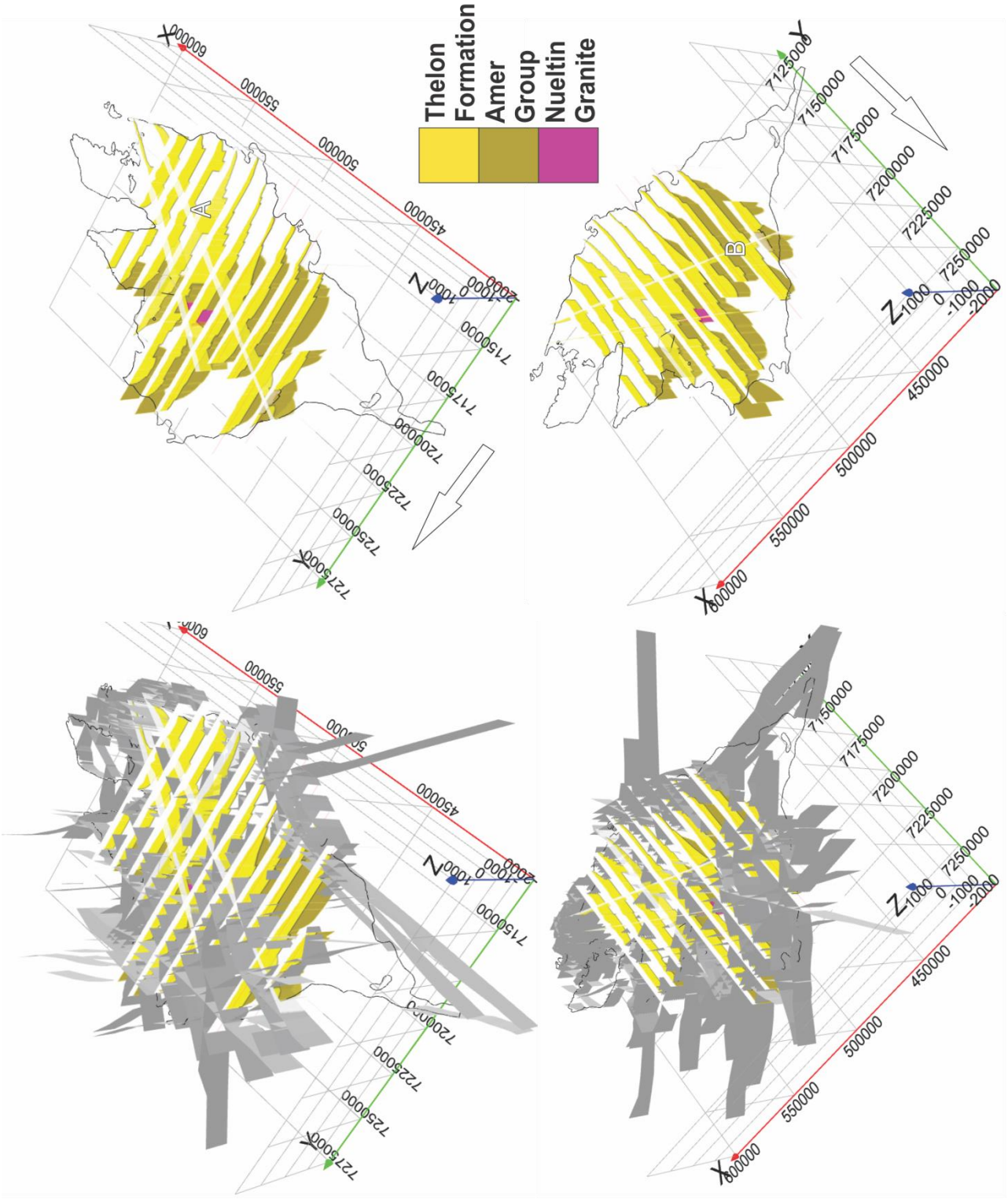
Thelon Formation
Amer Group
Nueltin Granite
A
B
X
Y
Z
600000
550000
500000
450000
7125000
7150000
7175000
7200000
7225000
7250000
1000
0
-1000
-2000

Figure 6.6 Pseudo 3D models of the Aberdeen Sub-basin showing all constructed cross-sections. Left images show fault distributions as mapped by the third author.

increased thickness of Thelon Formation and/or Amer Group. The Thelon Formation may continue to deepen toward the west where there are no high resolution data. An Overton refraction point is located here placing the depth to the unconformity surface at 771 m (Overton, 1979) suggesting the Thelon cover is fairly substantial.

The Five Mile Lake volcanics are mapped in outcrop by the third author as 0-200 m wide, with thickness increasing toward the southeast flank of the belt. Tschirhart et al. (2013a) model the Five Mile Lake volcanics in the northeast Amer Belt as a tightly folded vertically dipping synform 400 m wide and extending 500 m below the surface. This structure is bounded by non-magnetic Ayagaq quartzite. Three profiles are extracted from three separate Five Mile Lake volcanic packages each separated by faults. The models place the depth to the volcanic at ~ 525 m in the eastern extent of the Aberdeen Sub-basin, directly north of the Turqavik fault. An Overton depth estimate 6 km east of L11 has the thickness of Thelon Formation as 434 m, within the range of uncertainty surrounding the depth estimates. Contrasting with the apparent fault down-drop direction mapped by the third author, the Potent, source depth and inversion results place the bodies at increasing depth toward the east (Potent depths of 363 m to 627 m), suggesting that the Thelon Formation thickens slightly toward the Turqavik Fault (Figures 6.2, 6.5). Faults also separate each package, therefore the difference in depth between each model can be attributed to fault displacements, however the modeling in this paper suggests different faults and different offsets than previously inferred by Tschirhart et al. (in prep.) as reproduced in Figure 6.2. From the current modeling, the presence of previously unrecognized Mackenzie faults (trending ~150°) which have southwest-side-down offsets of ~70 m (eastern fault) and ~200 m (western fault) respectively. Alternatively, because these packages are located on the most southeastern flank of the Amer Belt, the Five Mile Lake volcanics may thin toward the east, making the body parameters used in the synthetic models less representative of the true shape. Without detailed drilling, there is no way to discern the actual scenario.

To the southeast, near the Kiggavik exploration camp, there are fewer geophysical constraints. The multiple DDH that intersect the subsurface provide most of the constraints for interpreting depth profiles in this area. Figure 6.7 shows the DDH data in conjunction with the Potent models of the McRae dykes and T01. In comparison to the deep part of the sub-basin, this area is relatively shallow; however it does exceed 500 m

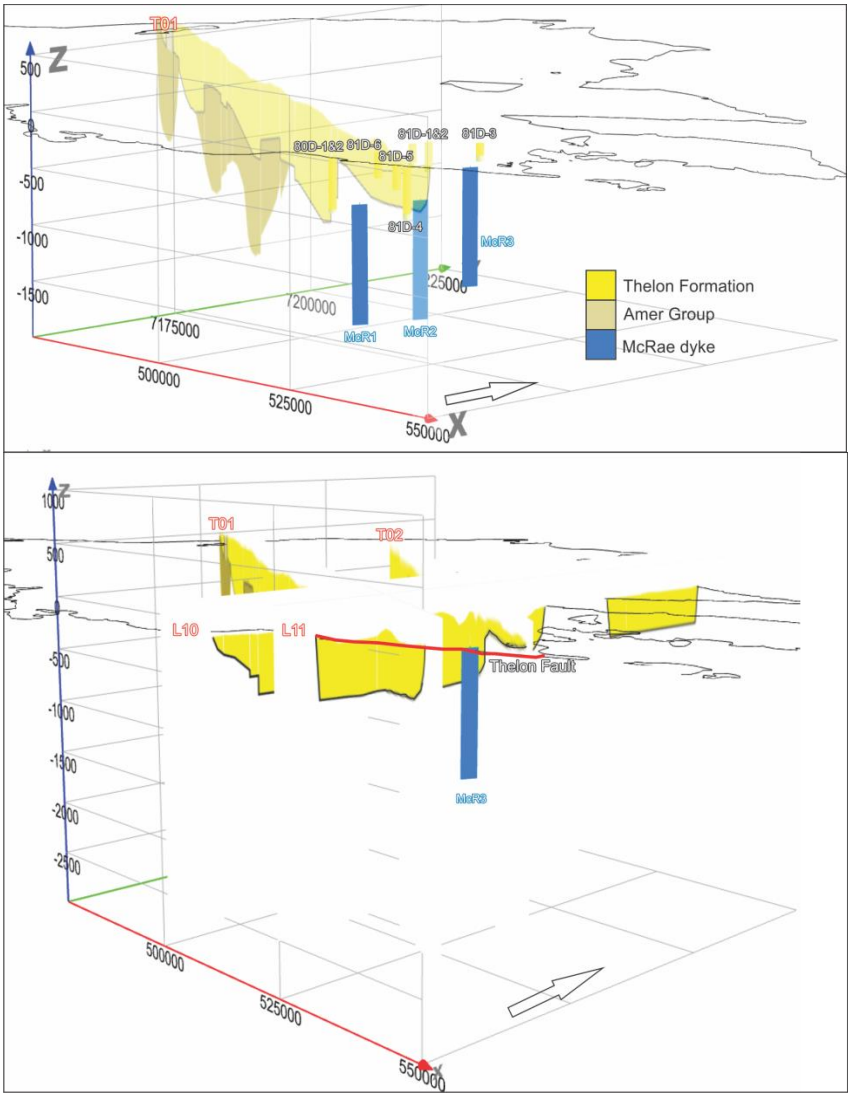

Figure 6.7a Location of DDH in relation to Potent McRae models and cross-section T01. **b)** Cross-sections T01, T02, L10 and L12 shown in relation to the Thelon Fault.

in some place. Moving south along T01 toward the Thelon Fault and past the ?5Tur graben, the Thelon Formation thickens toward the Thelon Fault (Figure 6.7a). Demagnetization of the McRae dykes transecting the southernmost section of T01 (Figure 6.3) suggests the Thelon Formation north of the Thelon fault is relatively deep and/or demagnetized due to hydrothermal fluid flow. Moving west and east along the Thelon Fault and the southern SLIC (Hudson granite and Martell syenite), the Thelon sandstone gently onlaps the Neoarchean metasedimentary gneiss of the Marjorie Hills assemblage, in agreement with drill-hole data and previous geophysical forward models (Figure 6.7b) (Tschirhart et al., 2013b). More detailed drilling would further test this interpretation as there are few discrete anomalies with which to ascertain magnetic source depths. Application of this methodology to an increased number of profiles at a smaller spacing with attention to relative fault history should develop a comprehensive 3D model for the Aberdeen Sub-basin surface and estimate the displacement of individual fault surfaces. This methodology also has potential for application to other related basins like the Athabasca, especially their less explored portions.

6.7.1 Limitations

Changes in the depth of the unconformity between profiles are most apparent when the model is rotated in a 3D viewer. We have not attempted to construct a 3D surface for the unconformity; this could be done by exporting digital results of this study into a full 3D modeling software system. Individual profiles were extracted at a uniform spacing of 10 km from a magnetic anomaly map which was gridded with a 100 m cell size. Actual depth control points defined by the magnetic data processing are irregularly distributed. For areas with subtle magnetic anomaly characteristics the unconformity surface is loosely constrained by extrapolation from adjacent regions where we have solutions. With a 10 km spacing between profiles there are many locations where multiple faults are proposed to exist between individual profiles. Estimating the amount of throw on each fault and incorporating this into a coherent fault history would require many more profiles than we have examined in this study. Some of the magnetic anomalies under consideration may be isolated, making it impossible to ascertain fault throw with respect to nearby blocks that do not contain magnetic marker units.

Throughout all of the magnetic interpretations it is assumed that the bodies being modeled have homogenous physical properties. This is often not the case in nature. Detailed petrophysical sampling has indicated a broad range of susceptibility values in all

the mapped units (ex. the Five Mile Lake volcanics range from 0.000003 SI to 0.05 SI; Tschirhart et al., in prep.), indicating a heterogeneous composition. Interference with adjacent bodies will also contribute to the observed magnetic field and subsequent depth calculation. Further error is introduced by deviation from an idealized source body. All depth estimations must therefore be considered to include uncertainties.

6.8 Conclusions

A combination method of generating a pseudo 3D model of a subsurface layer is presented as applied to the unconformity at the base of the Thelon Formation in the Aberdeen Sub-Basin of Nunavut, prospective for unconformity associated uranium deposits. The morphology of the unconformity surface along a series of profiles was initially derived through the integration of multiple semi-automated source depth algorithms: Werner deconvolution, Euler deconvolution, and Source Parameter Imaging. The basal unconformity surface was located using empirical basement indicators displayed by solutions which included: 1) lateral alignment; 2) truncations; 3) change of dip; 4) gap; 5) alignment into a cloud; and 6) bounded noise (Goussev and Pierece, 2010). These depth estimates were verified by inverse modeling of discrete object sources present on the unconformity surface that also serve as key basement lithotectonic marker units: the Five Mile Lake volcanics, McRae diabase dykes and inferred mafic intrusions along the Amer Mylonite Zone. Additional constraints on the model objects were provided by a 3D unconstrained inversion. Together these solutions constrain the most comprehensive model of a basal unconformity surface to-date. This model identifies several deep areas within the basin, the most notable being the ?Tur5 graben which is interpreted as a result of the 150° Mackenzie fault array. Within the Five Mile Lake volcanics the depth estimates obtained on each body are bounded by faults, and overall give an approximate thickening of Thelon Formation to the southeast, toward the Turqavik Fault. The cross-sections delineate the Thelon Fault as steeply north dipping, whereas northeast and southwest of the fault the Thelon Formation gently onlaps the basement metasedimentary gneiss and granite. A practical innovation used here is to combine the response from a series of search routines. By implementing stacking of depth estimates an increased confidence is placed on the final solution.

Future applications of this integrated method would provide greater understanding of other parts of the Thelon Basin and basins such as the Athabasca where much more company drill-hole data are available and ground gravity transects would be less

expensive to obtain. High resolution ground gravity transects across major faults provide information on the displacement and dip of the faults, thereby improving the resolution of the topography of the unconformity surface. Knowledge of the structure of major faults outside the basin that offset the basal unconformity beneath the basin can help constrain the geometry and architecture of the model. Where applied to answer exploration questions, this methodology identifies prospective areas on the basis of depth to unconformity and the intersection sites of reactivated faults – fundamental criteria for uranium deposits. Where coupled with a remotely predicted basement geological map and a sound knowledge of the fault history of a region, favorable areas for unconformity-associated uranium deposits can be prioritized. The example presented here for the northeastern Thelon Basin aims to improve the status of exploration there, as well as to serve as an example of what could be done to enhance a more advanced exploration region with many more and better populated data sets, such as the Athabasca Basin.

6.9 Acknowledgements

This project is part of the northeast Thelon compilation activity of the GEM Uranium project under the Geomapping for Energy and Minerals Program delivered by the Geological Survey of Canada (GSC). Some of the data reported here were obtained under the previous Secure Energy Supply of Canada Program at GSC. The high resolution geophysical data were acquired through a collaborative Letter of Agreement involving nine companies, the GSC and McMaster University, whereby GSC acquired new geophysics to fill priority gaps in the data. The Industry partners were AREVA Resources Canada, Cameco Corporation, Bayswater Uranium, Forum Uranium, Uranium North, Mega Uranium, Titan Uranium, Western Uranium and Nunavut Tunngavik Incorporated. These partners also shared logistics, geological data and knowledge and participated in ongoing multiple scientific exchanges, including field trips. Financial support to V. Tschirhart was provided by a NSERC Doctoral fellowship. Laboratory and computer costs at McMaster University were supported by an NRCan GEM Grant to WAM.

6.10 References

Buchan, K.L., Ernst, R.E. 2004. Dyke swarms and related units in Canada and adjacent regions. Geological Survey of Canada Map 2022A (scale 1:5,000,000) and accompanying booklet.

Card, C.D., Delaney, G., Bosman, S.A., Fairclough, M., Heath, P., Gouthas,G., and Baker, T. 2010. Modelling the 3D Architecture of rocks and structures of the Athabasca Basin: How Saskatchewan is tackling the challenge from down under. GeoCanada 2010 – Working with the Earth, 1-4 pp.

Calhoun, L.J., White, J.C., MacIssac, D., Jefferson, C.W. and Patterson, J.G. 2011. Basement-cover relationships in the Paleoproterozoic Amer Group, Nunavut (Abstract). Geological Association of Canada – Mineralogical Association of Canada – Society of Economic Geologists Joint Annual Meeting, Ottawa, May 2011, Abstract volume.

Chamberlain K.R., Schmitt A.K., Swapp S.M., Harrison T.M., Swoboda-Colberg N., Bleeker W. et al. 2010. In-situ U-Pb (IN_SIMS) micro-baddeleyite dating of mafic rocks: Method with examples. Precambrian Research 183, 379–387.

Davis, W.J., Gall, Q, Jefferson, C.W., and Rainbird, R.H. 2011. Diagenetic fluorapatite in the Paleoproterozoic Thelon Basin: structural-stratigraphic context, in situ ion microprobe U-Pb ages and fluid flow history. *Bulletin of the Geological Society of America*, 123, 1056-1073.

Gay, S.G. 2004. Glacial till: a troublesome source of near-surface magnetic anomalies. *The Leading Edge*, 23, 542-547.

Goussev, S.A. and Peirce, J.W. 2010. Magnetic basement: gravity-guided magnetic source depth analysis and interpretation. *Geophysical Prospecting*, 58, 321-334.

Grant, F.S. 1972. Review of data processing and interpretation methods in gravity and magnetics, 1964-1971. *Geophysics*, 37, 647-661.

Hansen, R. and Simmonds, M. 1993. Multiple-source Werner deconvolution. *Geophysics*, 58 (12), 1792–1800.

Harris, J R; Hillary, E M; Percival, J A; Buller, G; Buenviaje, R; Bazor, D; Baer, S; Kiessling, G M; Pehrsson, S J; Davis, W; Berman, R G; Wodicka, N; Beauchemin, M; Coyne, M; Therriault, A M. 2013. Geo-mapping Frontiers: Updated information on the regions covered by Operations Baker, Bathurst, Keewatin, Northern Keewatin, Thelon and Wager; Nunavut and Northwest Territories: GIS components; Geological Survey of Canada, Open File 7434; 31 p, doi:10.4095/292744

Hathor Exploration Ltd., 2009. Hathor Exploration's Roughrider zone; one year and a hell of a lot of core later [online]. Available from http://economy.gov.sk.ca/adx/aspx/adxGetMedia.aspx?DocID=11277,11276,11274,11265,11254,11228,3385,5460,2936,Documents&MediaID=33093&Filename=McCready+Open+House+2009.pdf, [accessed 09 September 2013].

Hasegawa, K., Davidson, G.I., Wollenberg, P. and Lida, Y. 1990. Geophysical exploration for unconformity-related uranium deposits in the northeastern part of the Thelon Basin, Northwest Territories, Canada. *Mining Geology*, 40, 83-95.

Jefferson, C.W., Thomas, D.J., Gandhi, S.S., Ramaekers, P., Delaney, G., Brisbin, D., Cutts, C., Portella, P., and Olson, R.A. 2007. Unconformity-associated uranium deposits of the Athabasca Basin, Saskatchewan and Alberta: *in* Jefferson, C.W. and Delaney, G. (eds.), EXTECH IV: Geology and Uranium EXploration TECHnology of the Proterozoic Athabasca Basin, Saskatchewan and Alberta Geological Survey of Canada, Bulletin 588, 23-68.

Jefferson, C.W.J., Pehrsson, S., Peterson, T., Wollenberg, P., Tschirhart, V., Riegler, T., McEwan, B., Tschirhart, P., Scott, J.M.J., Chorlton, L.B., Davis, W., Bethune, K., Riemer, W., Patterson, J., Morris, W.A., Anand, A., and Stieber, C. 2013. Bedrock geology of the western Marjorie-Tehek supracrustal belt and Northeast Thelon Basin margin in parts of NTS 66A and 66B, Nunavut: Geological Survey of Canada, Open File 7241.

Jessell, M. 2001. Three-dimensional geological modelling of potential-field data. *Computers & Geosciences*, 27, 455-465.

Keating, P. 2004. Residual total magnetic field, Athabasca Basin, Saskachewan and Alberta. Geological Survey of Canada, Open File 5674.

Li, X. 2003. On the use of different methods for estimating magnetic depth. *The Leading Edge*, 22, 1090-1099.

Li, Y. and Oldenburg, D.W. 1996. 3-D inversion of magnetic data. *Geophysics*, 61, 394-408.

McMartin, I., and Dredge, L.A. 2005. History of ice flow in the Schultz Lake and Wager Bay areas, Kivalliq region, Nunavut. Geological Survey of Canada, Current Research, B2, 1-12.

Miller, A. R., and LeCheminant, A.N. 1985. Geology and uranium metallogeny of Proterozoic supracrustal successions, central District of Keewatin, N.W.T. with comparisons to northern Saskatchewan*: in* Sibbald, T.I. and Petruk, W., (eds.), Geology of Uranium Deposits: Canadian Institute of Mining and Metallurgy Special Volume 32, 167-185.

Mwenifumbo, C.J., Elliot, B.E., Jefferson, C.W., Bernius, G.R. and Pflug, K.A. 2004. Physical rock properties from the Athabasca Group: designing geophysical exploration models for unconformity uranium deposits. *Journal of Applied Geophysics*, 55, 117-135.

Nabighian, M., Grauch, V., Hansen, R., LaFehr, T., Li, Y., Peirce, J., Phillips, J., and Ruder, M. 2005. The historical development of the magnetic method in exploration. *Geophysics*, 70(6), 33ND–61ND.

Overton, A. 1979. Seismic reconnaissance survey of the Dubawnt Group, districts of Keewatin and Mackenzie. Geological Survey of Canada, Current Research, Part B, Paper 79-1B, 397-400.

Peterson, T., Pehrsson, S., Jefferson, C., Scott, J., and Rainbird, R. 2010. The Dubawnt Supergroup, Canada: a LIP with a LISP. December 2010 LIP of the month [online]. Available from http://www.largeigneousprovinces.org/LOM.html, [accessed 18 September 2012].

Rainbird, R.H., Hadlari, T., Aspler, L.B., Donaldson, J.A., LeCheminant, A.N. and Peterson, T.P. 2003. Sequence stratigraphy and evolution of the Paleoproterozoic intracontinental Baker Lake and Thelon Basins, western Churchill Province, Nunavut, Canada. *Precambrian Research*, 125, 21-53.

Rainbird, R.H., Davis, W.J., Pehrsson, S.J., Wodicka, N., Rayner, N., and Skulski, T. 2010. Early Paleoproterozoic supracrustal assemblages of the Rae domain, Nunavut, Canada: Intracratonic basin development during supercontinent break-up and assembly: *Precambrian Research*, 181, 167-186.

Reeves, C.V., and MacLeod, I.N. 1983. Modelling of potential field anomalies – some applications for the microcomputer. *First Break*, 1(8), 18-24.

Reid, A., Allsop, J.M., Granser, H., Millet, A.J. and Somerton, I.W. 1990. Magnetic interpretation in three dimensions using Euler deconvolution. *Geophysics*, 55, 80-91.

Scott, J., Peterson, T.D., Jefferson, C.W., Cousens, B. 2010. Proterozoic (1.85-1.7 Ga) granitoid rocks and uranium in the Baker Lake – Thelon Basin region, Nunavut. *In* GeoCanada 2010 Extended Abstracts, Calgary, AB, 4 pp.

Scott, J.M.J. 2012. Paleoproterozoic (1.75 Ga) Granitoid rocks and uranium mineralization in the Baker Lake – Thelon Basin region, Nunavut: Unpublished M.Sc. Thesis, Carleton University, May 2012, 127 pp.

Spicer, B., Morris, B., Ugalde, H. 2011. Structure of the Rambler rhyolite, Baie Verte Peninsula, Newfoundland: inversions using UBC-GIF Grav 3D and Mag 3D. *Journal of Applied Geophysics*, 75 (1), 9-18.

Thomas, M.D. and McHardy, S. 2007. Magnetic insights into basement geology in the area of McArthur River uranium deposits, Athabasca Basin, Saskatchewa: *in* Jefferson,

C.W. and Delaney, G. (eds.), EXTECH IV: Geology and Uranium EXploration TECHnology of the Proterozoic Athabasca Basin, Saskatchewan and Alberta Geological Survey of Canada, Bulletin 588, 425-440.

Thomas, M. D. and Wood, G. 2007. Geological significance of gravity anomalies in the area of McArthur River uranium deposit, Athabasca Basin, Saskatchewan: *in* Jefferson, C.W. and Delaney, G. (eds.), EXTECH IV: Geology and Uranium EXploration TECHnology of the Proterozoic Athabasca Basin, Saskatchewan and Alberta Geological Survey of Canada, Bulletin 588, 441-464.

Thompson, D.T. 1982. EULDPH – A new technique for making computer-assisted depth estimates from magnetic data. *Geophysics*, 47, 31-37.

Thurston J.B. and Smith, R.S. 1997. Automatic conversion of magnetic data to depth, dip, and susceptibility contrast using the SPI™ method. *Geophysics*, 62, 807-813.

Tschirhart, P., Morris, W.A., and Jefferson, C.W. 2013. Geophysical modeling of the Neoarchean Woodburn Lake and Paleoproterozoic Ketyet River groups, and plutonic rocks in central Schultz Lake map area, Nunavut. Geological Survey of Canada, Current Research 2013-2, 19 pp., doi:10.4095/292116.

Tschirhart, V., Morris, W.A. and Oneschuk, D. 2011. Geophysical series, geophysical compilation project, Thelon Basin, Nunavut, NTS 66A, B, and parts of 65N, O, P, 66C, F, G and H. Geological Survey of Canada, Open File 6944. doi:10.4095/288806.

Tschirhart, V., Morris, W.A., Ugalde, H. and Jefferson, C.W. 2011. Preliminary 3D geophysical modelling of the Aberdeen sub-basin, northeast Thelon Bain region, Nunavut, Geological Survey of Canada, Current Research 2011-4, 12 p., doi: 10.4095/287165.

Tschirhart, V., Morris, W.A., Jefferson, C.W., Keating, P., White, J.C. and Calhoun, L. 2013a. 3D geophysical inversions of the north-east Amer Belt and their relationship to geologic structure. *Geophysical Prospecting*, 61, 547-560.

Tschirhart, V., Morris, W.A., Jefferson, C.W. 2013b. Framework geophysical modelling of granitoid vs supracrustal basement to the northeast Thelon Basin around the Kiggavik uranium camp, Nunavut. *Canadian Journal of Earth Sciences*, 50, 667-677.

7. Conclusions

Geophysical modelling continues to be a vital tool for companies operating in frontier areas because of its ability to remotely map geological units where traditional means of exploration has not yet reached. With continued development of these regions, it is imperative that a sound understanding of the subsurface geology and geometry is established to focus in on areas for detailed follow-up. This framework serves as a repository within which new data can be incorporated. It is anticipated that as new data is added there will be a resulting improvement in the accuracy and resolution of future models. The case studies presented herein demonstrate the utility of forward and inverse modelling techniques applied to potential field data sets in building a multi-dimensional geophysical framework for key rock packages within and peripheral to the Aberdeen Sub-basin. A collaborative feedback process ensures geometry and lithology deduced from past models feeds into the development of future geophysical models. Through the inclusion of petrophysical and geological constraints the geologic integrity of the model is maintained providing a best-hypothesis interpretation in the absence of abundant controls.

7.1 Chapter Summaries

Chapter 1 introduces the area of interest to this thesis, the northeast Thelon Basin, Nunavut. The GEM-U deliverables are outlined as the primary driver for this thesis. The geophysical methods implemented throughout the case studies are discussed, emphasizing the importance of petrophysical and geological constraints to geophysical models.

Chapter 2 focusses on structure of the northeast Amer synform as part of the larger Amer fold and thrust belt. Multiple hypotheses surround the subsurface form of this structure. The remote location of this area together with the limited outcrop compromises the ability to construct a structural interpretation. The morphology of the synform was investigated through the inversion of high resolution aeromagnetic imagery using the University of British Columbia Geophysical Inversion Facility (UBC-GIF) algorithm. This synform was deemed an appropriate candidate for this methodology as it is apparent on the map as an aeromagnetic bulls' eye. Parts of the larger aeromagnetic anomaly map comprise linear elongate segments. As such, they can be modeled using a series of individual 2D parametric inversion models. Integrating the derived geometry and physical property information into the full 3D inversion creates a geophysically constrained inversion and improves the chance of obtaining geologically feasible solutions The parametric models are correlated via physical properties to an upper magnetic iron

formation in the Three Lakes formation and magnetic Five Mile Lake volcanics, which form the central bulls' eye and southern brim to the synform, respectively. By incorporating geophysical 2D reference models that extend to considerable depth, the inversion was able to escape the "smooth blob" problem, wherein UBC-GIF code will focus all long wavelength magnetic anomalies at depth. This is unrealistic in terms of stratigraphic principles where unit thickness is presumed to be constant. In areas where little a priori information exists, this tool provides a way of maintaining a level of uniqueness in what would otherwise be a totally unconstrained inversion. The inversion generated a flat-bottomed canoe shaped synform in agreement with a forward model of a high resolution gravity transect and coincident geological cross-section. Knowledge of this structure can be extrapolated along the Amer Belt to where it delves below the Thelon Formation and provide invaluable knowledge for documenting the unconformity surface architecture.

Chapter 3 examines the relationship between the Neoarchean ore-hosting metasedimentary rocks and intruding Shultz Lake intrusive complex (SLIC). Recent drilling by Cameco Corporation has identified ore-hosting metasedimentary enclaves within demagnetized lineaments cross-cutting the SLIC. As such, knowledge of the geometry of the SLIC is an important exploration parameter. Samples collected during the 2006-2010 field seasons petrophysically characterize the main lithologic entities of interest and provide constraints to the forward modelling process. The intrusive SLIC is distinct from the metasedimentary packages in being considerably less dense and more magnetic. Within the SLIC, the density and susceptibility of the Martell syenite is laterally variable due to a mixed mineralogical composition. The Hudson granite shows unimodal density and susceptibility variances. The Neoarchean Pipedream and Marjorie Lake assemblages are geophysically indistinguishable from one another, but are modelled as two separate units with similar properties. Implementing joint forward modelling of gravity and magnetic data within petrophysical controls, three structural hypotheses are tested. It is concluded that that the SLIC, together with older metasedimentary and basement gneiss, has been structurally emplaced over the Neoarchean metasediments to the east. Hudson laccoloiths extend from the SLIC at depth. Corroborations between gravity, magnetic and structural mapping re-affirms the validity of the cross-sections. This model provides a semi-quantitative framework for the SLIC and adjacent rock masses, to a depth and spatial extent exceeding that of drilling to date.

Chapter 4 of this thesis develops a new method for the identification and timing of faults within sedimentary basins. Knowledge of the reactivation of basal faults is an important exploration parameter for unconformity-associated uranium deposits, as they will be focussed at high angle faults at or near the basement sandstone interface. Using the newly acquired aeromagnetic data over the Aberdeen Sub-basin the tilt horizontal gradient (TDX) and total field horizontal gradient magnitude (TF-hgm) are calculated, and the Blakely algorithm is used to define the source edge inflection point on these maps (Blakely and Simpson, 1986). For every inflection point, the Blakely algorithm calculates a dip direction, based on the symmetry of that point with respect to the down gradient direction of the magnetic source. Subsequent gridding of these data yields a color image with offsets and abrupt changes in dip direction demarcated by faults. By integrating the dip direction grid with a digital elevation model (DEM) derived from the Canadian Digital Elevation Database and knowledge of the positions of identified, inferred and newly mapped faults, the apparent fault timing can be deduced. Three groups of faults are identified. The first is seen only on the DEM and represent young brittle structures that have no effect on the basement unconformity and are not visible on the dip direction map. The second group is visible on the dip direction map but not the DEM. These are old basement structures that did not propagate upward through the Thelon Formation. The third group has an expression on both the DEM and the dip direction map; these faults are old structures that propagated upward during and/or after deposition of the Thelon Formation The third group of faults may be of greatest interest for uranium exploration, with reactivation increasing their potential to serve as conduits to transport uranium-rich fluids and focus uranium deposition. This method had never before been reported but demonstrates promise for comprehensive mapping of basin faults and tracking the tectonic development of the whole Thelon Basin.

A new remote predictive map (RPM) for the basal unconformity surface is presented in the fifth chapter. A petrophysical database compiling all archived samples through the 2006-2012 field seasons is constructed. These samples, coupled with detailed outcrop mapping provide the means to identify magnetic lithologic units that can be traced below the non-magnetic Thelon sedimentary cover. Augmenting the aeromagnetic imagery through the use of source edge detection routines enhances subtle contrasts that are not readily apparent in the total magnetic intensity image, and better discern subtle lateral contrasts. Correlating these images with outcrop mapping and a petrophysical

database six main magnetic lithologic units are defined: Archean mixed granitoid and amphibolitic gneiss; Neoarchean metasedimentary and metavolcanic rocks tentatively assigned to the 2.7 Ga Woodburn Lake group; the latest Neoarchean Marjorie Hills metasedimentary gneiss; the Amer Mylonite Zone with inferred associated 2.6 Ga mafic intrusions; other igneous intrusions of 2.6, 1.83 and 1.75 Ga vintage, and the <2.5 to <1.9 Ga Amer Group. Five late brittle fault arrays (040°, 075-90°, 120° and 170°) were involved in the development of accommodation space. Expanding the knowledge to the third dimension, four gravity forward models are constructed outside and within the basin under petrophysical controls. These profiles provide further knowledge of the structure and lithology at depth and verify aspects of the proposed geology, particularly the location of the 2.6 Ga Snow Island Suite (SIS) granite intrusions and geometry of the Amer Belt at depth. The new map is a platform for evolving geological interpretations that will be strengthened by advanced drilling.

Chapter six of this thesis is an investigation of integrated source depth routines to generate depth to basement estimates along strategic transects across the sub-basin. An extension of work done in Tschirhart et al. (2011), this manuscript improves on the pre-existing 3-dimensional geological framework and offers an alternative approach to basin modelling in the absence of a priori controls. Thirteen cross-sections are constructed within the bounds of the high resolution aeromagnetic imagery. Automatic source depth routines (Euler, Werner and SPI) are implemented along line to generate a series of source depth estimates for key magnetic lithologic units that abide to idealized source geometries. Where applicable 2 D inverse models transect anomalies and are input in the cross-section along with any drill-hole or seismic information, providing additional constraint. Comparison of multiple methodologies allows for a higher degree of certainty surrounding the depth estimates. The profiles all intersect at least one other section and abide to the pre-existing geological map, apparent down-drop direction of faults and basin extents. The Thelon Formation is modelled as generally flat-lying with abrupt changes in the thickness across previously mapped faults and consistent with neighbouring profiles. Information provided by these models proves that the unconformity surface has a highly variable topography, with the deepest areas located in the southwest Amer Belt and informally titled “?Tur5” graben which is interpreted as a result of the 150° Mackenzie fault array. Within the Five Mile Lake volcanics the depth estimates obtained on each body are bounded by faults, and give an approximate thickening of Thelon Formation

toward the Turqavik Fault to the southeast. The geometry of the Thelon fault is discriminated as steeply north dipping, reaching depths > 500 m on its northern side and consistent with nearby industry drilling. East and west of the Thelon Fault, the Thelon Formation can be seen as gently on-lapping. As new information becomes available, it can be incorporated into the model to improve the resolution and add additional absolute depth constraints.

7.2 Limitations

Geophysical modelling offers a non-invasive means to predict the subsurface distribution of geological units. Including constraints in the modelling process can guide the interpreter towards realistic solutions and limit inherent ambiguity. Unfortunately limitations exist in any geophysical interpretation process. From the initial acquisition of survey data to instrument sensitivity, sample size and availability of data, limitations affect the quality and accuracy of the results and must be addressed.

7.2.1 Constraints

The fundamental problem of non-uniqueness underlies any geophysical interpretation. That is, in the absence of geological constraints a finite number of solutions can replicate the observed potential field signal. It is only through the inclusion of constraints such as borehole data, geological maps, structural interpretations and petrophysical controls, that the geological integrity of the results can be maintained. The availability of information for an area is further correlated to the level of development of that region. More advanced projects will have access to greater repositories of information in comparison to those still in development. Therefore the level of control that can be placed on a potential field model is directly tied to project development. With respect to the Thelon Basin, the availability of information is continuously developing so that the primary publications of this thesis (Chapter 2 and Chapter 4) had limited control in comparison to the latter manuscripts (Chapter 3, 5 and 6). The geological maps used in earlier studies are based on a 800 m spaced regional aeromagnetic survey. The coarse resolution of the data did not permit discrimination of subtle aeromagnetic anomalies and much of the detailed geology was overlooked. The accuracy of the petrophysical controls used in the models is continuously improved as samples are added to the geodatabase. The interpretations in Chapter 5 use a comprehensive dataset that includes all the samples to date, while Chapter 4 uses archived samples, whose lithological groupings may have

changed. That is to say, what was deemed Woodburn Group at that time may not be considered Woodburn Group now or will be further subdivided into Pipedream versus Marjorie Lake assemblage. Knowledge of the subsurface structure in previous Chapters feeds into the development of models in the latter. Fundamental assumptions surrounding the geometry of key basement packages below the Thelon Formation cover are derived from earlier studies (Chapters 2 and 3) and are integrated into subsequent interpretations, specifically the form of fold belts. This sequential reasoning permits the development of more advanced interpretations, but any errors in the primary models are carried over into future analyses.

7.2.2 Modelling

During forward modelling of potential field data the lithological units in consideration are given an assigned physical property. This assumes that the unit as a whole is homogenous, which is not the case in nature. The units are highly heterogeneous due to variable mineralogical compositions. Any given unit can have a range of magnetic susceptibility and density values. By increasing the sample size a more representative average can be obtained, which will have a higher correlation with the observed potential field signal. The acquisition platform may further introduce error into the forward modelling process. The aeromagnetic data is acquired from a moving platform either within or being towed from an aircraft. The survey is flown along flight lines and records the sum contribution of the signal below the sensor. The data is interpolated via a gridding algorithm and fit across the flight-lines based on the chosen algorithm. This can alter the appearance of the observed signal by distorting the anomaly, especially where the strike of the anomaly is acute to the flight line and the flight lines are widely spaced. Forward modelling is undertaken from profiles extracted from the gridded survey data. Errors incurred during the processing stages will be carried over into the modelling process. While the effects are generally minimal, the issue is most notable in small wavelength high amplitude anomalies (i.e. dykes). The signal associated with these features will have a larger wavelength having been aliased across the flight lines. When modelling the body to match the observed signal the interpreter will often have to employ a larger body width than outcrop mapping dictates. Furthermore, forward modelling displays a 2-dimensional output of 3-dimension data and does not account for the 3D input of signal as recorded by the sensor. As the distance increases from source to sensor, signals from neighbouring bodies contribute to the recorded response. As such a 2D

forward model of airborne data may never fully represent the observed geophysical signal.

Depth ambiguity is present in any geophysical interpretation. A potential field signal can be replicated by a thin slab with variable magnetization near surface. Without the imposition of constraints there is no inherent depth information in the model. Geological knowledge must be brought into the forward modelling process to incur a level of control on the depth of the units. With respect to inverse modeling, a depth weighting function is imposed. This places longer wavelength features at increasing depth. Unfortunately this perpetuates the "smooth blob" problem, whereby long wavelength anomalies spread out from the main feature at depth. This feature does not abide to stratigraphic principles where unit thickness is presumed to be consistent.

Many of the constructed cross-sections incorporate an element of fault displacement. Present day fault mapping is through visual analysis of linear features on a DEM (Digital Elevation Model of topographic data), satellite imagery, air photographs, and total magnetic intensity (TMI) maps, in concert with traditional geological field work. Few actual displacements are known. Fault location as depicted in the models is a result of these surficial mapped features; the fault displacement is much more ambiguous. In areas of detailed gravity data a greater degree of certainty can be placed on the displacement (Chapters 3 and 5) by estimating fault geometry and displacement from anomalies in the observed gravity response. Chapter 6 is a much broader scale study. Down-drop direction is known (or hypothesized) but actual displacement is unknown. Displacements as modeled are based on correlations between source depth estimates and borehole data using the apparent down-drop direction across faults.

7.2.3 Physical Properties

Having an established database of petrophysical properties is essential before undertaking a geophysical modelling process. Without knowledge of the physical properties of the units, there is no way to determine whether a solution is geologically realistic. Having a larger database increases the population size and values will be more representative of the true lithology. Limitations in the sampling will directly affect the accuracy of the solution, especially in forward modelling, where the units are assumed to be heterogeneous. A better match between computed and observed responses will be related to the accuracy of the physical property assigned to the unit. Several of the rock

units modelled had no samples so analogies were made with lithologically similar units. Any deviations from this value will manifest itself as discrepancies in the model. Often samples are collected at surface and fail to record any mineralogical or compaction changes with depth. Specifically, the representative average does not account for increased density at depth. Modelling undertaken by Thomas and Wood (2007) model four stratigraphic horizons present in the Athabasca Group sandstone that record increasing density with depth. The limited sampling of the Thelon Formation sandstone did not permit such discrimination; it was modelled as one sequence.

Limitations of the data collection method must also be addressed. Specific gravity was calculated using an Archimedes submersion approach. This estimates density based on the ratio of dry to wet mass of a submersed sample multiplied by the density of the liquid. The value of 1.00 g/cc is used for the water, however it is not distilled. Any debris on the surface of the rock will alter the clarity of the water and affect its density. The level of accuracy is further limited by the precision of the scale used for weighing. Meaningful results require the scale to be absolutely level, which was not always possible depending on the laboratory setting. The magnetic susceptibility measurements were taken using multiple susceptibility meters. In such cases, different coil sizes were used. A larger coil provides a larger measurement surface area and thus a more representative magnetic susceptibility. When using a small-diameter sensor coil (Bartington MS2E) on coarse-grained igneous rocks, it is possible to experience localized nugget effects. For example, a local coarse magnetite crystal in a mass of feldspar and quartz can result in an inappropriate and artificially high magnetic susceptibility reading (Lee and Morris, 2012). To overcome the localized nugget effects multiple measurements were taken on varied surfaces on the same sample.

7.3 Future outlook

With the continued development of Canada's resource sector and the recent climb of the price of uranium, there is a high possibility that the Thelon Basin region will develop into a producing uranium camp. Once exploration progresses inwards to deposits similar to those in the Athabasca Basin located below hundreds of meters of sandstone, a thorough understanding of the geology, geometry and fault context is required. The work presented herein lays the groundwork for establishing the geological context of the sub-basin for exploration companies to build-upon and improve. In all the case studies, the

geophysical models represent regional geometries under few controls. Incorporating additional information, especially absolute controls such as borehole data, will serve to improve the resolution and accuracy of the models.

7.4 References

Blakely, R., and Simpson, R. 1986. Approximating edges of source bodies from magnetic or gravity anomalies. *Geophysics*, 51, 1494‑1498.

Lee, M. D., and Morris, W.A. 2012. Comparison of magnetic susceptibility meters using rock samples from the Wopmay orogen, Northwest Territories, Canada. Current Research. Geological Survey of Canada, Open File (in press).

Thomas, M.D. and Wood, G. 2007. Geological significance of gravity anomalies in the area of McArthur River uranium deposit, Athabasca Basin, Saskatchewan: *in* Jefferson, C.W. and Delaney, G., (eds.), EXTECH IV: Geology and Uranium EXploration TECHnology of the Proterozoic Athabasca Basin, Saskatchewan and Alberta; Geological Survey of Canada, Bulletin 588, 441-464.

Tschirhart, V., Morris, W.A., Ugalde, H. and Jefferson, C.W. 2011. Preliminary 3D geophysical modelling of the Aberdeen sub-basin, northeast Thelon Bain region, Nunavut. Geological Survey of Canada, Current Research 2011-4, 12 pp., doi: 10.4095/287165.